INTERPRETING CHANGES IN ANTHROPOGENIC EMISSIONS UNDERLYING ABRUPT CHANGES IN OBSERVED AIR QUALITY USING SURFACE AND SATELLITE OBSERVATIONS AND A CHEMICAL TRANSPORT MODEL

by

Gongda Lu

A thesis submitted to the University of Birmingham for the degree of

DOCTOR OF PHILOSOPHY

School of Geography, Earth and Environmental Science

College of Life and Environmental Sciences

University of Birmingham

April 2022

Abstract

Effective air quality policy is hindered by inaccurate estimates of precursor emissions, unvalidated, sparse or absent monitoring networks, and uncertain formation pathways of air pollution. Of particular concern are regions with severe air pollution, such as northern China and, large cities in South and Southeast Asia, and large cities in the world with high anthropogenic emissions. This work makes use of field campaign measurements, reference network measurements, satellite observations and a chemical transport model (CTM) to address these knowledge gaps in these regions.

In the Beijing-Tianjin-Hebei region (BTH) in northern China, the Chinese government implemented strict emission control measures in autumn-winter 2017/2018 to address fine particulate matter ($PM_{2.5}$) pollution. $PM_{2.5}$ reduction targets were met, so these controls are now adopted in other parts of China, even though the relative role of emission controls and meteorology was not assessed. Surface observations of air quality from monitoring networks (validated against field campaign measurements) and the GEOS-Chem CTM were used after addressing large biases in the regional bottom-up anthropogenic emission inventory for China. According to the model, emission controls accounted for less than half (at most 43%) the decline in total $PM_{2.5}$ while most (57%) was due to interannual variability in meteorology. Specifically, a deeper planetary boundary layer, stronger winds, and lower relative humidity during the emission control period. Emission controls alone would not achieve the $PM_{2.5}$ reduction targets of 15-25% in this region.

Cities in South and Southeast Asia are developing rapidly, but routine, up-to-date and publicly available inventories of emissions are lacking for this region. Nitrogen oxides (NO_x) emissions in cities are important precursors to health-hazardous $PM_{2.5}$ and tropospheric ozone (O_3) where it is a greenhouse gas. NO_x lifetimes and emissions over 10 large cities in South and Southeast Asia in 2019 were obtained by applying an exponentially modified Gaussian (EMG) approach with a wind rotation technique to the nitrogen dioxide (NO_2) tropospheric vertical column densities (VCDs) from the high spatial resolution TROPOspheric Monitoring Instrument (TROPOMI). Annual averaged NO_x emissions range from < 50 mol s^{-1} for Karachi, Ahmedabad, Mumbai, Lahore and Chennai, 50-100 mol s^{-1} for Manila and Jakarta, and > 100 mol s^{-1} for Delhi, Dhaka and Singapore. This is comparable to the range of emissions estimates for polluted cities in China. Bottom-up NO_x emissions from a widely used publicly available global inventory exceed the top-down estimates for most cities. The discrepancy is >100% for Chennai, Singapore and Jakarta. It was only possible to estimate top-down monthly NO_x estimates for 3 cities, due to issues with the line density fitting parameters at these fine temporal scales. These ranged from 63 to 148 mol s^{-1} for Singapore (annual mean 114 mol s^{-1}), 44 to 109 mol s^{-1} for Jakarta (68 mol s^{-1}), and 26 to 67 mol s^{-1} for Manila (53 mol s^{-1}). Month-to-month variability is absent in the bottom-up emission estimates. The discrepancies identified in this work need to be resolved to ensure the development of effective policies.

Abrupt changes in air quality during COVID-19 lockdowns presented an opportunity to investigate changes in observed $PM_{2.5}$, NO_x and O_3 pollution due to interventions. Surface observations of air quality in 11 cities worldwide were analysed. Observed NO_2 decreased substantially at urban background and roadside sites in all the cities, by 10-60% at urban background sites, and by 29-53% at roadside sites. In contrast, observed O_3 increased in all cities after the lockdowns, by 16-167% at urban background sites and by 20-156% at roadside sites. The percentage changes in observed $PM_{2.5}$ are -39 to 153% at urban background sites, -41 to 108% at roadside sites, and -34 to 165% at rural sites. But by comparing observations in 2020 to those in 2016-2019 during the equivalent periods, results here demonstrated that the observations of air quality alone cannot represent the changes in emissions due to COVID-19 lockdowns as the impact of meteorology should be considered.

Findings in this thesis demonstrate the application of observations from multiple platforms, innovative analytical techniques, and an advanced chemical transport model to abrupt changes in air quality in time and space to better understand air pollution precursor emissions and formation pathways and to interpret the relative contribution from changes in emissions and meteorology. Such information is vital for developing well-informed environmental policies.

Acknowledgments

First and foremost, I would like to thank my supervisors, Dr. Eloise A. Marais and Prof. Zongbo Shi. Without their encouragement and supervision, I would not have come this far into my education and research. I want to thank Dr. Eloise in particular, for making my dreams come true, as this once-in-a-lifetime PhD opportunity would not have happened without her.

I want to thank China Scholarship Council and the Education Section of the Chinese Embassy in London for supporting my PhD study in the UK.

I would like to thank our group members at University of Birmingham and at University College London. I am very lucky to have the chance to work with and learn from Clarissa, Karn, Alfred, Tuan, Congbo, Jingsha, Nana, Jamie, Kavitha, Bex and Rob. I want to thank Dr. John Roberts at University of Leicester for his help in improving my Python skills.

I am thankful to many people at the School of Geography, Earth and Environmental Sciences at University of Birmingham. They are Dr. Tom Pugh, Dr. Xiaoming Cai, Prof. Francis Pope, Dr. Salim Alam, Dr. Surindar Kishen Dhesi, Prof. Bill Bloss and Prof. Jon Sadler, Mrs. Gretchel Coldicott, Mr. James Peart, Mrs. Chantal Jackson, Mrs. Eileen Jackson and Mrs. Valerie Walker. Many of them have provided me all kinds of help and guidance since I came to GEES for my Masters degree in 2016.

Lastly, I would like to thank my friends in the UK, China, Denmark and the US, for all their support over the years. I am blessed to have you.

Thank you everyone for being a part of this journey!

Author’s contribution

This thesis is based on three manuscripts, the first one is under review in Atmospheric Environment, the second one is in preparation for submission to Geophysical Research Letters, and the last one has been published after peer-review in Science Advances.

CHAPTER 1: INTRODUCTION, is unique to this thesis.

CHAPTER 2: CONTRIBUTION OF AUTUMN-WINTER EMISSION CONTROLS TO AIR QUALITY IMPROVEMENTS IN THE BEIJING-TIANJIN-HEBEI REGION

Under review in **Atmospheric Environment** as:

G. Lu, E. A. Marais, T. V. Vu, J. Xu, Z. Shi, J. D. Lee, Q. Zhang, L. Shen, G. Luo, and F. Yu, Contribution of autumn-winter emission controls to air quality improvements in the Beijing-Tianjin-Hebei region

G. Lu performed the GEOS-Chem simulations, analysed the model and measurement data, and prepared the manuscript. E. A. Marais assisted in the writing and provided supervisory guidance, with co-supervision and editorial contributions from Z Shi. J. D. Lee provided APHH gas concentration data. Z. Shi, T. V. Vu and J. Xu performed PM composition analyses and provided guidance on using APHH data. Q. Zhang provided the original MEIC emission inventory that L. Shen processed for input to GEOS-Chem. G. Luo and F. Yu provided source codes for the updated wet scavenging scheme in GEOS-Chem

CHAPTER 3: TOP-DOWN ESTIMATE OF NO_X EMISSIONS IN CITIES IN SOUTH AND SOUTHEAST ASIA

To be submitted to **Geophysical Research Letters** as:

G. Lu, K. Vohra, E. A. Marais, and L. Zhu, Top-down estimate of NO_x *emissions in cities in South and Southeast Asia.*

G. Lu analysed the TROPOMI and ERA5 data, performed the HEMCO simulations, and prepared the manuscript. K. Vohra assisted in interpretation of the results. E. A. Marais assisted in the writing and provided supervisory guidance. L. Zhu provided source codes for the oversampling algorithm.

CHAPTER 4: CHANGES IN SURFACE AIR QUALITY DURING COVID-19 LOCKDOWNS

This chapter is a component of the paper published in **Science Advances** as:

Z. Shi, C. Song, B. Liu, G. Lu, J. Xu, T. V. Vu, R. J. R. Elliott, W. Li, W. J. Bloss, and R. M. Harisson (2021). Abrupt but smaller than expected changes in surface air quality attributable to COVID-19 lockdowns. Science advances, 7(3), eabd6696.

In the formal publication, author contribution to the paper is described as:

Z.S. conceived the research, designed the work, and drafted the original manuscript; G.L., J.X., B.L., and C.S. collected the air quality and meteorological data; C.S. collected the ERA5 reanalysis data, performed the back-trajectory clustering, and run the RF model, Monte Carlo simulation, and data visualization; T.V.V. and B.L. contributed to the development of the RF method for this study. W.J.B. contributed to the interpretation of the results regarding O_3-forming and O_3-depleting chemical processes. W.J.B., R.M.H., W.L., and R.J.R.E. contributed to drafting and revision of the manuscript.

In this chapter, some of the text relevant to my contribution is taken from the above paper. Other contents in this chapter are unique to this thesis. Following the university instructions, a detailed statement of author contribution is provided at the start of this chapter.

CHAPTER 5: SYNTHESIS, is unique to this thesis.

Tables of contents

List of figures

List of tables

List of abbreviations

AMF	Air Mass Factor
BC	Black Carbon
BJMEMN	Beijing Municipal Environmental Monitoring Network
BTH	Beijing-Tianjin-Hebei
CEDS	Community Emissions Data System
CNEMN	China National Environmental Monitoring Network
CO	Carbon Monoxide
CTM	Chemical Transport Model
DEFRA	Department for Environment, Food and Rural Affairs
DOAS	Differential Optical Absorption Spectroscopy
EC	Elemental Carbon
EDGAR	Emissions Database for Global Atmospheric Research
EMG	Exponentially Modified Gaussian
GC	GEOS-Chem
GFED	Global Fire Emissions Database
HCHO	Formaldehyde
HEMCO	Harmonized Emissions Component
IAP	Institute of Atmospheric Physics
MEE	Ministry of Environment and Ecology (China)
MEGAN	Model of Emissions of Gases and Aerosols from Nature
MEIC	Multi-resolution Emission Inventory for China
MERRA2	Modern-Era Retrospective analysis for Research and Applications, Version 2
NMB	Normalised Mean Bias
NMVOC	Non-methane Volatile Organic Compounds
NO	Nitrogen Oxide
NO_2	Nitrogen Dioxide
NO_X	Nitrogen Oxides
NH_3	Ammonia
OA	Organic Aerosol
OC	Organic Carbon
OM	Organic Matter
OMI	Ozone Monitoring Instrument
PAN	Peroxyacetyl Nitrate
PBL	Planetary Boundary Layer
PM	Particulate Matter
POA	Primary Organic Aerosol
RH	Relative Humidity
RMA	Reduced Major Axis Regression
SCD	Slant Column Density
SIA	Secondary Inorganic Aerosol
SOA	Secondary Organic Aerosol

SO_2	Sulfur Dioxide
TEMPO	Tropospheric Emissions: Monitoring of Pollution
TROPOMI	TROPOspheric Monitoring Instrument
VCD	Vertical Column Density
VOC	Volatile Organic Compounds
WHO	World Health Organization

Thesis overview

This thesis uses surface and satellite observations of air quality, meteorological reanalysis, emission inventories and a chemical transport model to interpret changes in emissions underlying abrupt changes in observed air quality in time and space at the local to regional scales.

Chapter 1 is the introduction to the thesis. It describes the impact of air pollution on human health and the environment, sources and formation of outdoor air pollution, surface and space-based monitoring or air quality, the GEOS-Chem chemical transport model, and the research gaps identified in this thesis.

Chapter 2 evaluates the relative role of strict seasonal air pollutant emission controls on improved air quality in the Beijing-Tianjin-Hebei region in northern China in autumn-winter 2017/2018. The work described in this chapter is under review in Atmospheric Environment as:

G. Lu, E. A. Marais, T. V. Vu, J. Xu, Z. Shi, J. D. Lee, Q. Zhang, L. Shen, G. Luo, and F. Yu, Contribution of autumn-winter emission controls to air quality improvements in the Beijing-Tianjin-Hebei region

Chapter 3 investigates the ability of satellite observations of NO_2 in estimating NO_x emissions from cities in South and Southeast Asia and compares the top-down NO_x emission estimates against commonly used bottom-up emission inventories. The findings in this chapter are in preparation for submission to Geophysical Research Letters as:

G. Lu, K. Vohra, E. A. Marais, and L. Zhu, Top-down estimate of NO_x *emissions in cities in South and Southeast Asia.*

Chapter 4 investigates changes in observed surface air quality due to COVID-19 lockdowns at 11cities around the world. This chapter is a component of the research paper published as:

Z. Shi, C. Song, B. Liu, G. Lu, J. Xu, T. V. Vu, R. J. R. Elliott, W. Li, W. J. Bloss, and R. M. Harrison (2021). Abrupt but smaller than expected changes in surface air quality attributable to COVID-19 lockdowns. Science advances, 7(3), eabd6696.

Chapter 5 summarises the key findings from work in this thesis and discusses opportunities for future research.

CHAPTER 1:INTRODUCTION

1.1 Impact of Air Pollution on Human Health and the Environment

Ambient air pollution causes adverse impacts on public health and the environment. Associations between air pollution and premature mortality have been evidenced from cohort studies during the last few decades, starting with the Harvard Six Cities Study (Dockery et al., 1993). Extensive subsequent epidemiological studies have demonstrated that long-term exposure to outdoor air pollution is linked to a range of morbidities, such as respiratory diseases (Guan et al., 2016; Turner et al., 2011; Xing et al., 2016), cardiovascular diseases (Lelieveld et al., 2019; Liang et al., 2020; Rajagopalan et al., 2018), increased risks of preterm birth (He et al., 2022; Qian et al., 2016), and loss of fertility (Li et al., 2021b). Long-term exposure to air pollution substantially reduces life expectancy (Apte et al., 2018; Lelieveld et al., 2015; Yin et al., 2020), particularly from endpoints such as ischemic heart disease, stroke, chronic obstructive pulmonary disease and lung cancer in adults, and acute respiratory lung infection in children under five years old (Apte et al., 2015). 3–9 million premature global deaths are attributed to exposure to outdoor air pollution each year (Burnett et al., 2018; Lelieveld et al., 2015; McDuffie et al., 2021; Murray et al., 2020), so air pollution is a leading risk factor for loss of life expectancy (Lelieveld et al., 2020). Exposure to air pollution also leads to decline in cognitive function, particularly for elder people (Power et al., 2011; Weuve et al., 2012; Zhang et al., 2018) and mental health problems, such as depression and anxiety (Bakian et al., 2015; Braithwaite et al., 2019; Newbury et al., 2019). Short-term exposure to severe air pollution is associated with cardiovascular, respiratory, and type 2 diabetes mortalities (Meng et al., 2021; Wu et al., 2021a; Wu et al., 2016a).

Major air pollutants that impact health directly or contribute to formation of health-hazardous pollutants include gaseous species such as nitrogen oxides ($NO_x \equiv NO + NO_2$), sulfur dioxide (SO_2), ammonia (NH_3), carbon monoxide (CO), non-methane volatile organic compounds (NMVOCs), tropospheric ozone (O_3), and fine particles with aerodynamic diameter ≤ 2.5 μm ($PM_{2.5}$). Most NO_x is emitted as nitric oxide (NO), but this reacts rapidly with the atmospheric oxidants peroxy radicals (HO_2 and RO_2), the nitrate radical (NO_3) and O_3 to form nitrogen dioxide (NO_2) (Monks, 2005). $PM_{2.5}$ is a mixture of chemical components often dominated by organics (OA), sulfate, nitrate, ammonium, mineral dust, black carbon (BC) and bound water (Philip et al., 2014; Xu et al., 2021). $PM_{2.5}$ has been strongly associated with adverse effects on human health (Apte et al., 2015; Feng et al., 2016; Kim et al., 2015; Lelieveld et al., 2015; McDuffie et al., 2021; Pope et al., 2009).

Over 90% of the global population lives in areas where air pollution exceeds the recently updated stricter World Health Organization (WHO) air quality guidelines of 5 $\mu g\ m^{-3}$ for annual mean $PM_{2.5}$ and 10 $\mu g\ m^{-3}$ for annual mean NO_2 (WHO, 2021). $PM_{2.5}$ pollution is particularly severe in developing countries such as China (Song et al., 2017b) and India (Vohra et al., 2021a); made worse by large population exposure to air pollution and related mortality (Lelieveld et al., 2015; Song et al., 2017a; Yue et al., 2020). These adverse health impacts further lead to economic losses due to reduced Gross Domestic Production (GDP), increased health expenditure and loss in the value of statistical life (Matus et al., 2012; Xie et al., 2019).

In addition to its adverse impacts on human health, ambient air pollution damages ecosystems. For example, exposure of plants to surface O_3 leads to oxidation of plant cells, thus impairing leaf photosynthesis and vegetation productivity and reducing global crop yields (Ainsworth et al., 2012; Avnery et al., 2011; Feng et al., 2019; Tai and Martin, 2017). Exposure to O_3 over decades may also alter the species composition of forests (Grulke and Heath, 2020). Ambient air pollution can also affect ecosystems indirectly through biogeochemical cycles, such as global nitrogen, sulfur and carbon cycles. For example, high levels of SO_2 and NO_x lead to formation of acid rain, which threatens the pH balance and vitality of aquatic ecosystems, soils and crops (Grennfelt et al., 2020).

Air pollution can also affect regional climate depending on the radiative forcing of some air pollutants as well as chemical reactions with greenhouse gases of O_3 and methane (CH_4) that alters their atmospheric abundance and persistence (lifetime). Chemical components of $PM_{2.5}$ also have opposite effects on climate: BC warms the atmosphere by absorbing sunlight (Peng et al., 2016). Sulfate, nitrate and ammonium cool the atmosphere by scattering sunlight (Lin et al., 2022; Zheng et al., 2020). Organic aerosols (OA) cool the atmosphere by scattering visible radiation, but also absorb light, leading to warming (Lin et al., 2014). The net effect of NO_x emissions on climate is complex, as NO_x emissions increase the abundance of O_3 in the troposphere where it is a greenhouse gas (Stevenson et al., 2013), but also form sunlight scattering PM and decrease abundance of CH_4 by oxidation, which both cool the atmosphere (Fiore et al., 2012).

1.2 Sources and Formation of Outdoor Air Pollution

Determination of the true environmental effects of air pollution on health, ecosystem functioning, and regional climate requires accurate estimates of the sources that degrade air quality. Dominant anthropogenic sources typically include energy production, industry, transportation, agriculture, and residential/domestic sources (Crippa et al., 2018; Li et al., 2017b; McDuffie et al., 2020). Worldwide, NO_x and SO_2 are mostly from combustion of the fossil fuels coal, natural gas and oil for industrial processes energy production, on-road vehicles and ships (McDuffie et al., 2020). Anthropogenic NH_3 is overwhelmingly dominated by the agricultural fertilizers and manure use, and livestock waste (Huang et al., 2012; Marais et al., 2021; Paulot et al., 2014). In urban areas, vehicles with three-ways catalytic converters and selective catalytic reduction devices also emit NH_3 (Cao et al., 2022; Farren et al., 2020; Liu et al., 2014; Perrino et al., 2002). Anthropogenic NMVOCs tend to be dominated by industrial solvent use, incomplete combustion of fossil fuels, open and domestic burning of biomass, and residential and commercial volatile chemical products (Li et al., 2019b; McDonald et al., 2018; Mo et al., 2021). Anthropogenic NMVOCs emissions may have increased in the last few decades according to both global and regional emission inventories (Li et al., 2019b; McDuffie et al., 2020), though estimates of these are uncertain and challenging to constrain. Primary CO is a ubiquitous product of inefficient combustion, so derives from all sources that burn fossil and biomass-based fuels (Goyal et al., 2013; Tang et al., 2016; Wei et al., 2012). Vehicles are also the dominant sources of BC in urban environments (Grivas et al., 2012; Joshi et al., 2021). Primary OA is also a consequence of inefficient combustion of fossil and biomass-based fuels (Jones and Harrison, 2005; Xu et al., 2021; Zhang et al., 2021). Anthropogenic fugitive dust from combustion, industrial processes, construction, brake and tire wear, and resuspended dust on roadways is likely underestimated in polluted regions (Philip et al., 2017). The contribution of different anthropogenic sources varies with time and location and is influenced by the emission controls imposed by governments (Zheng et al., 2018). Natural sources that influence air quality at a global scale include NO_x from lightning (Schumann and Huntrieser, 2007; Tie et al., 2002), most pollutant precursors from wildfires (van der Werf et al., 2017), soil NO_x from microbes in soils (Bertram et al., 2005; Huber et al., 2020), SO_2 from volcanic eruptions and degassing (Carn et al., 2017), biogenic volatile organic compounds from vegetation (Guenther et al., 2012; Hu et al., 2015; Marais et al., 2012), sea salt, desert dust, seabird NH_3, and marine DMS (Ginoux et al., 2004; Jaeglé et al., 2011).

Secondary air pollutants formed via chemical reactions of precursor compounds include secondary inorganic and organic aerosols and O_3 (Belis et al., 2013; Huang et al., 2014; Weagle et al., 2018; Zhang et al., 2017b). Secondary inorganic aerosols (SIA) include nitrate, sulfate and ammonium form as a result of chemical and physical processes. Sulfate aerosol is mainly formed via oxidation of SO_2 by hydrogen peroxide (H_2O_2) or O_3 to form sulfuric acid (H_2SO_4) (Khoder, 2002). NH_3 is alkaline and neutralizes H_2SO_4 to form ammonium sulfate $(NH_4)_2SO_4$ (Wang et al., 2013). Particulate nitrate is formed via two major pathways. During the daytime, NO_2 is oxidized by the hydroxyl radical (OH) to form nitric acid (HNO_3) that then reacts with NH_3 to form ammonium nitrate (NH_4NO_3), which partitions to the aerosol phase (Chen et al., 2020; Wang et al., 2017). At night, NO_2 is oxidized by O_3 to dinitrogen pentoxide (N_2O_5). N_2O_5 undergoes heterogeneous hydrolysis with water and chloride to form soluble nitrate including HNO_3, particulate nitrate, and nitryl chloride ($ClNO_2$) on chloride containing aerosol surface (Wang et al., 2020a). Secondary organic aerosols (SOA) are formed mainly via oxidation of NMVOCs by oxidizing agents such as OH, O_3, and NO_3 (Sun et al., 2016) or via aqueous aerosol-phase oxidation of primary OA (McNeill, 2015; Wang et al., 2021a). Detailed formation mechanisms of SOA remain unclear due to the large number of NMVOCs and pathways.

Surface O_3 pollution is mostly produced via photolysis of NO_2, following a sequence of chemical reactions with VOCs, CO and OH. VOCs and CO react with OH and generate organic peroxy radicals (RO_2) and hydroperoxy radicals (HO_2) (R1 and R2). RO_2 and HO_2 can oxidize NO to NO_2 (R3 and R4).

Then NO_2 is photolyzed to from atomic oxygen, which reacts with oxygen (O_2) to form O_3 (R5 and R6) (Atkinson, 2000; Sillman, 1999). O_3 chemistry is nonlinear and depends on the relative abundance of NO_x and VOCs. In typical urban environments, there are large emissions of NO_x, so O_3 formation is most sensitive to perturbations in VOCs and O_3 is titrated from prevalence of the reaction between NO with O_3 (Sillman, 1999).

$$\mathrm{VOCs + OH + O_2 \rightarrow RO_2 + H_2O} \tag{R1}$$

$$\mathrm{CO + OH + O_2 \rightarrow HO_2 + CO_2} \tag{R2}$$

$$\mathrm{RO_2 + NO + O_2 \rightarrow secondary\ VOCs + HO_2 + NO_2} \tag{R3}$$

$$\mathrm{HO_2 + NO \rightarrow OH + NO_2} \tag{R4}$$

$$\mathrm{NO_2 + hv \rightarrow NO + O} \tag{R5}$$

$$\mathrm{O + O_2 + M \rightarrow O_3 + M} \tag{R6}$$

Meteorology is also an important influencer of air pollution. In Northern China, for example, high daily mean $PM_{2.5} \geq 150$ µg m^{-3} are associated with calm conditions, shallow planetary boundary layer, thermal inversion contributing to build up of pollution and cool conditions and high relative humidity promoting formation of secondary inorganic aerosols (Ding et al., 2021; Li et al., 2019c; Miao et al., 2019; Su et al., 2020; Wu et al., 2019).

1.3 Surface and Space-based Monitoring of Air Quality

National and regional surface air quality monitoring networks are extensively used to constrain air pollution sources, to understand the underlying factors that influence the spatial and temporal variability of air pollution, to assess compliance against air quality standards, and to quantify the environmental impacts of ambient air pollution (Boldo et al., 2014; Borge et al., 2019; Guerreiro et al., 2014; Hou and Wu, 2016; Jiang et al., 2020; Ju et al., 2018; Oftedal et al., 2009; Sicard et al., 2021; Wang et al., 2019). These surface monitoring networks normally provide measurements of criteria air pollutants including NO_x, SO_2, CO, O_3, $PM_{2.5}$ and PM_{10} (particulate matter with an aerodynamic diameter $\leqslant 10$ μm).

Monitoring networks are well established in developed countries like the UK, European countries, and the US, providing long-term records of air quality for multiple pollutants since the 1990s (AQEG, 2015; Demerjian, 2000; Guerreiro et al., 2014; Liu and Peng, 2018). However, high costs associated with installation, maintenance, and quality control of in-situ reference measurement instruments contribute to limited global and temporal coverage of surface observations of air quality in many developing countries, hindering research on air quality and development of effective air quality policies to reduce air pollution. Many cities in South and Southeast Asia and Africa are devoid of reference monitors (Abera et al., 2021; Koplitz et al., 2016). On average in 2012-2014, there was one air quality monitoring station for every 30 million inhabitants in Pakistan, for every 25 million inhabitants in Indonesia, for every 3.8 million inhabitants in India, and for every 4.6 million inhabitants across the African continent (Carvalho, 2016). Significant premature deaths attributable to air pollution are found in highly populous countries with very poor air quality, such as China, India, and Nigeria (Lelieveld et al., 2015). Extensive and good quality surface network measurements are vital. To address severe air pollution in China, the China National Environmental Monitoring Network (CNEMN) was established in late 2013 to routinely monitor six criteria air pollutants (NO_2, SO_2, CO, O_3, $PM_{2.5}$ and PM_{10}). CNEMN was quickly extended from 74 cities in 2013 to more than 1400 monitoring sites in over 300 cities in 2015 (Zhang et al., 2020a). As a pioneer in local air quality monitoring in China, Beijing Municipal Environmental Monitoring Network (BJMEMN) was established to enhance the density of air quality measurements in Beijing (Wan et al., 2021).

Figure 1.1 shows the spatial distribution of the current (2022) distribution of CNEMN and BJMEMN sites. Both CNEMN and BJMEMN measurements have now been widely used to quantify changes in surface air pollution in China (Chu et al., 2020; Shen et al., 2020; Wan et al., 2021; Wu et al., 2018b; Yuan et al., 2021; Zhao et al., 2016), but independent evaluation with research-grade instruments is lacking. A previous study developed statistical techniques based on the z-score method (Lanzante, 1996) and used intercomparison of measurements of different air pollutants, such as ratios of $PM_{2.5}$ to PM_{10}, to determine that the contribution of outliers to measurements in 2014–2016 is small (0.65%–5.68%) and mostly due to issues with measurements of PM_{10} (Wu et al., 2018a). Many studies have also identified that reference measurements of NO_2, obtained almost exclusively with the chemiluminescence technique, are susceptible to interference from thermal decomposition of thermally unstable NO_x reservoir compounds, which may result in a positive bias of 6-22% (Dunlea et al., 2007; Reed et al., 2016; Shah et al., 2020).

Despite rapid expansion of CNEMN, there are still limitations in air quality monitoring in China. Sites are mostly in eastern China, and all are in urban areas, with a bias toward developed areas (Zhang et al., 2020a). Different from the well-established monitoring networks in the UK, information on site classification is not available for CNEMN, hindering assessment of representativeness of CNEMN measurements of urban air quality for comparison to models and satellite observations (Zhu et al., 2020). Measurements of the important aerosol precursor NH_3 and of major $PM_{2.5}$ components are covered with other networks that are proprietary. NH_3 emissions are either constant or increasing in China and this is reducing the effectiveness of $PM_{2.5}$ reductions achieved with emission controls targeting NO_x and SO_2 sources (Fu et al., 2017; Wu et al., 2016b). Surface measurements of NH_3 in China are limited to the proprietary Ammonia Monitoring Network in China (AMoN-China) (Pan et al., 2018), which started in September 2015 with 53 sites. Studies suggest there has been a persistent increase in anthropogenic NMVOCs emissions in China over the past thirty years (Li et al., 2019b; Shen et al., 2019), but there are no routine measurements of NMVOCs. Satellite observations of formaldehyde (HCHO), a commonly used proxy for NMVOCs due to ubiquitous and prompt formation of HCHO from oxidation of many NMVOCs (Souri et al., 2020), suggest there is a shift in the O_3 formation regime in some Chinese cities, from the VOC-limited to a transitionary regime (Wang et al. (2021b)). This has been attributed to rapid decline in anthropogenic NO_x emissions between 2016 and 2019 and further necessitates enhanced understanding of NMVOCs sources.

To aid in developing strategies to address $PM_{2.5}$ pollution in and around the very polluted Beijing-Tianjin-Hebei region in northern China, the National Aerosol Composition Monitoring Network (NACMON) was established in 2017 with 31 sites in 28 cities (Dao et al., 2019). The NACMON measures $PM_{2.5}$ components such as nitrate, sulfate, ammonium, OC, elemental carbon (EC), chloride, mineral dust, and trace elements (Dao et al., 2019). NACMON sites are only established in 28 cities in northern China and the measurements are also proprietary. Limited access to these valuable datasets hinders their use by the wider research community.

In addition to surface monitoring networks, intensive ground-based field campaigns have been conducted to obtain comprehensive measurements of atmospheric composition and meteorology, such as the Atmospheric Pollution and Human Health in a Chinese Megacity (APHH-Beijing) UK-China collaborative research programme (Shi et al., 2019). Though limited in time and space, these provide detailed insights into air pollution sources and composition, particularly when combined with numerical modelling tools such as trajectory models that track air parcels or chemical transport models that represent atmospheric chemistry in 3-dimensions.

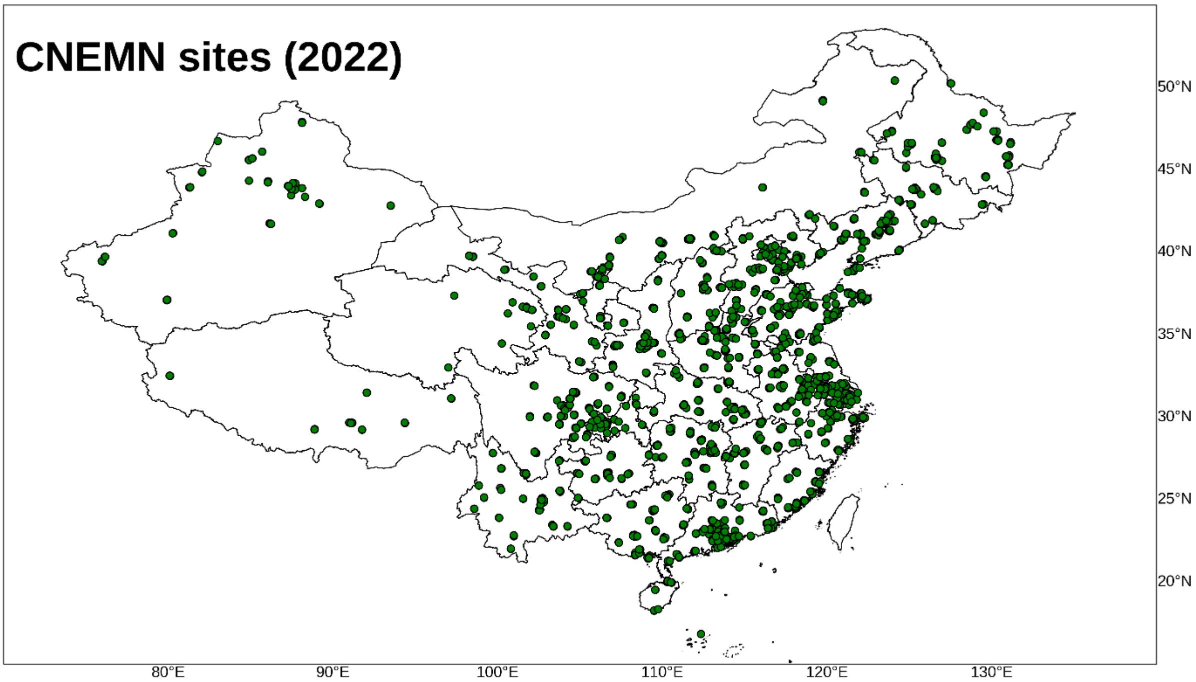

Figure 1.1: Map of CNEMN sites in 2022. Site list data source: https://quotsoft.net/air/ (last accessed: 1 April 2022)

Instruments onboard satellite platforms provide global coverage over multiple years for long-term and consistent monitoring of air quality (Duncan et al., 2014; Martin, 2008; Streets et al., 2013) In particular, satellite observations of tropospheric NO_2 vertical column densities (VCDs) have been extensively used to identify surface NO_2 pollution hotspots, to determine long-term trends in surface NO_2 pollution, to assess uncertainties and biases in bottom-up emission inventories, to evaluate the effectiveness of air quality policies, and to detect and quantify rapid changes in NO_2 pollution due to abrupt changes in anthropogenic activity such as COVID-19 lockdowns (Cooper et al., 2022; Lamsal et al., 2008; Li et al., 2021a; Martin et al., 2003; Silvern et al., 2019; Vohra et al., 2021a). For example, Liu et al. (2016) used NO_2 column densities provided by the Ozone Monitoring Instrument (OMI) to estimate a 32% decline in OMI NO_2 from 2011 to 2015 in China, which corresponds to a 21% decline in emissions. Vohra et al. (2022) has used OMI NO_2 observations to report a rapid increase of 0.8-7.7 % a^{-1} in NO_2 concentrations in cities in South and Southeast Asia in 2005-2018.

OMI is at relatively coarse resolution (13 × 24 km^2 at nadir), has substantial data loss due to the row anomaly and has been in space since 2005, so is beyond its expected lifetime of 3-4 years (Schenkeveld et al., 2017). Following the success of OMI (Levelt et al., 2018), the TROPOspheric Monitoring Instrument (TROPOMI) was launched into sun synchronous orbit onboard the Copernicus Sentinel - 5P satellite on 13 October 2017. TPOPOMI passes overhead at around 13:30 pm local time, providing daily global coverage with a swath width of ~2600 km. The ground pixel nadir resolution was 7 × 3.5 km^2 before 6 August 2019 and increased to 5.5 × 3.5 km^2 afterwards (van Geffen et al., 2021; Veefkind et al., 2012). Tropospheric NO_2 VCDs are retrieved from TROPOMI following three steps (van Geffen et al., 2021). The first step is to retrieve the total NO_2 slant column density (SCD) (the concentrations of NO_2 along the light path) (Figure 1.2) using the differential optical absorption spectroscopy (DOAS) technique in the wavelength range of 405-465 nm (Platt and Stutz, 2008). Then the NO_2 tropospheric slant column is separated from the total slant NO_2 column using a chemistry transport model (CTM) by way of data assimilation (Boersma et al., 2018). In the end, the tropospheric NO_2 slant column densities are converted to physical tropospheric NO_2 VCDs (Figure 1.2) using an air mass factor (AMF) estimated with a radiative transfer model (Boersma et al., 2018). TROPOMI NO_2 shows improved data quality with lower uncertainties (noise) compared to OMI NO_2 (van Geffen et al., 2020), and is highly correlated with surface and aircraft measurements of NO_2 in time and space (Griffin et al., 2019; Judd et al., 2020; Tack et al., 2021; Verhoelst et al., 2021; Wang et al., 2022a; Zhao et al., 2020).

TROPOMI NO_2 has been extensively used to estimate changes in NO_2 during worldwide lockdowns in response to the COVID-19 pandemic (Cooper et al., 2022; Goldberg et al., 2020; Le et al., 2020; Liu et al., 2020; Pazmiño et al., 2021; Potts et al., 2021; Qu et al., 2021; Solberg et al., 2021; Wang et al., 2021c). Zhang et al. (2020b) reported that NO_x emissions in East China decreased by 50% compared to those before lockdowns in January 2020, and NO_x emissions increased by 26% after the lockdowns in February-March 2020. Potts et al. (2021) reported that NO_x emissions declined by ~20% in the UK during the lockdown (23 March to 31 May 2020), ranging from 22-23% in the western portion of the country to 29% in the southeast and in Manchester, and >40% in London.

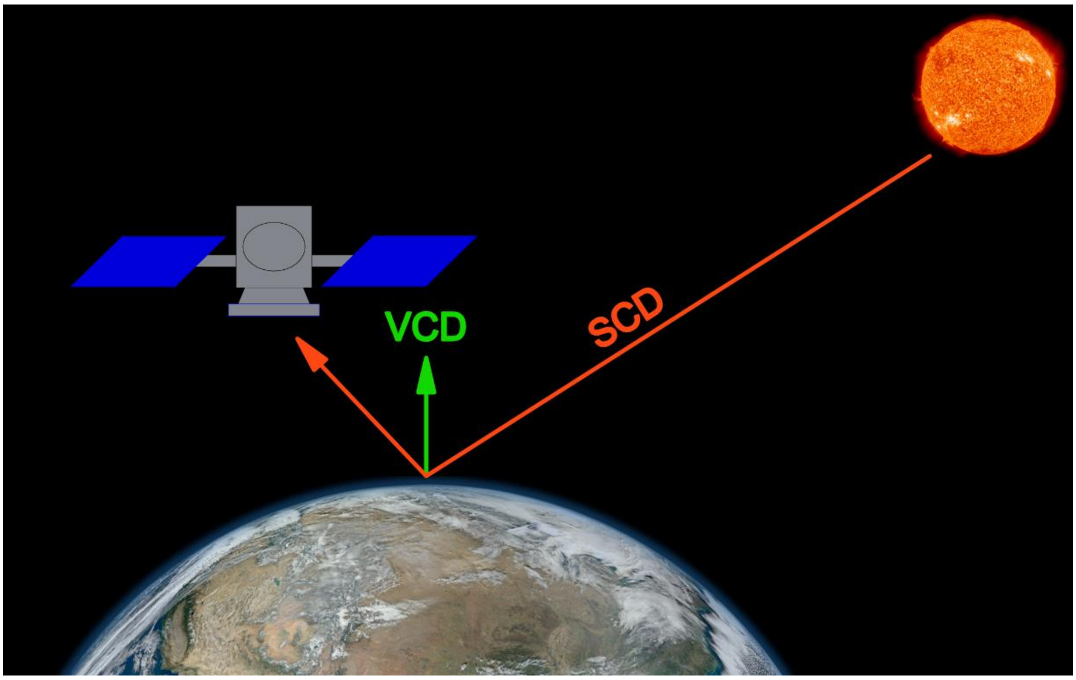

Figure 1.2: Schematic of the light path from the sun to the instrument (the slant column) and the true vertical column. SCD = slant column density; VCD = vertical column density.

The horizontal resolution of satellite instruments can be further improved using so-called oversampling. This technique represents each satellite observation as a sensitivity distribution on the ground, instead of a point or a polygon (Sun et al., 2018). For each satellite sensor, its sensitivity distribution is determined by its spatial response function. A generalized 2D super Gaussian function is proposed to characterize the spatial response functions of imaging grating spectrometers such as TROPOMI. Recent studies have applied this technique to TROPOMI NO_2 to grid the data to very fine resolutions of 0.01° × 0.01° and 0.02° × 0.02° to further refine trace gas plumes over NO_2 hotspots (Demetillo et al., 2021; Sun et al., 2021; Wang et al., 2022b). When this technique is applied to relatively coarse OMI instruments, averaging over long time periods (years) is required to accommodate low data coverage. The higher data density of TROPOMI can accommodate sampling over a relatively short period of time of one month. The fine spatial resolution of oversampled TROPOMI NO_2 VCDs is shown in Figure 1.3 over ten cities in South and Southeast Asia at 0.05° × 0.05° in 2019.

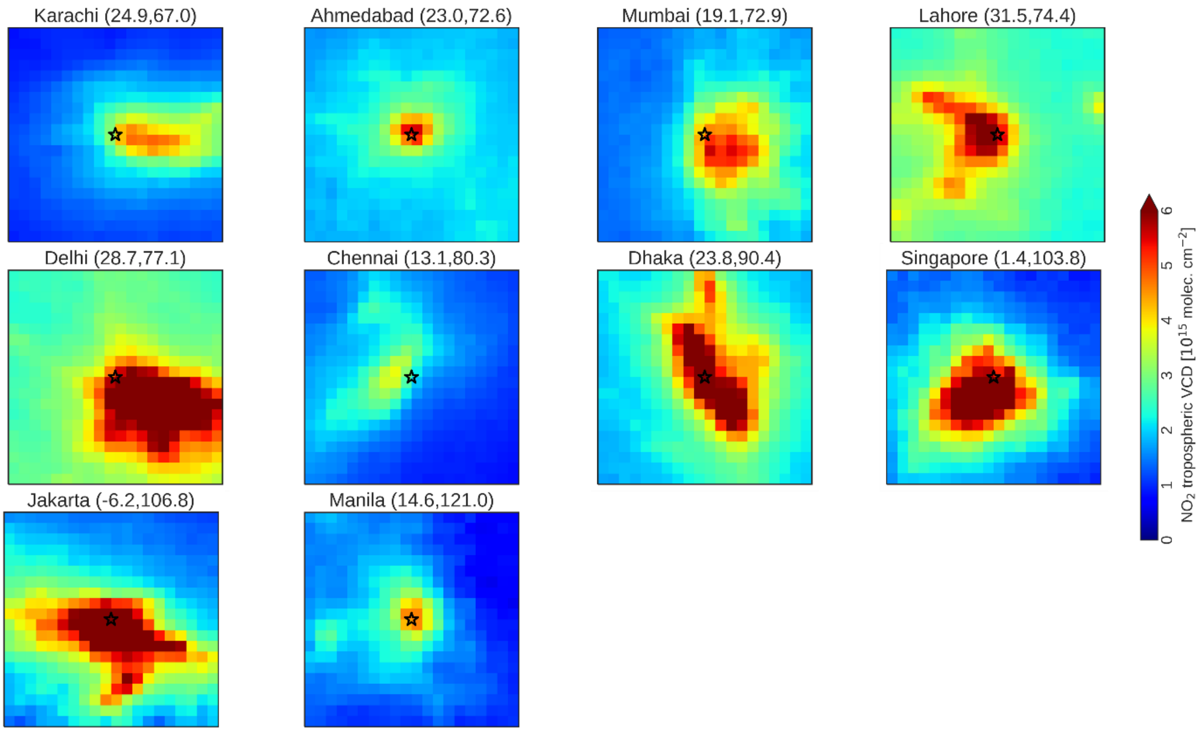

Figure 1.3: Oversampled TROPOMI NO_2 over ten cities in South and Southeast Asia in 2019. The name of each city is shown at the top of each map. Coordinates (latitude, longitude) are provided for each city centre next to each city name. Each map is provided at 0.05° × 0.05° resolution over a 1° × 1° domain surrounding the city centre.

NO_x emissions can be estimated from satellite observations of tropospheric NO_2 VCDs using a range of techniques, such as the mass balance approach using a CTM (Martin et al., 2003), the four-dimensional variational (4D-Var) method (Chai et al., 2009; Cooper et al., 2017; Qu et al., 2022), and an Ensemble Kalman Filter (Ding et al., 2015; Hanea et al., 2004; Miyazaki et al., 2012; Wu et al., 2020). For estimating NO_x emissions from isolated cities, Beirle et al. (2011) first proposed an exponentially modified Gaussian (EMG) method using tropospheric NO_2 VCDs and wind data from meteorology reanalysis. In brief, this method is based on the downwind decay of an NO_2 plume from the city. As shown in Figure 1.4, the 2D map of satellite NO_2 is converted to a 1D NO_2 line density by integrating NO_2 along the wind direction. The observed line densities show the distribution of NO_2 near the point source as a function of distance to the source along the dominant wind direction (x). The values of observed line densities are obtained by integrating satellite NO_2 in the across-wind direction

(y) over the interval b. City plume NO_x emissions are then derived with parameters obtained from the EMG fit to the observed NO_2 line densities and the city mean wind speed. Beirle et al. (2011) found that for isolated high polluting cities, NO_x emissions derived by this method are in good agreement with bottom-up emission inventories. Many studies have since adopted similar methods to estimate city NO_x emissions (Ialongo et al., 2014; Laughner and Cohen, 2019; Verstraeten et al., 2018; Xue et al., 2022). For example, Laughner and Cohen (2019) applied this method to OMI NO_2 in 30 cities in the US and found that changes in NO_x lifetime are of the same order as changes in NO_x emissions over the study periods. Their results suggest that change in NO_x lifetime must be accounted for when relating NO_x emissions and concentrations. Verstraeten et al. (2018) selected 23 cities in Europe and applied the EMG method to NO_2 columns from OMI and the LOTOS-EUROS (Long Term Ozone Simulation-European Ozone Simulation) CTM. Their results show that NO_x emissions estimated by the EMG method are consistent with the bottom-up emission inventory and thus can be used for real-time updates of the bottom-up emission inventory over urban areas. These studies normally need to average a long record of satellite NO_2 observations along different wind directions and then estimate NO_x emissions from the city under each wind direction.

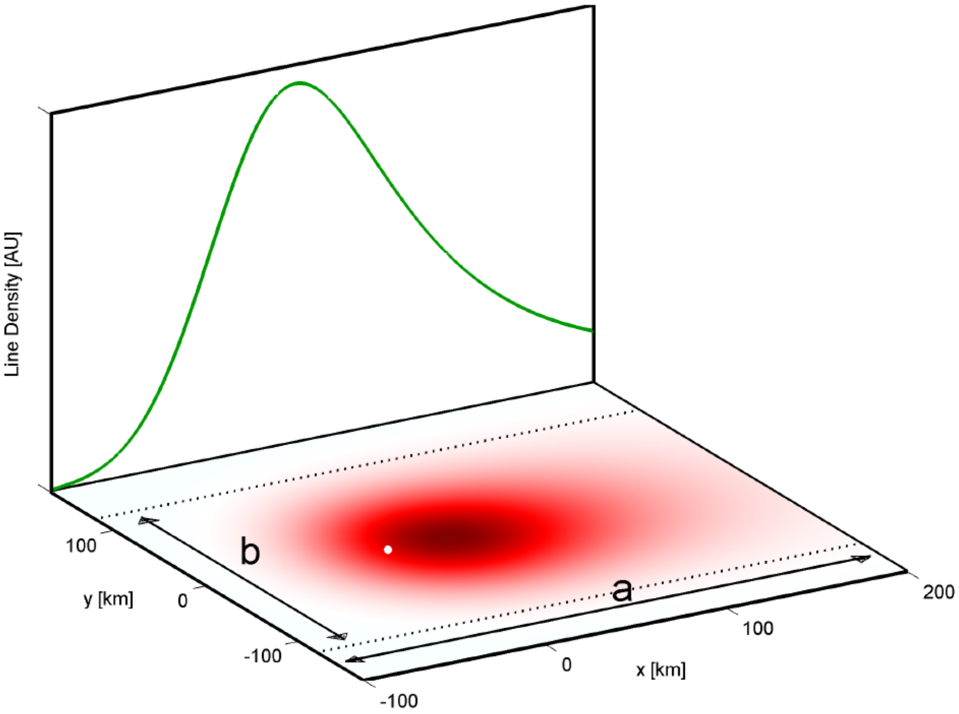

Figure 1.4: Sketch of the definition of line densities. The averaged NO_2 concentrations are mapped (red shade) for each wind direction sector. The white dot represents the location of the source (city centre). NO_2 are integrated in across-wind direction (y) over the interval b (units: km), yielding the NO_2 line densities (green) (artificial units (AU) can be used, such as moles m^{-1}). The EMG fit is performed over the interval a (units: km). Source: (Beirle et al., 2011)

The approach of Beirle et al. (2011) requires large dataset to average over multiple wind speeds. Valin et al. (2013) addressed this issue by developing a wind rotation technique that combines satellite observations under different wind directions and from different days by rotating NO_2 observations about the source centre by $-\theta$, where θ is the near-surface wind direction averaged over each satellite pixel, as illustrated in Figure 1.5. This preserves each satellite NO_2 pixel, its distance to the source (city) centre and upwind-downwind character. After wind rotation is applied, all satellite NO_2 pixels are oriented in the North to South direction. Based on the EMG approach proposed by Beirle et al. (2011) and the wind rotation technique proposed by Valin et al. (2013), following studies adopted similar approaches to estimate NO_x emissions from large point sources such as cities and power plants (de Foy et al., 2015; Goldberg et al., 2021; Lange et al., 2022; Lu et al., 2015; Wu et al., 2021b). This wind rotation and EMG approach is yet to be applied across cities in South and Southeast Asia where constraints on air pollution sources are lacking.

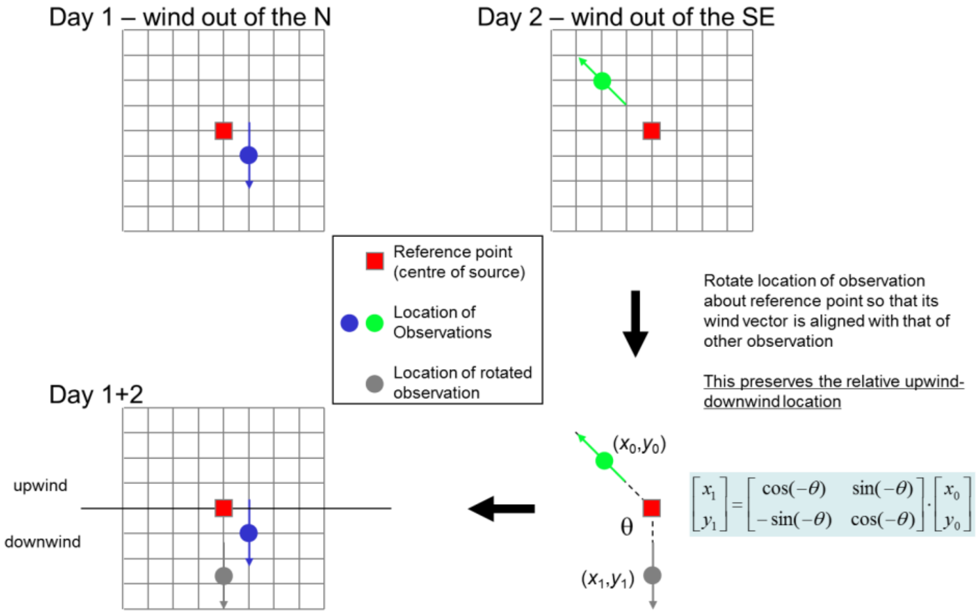

Figure 1.5: **Schematic diagram showing the wind rotation technique. If the wind direction at a certain satellite observation is θ, then each satellite pixel is rotated about the source centre with an angle of -θ. This approach preserves the relative location of the satellite pixel to the source. After rotation, the effective wind direction is North-South for all satellite observations. Source: (Fioletov et al., 2015)**

1.4 The Chemical Transport Model GEOS-Chem

Information on air quality from observations provided by surface networks, field campaigns and space-based instruments are substantially enhanced by interpretation with a detailed comprehensive chemical transport model (CTM) (Chen et al., 2019). The GEOS-Chem CTM (https://geos-chem.seas.harvard.edu/; last accessed: 31 March 2022) is a global three-dimensional numerical model that simulates global and regional atmospheric composition. It was first described by Bey et al. (2001), and undergoes substantial and routine scientific and coding updates to keep pace with the state of the science (https://geos-chem.seas.harvard.edu/; last accessed: 31 March 2022). The model is driven with assimilated meteorology provided by the NASA Global Modeling and Assimilation Office (GMAO). Depending on the horizontal resolutions of input meteorology, the model is available at coarse resolution of 4° × 5° (latitude × longitude) and 2° × 2.5° for global simulations and at finer resolutions of 0.5° × 0.625° and 0.25° × 0.3125° for regional nested simulations. The model includes vertical layers from the surface to the top of atmosphere.

A wide selection of global and regional anthropogenic and natural emission inventories is available for use with GEOS-Chem. For example, the Multi-resolution Emission Inventory for China (MEIC) (http://www.meicmodel.org/; last accessed: 31 March 2022) provides monthly anthropogenic emissions for 2008-2017 in China. It includes emissions of SO_2, NO_x, CO, NMVOCs, NH_3, and primary particles from ~700 anthropogenic sources (Li et al., 2017a; Zheng et al., 2018). GEOS-Chem uses the Harmonized Emissions Component (HEMCO) emission package to calculate and grid user-selected inventories to the same horizontal resolution for input to GEOS-Chem (Keller et al., 2014; Lin et al., 2021). The model includes detailed coupled gas- and aerosol-phase chemistry to represent chemical formation and loss of air pollutants. Formation of secondary sulfate-nitrate-ammonium aerosols is computed with the ISORROPIA-II thermodynamic equilibrium model (Fountoukis and Nenes, 2007). SOA can be simulated by GEOS-Chem using two different schemes. The “simple scheme” simulates primary organic aerosols (POA) as non-volatile and takes a fixed-yield approach to SOA formation. The “complex scheme” simulates POA as semi-volatile and uses a more sophisticated volatility basis set approach for non-isoprene SOA, with an explicit aqueous uptake mechanism to model isoprene SOA (Pai et al., 2020). Physical loss processes include dry and wet deposition (Amos et al., 2012; Liu et al., 2001; Wang et al., 1998). GEOS-Chem is widely used to assess health impact of regional and global air pollution (Paulot and Jacob, 2014; Vohra et al., 2021b; Zhang et al., 2017a), estimate emissions of air pollutants from satellite observations (Cooper et al., 2022; Marais et al., 2021; Martin et al., 2003; Qu et al., 2022; Streets et al., 2013), and interpret factors contributing to air pollution (Li et al., 2019a; Li et al., 2020; Potts et al., 2021; Zhai et al., 2021). The model has been demonstrated to capture the trends in air pollution and reproduce observed total $PM_{2.5}$ mass measured by reference monitors (Dang and Liao, 2019; Weagle et al., 2018). Even so, the model still misses or misrepresents physical and chemical mechanisms leading to $PM_{2.5}$ formation, includes errors in meteorological parameters in the assimilated meteorology, and uses emission inventories that are subject to large uncertainties and biases and that are challenging to keep current (Bates et al., 2021; Li et al., 2018; Luo et al., 2019; Miao et al., 2020; Wang et al., 2014; Yu et al., 2018).

1.5 Research Gaps

Surface monitoring networks have been extensively used to assess compliance with air quality standards and effectiveness of air quality policies. The Chinese government judges whether cities have met their emission reduction targets solely based on observations of $PM_{2.5}$ from surface monitoring networks (MEE, 2018). This is not scientific, as factors such as meteorology can also affect the effectiveness of $PM_{2.5}$ abatement measures and, hence the observed air quality. The challenge of achieving the same level of $PM_{2.5}$ reduction varies from city to city. Incorrect assessment of the effectiveness of emissions controls hinders developing effective air quality policies. Effective air quality policies are also lacking in regions such as South and Southeast Asia, where there is limited understanding of surface air pollution due to sparse or missing surface monitoring networks. Satellite observations of air quality can be used to infer surface emissions. But the relationship between observations of air quality and actual emissions is complex. In addition to the importance to air quality policymaking, observations of air quality are also used to detect short-term changes in air quality and emissions due to interventions, for example the worldwide COVID-19 lockdowns. A common approach is to conduct a simple statistical analysis that compares air quality before and after the lockdowns began or during the lockdowns with the same periods in previous years (Fu et al., 2021; Sharma et al., 2020; Wang et al., 2020b). But year-to-year changes in meteorology moderates the link between emissions and pollutant concentrations and is not accounted for in such studies. Scientific knowledge of anthropogenic emissions and changes in observed air quality is essential for developing effective emission control measures to reduce pollution and protect human health. This thesis seeks to address the following science questions and research gaps.

1. What is the true efficacy of strict emission controls in addressing $PM_{2.5}$ pollution? The Chinese government imposed strict emission controls in 28 cities in and around the Beijing-Tianjin-Hebei region in northern China in autumn-winter 2017/2018. This approach is now adopted in

many regions in China, despite limited assessment of the relative contribution of emissions reductions and other factors like meteorology that is necessary for successful implementation of these control measures elsewhere (Chapter 2).

2. NO_x emissions in cities are important precursors to health-hazardous $PM_{2.5}$ and tropospheric O_3. Surface air quality monitoring is very limited in cities in South and Southeast Asia and estimates of NO_x emissions from bottom-up emission inventories are under validated. This is addressed by applying the wind rotation and EMG fit method to TROPOMI tropospheric NO_2 columns to estimate NO_x emissions in 10 large cities in South and Southeast Asia and to evaluate widely used bottom-up inventories used to inform policies and assess the environmental impacts of air pollution (Chapter 3).
3. Lessons learned about complex atmospheric processes affecting $PM_{2.5}$, NO_x and O_3 pollution using abrupt changes in anthropogenic emissions during COVID-19 lockdowns. In response to the outbreak of COVID-19, governments worldwide imposed strict restrictions on a range of human activities or lockdowns, which led to an abrupt reduction in anthropogenic emissions of air pollutants. The rapid and unprecedented lockdowns provide a unique opportunity to assess the impact of intervention on air quality at 11 global air pollution hotspots (Chapter 4).

1.6 References

Abera, A., Friberg, J., Isaxon, C., Jerrett, M., Malmqvist, E., Sjostrom, C., Taj, T., and Vargas, A. M.: Air Quality in Africa: Public Health Implications, in: Annual Review of Public Health, Vol 42, 2021, edited by: Fielding, J. E., Annual Review of Public Health, 193-210, 10.1146/annurev-publhealth-100119-113802, 2021.

Ainsworth, E. A., Yendrek, C. R., Sitch, S., Collins, W. J., and Emberson, L. D.: The Effects of Tropospheric Ozone on Net Primary Productivity and Implications for Climate Change, in: Annual Review of Plant Biology, Vol 63, edited by: Merchant, S. S., Annual Review of Plant Biology, 637-661, 10.1146/annurev-arplant-042110-103829, 2012.

Amos, H. M., Jacob, D. J., Holmes, C. D., Fisher, J. A., Wang, Q., Yantosca, R. M., Corbitt, E. S., Galarneau, E., Rutter, A. P., Gustin, M. S., Steffen, A., Schauer, J. J., Graydon, J. A., St Louis, V. L., Talbot, R. W., Edgerton, E. S., Zhang, Y., and Sunderland, E. M.: Gas-particle partitioning of atmospheric Hg(II) and its effect on global mercury deposition, Atmos. Chem. Phys., 12, 591-603, https://doi.org/10.5194/acp-12-591-2012, 2012.

Apte, J. S., Brauer, M., Cohen, A. J., Ezzati, M., and Pope, C. A.: Ambient PM2.5 Reduces Global and Regional Life Expectancy, Environmental Science & Technology Letters, 5, 546-551, 10.1021/acs.estlett.8b00360, 2018.

Apte, J. S., Marshall, J. D., Cohen, A. J., and Brauer, M.: Addressing Global Mortality from Ambient $PM_{2.5}$, Environmental Science & Technology, 49, 8057-8066, 10.1021/acs.est.5b01236, 2015.

AQEG: Evidential Value of Defra Air Quality Compliance Monitoring, Air Quality Expert Group, 2015.

Atkinson, R.: Atmospheric chemistry of VOCs and NOx, Atmospheric Environment, 34, 2063-2101, 10.1016/s1352-2310(99)00460-4, 2000.

Avnery, S., Mauzerall, D. L., Liu, J. F., and Horowitz, L. W.: Global crop yield reductions due to surface ozone exposure: 1. Year 2000 crop production losses and economic damage, Atmospheric Environment, 45, 2284-2296, 10.1016/j.atmosenv.2010.11.045, 2011.

Bakian, A. V., Huber, R. S., Coon, H., Gray, D., Wilson, P., McMahon, W. M., and Renshaw, P. F.: Acute Air Pollution Exposure and Risk of Suicide Completion, American Journal of Epidemiology, 181, 295-303, 10.1093/aje/kwu341, 2015.

Bates, K. H., Jacob, D. J., Li, K., Ivatt, P. D., Evans, M. J., Yan, Y., and Lin, J.: Development and evaluation of a new compact mechanism for aromatic oxidation in atmospheric models, Atmos. Chem. Phys., 21, 18351-18374, 10.5194/acp-21-18351-2021, 2021.

Beirle, S., Boersma, K. F., Platt, U., Lawrence, M. G., and Wagner, T.: Megacity Emissions and Lifetimes of Nitrogen Oxides Probed from Space, Science, 333, 1737-1739, 10.1126/science.1207824, 2011.

Belis, C. A., Karagulian, F., Larsen, B. R., and Hopke, P. K.: Critical review and meta-analysis of ambient particulate matter source apportionment using receptor models in Europe, Atmospheric Environment, 69, 94-108, 10.1016/j.atmosenv.2012.11.009, 2013.

Bertram, T. H., Heckel, A., Richter, A., Burrows, J. P., and Cohen, R. C.: Satellite measurements of daily variations in soil NOx emissions, Geophysical Research Letters, 32, 10.1029/2005gl024640, 2005.

Bey, I., Jacob, D. J., Yantosca, R. M., Logan, J. A., Field, B. D., Fiore, A. M., Li, Q. B., Liu, H. G. Y., Mickley, L. J., and Schultz, M. G.: Global modeling of tropospheric chemistry with assimilated meteorology: Model description and evaluation, Journal of Geophysical Research-Atmospheres, 106, 23073-23095, Doi 10.1029/2001jd000807, 2001.

Boersma, K. F., Eskes, H. J., Richter, A., De Smedt, I., Lorente, A., Beirle, S., van Geffen, J. H. G. M., Zara, M., Peters, E., Van Roozendael, M., Wagner, T., Maasakkers, J. D., van der A, R. J., Nightingale, J., De Rudder, A., Irie, H., Pinardi, G., Lambert, J. C., and Compernolle, S. C.: Improving algorithms and uncertainty estimates for satellite NO2 retrievals: results from the quality assurance for the essential climate variables (QA4ECV) project, Atmos. Meas. Tech., 11, 6651-6678, 10.5194/amt-11-6651-2018, 2018.

Boldo, E., Linares, C., Aragones, N., Lumbreras, J., Borge, R., de la Paz, D., Perez-Gomez, B., Fernandez-Navarro, P., Garcia-Perez, J., Pollan, M., Ramis, R., Moreno, T., Karanasiou, A., and Lopez-Abente, G.: Air quality modeling and mortality impact of fine particles reduction policies in Spain, Environmental Research, 128, 15-26, 10.1016/j.envres.2013.10.009, 2014.

Borge, R., Requia, W. J., Yague, C., Jhun, I., and Koutrakis, P.: Impact of weather changes on air quality and related mortality in Spain over a 25 year period 1993-2017, Environment International, 133, 10.1016/j.envint.2019.105272, 2019.

Braithwaite, I., Zhang, S., Kirkbride, J. B., Osborn, D. P. J., and Hayes, J. F.: Air Pollution (Particulate Matter) Exposure and Associations with Depression, Anxiety, Bipolar, Psychosis and Suicide Risk: A Systematic Review and Meta-Analysis, Environmental Health Perspectives, 127, 10.1289/ehp4595, 2019.

Burnett, R., Chen, H., Szyszkowicz, M., Fann, N., Hubbell, B., Pope, C. A., Apte, J. S., Brauer, M., Cohen, A., Weichenthal, S., Coggins, J., Di, Q., Brunekreef, B., Frostad, J., Lim, S. S., Kan, H. D., Walker, K. D., Thurston, G. D., Hayes, R. B., Lim, C. C., Turner, M. C., Jerrett, M., Krewski, D., Gapstur, S. M., Diver, W. R., Ostro, B., Goldberg, D., Crouse, D. L., Martin, R. V., Peters, P., Pinault, L., Tjepkema, M., Donkelaar, A., Villeneuve, P. J., Miller, A. B., Yin, P., Zhou, M. G., Wang, L. J., Janssen, N. A. H., Marra, M., Atkinson, R. W., Tsang, H., Thach, Q., Cannon, J. B., Allen, R. T., Hart, J. E., Laden, F., Cesaroni, G., Forastiere, F., Weinmayr, G., Jaensch, A., Nagel, G., Concin, H., and Spadaro, J. V.: Global estimates of mortality associated with long-term exposure to outdoor fine particulate matter, Proceedings of the National Academy of Sciences of the United States of America, 115, 9592-9597, 10.1073/pnas.1803222115, 2018.

Cao, H., Henze, D. K., Cady-Pereira, K., McDonald, B. C., Harkins, C., Sun, K., Bowman, K. W., Fu, T.-M., and Nawaz, M. O.: COVID-19 Lockdowns Afford the First Satellite-Based Confirmation That Vehicles Are an Under-recognized Source of Urban NH3 Pollution in Los Angeles, Environmental Science & Technology Letters, 9, 3-9, 10.1021/acs.estlett.1c00730, 2022.

Carn, S. A., Fioletov, V. E., McLinden, C. A., Li, C., and Krotkov, N. A.: A decade of global volcanic SO2 emissions measured from space, Scientific Reports, 7, 10.1038/srep44095, 2017.

Carvalho, H.: The air we breathe: differentials in global air quality monitoring, Lancet Respiratory Medicine, 4, 603-605, 10.1016/s2213-2600(16)30180-1, 2016.

Chai, T. F., Carmichael, G. R., Tang, Y. H., Sandu, A., Heckel, A., Richter, A., and Burrows, J. P.: Regional NOx emission inversion through a four-dimensional variational approach using SCIAMACHY tropospheric NO2 column observations, Atmospheric Environment, 43, 5046-5055, 10.1016/j.atmosenv.2009.06.052, 2009.

Chen, L., Gao, Y., Zhang, M. G., Fu, J. S., Zhu, J., Liao, H., Li, J. L., Huang, K., Ge, B. Z., Wang, X. M., Lam, Y. F., Lin, C. Y., Itahashi, S., Nagashima, T., Kajino, M., Yamaji, K., Wang, Z. F., and

Kurokawa, J.: MICS-Asia III: multi-model comparison and evaluation of aerosol over East Asia, Atmos. Chem. Phys., 19, 11911-11937, https://doi.org/10.5194/acp-19-11911-2019, 2019.

Chen, X., Wang, H., Lu, K., Li, C., Zhai, T., Tan, Z., Ma, X., Yang, X., Liu, Y., Chen, S., Dong, H., Li, X., Wu, Z., Hu, M., Zeng, L., and Zhang, Y.: Field Determination of Nitrate Formation Pathway in Winter Beijing, Environ Sci Technol, 54, 9243-9253, 10.1021/acs.est.0c00972, 2020.

Chu, B. W., Ma, Q. X., Liu, J., Ma, J. Z., Zhang, P., Chen, T. Z., Feng, Q. C., Wang, C. Y., Yang, N., Ma, H. N., Ma, J. J., Russell, A. G., and He, H.: Air Pollutant Correlations in China: Secondary Air Pollutant Responses to NOx and SO2 Control, Environmental Science & Technology Letters, 7, 695-700, 10.1021/acs.estlett.0c00403, 2020.

Cooper, M., Martin, R. V., Padmanabhan, A., and Henze, D. K.: Comparing mass balance and adjoint methods for inverse modeling of nitrogen dioxide columns for global nitrogen oxide emissions, Journal of Geophysical Research-Atmospheres, 122, 4718-4734, 10.1002/2016jd025985, 2017.

Cooper, M. J., Martin, R. V., Hammer, M. S., Levelt, P. F., Veefkind, P., Lamsal, L. N., Krotkov, N. A., Brook, J. R., and McLinden, C. A.: Global fine-scale changes in ambient NO2 during COVID-19 lockdowns, Nature, 601, 380-387, 10.1038/s41586-021-04229-0, 2022.

Crippa, M., Guizzardi, D., Muntean, M., Schaaf, E., Dentener, F., van Aardenne, J. A., Monni, S., Doering, U., Olivier, J. G. J., Pagliari, V., and Janssens-Maenhout, G.: Gridded emissions of air pollutants for the period 1970-2012 within EDGAR v4.3.2, Earth System Science Data, 10, 1987-2013, 10.5194/essd-10-1987-2018, 2018.

Dang, R. J. and Liao, H.: Severe winter haze days in the Beijing-Tianjin-Hebei region from 1985 to 2017 and the roles of anthropogenic emissions and meteorology, Atmospheric Chemistry and Physics, 19, 10801-10816, 10.5194/acp-19-10801-2019, 2019.

Dao, X., Lin, Y. C., Cao, F., Di, S. Y., Hong, Y. H., Xing, G. H., Li, J. J., Fu, P. Q., and Zhang, Y. L.: Introduction to the National Aerosol Chemical Composition Monitoring Network of China: Objectives, Current Status, and Outlook, Bulletin of the American Meteorological Society, 100, Es337-Es351, 10.1175/Bams-D-18-0325.1, 2019.

de Foy, B., Lu, Z. F., Streets, D. G., Lamsal, L. N., and Duncan, B. N.: Estimates of power plant NOx emissions and lifetimes from OMI NO2 satellite retrievals, Atmospheric Environment, 116, 1-11, 10.1016/j.atmosenv.2015.05.056, 2015.

Demerjian, K. L.: A review of national monitoring networks in North America, Atmospheric Environment, 34, 1861-1884, 10.1016/s1352-2310(99)00452-5, 2000.

Demetillo, M. A. G., Harkins, C., McDonald, B. C., Chodrow, P. S., Sun, K., and Pusede, S. E.: Space-Based Observational Constraints on NO2 Air Pollution Inequality From Diesel Traffic in Major US Cities, Geophysical Research Letters, 48, 10.1029/2021gl094333, 2021.

Ding, J., Dai, Q. L., Zhang, Y. F., Xu, J., Huangfu, Y. Q., and Feng, Y. C.: Air humidity affects secondary aerosol formation in different pathways, Science of the Total Environment, 759, 10.1016/j.scitotenv.2020.143540, 2021.

Ding, J., van der A, R. J., Mijling, B., Levelt, P. F., and Hao, N.: NO_x emission estimates during the 2014 Youth Olympic Games in Nanjing, Atmos. Chem. Phys., 15, 9399-9412, 10.5194/acp-15-9399-2015, 2015.

Dockery, D. W., Pope, C. A., Xu, X. P., Spengler, J. D., Ware, J. H., Fay, M. E., Ferris, B. G., and Speizer, F. E.: AN ASSOCIATION BETWEEN AIR-POLLUTION AND MORTALITY IN 6 UNITED-STATES CITIES, New England Journal of Medicine, 329, 1753-1759, 10.1056/nejm199312093292401, 1993.

Duncan, B. N., Prados, A. I., Lamsal, L. N., Liu, Y., Streets, D. G., Gupta, P., Hilsenrath, E., Kahn, R. A., Nielsen, J. E., Beyersdorf, A. J., Burton, S. P., Fiore, A. M., Fishman, J., Henze, D. K., Hostetler, C. A., Krotkov, N. A., Lee, P., Lin, M. Y., Pawson, S., Pfister, G., Pickering, K. E., Pierce, R. B., Yoshida, Y., and Ziemba, L. D.: Satellite data of atmospheric pollution for US air quality applications: Examples of applications, summary of data end-user resources, answers to FAQs, and common mistakes to avoid, Atmospheric Environment, 94, 647-662, 10.1016/j.atmosenv.2014.05.061, 2014.

Dunlea, E. J., Herndon, S. C., Nelson, D. D., Volkamer, R. M., San Martini, F., Sheehy, P. M., Zahniser, M. S., Shorter, J. H., Wormhoudt, J. C., Lamb, B. K., Allwine, E. J., Gaffney, J. S., Marley, N. A., Grutter, M., Marquez, C., Blanco, S., Cardenas, B., Retama, A., Villegas, C. R. R., Kolb, C. E., Molina, L. T., and Molina, M. J.: Evaluation of nitrogen dioxide chemiluminescence monitors in a polluted urban environment, Atmos. Chem. Phys., 7, 2691-2704, https://doi.org/10.5194/acp-7-2691-2007, 2007.

Farren, N. J., Davison, J., Rose, R. A., Wagner, R. L., and Carslaw, D. C.: Underestimated Ammonia Emissions from Road Vehicles, Environmental Science & Technology, 54, 15689-15697, 10.1021/acs.est.0c05839, 2020.

Feng, S. L., Gao, D., Liao, F., Zhou, F. R., and Wang, X. M.: The health effects of ambient PM2.5 and potential mechanisms, Ecotoxicology and Environmental Safety, 128, 67-74, 10.1016/j.ecoenv.2016.01.030, 2016.

Feng, Z. Z., De Marco, A., Anav, A., Gualtieri, M., Sicard, P., Tian, H. Q., Fornasier, F., Tao, F. L., Guo, A. H., and Paoletti, E.: Economic losses due to ozone impacts on human health, forest productivity and crop yield across China, Environment International, 131, 10.1016/j.envint.2019.104966, 2019.

Fioletov, V. E., McLinden, C. A., Krotkov, N., and Li, C.: Lifetimes and emissions of SO2 from point sources estimated from OMI, Geophysical Research Letters, 42, 1969-1976, 10.1002/2015gl063148, 2015.

Fiore, A. M., Naik, V., Spracklen, D. V., Steiner, A., Unger, N., Prather, M., Bergmann, D., Cameron-Smith, P. J., Cionni, I., Collins, W. J., Dalsoren, S., Eyring, V., Folberth, G. A., Ginoux, P., Horowitz, L. W., Josse, B., Lamarque, J. F., MacKenzie, I. A., Nagashima, T., O'Connor, F. M., Righi, M., Rumbold, S. T., Shindell, D. T., Skeie, R. B., Sudo, K., Szopa, S., Takemura, T., and Zeng, G.: Global air quality and climate, Chemical Society Reviews, 41, 6663-6683, 10.1039/c2cs35095e, 2012.

Fountoukis, C. and Nenes, A.: ISORROPIA II: a computationally efficient thermodynamic equilibrium model for K^+-Ca^{2+}-Mg^{2+}-NH_4^+-Na^+-SO_4^{2-}-NO_3^--Cl^--H_2O aerosols, Atmos. Chem. Phys., 7, 4639-4659, https://doi.org/10.5194/acp-7-4639-2007, 2007.

Fu, S., Guo, M. X., Fan, L. P., Deng, Q. Y., Han, D. M., Wei, Y., Luo, J. M., Qin, G. M., and Cheng, J. P.: Ozone pollution mitigation in guangxi (south China) driven by meteorology and anthropogenic emissions during the COVID-19 lockdown, Environmental Pollution, 272, 10.1016/j.envpol.2020.115927, 2021.

Fu, X., Wang, S. X., Xing, J., Zhang, X. Y., Wang, T., and Hao, J. M.: Increasing Ammonia Concentrations Reduce the Effectiveness of Particle Pollution Control Achieved via SO_2 and NO_X Emissions Reduction in East China, Environ. Sci. Tech. Lett., 4, 221-227, https://doi.org/10.1021/acs.estlett.7b00143, 2017.

Ginoux, P., Prospero, J. M., Torres, O., and Chin, M.: Long-term simulation of global dust distribution with the GOCART model: correlation with North Atlantic Oscillation, Environmental Modelling & Software, 19, 113-128, 10.1016/s1364-8152(03)00114-2, 2004.

Goldberg, D. L., Anenberg, S. C., Griffin, D., McLinden, C. A., Lu, Z., and Streets, D. G.: Disentangling the impact of the COVID-19 lockdowns on urban NO_2 from natural variability, Geophys Res Lett, 47, e2020GL089269, 10.1029/2020GL089269, 2020.

Goldberg, D. L., Anenberg, S. C., Lu, Z. F., Streets, D. G., Lamsal, L. N., McDuffie, E. E., and Smith, S. J.: Urban NOx emissions around the world declined faster than anticipated between 2005 and 2019, Environmental Research Letters, 16, 10.1088/1748-9326/ac2c34, 2021.

Goyal, P., Mishra, D., and Kumar, A.: Vehicular emission inventory of criteria pollutants in Delhi, Springerplus, 2, 10.1186/2193-1801-2-216, 2013.

Grennfelt, P., Engleryd, A., Forsius, M., Hov, O., Rodhe, H., and Cowling, E.: Acid rain and air pollution: 50 years of progress in environmental science and policy, Ambio, 49, 849-864, 10.1007/s13280-019-01244-4, 2020.

Griffin, D., Zhao, X. Y., McLinden, C. A., Boersma, F., Bourassa, A., Dammers, E., Degenstein, D., Eskes, H., Fehr, L., Fioletov, V., Hayden, K., Kharol, S. K., Li, S. M., Makar, P., Martin, R. V., Mihele, C., Mittermeier, R. L., Krotkov, N., Sneep, M., Lamsal, L. N., ter Linden, M., van Geffen, J., Veefkind, P., and Wolde, M.: High-Resolution Mapping of Nitrogen Dioxide With TROPOMI: First Results and Validation Over the Canadian Oil Sands, Geophysical Research Letters, 46, 1049-1060, 10.1029/2018gl081095, 2019.

Grivas, G., Cheristanidis, S., and Chaloulakou, A.: Elemental and organic carbon in the urban environment of Athens. Seasonal and diurnal variations and estimates of secondary organic carbon, Science of the Total Environment, 414, 535-545, 10.1016/j.scitotenv.2011.10.058, 2012.

Grulke, N. E. and Heath, R. L.: Ozone effects on plants in natural ecosystems, Plant Biology, 22, 12-37, 10.1111/plb.12971, 2020.

Guan, W. J., Zheng, X. Y., Chung, K. F., and Zhong, N. S.: Impact of air pollution on the burden of chronic respiratory diseases in China: time for urgent action, Lancet, 388, 1939-1951, 2016.

Guenther, A. B., Jiang, X., Heald, C. L., Sakulyanontvittaya, T., Duhl, T., Emmons, L. K., and Wang, X.: The Model of Emissions of Gases and Aerosols from Nature version 2.1 (MEGAN2.1): an extended and updated framework for modeling biogenic emissions, Geosci. Model Dev., 5, 1471-1492, 10.5194/gmd-5-1471-2012, 2012.

Guerreiro, C. B. B., Foltescu, V., and de Leeuw, F.: Air quality status and trends in Europe, Atmospheric Environment, 98, 376-384, 10.1016/j.atmosenv.2014.09.017, 2014.

Hanea, R. G., Velders, G. J. M., and Heemink, A.: Data assimilation of ground-level ozone in Europe with a Kalman filter and chemistry transport model, Journal of Geophysical Research-Atmospheres, 109, 10.1029/2003jd004283, 2004.

He, Y., Jiang, Y. X., Yang, Y., Xu, J. H., Zhang, Y., Wang, Q. M., Shen, H. P., Zhang, Y. P., Yan, D. H., Peng, Z. Q., Liu, C., Wang, W. D., Schikowski, T., Li, H. C., Yan, B. Z., Ji, J. S., Chen, A. M., van Donkelaar, A., Martin, R., Chen, R. J., Kan, H. D., Cai, J., and Ma, X.: Composition of fine particulate matter and risk of preterm birth: A nationwide birth cohort study in 336 Chinese cities, Journal of Hazardous Materials, 425, 10.1016/j.jhazmat.2021.127645, 2022.

Hou, P. and Wu, S. L.: Long-term Changes in Extreme Air Pollution Meteorology and the Implications for Air Quality, Scientific Reports, 6, 10.1038/srep23792, 2016.

Hu, L., Millet, D. B., Baasandorj, M., Griffis, T. J., Turner, P., Helmig, D., Curtis, A. J., and Hueber, J.: Isoprene emissions and impacts over an ecological transition region in the US Upper Midwest inferred from tall tower measurements, Journal of Geophysical Research-Atmospheres, 120, 3553-3571, 10.1002/2014jd022732, 2015.

Huang, R. J., Zhang, Y., Bozzetti, C., Ho, K. F., Cao, J. J., Han, Y., Daellenbach, K. R., Slowik, J. G., Platt, S. M., Canonaco, F., Zotter, P., Wolf, R., Pieber, S. M., Bruns, E. A., Crippa, M., Ciarelli, G., Piazzalunga, A., Schwikowski, M., Abbaszade, G., Schnelle-Kreis, J., Zimmermann, R., An, Z., Szidat, S., Baltensperger, U., El Haddad, I., and Prevot, A. S.: High secondary aerosol contribution to particulate pollution during haze events in China, Nature, 514, 218-222, https://doi.org/10.1038/nature13774, 2014.

Huang, X., Song, Y., Li, M. M., Li, J. F., Huo, Q., Cai, X. H., Zhu, T., Hu, M., and Zhang, H. S.: A high-resolution ammonia emission inventory in China, Global Biogeochem. Cy., 26, GB1030, https://doi.org/10.1029/2011gb004161, 2012.

Huber, D. E., Steiner, A. L., and Kort, E. A.: Daily Cropland Soil NOx Emissions Identified by TROPOMI and SMAP, Geophysical Research Letters, 47, 10.1029/2020gl089949, 2020.

Ialongo, I., Hakkarainen, J., Hyttinen, N., Jalkanen, J. P., Johansson, L., Boersma, K. F., Krotkov, N., and Tamminen, J.: Characterization of OMI tropospheric NO2 over the Baltic Sea region, Atmospheric Chemistry and Physics, 14, 7795-7805, 10.5194/acp-14-7795-2014, 2014.

Jaeglé, L., Quinn, P. K., Bates, T. S., Alexander, B., and Lin, J. T.: Global distribution of sea salt aerosols: new constraints from in situ and remote sensing observations, Atmospheric Chemistry and Physics, 11, 3137-3157, 10.5194/acp-11-3137-2011, 2011.

Jiang, Z., Jolleys, M. D., Fu, T. M., Palmer, P. I., Ma, Y., Tian, H., Li, J., and Yang, X.: Spatiotemporal and probability variations of surface PM2.5 over China between 2013 and 2019 and the associated changes in health risks: An integrative observation and model analysis, Sci Total Environ, 723, 137896, 10.1016/j.scitotenv.2020.137896, 2020.

Jones, A. M. and Harrison, R. M.: Interpretation of particulate elemental and organic carbon concentrations at rural, urban and kerbside sites, Atmospheric Environment, 39, 7114-7126, 10.1016/j.atmosenv.2005.08.017, 2005.

Joshi, R., Liu, D. T., Nemitz, E., Langford, B., Mullinger, N., Squires, F., Lee, J., Wu, Y. F., Pan, X. L., Fu, P. Q., Kotthaus, S., Grimmond, S., Zhang, Q., Wu, R. L., Wild, O., Flynn, M., Coe, H., and Allan, J.: Direct measurements of black carbon fluxes in central Beijing using the eddy covariance method, Atmos. Chem. Phys., 21, 147-162, https://doi.org/10.5194/acp-21-147-2021, 2021.

Ju, H., Kim, H. C., Kim, B. U., Ghim, Y. S., Shin, H. J., and Kim, S.: Long-term Trend Analysis of Key Criteria Air Pollutants over Air Quality Control Regions in South Korea using Observation Data and Air Quality Simulation, Journal of Korean Society for Atmospheric Environment, 34, 101-119, 10.5572/kosae.2018.34.1.101, 2018.

Judd, L. M., Al-Saadi, J. A., Szykman, J. J., Valin, L. C., Janz, S. J., Kowalewski, M. G., Eskes, H. J., Veefkind, J. P., Cede, A., Mueller, M., Gebetsberger, M., Swap, R., Pierce, R. B., Nowlan, C. R., Abad, G. G., Nehrir, A., and Williams, D.: Evaluating Sentinel-5P TROPOMI tropospheric NO2 column densities with airborne and Pandora spectrometers near New York City and Long Island Sound, Atmospheric Measurement Techniques, 13, 6113-6140, 10.5194/amt-13-6113-2020, 2020.

Keller, C. A., Long, M. S., Yantosca, R. M., Da Silva, A. M., Pawson, S., and Jacob, D. J.: HEMCO v1.0: a versatile, ESMF-compliant component for calculating emissions in atmospheric models, Geoscientific Model Development, 7, 1409-1417, 10.5194/gmd-7-1409-2014, 2014.

Khoder, M. I.: Atmospheric conversion of sulfur dioxide to particulate sulfate and nitrogen dioxide to particulate nitrate and gaseous nitric acid in an urban area, Chemosphere, 49, 675-684, 10.1016/s0045-6535(02)00391-0, 2002.

Kim, K. H., Kabir, E., and Kabir, S.: A review on the human health impact of airborne particulate matter, Environment International, 74, 136-143, 10.1016/j.envint.2014.10.005, 2015.

Koplitz, S. N., Mickley, L. J., Marlier, M. E., Buonocore, J. J., Kim, P. S., Liu, T. J., Sulprizio, M. P., DeFries, R. S., Jacob, D. J., Schwartz, J., Pongsiri, M., and Myers, S. S.: Public health impacts of the severe haze in Equatorial Asia in September-October 2015: demonstration of a new framework for informing fire management strategies to reduce downwind smoke exposure, Environmental Research Letters, 11, 10.1088/1748-9326/11/9/094023, 2016.

Lamsal, L. N., Martin, R. V., van Donkelaar, A., Steinbacher, M., Celarier, E. A., Bucsela, E., Dunlea, E. J., and Pinto, J. P.: Ground-level nitrogen dioxide concentrations inferred from the satellite-borne Ozone Monitoring Instrument, Journal of Geophysical Research-Atmospheres, 113, 10.1029/2007jd009235, 2008.

Lange, K., Richter, A., and Burrows, J. P.: Variability of nitrogen oxide emission fluxes and lifetimes estimated from Sentinel-5P TROPOMI observations, Atmos. Chem. Phys., 22, 2745-2767, 10.5194/acp-22-2745-2022, 2022.

Lanzante, J. R.: Resistant, robust and non-parametric techniques for the analysis of climate data: Theory and examples, including applications to historical radiosonde station data, International Journal of Climatology, 16, 1197-1226, 10.1002/(sici)1097-0088(199611)16:11<1197::Aid-joc89>3.0.Co;2-l, 1996.

Laughner, J. L. and Cohen, R. C.: Direct observation of changing NO_x lifetime in North American cities, Science, 366, 723-727, 10.1126/science.aax6832, 2019.

Le, T., Wang, Y., Liu, L., Yang, J., Yung, Y. L., Li, G., and Seinfeld, J. H.: Unexpected air pollution with marked emission reductions during the COVID-19 outbreak in China, Science, 369, 702-706, https://doi.org/10.1126/science.abb7431, 2020.

Lelieveld, J., Evans, J. S., Fnais, M., Giannadaki, D., and Pozzer, A.: The contribution of outdoor air pollution sources to premature mortality on a global scale, Nature, 525, 367-+, 10.1038/nature15371, 2015.

Lelieveld, J., Klingmuller, K., Pozzer, A., Poschl, U., Fnais, M., Daiber, A., and Munzel, T.: Cardiovascular disease burden from ambient air pollution in Europe reassessed using novel hazard ratio functions, European Heart Journal, 40, 1590-1596, 10.1093/eurheartj/ehz135, 2019.

Lelieveld, J., Pozzer, A., Poschl, U., Fnais, M., Haines, A., and Munzel, T.: Loss of life expectancy from air pollution compared to other risk factors: a worldwide perspective, Cardiovascular Research, 116, 1910-1917, 10.1093/cvr/cvaa025, 2020.

Levelt, P. F., Joiner, J., Tamminen, J., Veefkind, J. P., Bhartia, P. K., Zweers, D. C. S., Duncan, B. N., Streets, D. G., Eskes, H., van der A, R., McLinden, C., Fioletov, V., Carn, S., de Laat, J., DeLand, M., Marchenko, S., McPeters, R., Ziemke, J., Fu, D. J., Liu, X., Pickering, K., Apituley, A., Abad, G. G., Arola, A., Boersma, F., Miller, C. C., Chance, K., de Graaf, M., Hakkarainen, J., Hassinen, S., Ialongo, I., Kleipool, Q., Krotkov, N., Li, C., Lamsal, L., Newman, P., Nowlan, C., Suleiman, R., Tilstra, L. G., Torres, O., Wang, H. Q., and Wargan, K.: The Ozone Monitoring Instrument: overview of 14 years in space, Atmospheric Chemistry and Physics, 18, 5699-5745, 10.5194/acp-18-5699-2018, 2018.

Li, K., Jacob, D. J., Liao, H., Shen, L., Zhang, Q., and Bates, K. H.: Anthropogenic drivers of 2013-2017 trends in summer surface ozone in China, Proc. Natl. Acad. Sci. USA, 116, 422-427, https://doi.org/10.1073/pnas.1812168116, 2019a.

Li, M., Klimont, Z., Zhang, Q., Martin, R. V., Zheng, B., Heyes, C., Cofala, J., Zhang, Y. X., and He, K. B.: Comparison and evaluation of anthropogenic emissions of SO2 and NOx over China, Atmospheric Chemistry and Physics, 18, 3433-3456, 10.5194/acp-18-3433-2018, 2018.

Li, M., Liu, H., Geng, G. N., Hong, C. P., Liu, F., Song, Y., Tong, D., Zheng, B., Cui, H. Y., Man, H. Y., Zhang, Q., and He, K. B.: Anthropogenic emission inventories in China: a review, Natl. Sci. Rev., 4, 834-866, https://doi.org/10.1093/nsr/nwx150, 2017a.

Li, M., McDonald, B. C., McKeen, S. A., Eskes, H., Levelt, P., Francoeur, C., Harkins, C., He, J., Barth, M., Henze, D. K., Bela, M. M., Trainer, M., Gouw, J. A., and Frost, G. J.: Assessment of Updated Fuel-Based Emissions Inventories Over the Contiguous United States Using TROPOMI NO2 Retrievals, Journal of Geophysical Research-Atmospheres, 126, 10.1029/2021jd035484, 2021a.

Li, M., Zhang, Q., Kurokawa, J., Woo, J. H., He, K. B., Lu, Z. F., Ohara, T., Song, Y., Streets, D. G., Carmichael, G. R., Cheng, Y. F., Hong, C. P., Huo, H., Jiang, X. J., Kang, S. C., Liu, F., Su, H., and Zheng, B.: MIX: a mosaic Asian anthropogenic emission inventory under the international collaboration framework of the MICS-Asia and HTAP, Atmospheric Chemistry and Physics, 17, 935-963, 10.5194/acp-17-935-2017, 2017b.

Li, M., Zhang, Q., Zheng, B., Tong, D., Lei, Y., Liu, F., Hong, C. P., Kang, S. C., Yan, L., Zhang, Y. X., Bo, Y., Su, H., Cheng, Y. F., and He, K. B.: Persistent growth of anthropogenic non-methane volatile organic compound (NMVOC) emissions in China during 1990-2017: drivers, speciation and ozone formation potential, Atmos. Chem. Phys., 19, 8897-8913, https://doi.org/10.5194/acp-19-8897-2019, 2019b.

Li, Q., Zheng, D. N., Wang, Y. Y., Li, R., Wu, H. P., Xu, S. X., Kang, Y. F., Cao, Y. X., Chen, X. J., Zhu, Y. M., Xu, S. G., Chen, Z. J., Liu, P., and Qiao, J.: Association between exposure to airborne particulate matter less than 2.5 μm and human fecundity in China, Environment International, 146, 10.1016/j.envint.2020.106231, 2021b.

Li, R., Wang, Z., Cui, L., Fu, H., Zhang, L., Kong, L., Chen, W., and Chen, J.: Air pollution characteristics in China during 2015-2016: Spatiotemporal variations and key meteorological factors, Sci Total Environ, 648, 902-915, 10.1016/j.scitotenv.2018.08.181, 2019c.

Li, S. X., Chen, L. L., Huang, G., Lin, J. T., Yan, Y. Y., Ni, R. J., Huo, Y. F., Wang, J. X., Liu, M. Y., Weng, H. J., Wang, Y. H., and Wang, Z. F.: Retrieval of surface $PM_{2.5}$ mass concentrations over North China using visibility measurements and GEOS-Chem simulations, Atmospheric Environment, 222, https://doi.org/10.1016/j.atmosenv.2019.117121, 2020.

Liang, F., Liu, F., Huang, K., Yang, X., Li, J., Xiao, Q., Chen, J., Liu, X., Cao, J., Shen, C., Yu, L., Lu, F., Wu, X., Wu, X., Li, Y., Hu, D., Huang, J., Liu, Y., Lu, X., and Gu, D.: Long-Term Exposure to Fine Particulate Matter and Cardiovascular Disease in China, J Am Coll Cardiol, 75, 707-717, 10.1016/j.jacc.2019.12.031, 2020.

Lin, G. X., Penner, J. E., Flanner, M. G., Sillman, S., Xu, L., and Zhou, C.: Radiative forcing of organic aerosol in the atmosphere and on snow: Effects of SOA and brown carbon, Journal of Geophysical Research-Atmospheres, 119, 7453-7476, 10.1002/2013jd021186, 2014.

Lin, H., Jacob, D. J., Lundgren, E. W., Sulprizio, M. P., Keller, C. A., Fritz, T. M., Eastham, S. D., Emmons, L. K., Campbell, P. C., Baker, B., Saylor, R. D., and Montuoro, R.: Harmonized Emissions Component (HEMCO) 3.0 as a versatile emissions component for atmospheric models: application in the GEOS-Chem, NASA GEOS, WRF-GC, CESM2, NOAA GEFS-Aerosol, and NOAA UFS models, Geosci. Model Dev., 14, 5487-5506, 10.5194/gmd-14-5487-2021, 2021.

Lin, J., Zhou, C., Chen, L., Huang, G., Lamarque, J. F., Nie, J., Yang, J., Hu, K., Liu, P., Wang, J., Xia, Y., Yang, Y., and Hu, Y.: Sulfur emissions from consumption by developed and developing countries produce comparable climate impacts, Nature Geoscience, 10.1038/s41561-022-00898-2, 2022.

Liu, F., Page, A., Strode, S. A., Yoshida, Y., Choi, S., Zheng, B., Lamsal, L. N., Li, C., Krotkov, N. A., Eskes, H., van der A, R., Veefkind, P., Levelt, P. F., Hauser, O. P., and Joiner, J.: Abrupt decline in tropospheric nitrogen dioxide over China after the outbreak of COVID-19, Science Advances, 6, 10.1126/sciadv.abc2992, 2020.

Liu, F., Zhang, Q., Ronald, J. V., Zheng, B., Tong, D., Yan, L., Zheng, Y. X., and He, K. B.: Recent reduction in NOx emissions over China: synthesis of satellite observations and emission inventories, Environmental Research Letters, 11, 10.1088/1748-9326/11/11/114002, 2016.

Liu, H., Jacob, D. J., Bey, I., and Yantosca, R. M.: Constraints from ^{210}Pb and ^{7}Be on wet deposition and transport in a global three-dimensional chemical tracer model driven by assimilated meteorological fields, J. Geophys. Res. Atmos., 106, 12109-12128, https://doi.org/10.1029/2000jd900839, 2001.

Liu, J. C. and Peng, R. D.: Health effect of mixtures of ozone, nitrogen dioxide, and fine particulates in 85 US counties, Air Quality Atmosphere and Health, 11, 311-324, 10.1007/s11869-017-0544-2, 2018.

Liu, T. Y., Wang, X. M., Wang, B. G., Ding, X., Deng, W., Lu, S. J., and Zhang, Y. L.: Emission factor of ammonia (NH3) from on-road vehicles in China: tunnel tests in urban Guangzhou, Environmental Research Letters, 9, 10.1088/1748-9326/9/6/064027, 2014.

Lu, Z., Streets, D. G., de Foy, B., Lamsal, L. N., Duncan, B. N., and Xing, J.: Emissions of nitrogen oxides from US urban areas: estimation from Ozone Monitoring Instrument retrievals for 2005-2014, Atmospheric Chemistry and Physics, 15, 10367-10383, 10.5194/acp-15-10367-2015, 2015.

Luo, G., Yu, F. Q., and Schwab, J.: Revised treatment of wet scavenging processes dramatically improves GEOS-Chem 12.0.0 simulations of surface nitric acid, nitrate, and ammonium over the United States, Geosci. Model Dev., 12, 3439-3447, https://doi.org/10.5194/gmd-12-3439-2019, 2019.

Marais, E. A., Jacob, D. J., Kurosu, T. P., Chance, K., Murphy, J. G., Reeves, C., Mills, G., Casadio, S., Millet, D. B., Barkley, M. P., Paulot, F., and Mao, J.: Isoprene emissions in Africa inferred from OMI observations of formaldehyde columns, Atmospheric Chemistry and Physics, 12, 6219-6235, 10.5194/acp-12-6219-2012, 2012.

Marais, E. A., Pandey, A. K., Van Damme, M., Clarisse, L., Coheur, P. F., Shephard, M. W., Cady-Pereira, K. E., Misselbrook, T., Zhu, L., Luo, G., and Yu, F. Q.: UK Ammonia Emissions Estimated With Satellite Observations and GEOS-Chem, Journal of Geophysical Research-Atmospheres, 126, 10.1029/2021jd035237, 2021.

Martin, R. V.: Satellite remote sensing of surface air quality, Atmospheric Environment, 42, 7823-7843, 10.1016/j.atmosenv.2008.07.018, 2008.

Martin, R. V., Jacob, D. J., Chance, K., Kurosu, T. P., Palmer, P. I., and Evans, M. J.: Global inventory of nitrogen oxide emissions constrained by space-based observations of NO_2 columns, Journal of Geophysical Research-Atmospheres, 108, Artn 4537

10.1029/2003jd003453, 2003.

Matus, K., Nam, K. M., Selin, N. E., Lamsal, L. N., Reilly, J. M., and Paltsev, S.: Health damages from air pollution in China, Global Environmental Change-Human and Policy Dimensions, 22, 55-66, 10.1016/j.gloenvcha.2011.08.006, 2012.

McDonald, B. C., de Gouw, J. A., Gilman, J. B., Jathar, S. H., Akherati, A., Cappa, C. D., Jimenez, J. L., Lee-Taylor, J., Hayes, P. L., McKeen, S. A., Cui, Y. Y., Kim, S. W., Gentner, D. R., Isaacman-VanWertz, G., Goldstein, A. H., Harley, R. A., Frost, G. J., Roberts, J. M., Ryerson, T. B., and Trainer, M.: Volatile chemical products emerging as largest petrochemical source of urban organic emissions, Science, 359, 760-764, 10.1126/science.aaq0524, 2018.

McDuffie, E. E., Martin, R. V., Spadaro, J. V., Burnett, R., Smith, S. J., O'Rourke, P., Hammer, M. S., van Donkelaar, A., Bindle, L., Shah, V., Jaegle, L., Luo, G., Yu, F. Q., Adeniran, J. A., Lin, J. T., and Brauer, M.: Source sector and fuel contributions to ambient PM2.5 and attributable mortality across multiple spatial scales, Nature Communications, 12, 10.1038/s41467-021-23853-y, 2021.

McDuffie, E. E., Smith, S. J., O'Rourke, P., Tibrewal, K., Venkataraman, C., Marais, E. A., Zheng, B., Crippa, M., Brauer, M., and Martin, R. V.: A global anthropogenic emission inventory of atmospheric pollutants from sector- and fuel-specific sources (1970-2017): an application of the Community Emissions Data System (CEDS), Earth System Science Data, 12, 3413-3442, 10.5194/essd-12-3413-2020, 2020.

McNeill, V. F.: Aqueous Organic Chemistry in the Atmosphere: Sources and Chemical Processing of Organic Aerosols, Environmental Science & Technology, 49, 1237-1244, 10.1021/es5043707, 2015.

Ministry of Ecology and Environment, the People's Republic of China (MEE).Letter on notifying the completion of air quality targets in the Beijing-Tianjin-Hebei air pollution transmission channel cities in autumn and winter (in Chinese), available at: http://www.mee.gov.cn/gkml/sthjbgw/stbgth/201805/t20180503_435855.htm (last access: 04 March 2021), 2018.

Meng, X., Liu, C., Chen, R. J., Sera, F., Vicedo-Cabrera, A. M., Milojevic, A., Guo, Y. M., Tong, S. L., Coelho, M., Saldiva, P. H. N., Lavigne, E., Correa, P. M., Ortega, N. V., Garcia, S. O., Kysely, J., Urban, A., Orru, H., Maasikmets, M., Jaakkola, J. J. K., Ryti, N., Huber, V., Schneider, A., Katsouyanni, K., Analitis, A., Hashizume, M., Honda, Y., Ng, C. F. S., Nunes, B., Teixeira, J. P., Holobaca, I. H., Fratianni, S., Kim, H., Tobias, A., Iniguez, C., Forsberg, B., Astrom, C., Ragettli, M. S., Guo, Y. L. L., Pan, S. C., Li, S. S., Bell, M. L., Zanobetti, A., Schwartz, J., Wu, T. C., Gasparrini, A., and Kan, H. D.: Short term associations of ambient nitrogen dioxide with daily total, cardiovascular, and respiratory mortality: multilocation analysis in 398 cities, Bmj-British Medical Journal, 372, 10.1136/bmj.n534, 2021.

Miao, R. Q., Chen, Q., Zheng, Y., Cheng, X., Sun, Y. L., Palmer, P. I., Shrivastava, M., Guo, J. P., Zhang, Q., Liu, Y. H., Tan, Z. F., Ma, X. F., Chen, S. Y., Zeng, L. M., Lu, K. D., and Zhang, Y. H.: Model bias in simulating major chemical components of $PM_{2.5}$ in China, Atmos. Chem. Phys., 20, 12265-12284, https://doi.org/10.5194/acp-20-12265-2020, 2020.

Miao, Y., Liu, S., and Huang, S.: Synoptic pattern and planetary boundary layer structure associated with aerosol pollution during winter in Beijing, China, Sci Total Environ, 682, 464-474, 10.1016/j.scitotenv.2019.05.199, 2019.

Miyazaki, K., Eskes, H. J., and Sudo, K.: Global NOx emission estimates derived from an assimilation of OMI tropospheric NO2 columns, Atmospheric Chemistry and Physics, 12, 2263-2288, 10.5194/acp-12-2263-2012, 2012.

Mo, Z. W., Cui, R., Yuan, B., Cai, H. H., McDonald, B. C., Li, M., Zheng, J. Y., and Shao, M.: A mass-balance-based emission inventory of non-methane volatile organic compounds (NMVOCs) for solvent use in China, Atmospheric Chemistry and Physics, 21, 13655-13666, 10.5194/acp-21-13655-2021, 2021.

Monks, P. S.: Gas-phase radical chemistry in the troposphere, Chemical Society Reviews, 34, 376-395, 10.1039/b307982c, 2005.

Murray, C. J. L. and Aravkin, A. Y. and Zheng, P. and Abbafati, C. and Abbas, K. M. and Abbasi-Kangevari, M. and Abd-Allah, F. and Abdelalim, A. and Abdollahi, M. and Abdollahpour, I. and Abegaz, K. H. and Abolhassani, H. and Aboyans, V. and Abreu, L. G. and Abrigo, M. R. M. and Abualhasan, A. and Abu-Raddad, L. J. and Abushouk, A. I. and Adabi, M. and Adekanmbi, V. and Adeoye, A. M. and Adetokunboh, O. O. and Adham, D. and Advani, S. M. and Agarwal, G. and Aghamir, S. M. K. and Agrawal, A. and Ahmad, T. and Ahmadi, K. and Ahmadi, M. and Ahmadieh, H. and Ahmed, M. B. and Akalu, T. Y. and Akinyemi, R. O. and Akinyemiju, T. and Akombi, B. and

Akunna, C. J. and Alahdab, F. and Al-Aly, Z. and Alam, K. and Alam, S. and Alam, T. and Alanezi, F. M. and Alanzi, T. M. and Alemu, B. W. and Alhabib, K. F. and Ali, M. and Ali, S. and Alicandro, G. and Alinia, C. and Alipour, V. and Alizade, H. and Aljunid, S. M. and Alla, F. and Allebeck, P. and Almasi-Hashiani, A. and Al-Mekhlafi, H. M. and Alonso, J. and Altirkawi, K. A. and Amini-Rarani, M. and Amiri, F. and Amugsi, D. A. and Ancuceanu, R. and Anderlini, D. and Anderson, J. A. and Andrei, C. L. and Andrei, T. and Angus, C. and Anjomshoa, M. and Ansari, F. and Ansari-Moghaddam, A. and Antonazzo, I. C. and Antonio, C. A. T. and Antony, C. M. and Antriyandarti, E. and Anvari, D. and Anwer, R. and Appiah, S. C. Y. and Arabloo, J. and Arab-Zozani, M. and Ariani, F. and Armoon, B. and Arnlov, J. and Arzani, A. and Asadi-Aliabadi, M. and Asadi-Pooya, A. A. and Ashbaugh, C. and Assmus, M. and Atafar, Z. and Atnafu, D. D. and Atout, M. M. W. and Ausloos, F. and Ausloos, M. and Quintanilla, B. P. A. and Ayano, G. and Ayanore, M. A. and Azari, S. and Azarian, G. and Azene, Z. N. and Badawi, A. and Badiye, A. D. and Bahrami, M. A. and Bakhshaei, M. H. and Bakhtiari, A. and Bakkannavar, S. M. and Baldasseroni, A. and Ball, K. and Ballew, S. H. and Balzi, D. and Banach, M. and Banerjee, S. K. and Bante, A. B. and Baraki, A. G. and Barker-Collo, S. L. and Barnighausen, T. W. and Barrero, L. H. and Barthelemy, C. M. and Barua, L. and Basu, S. and Baune, B. T. and Bayati, M. and Becker, J. S. and Bedi, N. and Beghi, E. and Bejot, Y. and Bell, M. L. and Bennitt, F. B. and Bensenor, I. M. and Berhe, K. and Berman, A. E. and Bhagavathula, A. S. and Bhageerathy, R. and Bhala, N. and Bhandari, D. and Bhattacharyya, K. and Bhutta, Z. A. and Bijani, A. and Bikbov, B. and Bin Sayeed, M. S. and Biondi, A. and Birihane, B. M. and Bisignano, C. and Biswas, R. K. and Bitew, H. and Bohlouli, S. and Bohluli, M. and Boon-Dooley, A. S. and Borges, G. and Borzi, A. M. and Borzouei, S. and Bosetti, C. and Boufous, S. and Braithwaite, D. and Breitborde, N. J. K. and Breitner, S. and Brenner, H. and Briant, P. S. and Briko, A. N. and Briko, N. I. and Britton, G. B. and Bryazka, D. and Bumgarner, B. R. and Burkart, K. and Burnett, R. T. and Nagaraja, S. B. and Butt, Z. A. and dos Santos, F. L. C. and Cahill, L. E. and Camera, L. A. and Campos-Nonato, I. R. and Cardenas, R. and Carreras, G. and Carrero, J. J. and Carvalho, F. and Castaldelli-Maia, J. M. and Castaneda-Orjuela, C. A. and Castelpietra, G. and Castro, F. and Causey, K. and Cederroth, C. R. and Cercy, K. M. and Cerin, E. and Chandan, J. S. and Chang, K. L. and Charlson, F. J. and Chattu, V. K. and Chaturvedi, S. and Cherbuin, N. and Chimed-Ochir, O. and Cho, D. Y. and Choi, J. Y. J. and Christensen, H. and Chu, D. T. and Chung, M. T. and Chung, S. C. and Cicuttini, F. M. and Ciobanu, L. G. and Cirillo, M. and Classen, T. K. D. and Cohen, A. J. and Compton, K. and Cooper, O. R. and Costa, V. M. and Cousin, E. and Cowden, R. G. and Cross, D. H. and Cruz, J. A. and Dahlawi, S. M. A. and Damasceno, A. A. M. and Damiani, G. and Dandona, L. and Dandona, R. and Dangel, W. J. and Danielsson, A. K. and Dargan, P. I. and Darwesh, A. M. and Daryani, A. and Das, J. K. and Das Gupta, R. and Das Neves, J. and Davila-Cervantes, C. A. and Davitoiu, D. V. and De Leo, D. and Degenhardt, L. and DeLang, M. and Dellavalle, R. P. and Demeke, F. M. and Demoz, G. T. and Demsie, D. G. and Denova-Gutierrez, E. and Dervenis, N. and Dhungana, G. P. and Dianatinasab, M. and da Silva, D. D. and Diaz, D. and Forooshani, Z. S. D. and Djalalinia, S. and Do, H. T. and Dokova, K. and Dorostkar, F. and Doshmangir, L. and Driscoll, T. R. and Duncan, B. B. and Duraes, A. R. and Eagan, A. W. and Edvardsson, D. and El Nahas, N. and El Sayed, I. and El Tantawi, M. and Elbarazi, I. and Elgendy, I. Y. and El-Jaafary, S. I. and Elyazar, I. R. F. and Emmons-Bell, S. and Erskine, H. E. and Eskandarieh, S. and Esmaeilnejad, S. and Esteghamati, A. and Estep, K. and Etemadi, A. and Etisso, A. E. and Fanzo, J. and Farahmand, M. and Fareed, M. and Faridnia, R. and Farioli, A. and Faro, A. and Faruque, M. and Farzadfar, F. and Fattahi, N. and Fazlzadeh, M. and Feigin, V. L. and Feldman, R. and Fereshtehnejad, S. M. and Fernandes, E. and Ferrara, G. and Ferrari, A. J. and Ferreira, M. L. and Filip, I. and Fischer, F. and Fisher, J. L. and Flor, L. S. and Foigt, N. A. and Folayan, M. O. and Fomenkov, A. A. and Force, L. M. and Foroutan, M. and Franklin, R. C. and Freitas, M. and Fu, W. J. and Fukumoto, T. and Furtado, J. M. and Gad, M. M. and Gakidou, E. and Gallus, S. and Garcia-Basteiro, A. L. and Gardner, W. M. and Geberemariyam, B. S. and Gebreslassie, A. and Geremew, A. and Hayoon, A. G. and Gething, P. W. and Ghadimi, M. and Ghadiri, K. and Ghaffarifar, F. and Ghafourifard, M. and Ghamari, F. and Ghashghaee, A. and Ghiasvand, H. and Ghith, N. and Gholamian, A. and Ghosh, R. and Gill, P. S. and Ginindza, T. G. and Giussani, G. and Gnedovskaya, E. V. and Goharinezhad, S. and Gopalani, S. V. and Gorini, G. and Goudarzi, H. and Goulart, A. C. and Greaves, F. and Grivna, M. and Grosso, G. and Gubari, M. I. M. and Gugnani, H. C. and Guimaraes, R. A. and Guled, R. A. and Guo, G. R. and Guo, Y. M. and Gupta, R. and Gupta, T. and Haddock, B. and Hafezi-Nejad, N. and Hafiz, A. and Haj-

Mirzaian, A. and Haj-Mirzaian, A. and Hall, B. J. and Halvaei, I. and Hamadeh, R. R. and Hamidi, S. and Hammer, M. S. and Hankey, G. J. and Haririan, H. and Haro, J. M. and Hasaballah, A. I. and Hasan, M. M. and Hasanpoor, E. and Hashi, A. and Hassanipour, S. and Hassankhani, H. and Havmoeller, R. J. and Hay, S. I. and Hayat, K. and Heidari, G. and Heidari-Soureshjani, R. and Henrikson, H. J. and Herbert, M. E. and Herteliu, C. and Heydarpour, F. and Hird, T. R. and Hoek, H. W. and Holla, R. and Hoogar, P. and Hosgood, H. D. and Hossain, N. and Hosseini, M. and Hosseinzadeh, M. and Hostiuc, M. and Hostiuc, S. and Househ, M. and Hsairi, M. and Hsieh, V. C. R. and Hu, G. Q. and Hu, K. J. and Huda, T. M. and Humayun, A. and Huynh, C. K. and Hwang, B. F. and Iannucci, V. C. and Ibitoye, S. E. and Ikeda, N. and Ikuta, K. S. and Ilesanmi, O. S. and Ilic, I. M. and Ilic, M. D. and Inbaraj, L. R. and Ippolito, H. and Iqbal, U. and Irvani, S. S. N. and Irvine, C. M. S. and Islam, M. M. and Islam, S. M. S. and Iso, H. and Ivers, R. Q. and Iwu, C. C. D. and Iwu, C. J. and Iyamu, I. O. and Jaafari, J. and Jacobsen, K. H. and Jafari, H. and Jafarinia, M. and Jahani, M. A. and Jakovljevic, M. and Jalilian, F. and James, S. L. and Janjani, H. and Javaheri, T. and Javidnia, J. and Jeemon, P. and Jenabi, E. and Jha, R. P. and Jha, V. and Ji, J. S. and Johansson, L. and John, O. and John-Akinola, Y. O. and Johnson, C. O. and Jonas, J. B. and Joukar, F. and Jozwiak, J. J. and Jurisson, M. and Kabir, A. and Kabir, Z. and Kalani, H. and Kalani, R. and Kalankesh, L. R. and Kalhor, R. and Kanchan, T. and Kapoor, N. and Matin, B. K. and Karch, A. and Karim, M. A. and Kassa, G. M. and Katikireddi, S. V. and Kayode, G. A. and Karyani, A. K. and Keiyoro, P. N. and Keller, C. and Kemmer, L. and Kendrick, P. J. and Khalid, N. and Khammarnia, M. and Khan, E. A. and Khan, M. and Khatab, K. and Khater, M. M. and Khatib, M. N. and Khayamzadeh, M. and Khazaei, S. and Kieling, C. and Kim, Y. J. and Kimokoti, R. W. and Kisa, A. and Kisa, S. and Kivimaki, M. and Knibbs, L. D. and Knudsen, A. K. S. and Kocarnik, J. M. and Kochhar, S. and Kopec, J. A. and Korshunov, V. A. and Koul, P. A. and Koyanagi, A. and Kraemer, M. U. G. and Krishan, K. and Krohn, K. J. and Kromhout, H. and Defo, B. K. and Kumar, G. A. and Kumar, V. and Kurmi, O. P. and Kusuma, D. and La Vecchia, C. and Ben, L. and Lal, D. K. and Lalloo, R. and Lallukka, T. and Lami, F. H. and Landires, I. and Lang, J. J. and Langan, S. M. and Larsson, A. O. and Lasrado, S. and Lauriola, P. and Lazarus, J. V. and Lee, P. H. and Lee, S. W. H. and LeGrand, K. E. and Leigh, J. and Leonardi, M. and Lescinsky, H. and Leung, J. and Levi, M. and Li, S. S. and Lim, L. L. and Linn, S. and Liu, S. W. and Liu, S. M. and Liu, Y. and Lo, J. and Lopez, A. D. and Lopez, J. C. F. and Lopukhov, P. D. and Lorkowski, S. and Lotufo, P. A. and Lu, A. and Lugo, A. and Maddison, E. R. and Mahasha, P. W. and Mahdavi, M. M. and Mahmoudi, M. and Majeed, A. and Maleki, A. and Maleki, S. and Malekzadeh, R. and Malta, D. C. and Mamun, A. A. and Manda, A. L. and Manguerra, H. and Mansour-Ghanaei, F. and Mansouri, B. and Mansournia, M. A. and Herrera, A. M. M. and Maravilla, J. C. and Marks, A. and Martin, R. V. and Martini, S. and Martins-Melo, F. R. and Masaka, A. and Masoumi, S. Z. and Mathur, M. R. and Matsushita, K. and Maulik, P. K. and McAlinden, C. and McGrath, J. J. and McKee, M. and Mehndiratta, M. M. and Mehri, F. and Mehta, K. M. and Memish, Z. A. and Mendoza, W. and Menezes, R. G. and Mengesha, E. W. and Mereke, A. and Mereta, S. T. and Meretoja, A. and Meretoja, T. J. and Mestrovic, T. and Miazgowski, B. and Miazgowski, T. and Michalek, I. M. and Miller, T. R. and Mills, E. J. and Mini, G. K. and Miri, M. and Mirica, A. and Mirrakhimov, E. M. and Mirzaei, H. and Mirzaei, M. and Mirzaei, R. and Mirzaei-Alavijeh, M. and Misganaw, A. T. and Mithra, P. and Moazen, B. and Mohammad, D. K. and Mohammad, Y. and Mezerji, N. M. G. and Mohammadian-Hafshejani, A. and Mohammadifard, N. and Mohammadpourhodki, R. and Mohammed, A. S. and Mohammed, H. and Mohammed, J. A. and Mohammed, S. and Mokdad, A. H. and Molokhia, M. and Monasta, L. and Mooney, M. D. and Moradi, G. and Moradi, M. and Moradi-Lakeh, M. and Moradzadeh, R. and Moraga, P. and Morawska, L. and Morgado-da-Costa, J. and Morrison, S. D. and Mosapour, A. and Mosser, J. F. and Mouodi, S. and Mousavi, S. M. and Khaneghah, A. M. and Mueller, U. O. and Mukhopadhyay, S. and Mullany, E. C. and Musa, K. I. and Muthupandian, S. and Nabhan, A. F. and Naderi, M. and Nagarajan, A. J. and Nagel, G. and Naghavi, M. and Naghshtabrizi, B. and Naimzada, M. D. and Najafi, F. and Nangia, V. and Nansseu, J. R. and Naserbakht, M. and Nayak, V. C. and Negoi, I. and Ngunjiri, J. W. and Nguyen, C. T. and Nguyen, H. L. T. and Nguyen, M. and Nigatu, Y. T. and Nikbakhsh, R. and Nixon, M. R. and Nnaji, C. A. and Nomura, S. and Norrving, B. and Noubiap, J. J. and Nowak, C. and Nunez-Samudio, V. and Oiu, A. O. and Oancea, B. and Odell, C. M. and Ogbo, F. A. and Oh, I. H. and Okunga, E. W. and Oladnabi, M. and Olagunju, A. T. and Olusanya, B. O. and Olusanya, J. O. and Omer, M. O. and Ong, K. L. and Onwujekwe, O. E. and Orpana, H. M. and Ortiz, A. and Osarenotor, O. and Osei, F. B.

and Ostroff, S. M. and Otstavnov, N. and Otstavnov, S. S. and Overland, S. and Owolabi, M. O. and Section, M. P. A. and Padubidri, J. R. and Palladino, R. and Panda-Jonas, S. and Pandey, A. and Parry, C. D. H. and Pasovic, M. and Pasupula, D. K. and Patel, S. K. and Pathak, M. and Patten, S. B. and Patton, G. C. and Toroudi, H. P. and Peden, A. E. and Pennini, A. and Pepito, V. C. F. and Peprah, E. K. and Pereira, D. M. and Pesudovs, K. and Pham, H. Q. and Phillips, M. R. and Piccinelli, C. and Pilz, T. M. and Piradov, M. A. and Pirsaheb, M. and Plass, D. and Polinder, S. and Polkinghorne, K. R. and Pond, C. D. and Postma, M. J. and Pourjafar, H. and Pourmalek, F. and Poznanska, A. and Prada, S. I. and Prakash, V. and Pribadi, D. R. A. and Pupillo, E. and Quazi Syed, Z. and Rabiee, M. and Rabiee, N. and Radfar, A. and Rafiee, A. and Raggi, A. and Rahman, M. A. and Rajabpour-Sanati, A. and Rajati, F. and Rakovac, I. and Ram, P. and Ramezanzadeh, K. and Ranabhat, C. L. and Rao, P. C. and Rao, S. J. and Rashedi, V. and Rathi, P. and Rawaf, D. L. and Rawaf, S. and Rawal, L. and Rawassizadeh, R. and Rawat, R. and Razo, C. and Boston, S. and Reiner, R. C. and Reitsma, M. B. and Remuzzi, G. and Renjith, V. and Renzaho, A. M. N. and Resnikoff, S. and Rezaei, N. and Rezaei, N. and Rezapour, A. and Rhinehart, P. A. and Riahi, S. M. and Ribeiro, D. C. and Ribeiro, D. and Rickard, J. and Rivera, J. A. and Roberts, N. L. S. and Rodriguez-Ramirez, S. and Roever, L. and Ronfani, L. and Room, R. and Roshandel, G. and Roth, G. A. and Rothenbacher, D. and Rubagotti, E. and Rwegerera, G. M. and Sabour, S. and Sachdev, P. S. and Saddik, B. and Sadeghi, E. and Sadeghi, M. and Saeedi, R. and Moghaddam, S. S. and Safari, Y. and Safi, S. and Safiri, S. and Sagar, R. and Sahebkar, A. and Sajadi, S. M. and Salam, N. and Salamati, P. and Salem, H. and Salem, M. R. and Salimzadeh, H. and Salman, O. M. and Salomon, J. A. and Samad, Z. and Kafil, H. S. and Sambala, E. Z. and Samy, A. M. and Sanabria, J. and Sanchez-Pimienta, T. G. and Santomauro, D. F. and Santos, I. S. and Santos, J. V. and Santric-Milicevic, M. M. and Saraswathy, S. Y. I. and Sarmiento-Suarez, R. and Sarrafzadegan, N. and Sartorius, B. and Sarveazad, A. and Sathian, B. and Sathish, T. and Sattin, D. and Saxena, S. and Schaeffer, L. E. and Schiavolin, S. and Schlaich, M. P. and Schmidt, M. I. and Schutte, A. E. and Schwebel, D. C. and Schwendicke, F. and Senbeta, A. M. and Senthilkumaran, S. and Sepanlou, S. G. and Serdar, B. and Serre, M. L. and Shadid, J. and Shafaat, O. and Shahabi, S. and Shaheen, A. A. and Shaikh, M. A. and Shalash, A. S. and Shams-Beyranvand, M. and Shamsizadeh, M. and Sharafi, K. and Sheikh, A. and Sheikhtaheri, A. and Shibuya, K. and Shield, K. D. and Shigematsu, M. and Shin, J. I. and Shin, M. J. and Shiri, R. and Shirkoohi, R. and Shuval, K. and Siabani, S. and Sierpinski, R. and Sigfusdottir, I. D. and Sigurvinsdottir, R. and Silva, J. P. and Simpson, K. E. and Singh, J. A. and Singh, P. and Skiadaresi, E. and Skou, S. T. and Skryabin, V. Y. and Smith, E. U. R. and Soheili, A. and Soltani, S. and Soofi, M. and Sorensen, R. J. D. and Soriano, J. B. and Sorrie, M. B. and Soshnikov, S. and Soyiri, I. N. and Spencer, C. N. and Spotin, A. and Sreeramareddy, C. T. and Srinivasan, V. and Stanaway, J. D. and Stein, C. and Stein, D. J. and Steiner, C. and Stockfelt, L. and Stokes, M. A. and Straif, K. and Stubbs, J. L. and Sufiyan, M. B. and Suleria, H. A. R. and Abdulkader, R. S. and Sulo, G. and Sultan, I. and Szumowski, L. and Tabares-Seisdedos, R. and Tabb, K. M. and Tabuchi, T. and Taherkhani, A. and Tajdini, M. and Takahashi, K. and Takala, J. S. and Tamiru, A. T. and Taveira, N. and Tehrani-Banihashemi, A. and Temsah, M. H. and Tesema, G. A. and Tessema, Z. T. and Thurston, G. D. and Titova, M. V. and Tohidinik, H. R. and Tonelli, M. and Topor-Madry, R. and Topouzis, F. and Torre, A. E. and Touvier, M. and Tovani-Palone, M. R. and Tran, B. X. and Travillian, R. and Tsatsakis, A. and Car, L. T. and Tyrovolas, S. and Uddin, R. and Umeokonkwo, C. D. and Unnikrishnan, B. and Upadhyay, E. and Vacante, M. and Valdez, P. R. and Van Donkelaar, A. and Vasankari, T. J. and Vasseghian, Y. and Veisani, Y. and Venketasubramanian, N. and Violante, F. S. and Vlassov, V. and Vollset, S. E. and Vos, T. and Vukovic, R. and Waheed, Y. and Wallin, M. T. and Wang, Y. F. and Wang, Y. P. and Watson, A. and Wei, J. K. and Wei, M. Y. W. and Weintraub, R. G. and Weiss, J. and Werdecker, A. and Westerman, R. and Whisnant, J. L. and Whiteford, H. A. and Wiens, K. E. and Wolfe, C. D. A. and Wozniak, S. S. and Wu, A. M. and Wu, J. J. and Hanson, S. W. and Xu, G. L. and Xu, R. and Yadgir, S. and Jabbari, S. H. Y. and Yamagishi, K. and Yaminfirooz, M. and Yano, Y. and Yaya, S. and Yazdi-Feyzabadi, V. and Yeheyis, T. Y. and Yilgwan, C. S. and Yilma, M. T. and Yip, P. and Yonemoto, N. and Younis, M. Z. and Younker, T. P. and Yousefi, B. and Yousefi, Z. and Yousefinezhadi, T. and Yousuf, A. Y. and Yu, C. H. and Yusefzadeh, H. and Moghadam, T. Z. and Zamani, M. and Zamanian, M. and Zandian, H. and Zastrozhin, M. S. and Zhang, Y. Q. and Zhang, Z. J. and Zhao, J. T. and Zhao, X. J. G. and Zhao, Y. X. and Zhou, M. G. and Ziapour, A. and Zimsen, S. R. M. and Brauer, M. and Afshin, A. and Lim, S. S. and Factors, G. B. D. R.: Global burden of 87 risk factors in 204 countries and territories, 1990-2019: a systematic analysis for the Global Burden of Disease Study 2019, Lancet, 396, 1223-1249, 10.1016/s0140-6736(20)30752-2, 2020.

Newbury, J. B., Arseneault, L., Beevers, S., Kitwiroon, N., Roberts, S., Pariante, C. M., Kelly, F. J., and Fisher, H. L.: Association of Air Pollution Exposure With Psychotic Experiences During Adolescence, Jama Psychiatry, 76, 614-623, 10.1001/jamapsychiatry.2019.0056, 2019.

Oftedal, B., Walker, S. E., Gram, F., McInnes, H., and Nafstad, P.: Modelling long-term averages of local ambient air pollution in Oslo, Norway: evaluation of nitrogen dioxide, PM10 and PM2.5, International Journal of Environment and Pollution, 36, 110-126, 10.1504/ijep.2009.021820, 2009.

Pai, S. J., Heald, C. L., Pierce, J. R., Farina, S. C., Marais, E. A., Jimenez, J. L., Campuzano-Jost, P., Nault, B. A., Middlebrook, A. M., Coe, H., Shilling, J. E., Bahreini, R., Dingle, J. H., and Vu, K.: An evaluation of global organic aerosol schemes using airborne observations, Atmospheric Chemistry and Physics, 20, 2637-2665, 10.5194/acp-20-2637-2020, 2020.

Pan, Y., Tian, S., Zhao, Y., Zhang, L., Zhu, X., Gao, J., Huang, W., Zhou, Y., Song, Y., Zhang, Q., and Wang, Y.: Identifying Ammonia Hotspots in China Using a National Observation Network, Environ. Sci. Technol., 52, 3926-3934, https://doi.org/10.1021/acs.est.7b05235, 2018.

Paulot, F. and Jacob, D. J.: Hidden Cost of U.S. Agricultural Exports: Particulate Matter from Ammonia Emissions, Environmental Science & Technology, 48, 903-908, 10.1021/es4034793, 2014.

Paulot, F., Jacob, D. J., Pinder, R. W., Bash, J. O., Travis, K., and Henze, D. K.: Ammonia emissions in the United States, European Union, and China derived by high-resolution inversion of ammonium wet deposition data: Interpretation with a new agricultural emissions inventory (MASAGE_NH3), Journal of Geophysical Research-Atmospheres, 119, 4343-4364, 10.1002/2013jd021130, 2014.

Pazmiño, A., Beekmann, M., Goutail, F., Ionov, D., Bazureau, A., Nunes-Pinharanda, M., Hauchecorne, A., and Godin-Beekmann, S.: Impact of the COVID-19 pandemic related to lockdown measures on tropospheric NO2 columns over Île-de-France, Atmos. Chem. Phys., 21, 18303-18317, 10.5194/acp-21-18303-2021, 2021.

Peng, J. F., Hu, M., Guo, S., Du, Z. F., Zheng, J., Shang, D. J., Zamora, M. L., Zeng, L. M., Shao, M., Wu, Y. S., Zheng, J., Wang, Y., Glen, C. R., Collins, D. R., Molina, M. J., and Zhang, R. Y.: Markedly enhanced absorption and direct radiative forcing of black carbon under polluted urban environments, Proceedings of the National Academy of Sciences of the United States of America, 113, 4266-4271, 10.1073/pnas.1602310113, 2016.

Perrino, C., Catrambone, M., Di Bucchianico, A. D. M., and Allegrini, I.: Gaseous ammonia in the urban area of Rome, Italy and its relationship with traffic emissions, Atmospheric Environment, 36, 5385-5394, 10.1016/s1352-2310(02)00469-7, 2002.

Philip, S., Martin, R. V., Snider, G., Weagle, C. L., van Donkelaar, A., Brauer, M., Henze, D. K., Klimont, Z., Venkataraman, C., Guttikunda, S. K., and Zhang, Q.: Anthropogenic fugitive, combustion and industrial dust is a significant, underrepresented fine particulate matter source in global atmospheric models, Environmental Research Letters, 12, 10.1088/1748-9326/aa65a4, 2017.

Philip, S., Martin, R. V., van Donkelaar, A., Lo, J. W. H., Wang, Y. X., Chen, D., Zhang, L., Kasibhatla, P. S., Wang, S. W., Zhang, Q., Lu, Z. F., Streets, D. G., Bittman, S., and Macdonald, D. J.: Global Chemical Composition of Ambient Fine Particulate Matter for Exposure Assessment, Environmental Science & Technology, 48, 13060-13068, 10.1021/es502965b, 2014.

Platt, U. and Stutz, J.: Differential Optical Absorption Spectroscopy, Springer, https://doi.org/10.1007/978-3-540-75776-4, 2008.

Pope, C. A., Ezzati, M., and Dockery, D. W.: Fine-Particulate Air Pollution and Life Expectancy in the United States, New England Journal of Medicine, 360, 376-386, 10.1056/NEJMsa0805646, 2009.

Potts, D. A., Marais, E. A., Boesch, H., Pope, R. J., Lee, J., Drysdale, W., Chipperfield, M. P., Kerridge, B., Siddans, R., Moore, D. P., and Remedios, J.: Diagnosing air quality changes in the UK during the COVID-19 lockdown using TROPOMI and GEOS-Chem, Environmental Research Letters, 16, 10.1088/1748-9326/abde5d, 2021.

Power, M. C., Weisskopf, M. G., Alexeeff, S. E., Coull, B. A., Spiro, A., and Schwartz, J.: Traffic-Related Air Pollution and Cognitive Function in a Cohort of Older Men, Environmental Health Perspectives, 119, 682-687, 10.1289/ehp.1002767, 2011.

Qian, Z. M., Liang, S. W., Yang, S. P., Trevathan, E., Huang, Z., Yang, R., Wang, J., Hu, K., Zhang, Y. M., Vaughn, M., Shen, L. J., Liu, W. J., Li, P., Ward, P., Yang, L., Zhang, W., Chen, W., Dong, G. H., Zheng, T. Z., Xu, S. Q., and Zhang, B.: Ambient air pollution and preterm birth: A prospective birth cohort study in Wuhan, China, International Journal of Hygiene and Environmental Health, 219, 195-203, 10.1016/j.ijheh.2015.11.003, 2016.

Qu, Z., Henze, D. K., Worden, H. M., Jiang, Z., Gaubert, B., Theys, N., and Wang, W.: Sector-Based Top-Down Estimates of NOx, SO2, and CO Emissions in East Asia, Geophysical Research Letters, 49, 10.1029/2021gl096009, 2022.

Qu, Z., Jacob, D. J., Silvern, R. F., Shah, V., Campbell, P. C., Valin, L. C., and Murray, L. T.: US COVID-19 Shutdown Demonstrates Importance of Background NO2 in Inferring NOx Emissions From Satellite NO2 Observations, Geophysical Research Letters, 48, 10.1029/2021gl092783, 2021.

Rajagopalan, S., Al-Kindi, S. G., and Brook, R. D.: Air Pollution and Cardiovascular Disease JACC State-of-the-Art Review, Journal of the American College of Cardiology, 72, 2054-2070, 10.1016/j.jacc.2018.07.099, 2018.

Reed, C., Evans, M. J., Di Carlo, P., Lee, J. D., and Carpenter, L. J.: Interferences in photolytic NO_2 measurements: explanation for an apparent missing oxidant?, Atmos. Chem. Phys., 16, 4707-4724, https://doi.org/10.5194/acp-16-4707-2016, 2016.

Schenkeveld, V. M. E., Jaross, G., Marchenko, S., Haffner, D., Kleipool, Q. L., Rozemeijer, N. C., Veefkind, J. P., and Levelt, P. F.: In-flight performance of the Ozone Monitoring Instrument, Atmospheric Measurement Techniques, 10, 1957-1986, 10.5194/amt-10-1957-2017, 2017.

Schumann, U. and Huntrieser, H.: The global lightning-induced nitrogen oxides source, Atmos. Chem. Phys., 7, 3823-3907, 10.5194/acp-7-3823-2007, 2007.

Shah, V., Jacob, D. J., Li, K., Silvern, R. F., Zhai, S. X., Liu, M. Y., Lin, J. T., and Zhang, Q.: Effect of changing NO_x lifetime on the seasonality and long-term trends of satellite-observed tropospheric NO_2 columns over China, Atmos. Chem. Phys., 20, 1483-1495, https://doi.org/10.5194/acp-20-1483-2020, 2020.

Sharma, S., Zhang, M. Y., Anshika, Gao, J. S., Zhang, H. L., and Kota, S. H.: Effect of restricted emissions during COVID-19 on air quality in India, Science of the Total Environment, 728, 10.1016/j.scitotenv.2020.138878, 2020.

Shen, F., Zhang, L., Jiang, L., Tang, M., Gai, X., Chen, M., and Ge, X.: Temporal variations of six ambient criteria air pollutants from 2015 to 2018, their spatial distributions, health risks and relationships with socioeconomic factors during 2018 in China, Environ Int, 137, 105556, 10.1016/j.envint.2020.105556, 2020.

Shen, L., Jacob, D. J., Zhu, L., Zhang, Q., Zheng, B., Sulprizio, M. P., Li, K., De Smedt, I., Abad, G. G., Cao, H. S., Fu, T. M., and Liao, H.: The 2005-2016 Trends of Formaldehyde Columns Over China Observed by Satellites: Increasing Anthropogenic Emissions of Volatile Organic Compounds and Decreasing Agricultural Fire Emissions, Geophysical Research Letters, 46, 4468-4475, 10.1029/2019gl082172, 2019.

Shi, Z. B., Vu, T., Kotthaus, S., Harrison, R. M., Grimmond, S., Yue, S., Zhu, T., Lee, J., Han, Y., Demuzere, M., Dunmore, R. E., Ren, L. J., Liu, D., Wang, Y. L., Wild, O., Allan, J., Acton, W. J., Barlow, J., Barratt, B., Beddows, D., Bloss, W. J., Calzolai, G., Carruthers, D., Carslaw, D. C., Chan, Q., Chatzidiakou, L., Chen, Y., Crilley, L., Coe, H., Dai, T., Doherty, R., Duan, F., Fu, P., Ge, B., Ge, M., Guan, D., Hamilton, J. F., He, K., Heal, M., Heard, D., Hewitt, C. N., Hollaway, M., Hu, M., Ji, D., Jiang, X. J., Jones, R., Kalberer, M., Kelly, F. J., Kramer, L., Langford, B., Lin, C., Lewis, A. C., Li, J., Li, W., Liu, H., Liu, J. F., Loh, M., Lu, K. D., Lucarelli, F., Mann, G., McFiggans, G., Miller, M. R., Mills, G., Monk, P., Nemitz, E., O'Connor, F., Ouyang, B., Palmer, P. I., Percival, C., Popoola, O., Reeves, C., Rickard, A. R., Shao, L. Y., Shi, G. Y., Spracklen, D., Stevenson, D., Sun, Y., Sun, Z. W., Tao, S., Tong, S. R., Wang, Q. Q., Wang, W. H., Wang, X. M., Wang, X. J., Wang, Z. F., Wei, L. F., Whalley, L., Wu, X. F., Wu, Z. J., Xie, P. H., Yang, F. M., Zhang, Q., Zhang, Y. L., Zhang, Y. H., and Zheng, M.: Introduction to the special issue "In-depth study of air pollution sources and processes within Beijing and its surrounding region (APHH-Beijing)", Atmos. Chem. Phys., 19, 7519-7546, https://doi.org/10.5194/acp-19-7519-2019, 2019.

Sicard, P., Agathokleous, E., De Marco, A., Paoletti, E., and Calatayud, V.: Urban population exposure to air pollution in Europe over the last decades, Environmental Sciences Europe, 33, 10.1186/s12302-020-00450-2, 2021.

Sillman, S.: The relation between ozone, NO_x and hydrocarbons in urban and polluted rural environments, Atmospheric Environment, 33, 1821-1845, Doi 10.1016/S1352-2310(98)00345-8, 1999.

Silvern, R. F., Jacob, D. J., Mickley, L. J., Sulprizio, M. P., Travis, K. R., Marais, E. A., Cohen, R. C., Laughner, J. L., Choi, S., Joiner, J., and Lamsal, L. N.: Using satellite observations of tropospheric NO2 columns to infer long-term trends in US NOx emissions: the importance of accounting for the free tropospheric NO2 background, Atmospheric Chemistry and Physics, 19, 8863-8878, 10.5194/acp-19-8863-2019, 2019.

Solberg, S., Walker, S. E., Schneider, P., and Guerreiro, C.: Quantifying the Impact of the Covid-19 Lockdown Measures on Nitrogen Dioxide Levels throughout Europe, Atmosphere, 12, 10.3390/atmos12020131, 2021.

Song, C. B., He, J. J., Wu, L., Jin, T. S., Chen, X., Li, R. P., Ren, P. P., Zhang, L., and Mao, H. J.: Health burden attributable to ambient PM2.5 in China, Environmental Pollution, 223, 575-586, 10.1016/j.envpol.2017.01.060, 2017a.

Song, C. B., Wu, L., Xie, Y. C., He, J. J., Chen, X., Wang, T., Lin, Y. C., Jin, T. S., Wang, A. X., Liu, Y., Dai, Q. L., Liu, B. S., Wang, Y. N., and Mao, H. J.: Air pollution in China: Status and spatiotemporal variations, Environmental Pollution, 227, 334-347, 10.1016/j.envpol.2017.04.075, 2017b.

Souri, A. H., Nowlan, C. R., Wolfe, G. M., Lamsal, L. N., Miller, C. E. C., Abad, G. G., Janz, S. J., Fried, A., Blake, D. R., Weinheimer, A. J., Diskin, G. S., Liu, X., and Chance, K.: Revisiting the effectiveness of HCHO/NO2 ratios for inferring ozone sensitivity to its precursors using high resolution airborne remote sensing observations in a high ozone episode during the KORUS-AQ campaign, Atmospheric Environment, 224, 10.1016/j.atmosenv.2020.117341, 2020.

Stevenson, D. S., Young, P. J., Naik, V., Lamarque, J. F., Shindell, D. T., Voulgarakis, A., Skeie, R. B., Dalsoren, S. B., Myhre, G., Berntsen, T. K., Folberth, G. A., Rumbold, S. T., Collins, W. J., MacKenzie, I. A., Doherty, R. M., Zeng, G., van Noije, T. P. C., Strunk, A., Bergmann, D., Cameron-Smith, P., Plummer, D. A., Strode, S. A., Horowitz, L., Lee, Y. H., Szopa, S., Sudo, K., Nagashima, T., Josse, B., Cionni, I., Righi, M., Eyring, V., Conley, A., Bowman, K. W., Wild, O., and Archibald, A.: Tropospheric ozone changes, radiative forcing and attribution to emissions in the Atmospheric Chemistry and Climate Model Intercomparison Project (ACCMIP), Atmospheric Chemistry and Physics, 13, 3063-3085, 10.5194/acp-13-3063-2013, 2013.

Streets, D. G., Canty, T., Carmichael, G. R., de Foy, B., Dickerson, R. R., Duncan, B. N., Edwards, D. P., Haynes, J. A., Henze, D. K., Houyoux, M. R., Jacobi, D. J., Krotkov, N. A., Lamsal, L. N., Liu, Y., Lu, Z. F., Martini, R. V., Pfister, G. G., Pinder, R. W., Salawitch, R. J., and Wechti, K. J.: Emissions estimation from satellite retrievals: A review of current capability, Atmospheric Environment, 77, 1011-1042, 10.1016/j.atmosenv.2013.05.051, 2013.

Su, T. N., Li, Z. Q., Li, C. C., Li, J., Han, W. C., Shen, C. Y., Tan, W. S., Wei, J., and Guo, J. P.: The significant impact of aerosol vertical structure on lower atmosphere stability and its critical role in aerosol-planetary boundary layer (PBL) interactions, Atmospheric Chemistry and Physics, 20, 3713-3724, 10.5194/acp-20-3713-2020, 2020.

Sun, J., Wu, F. K., Hu, B., Tang, G. Q., Zhang, J. K., and Wang, Y. S.: VOC characteristics, emissions and contributions to SOA formation during hazy episodes, Atmospheric Environment, 141, 560-570, 10.1016/j.atmosenv.2016.06.060, 2016.

Sun, K., Li, L. B., Jagini, S., and Li, D.: A satellite-data-driven framework to rapidly quantify air-basin-scale NOx emissions and its application to the Po Valley during the COVID-19 pandemic, Atmospheric Chemistry and Physics, 21, 13311-13332, 10.5194/acp-21-13311-2021, 2021.

Sun, K., Zhu, L., Cady-Pereira, K., Miller, C. C., Chance, K., Clarisse, L., Coheur, P. F., Abad, G. G., Huang, G. Y., Liu, X., Van Damme, M., Yang, K., and Zondlo, M.: A physics-based approach to oversample multi-satellite, multispecies observations to a common grid, Atmospheric Measurement Techniques, 11, 6679-6701, 10.5194/amt-11-6679-2018, 2018.

Tack, F., Merlaud, A., Iordache, M. D., Pinardi, G., Dimitropoulou, E., Eskes, H., Bomans, B., Veefkind, P., and Van Roozendael, M.: Assessment of the TROPOMI tropospheric NO2 product based on airborne APEX observations, Atmospheric Measurement Techniques, 14, 615-646, 10.5194/amt-14-615-2021, 2021.

Tai, A. P. K. and Martin, M. V.: Impacts of ozone air pollution and temperature extremes on crop yields: Spatial variability, adaptation and implications for future food security, Atmospheric Environment, 169, 11-21, 10.1016/j.atmosenv.2017.09.002, 2017.

Tang, G. Q., Chao, N., Wang, Y. S., and Chen, J. S.: Vehicular emissions in China in 2006 and 2010, Journal of Environmental Sciences, 48, 179-192, 10.1016/j.jes.2016.01.031, 2016.

Tie, X. X., Zhang, R. Y., Brasseur, G., and Lei, W. F.: Global NOx production by lightning, Journal of Atmospheric Chemistry, 43, 61-74, 10.1023/a:1016145719608, 2002.

Turner, M. C., Krewski, D., Pope, C. A., Chen, Y., Gapstur, S. M., and Thun, M. J.: Long-term Ambient Fine Particulate Matter Air Pollution and Lung Cancer in a Large Cohort of Never-Smokers, American Journal of Respiratory and Critical Care Medicine, 184, 1374-1381, 10.1164/rccm.201106-1011OC, 2011.

Valin, L. C., Russell, A. R., and Cohen, R. C.: Variations of OH radical in an urban plume inferred from NO2 column measurements, Geophysical Research Letters, 40, 1856-1860, 10.1002/grl.50267, 2013.

van der Werf, G. R., Randerson, J. T., Giglio, L., van Leeuwen, T. T., Chen, Y., Rogers, B. M., Mu, M., van Marle, M. J. E., Morton, D. C., Collatz, G. J., Yokelson, R. J., and Kasibhatla, P. S.: Global fire emissions estimates during 1997–2016, Earth Syst. Sci. Data, 9, 697-720, 10.5194/essd-9-697-2017, 2017.

van Geffen, J., Boersma, K. F., Eskesl, H., Sneep, M., ter Linden, M., Zara, M., and Veefkind, J. P.: S5P TROPOMI NO2 slant column retrieval: method, stability, uncertainties and comparisons with OMI, Atmospheric Measurement Techniques, 13, 1315-1335, 10.5194/amt-13-1315-2020, 2020.

van Geffen, J., Eskes, H. J., Boersma, K. F., and Veefkind, J. P.: TROPOMI ATBD of the total and tropospheric NO_2 data products (issue 2.2.0), Royal Netherlands Meteorological Institute (KNMI), De Bilt, the Netherlands, 2021.

Veefkind, J. P., Aben, I., McMullan, K., Forster, H., de Vries, J., Otter, G., Claas, J., Eskes, H. J., de Haan, J. F., Kleipool, Q., van Weele, M., Hasekamp, O., Hoogeveen, R., Landgraf, J., Snel, R., Tol, P., Ingmann, P., Voors, R., Kruizinga, B., Vink, R., Visser, H., and Levelt, P. F.: TROPOMI on the ESA Sentinel-5 Precursor: A GMES mission for global observations of the atmospheric composition for climate, air quality and ozone layer applications, Remote Sensing of Environment, 120, 70-83, 10.1016/j.rse.2011.09.027, 2012.

Verhoelst, T., Compernolle, S., Pinardi, G., Lambert, J. C., Eskes, H. J., Eichmann, K. U., Fjaeraa, A. M., Granville, J., Niemeijer, S., Cede, A., Tiefengraber, M., Hendrick, F., Pazmino, A., Bais, A., Bazureau, A., Boersma, K. F., Bognar, K., Dehn, A., Donner, S., Elokhov, A., Gebetsberger, M., Goutail, F., de la Mora, M. G., Gruzdev, A., Gratsea, M., Hansen, G. H., Irie, H., Jepsen, N., Kanaya, Y., Karagkiozidis, D., Kivi, R., Kreher, K., Levelt, P. F., Liu, C., Muller, M., Comas, M. N., Piters, A. J. M., Pommereau, J. P., Portafaix, T., Prados-Roman, C., Puentedura, O., Querel, R., Remmers, J., Richter, A., Rimmer, J., Cardenas, C. R., de Miguel, L. S., Sinyakov, V. P., Stremme, W., Strong, K., Van Roozendael, M., Veefkind, J. P., Wagner, T., Wittrock, F., Gonzalez, M. Y., and Zehner, C.: Ground-based validation of the Copernicus Sentinel-5P TROPOMI NO2 measurements with the NDACC ZSL-DOAS, MAX-DOAS and Pandonia global networks, Atmospheric Measurement Techniques, 14, 481-510, 10.5194/amt-14-481-2021, 2021.

Verstraeten, W. W., Boersma, K. F., Douros, J., Williams, J. E., Eskes, H., Liu, F., Beirle, S., and Delcloo, A.: Top-Down NOX Emissions of European Cities Based on the Downwind Plume of Modelled and Space-Borne Tropospheric NO2 Columns, Sensors, 18, 10.3390/s18092893, 2018.

Vohra, K., Marais, E. A., Bloss, W. J., Schwartz, J., Mickley, L. J., Van Damme, M., Clarisse, L., and Coheur, P. F.: Rapid rise in premature mortality due to anthropogenic air pollution in fast-growing tropical cities from 2005 to 2018, Science Advances, 8, 10.1126/sciadv.abm4435, 2022.

Vohra, K., Marais, E. A., Suckra, S., Kramer, L., Bloss, W. J., Sahu, R., Gaur, A., Tripathi, S. N., Van Damme, M., Clarisse, L., and Coheur, P. F.: Long-term trends in air quality in major cities in the UK and India: a view from space, Atmospheric Chemistry and Physics, 21, 6275-6296, 10.5194/acp-21-6275-2021, 2021a.

Vohra, K., Vodonos, A., Schwartz, J., Marais, E. A., Sulprizio, M. P., and Mickley, L. J.: Global mortality from outdoor fine particle pollution generated by fossil fuel combustion: Results from GEOS-Chem, Environmental Research, 195, 10.1016/j.envres.2021.110754, 2021b.

Wan, Y. T., Xu, M. Y., Huang, H., and Chen, S. X.: A spatio-temporal model for the analysis and prediction of fine particulate matter concentration in Beijing, Environmetrics, 32, e2648, https://doi.org/10.1002/env.2648, 2021.

Wang, C. J., Wang, T., Wang, P. C., and Wang, W. N.: Assessment of the Performance of TROPOMI NO2 and SO2 Data Products in the North China Plain: Comparison, Correction and Application, Remote Sensing, 14, 10.3390/rs14010214, 2022a.

Wang, H. C., Chen, X. R., Lu, K. D., Tan, Z. F., Ma, X. F., Wu, Z. J., Li, X., Liu, Y. H., Shang, D. J., Wu, Y. S., Zeng, L. M., Hu, M., Schmitt, S., Kiendler-Scharr, A., Wahner, A., and Zhang, Y. H.: Wintertime N2O5 uptake coefficients over the North China Plain, Science Bulletin, 65, 765-774, 10.1016/j.scib.2020.02.006, 2020a.

Wang, H. C., Lu, K. D., Chen, X. R., Zhu, Q. D., Chen, Q., Guo, S., Jiang, M. Q., Li, X., Shang, D. J., Tan, Z. F., Wu, Y. S., Wu, Z. J., Zou, Q., Zheng, Y., Zeng, L. M., Zhu, T., Hu, M., and Zhang, Y. H.: High N2O5 Concentrations Observed in Urban Beijing: Implications of a Large Nitrate Formation Pathway, Environmental Science & Technology Letters, 4, 416-420, 10.1021/acs.estlett.7b00341, 2017.

Wang, J., Ye, J., Zhang, Q., Zhao, J., Wu, Y., Li, J., Liu, D., Li, W., Zhang, Y., Wu, C., Xie, C., Qin, Y., Lei, Y., Huang, X., Guo, J., Liu, P., Fu, P., Li, Y., Lee, H. C., Choi, H., Zhang, J., Liao, H., Chen, M., Sun, Y., Ge, X., Martin, S. T., and Jacob, D. J.: Aqueous production of secondary organic aerosol from fossil-fuel emissions in winter Beijing haze, Proc. Natl. Acad. Sci. USA, 118, e2022179118, https://doi.org/10.1073/pnas.2022179118, 2021a.

Wang, K., Wu, K., Wang, C. L., Tong, Y. L., Gao, J. J., Zuo, P. L., Zhang, X. X., and Yue, T.: Identification of NOx hotspots from oversampled TROPOMI NO2 column based on image segmentation method, Science of the Total Environment, 803, 10.1016/j.scitotenv.2021.150007, 2022b.

Wang, W., van der A, R., Ding, J., van Weele, M., and Cheng, T.: Spatial and temporal changes of the ozone sensitivity in China based on satellite and ground-based observations, Atmos. Chem. Phys., 21, 7253-7269, 10.5194/acp-21-7253-2021, 2021b.

Wang, Y., Jacob, D. J., and Logan, J. A.: Global simulation of tropospheric O_3-NO_x-hydrocarbon chemistry: 1. Model formulation, J. Geophys. Res. Atmos., 103, 10713-10725, https://doi.org/10.1029/98jd00158, 1998.

Wang, Y., Zhang, Q. Q., He, K., Zhang, Q., and Chai, L.: Sulfate-nitrate-ammonium aerosols over China: response to 2000-2015 emission changes of sulfur dioxide, nitrogen oxides, and ammonia, Atmos. Chem. Phys., 13, 2635-2652, https://doi.org/10.5194/acp-13-2635-2013, 2013.

Wang, Y. C., Yuan, Y., Wang, Q. Y., Liu, C. G., Zhi, Q., and Cao, J. J.: Changes in air quality related to the control of coronavirus in China: Implications for traffic and industrial emissions, Science of the Total Environment, 731, 10.1016/j.scitotenv.2020.139133, 2020b.

Wang, Y. S., Li, W. J., Gao, W. K., Liu, Z. R., Tian, S. L., Shen, R. R., Ji, D. S., Wang, S., Wang, L. L., Tang, G. Q., Song, T., Cheng, M. T., Wang, G. H., Gong, Z. Y., Hao, J. M., and Zhang, Y. H.: Trends in particulate matter and its chemical compositions in China from 2013-2017, Sci. China Earth Sci., 62, 1857-1871, https://doi.org/10.1007/s11430-018-9373-1, 2019.

Wang, Y. X., Zhang, Q. Q., Jiang, J. K., Zhou, W., Wang, B. Y., He, K. B., Duan, F. K., Zhang, Q., Philip, S., and Xie, Y. Y.: Enhanced sulfate formation during China's severe winter haze episode in January 2013 missing from current models, Journal of Geophysical Research-Atmospheres, 119, 16, 10.1002/2013jd021426, 2014.

Wang, Z., Uno, I., Yumimoto, K., Itahashi, S., Chen, X. S., Yang, W. Y., and Wang, Z. F.: Impacts of COVID-19 lockdown, Spring Festival and meteorology on the NO2 variations in early 2020 over China based on in-situ observations, satellite retrievals and model simulations, Atmospheric Environment, 244, 10.1016/j.atmosenv.2020.117972, 2021c.

Weagle, C. L., Snider, G., Li, C., van Donkelaar, A., Philip, S., Bissonnette, P., Burke, J., Jackson, J., Latimer, R., Stone, E., Abboud, I., Akoshile, C., Anh, N. X., Brook, J. R., Cohen, A., Dong, J., Gibson, M. D., Griffith, D., He, K. B., Holben, B. N., Kahn, R., Keller, C. A., Kim, J. S., Lagrosas, N., Lestari, P., Khian, Y. L., Liu, Y., Marais, E. A., Martins, J. V., Misra, A., Muliane, U., Pratiwi, R., Quel, E. J., Salam, A., Segev, L., Tripathi, S. N., Wang, C., Zhang, Q., Brauer, M., Rudich, Y., and Martin, R. V.: Global Sources of Fine Particulate Matter: Interpretation of PM2.5 Chemical Composition Observed by SPARTAN using a Global Chemical Transport Model, Environmental Science & Technology, 52, 11670-11681, 10.1021/acs.est.8b01658, 2018.

Wei, W., Zhang, W., Hu, D., Ou, L. B., Tong, Y. D., Shen, G. F., Shen, H. Z., and Wang, X. J.: Emissions of carbon monoxide and carbon dioxide from uncompressed and pelletized biomass fuel burning in typical household stoves in China, Atmospheric Environment, 56, 136-142, 10.1016/j.atmosenv.2012.03.060, 2012.

Weuve, J., Puett, R. C., Schwartz, J., Yanosky, J. D., Laden, F., and Grodstein, F.: Exposure to Particulate Air Pollution and Cognitive Decline in Older Women, Archives of Internal Medicine, 172, 219-227, 10.1001/archinternmed.2011.683, 2012.

WHO (World Health Organization). (2021). WHO global air quality guidelines: particulate matter (PM2.5 and PM10), ozone, nitrogen dioxide, sulfur dioxide and carbon monoxide. World Health Organization. https://apps.who.int/iris/handle/10665/345329. License: CC BY-NC-SA 3.0 IGO

Wu, C. X., Yan, Y. Q., Chen, X., Gong, J., Guo, Y., Zhao, Y. Y., Yang, N. N., Dai, J., Zhang, F. X., and Xiang, H.: Short-term exposure to ambient air pollution and type 2 diabetes mortality: A population-based time series study, Environmental Pollution, 289, 10.1016/j.envpol.2021.117886, 2021a.

Wu, H. J., Tang, X., Wang, Z. F., Wu, L., Li, J. J., Wang, W., Yang, W. Y., and Zhu, J.: High-spatiotemporal-resolution inverse estimation of CO and NOx emission reductions during emission control periods with a modified ensemble Kalman filter, Atmospheric Environment, 236, 10.1016/j.atmosenv.2020.117631, 2020.

Wu, H. J., Tang, X., Wang, Z. F., Wu, L., Lu, M. M., Wei, L. F., and Zhu, J.: Probabilistic Automatic Outlier Detection for Surface Air Quality Measurements from the China National Environmental Monitoring Network, Adv. Atmos. Sci., 35, 1522-1532, https://doi.org/10.1007/s00376-018-8067-9, 2018a.

Wu, J., Bei, N., Hu, B., Liu, S., Zhou, M., Wang, Q., Li, X., Liu, L., Feng, T., Liu, Z., Wang, Y., Cao, J., Tie, X., Wang, J., Molina, L. T., and Li, G.: Is water vapor a key player of the wintertime haze in North China Plain?, Atmos. Chem. Phys., 19, 8721-8739, https://doi.org/10.5194/acp-19-8721-2019, 2019.

Wu, N., Geng, G. N., Yan, L., Bi, J. Z., Li, Y. S., Tong, D., Zheng, B., and Zhang, Q.: Improved spatial representation of a highly resolved emission inventory in China: evidence from TROPOMI measurements, Environmental Research Letters, 16, 10.1088/1748-9326/ac175f, 2021b.

Wu, S. W., Ni, Y., Li, H. Y., Pan, L., Yang, D., Baccarelli, A. A., Deng, F. R., Chen, Y. H., Shima, M., and Guo, X. B.: Short-term exposure to high ambient air pollution increases airway inflammation and respiratory symptoms in chronic obstructive pulmonary disease patients in Beijing, China, Environment International, 94, 76-82, 10.1016/j.envint.2016.05.004, 2016a.

Wu, X. G., Ding, Y. Y., Zhou, S. B., and Tan, Y.: Temporal characteristic and source analysis of PM2.5 in the most polluted city agglomeration of China, Atmospheric Pollution Research, 9, 1221-1230, 10.1016/j.apr.2018.05.008, 2018b.

Wu, Y., Gu, B., Erisman, J. W., Reis, S., Fang, Y., Lu, X., and Zhang, X.: PM2.5 pollution is substantially affected by ammonia emissions in China, Environ Pollut, 218, 86-94, 10.1016/j.envpol.2016.08.027, 2016b.

Xie, Y., Dai, H. C., Zhang, Y. X., Wu, Y. Z., Hanaoka, T., and Masui, T.: Comparison of health and economic impacts of PM2.5 and ozone pollution in China, Environment International, 130, 10.1016/j.envint.2019.05.075, 2019.

Xing, Y. F., Xu, Y. H., Shi, M. H., and Lian, Y. X.: The impact of PM2.5 on the human respiratory system, Journal of Thoracic Disease, 8, E69-E74, 10.3978/j.issn.2072-1439.2016.01.19, 2016.

Xu, J., Liu, D., Wu, X., Vu, T. V., Zhang, Y., Fu, P., Sun, Y., Xu, W., Zheng, B., Harrison, R. M., and Shi, Z.: Source apportionment of fine organic carbon at an urban site of Beijing using a chemical mass balance model, Atmos. Chem. Phys., 21, 7321-7341, https://doi.org/10.5194/acp-21-7321-2021, 2021.

Xue, R., Wang, S., Zhang, S., He, S., Liu, J., Tanvir, A., and Zhou, B.: Estimating city NOX emissions from TROPOMI high spatial resolution observations – A case study on Yangtze River Delta, China, Urban Climate, 43, 101150, https://doi.org/10.1016/j.uclim.2022.101150, 2022.

Yin, P., Brauer, M., Cohen, A. J., Wang, H., Li, J., Burnett, R. T., Stanaway, J. D., Causey, K., Larson, S., Godwin, W., Frostad, J., Marks, A., Wang, L., Zhou, M., and Murray, C. J. L.: The effect of air pollution on deaths, disease burden, and life expectancy across China and its provinces, 1990-2017: an analysis for the Global Burden of Disease Study 2017, Lancet Planet Health, 4, e386-e398, 10.1016/S2542-5196(20)30161-3, 2020.

Yu, K., Keller, C. A., Jacob, D. J., Molod, A. M., Eastham, S. D., and Long, M. S.: Errors and improvements in the use of archived meteorological data for chemical transport modeling: an analysis using GEOS-Chem v11-01 driven by GEOS-5 meteorology, Geosci. Model Dev., 11, 305-319, 10.5194/gmd-11-305-2018, 2018.

Yuan, L., Popoola, O. A. M., Hood, C., Carruthers, D., Jones, R. L., Liu, H., Lv, Z. F., Zhang, Q., and Archibald, A. T.: Constraining emission estimates of carbon monoxide using a perturbed emissions ensemble with observations: a focus on Beijing, Air Quality Atmosphere and Health, 10.1007/s11869-021-01041-7, 2021.

Yue, H., He, C., Huang, Q., Yin, D., and Bryan, B. A.: Stronger policy required to substantially reduce deaths from PM2.5 pollution in China, Nat Commun, 11, 1462, 10.1038/s41467-020-15319-4, 2020.

Zhai, S. X., Jacob, D. J., Wang, X., Liu, Z. R., Wen, T. X., Shah, V., Li, K., Moch, J. M., Bates, K. H., Song, S. J., Shen, L., Zhang, Y. Z., Luo, G., Yu, F. Q., Sun, Y. L., Wang, L. T., Qi, M. Y., Tao, J., Gui, K., Xu, H. H., Zhang, Q., Zhao, T. L., Wang, Y. S., Lee, H. C., Choi, H., and Liao, H.: Control of particulate nitrate air pollution in China, Nature Geoscience, 10.1038/s41561-021-00726-z, 2021.

Zhang, F., Shi, Y., Fang, D., Ma, G., Nie, C., Krafft, T., He, L., and Wang, Y.: Monitoring history and change trends of ambient air quality in China during the past four decades, J. Environ. Manage, 260, 110031, https://doi.org/10.1016/j.jenvman.2019.110031, 2020a.

Zhang, Q., Jiang, X. J., Tong, D., Davis, S. J., Zhao, H. Y., Geng, G. N., Feng, T., Zheng, B., Lu, Z. F., Streets, D. G., Ni, R. J., Brauer, M., van Donkelaar, A., Martin, R. V., Huo, H., Liu, Z., Pan, D., Kan, H. D., Yan, Y. Y., Lin, J. T., He, K. B., and Guan, D. B.: Transboundary health impacts of transported global air pollution and international trade, Nature, 543, 705-+, 10.1038/nature21712, 2017a.

Zhang, R. X., Zhang, Y. Z., Lin, H. P., Feng, X., Fu, T. M., and Wang, Y. H.: NOx Emission Reduction and Recovery during COVID-19 in East China, Atmosphere, 11, 10.3390/atmos11040433, 2020b.

Zhang, X., Chen, X., and Zhang, X. B.: The impact of exposure to air pollution on cognitive performance, Proceedings of the National Academy of Sciences of the United States of America, 115, 9193-9197, 10.1073/pnas.1809474115, 2018.

Zhang, Y., Cai, J., Wang, S., He, K., and Zheng, M.: Review of receptor-based source apportionment research of fine particulate matter and its challenges in China, Sci. Total. Environ., 586, 917-929, https://doi.org/10.1016/j.scitotenv.2017.02.071, 2017b.

Zhang, Y. X., Shi, Z. B., Wang, Y. Y., Liu, L., Zhang, J., Li, J. F., Xia, Y., Ding, X. K., Liu, D. T., Kong, S. F., Niu, H. Y., Fu, P. Q., Zhang, X. Y., and Li, W. J.: Fine particles from village air in northern China in winter: Large contribution of primary organic aerosols from residential solid fuel burning, Environmental Pollution, 272, 10.1016/j.envpol.2020.116420, 2021.

Zhao, S., Yu, Y., Yin, D., He, J., Liu, N., Qu, J., and Xiao, J.: Annual and diurnal variations of gaseous and particulate pollutants in 31 provincial capital cities based on in situ air quality monitoring data from China National Environmental Monitoring Center, Environ Int, 86, 92-106, 10.1016/j.envint.2015.11.003, 2016.

Zhao, X., Griffin, D., Fioletov, V., McLinden, C., Cede, A., Tiefengraber, M., Mueller, M., Bognar, K., Strong, K., Boersma, F., Eskes, H., Davies, J., Ogyu, A., and Lee, S. C.: Assessment of the quality of TROPOMI high-spatial-resolution NO2 data products in the Greater Toronto Area, Atmospheric Measurement Techniques, 13, 2131-2159, 10.5194/amt-13-2131-2020, 2020.

Zheng, B., Tong, D., Li, M., Liu, F., Hong, C. P., Geng, G. N., Li, H. Y., Li, X., Peng, L. Q., Qi, J., Yan, L., Zhang, Y. X., Zhao, H. Y., Zheng, Y. X., He, K. B., and Zhang, Q.: Trends in China's anthropogenic emissions since 2010 as the consequence of clean air actions, Atmos. Chem. Phys., 18, 14095-14111, https://doi.org/10.5194/acp-18-14095-2018, 2018.

Zheng, Y. X., Zhang, Q., Tong, D., Davis, S. J., and Caldeira, K.: Climate effects of China's efforts to improve its air quality, Environmental Research Letters, 15, https://doi.org/10.1088/1748-9326/ab9e21, 2020.

Zhu, Y., Chen, J., Bi, X., Kuhlmann, G., Chan, K. L., Dietrich, F., Brunner, D., Ye, S., and Wenig, M.: Spatial and temporal representativeness of point measurements for nitrogen dioxide pollution levels in cities, Atmospheric Chemistry and Physics, 20, 13241-13251, 10.5194/acp-20-13241-2020, 2020.

CHAPTER 2:CONTRIBUTION OF AUTUMN-WINTER EMISSION CONTROLS TO AIR QUALITY IMPROVEMENTS IN THE BEIJING-TIANJIN-HEBEI REGION

2.1 Abstract

Cold season emission controls are an increasingly popular strategy in China to address severe fine particulate matter ($PM_{2.5}$) pollution. Here we evaluate the efficacy of such measures, focusing on the influence of emission controls imposed on pollution sources in 28 cities in and around the Beijing-Tianjin-Hebei region (BTH) in autumn-winter 2017/2018 compared to the contribution from interannual variability in meteorology. For this, we use the GEOS-Chem chemical transport model driven with the Multi-resolution Emission Inventory for China (MEIC) after correcting underestimates in emissions (50% for NO_x, >100% for point sources of SO_2) using air pollutant observations from national and Beijing local monitoring network sites. Decline in observed $PM_{2.5}$ averaged across all sites in BTH in autumn-winter 2017/2018 relative to the previous year is 29%, declining from 103 to 74 µg m^{-3} and surpassing the regional target of 15%. Decline in modelled $PM_{2.5}$ is similar for grids coincident with the network sites (25%) and 20% across BTH. According to the model, pollution control measures led to decline in $PM_{2.5}$ precursor emissions of 0.27 Tg NO_x (as NO), 0.66 Tg sulfur dioxide (SO_2), 70 Gg organic carbon (OC), and 50 Gg black carbon (BC). These alone contribute less than half (at most 43%) of the total decline in $PM_{2.5}$ compared to a 57% contribution from interannual variability in meteorology. Specifically, stronger winds, deeper planetary boundary layer, and drier conditions in autumn-winter 2017/2018 than the previous year. The relative role of emissions and meteorology should be considered for successful application of future seasonal emissions controls in BTH and other polluted regions in China.

2.2 Introduction

Cold season emission controls are an increasingly popular measure to reduce air pollution in China, in particular elevated concentrations of fine particles, or $PM_{2 5}$. The Chinese government imposed such measures in 28 cities in and around the Beijing-Tianjin-Hebei region (BTH) (so-called “2+26” cities) in northern China in autumn-winter 2017/2018. Targets were set to reduce regional mean $PM_{2 5}$ by 15% and city-specific $PM_{2 5}$ by 10-25% relative to the previous year (MEE, 2017). The Chinese Ministry of Ecology and Environment (MEE) used national network observations of $PM_{2 5}$ to determine that regional reduction targets were achieved and that only 3 of the 28 cities did not meet their city-specific targets (MEE, 2018). This approach is now adopted in many regions in China (MEE, 2020a, b), despite limited assessment of the relative contribution of emissions reductions and other factors like meteorology that is necessary for successful implementation of these control measures elsewhere.

Severe air pollution persists in BTH, despite substantial decline in $PM_{2 5}$ of ~40% from 2013 to 2017 from enacting emission controls as part of the 5-year Action Plans (Zhang et al., 2019). Annual mean $PM_{2 5}$ in BTH in 2017 was 64 µg m^{-3} (Wang et al., 2019); almost double the national standard of 35 µg m^{-3} (MEE, 2012) and 12 times the recently updated World Health Organization (WHO) guideline of 5 µg m^{-3} (WHO, 2021). Severe $PM_{2 5}$ pollution is due to a combination of primary emissions of particles and gas-phase precursors from multiple sources (Zhang et al., 2018), active heterogeneous chemistry enhancing formation of secondary inorganic and organic aerosols (Huang et al., 2014), and accumulation of pollution due to meteorological conditions such as low wind speeds, a shallow planetary boundary layer and high relative humidity (RH) (An et al., 2019; Bei et al., 2020; Le et al., 2020; Wu et al., 2019). Dominant local $PM_{2 5}$ sources in autumn-winter include sustained contributions from the energy sector and road traffic (Tong et al., 2020), seasonal industrial and residential combustion of coal and other solid fuels (Ma et al., 2017; Yun et al., 2020), and widespread burning of crop residue (Li et al., 2020). Mitigation measures in China have led to a nationwide decline in emissions of the primary $PM_{2 5}$ components black carbon (BC) and organic carbon (OC) of 28 % for BC and 32 % for OC from 2013 to 2017 (Zheng et al., 2018). Emissions of the gas-phase $PM_{2 5}$ precursors nitrogen oxides ($NO_x \equiv NO + NO_2$) and sulfur dioxide (SO_2) have declined by 21% for NO_x

and 59% for SO_2 over the same period. Trends in other $PM_{2.5}$ precursors are less certain. Emissions of ammonia (NH_3), mostly from agriculture, have likely increased or remained constant (Liu et al., 2018; Zhang et al., 2017a; Zheng et al., 2018). Emissions of non-methane volatile organic compounds (NMVOCs), mostly from industrial activity and solvent use, are either stable or increasing (Li et al., 2019b). Non-local sources also contribute to $PM_{2.5}$ in BTH throughout the year. Dong et al. (2020) used a regional air quality model to estimate that, in 2017, transport of non-local $PM_{2.5}$ accounted for 33-68% of total monthly mean $PM_{2.5}$ in BTH.

Many mitigation measures were implemented in autumn-winter 2017/2018. These are detailed in the "Air Pollution Action Plan in Autumn and Winter of 2017-2018 for the Beijing-Tianjin-Hebei Region and its Surrounding Areas" report by the MEE (MEE, 2017). Briefly, these include a sector-wide cap on total consumption of coal, phaseout of small inefficient and outdated industrial coal-fired boilers, reduction in production capacity of heavy industries such as iron and cement, switching from coal to cleaner fuels in homes, and mandated controls on construction site fugitive dust emissions. Other short-term and reactionary measures included shutdown of intensive industries and construction sites throughout the emission control period and instantaneous shutdown of additional industrial plants in response to forecasts of elevated $PM_{2.5}$. Tougher emission standards were imposed and higher quality vehicular fuel was mandated for on-road vehicles. Agricultural residue burning was banned and strictly enforced, and installation of emission control technologies was required for all large emitters of industrial NMVOCs.

A recent regional modelling study by Zhang et al. (2021) has assessed changes in air quality in each of the 28 cities in 2017/2018 relative to the previous year. In that study, they used the high-resolution Community Multi-Scale Air Quality model coupled to the Weather Research and Forecasting Model for meteorology (CMAQ-WRF). The contribution of emission controls to the decrease in simulated $PM_{2.5}$ in each city ranged from 2% to 82% and meteorology was often the dominant contributor, ranging from 18% to 98%. Their study used a regional bottom-up emission inventory that is susceptible to large biases. Error estimates of bottom-up inventories for China determined with satellite observations and intercomparison of inventories are 12-31% for SO_2, 13-37% for NO_x, 18-86% for CO, and 17% to >100% for primary $PM_{2.5}$ (Koukouli et al., 2018; Li et al., 2017).

Similar control measures to those adopted in BTH in autumn-winter 2017/2018 are now widely used in China, necessitating evaluation of the efficacy of these policies. Here we use the extensive national and regional (Beijing) air quality monitoring networks, evaluated with independent measurements, to address biases in the Multi-resolution Emission Inventory for China (MEIC). We then implement the bias-corrected MEIC in the GEOS-Chem chemical transport model (CTM) to quantify the relative role of emission controls and meteorology in meeting the regional $PM_{2.5}$ targets in BTH in autumn-winter 2017/2018 to guide continued use of emission controls to address air pollution.

2.3 Data and methods

2.3.1 Surface measurements of air pollution in BTH

Routine monitoring of ambient $PM_{2.5}$ and trace gases in BTH occur at China National Environmental Monitoring Network (CNEMN) and local Beijing Municipal Environmental Monitoring Network (BJMEMN) sites (Zhang et al., 2020). We use observations of hourly SO_2, NO_2, CO, and $PM_{2.5}$ for the autumn-winter emission reduction period (October 2017-March 2018) and the preceding year (October 2016-March 2017) at sites operational in both years. These include 129 CNEMN sites and 35 BJMEMN sites within the BTH control region and 273 CNEMN sites in the surrounding area. Data from both networks are from the Sina Air Quality Data Platform (http://beijingair.sinaapp.com/; last accessed 17 October 2020, now hosted at https://quotsoft.net/air/). CNEMN and BJMEMN trace gas measurements are obtained with chemiluminescence for NO_2, UV fluorescence for SO_2, and IR absorption for CO. Data from both networks have been widely used to quantify changes in surface air pollution (Li et al., 2019a; Silver et al., 2018; Wan et al., 2021; Wang et al., 2014; Zhai et al., 2019), but independent evaluation is limited. A previous study used statistical techniques and intercomparison of measurements of different pollutants to determine that outliers are $\leq$ 1% of all measurements of air pollutants relevant to this work (Wu et al., 2018).

We assess CNEMN and BJMEMN network measurements with total $PM_{2.5}$ concentration measurements from the US Embassy in Beijing and total $PM_{2.5}$, $PM_{2.5}$ components and trace gas (SO_2, NO_2, and CO) measurements from the winter portion of the intensive Atmospheric Pollution & Human Health in a Chinese Megacity (APHH) campaign (Table S2.1). US Embassy $PM_{2.5}$ in Beijing is measured following US EPA quality control protocols (Martini et al., 2015). APHH included a comprehensive suite of aerosols and trace gases from the 325-m tower at the urban Institute of Atmospheric Physics (IAP) measurement site and a few air quality measurements at a rural site (Pinggu) located ~60 km from the Beijing city centre (Shi et al., 2019). APHH NO_2 measurements are from a Teledyne T500U Cavity Attenuated Phase Shift (CAPS) analyser (Kebabian et al., 2005; Shi et al., 2019). $PM_{2.5}$ components are measured with thermal-optical carbon analyzers for OC and BC and ion chromatography for sulfate, nitrate, and ammonium (Srivastava et al., 2021) at 33% RH (Xu et al., 2021).

2.3.2 GEOS-Chem simulations of surface air pollution in BTH

We use the GEOS-Chem model (version 12.0.0; https://doi.org/10.5281/zenodo.1343547) with the surface network measurements to quantify precursor emissions of $PM_{2.5}$ in and around BTH and assess the relative role of emissions and meteorology to the observed changes in $PM_{2.5}$ in AW2017 relative to the previous year. The model is nested over East Asia (11°S-55°N, 60-150°E) at a horizontal resolution of 0.5° × 0.625° (latitude × longitude). The model is driven with assimilated meteorology from the NASA Modern-Era Retrospective analysis for Research and Applications version 2 (MERRA-2). These are updated hourly for 2D fields and every 3 hours for 3D fields. Dynamic (3-hourly) boundary conditions are from a global simulation at 4° × 5°. Monthly anthropogenic emissions for China in October 2016-March 2017 are from the regional bottom-up Multi-resolution Emission Inventory for China (MEIC) (http://www.meicmodel.org/; last accessed 04 March 2020) available for 2000-2017 at 0.5° × 0.625°. The MEIC includes emissions of SO_2, NO_x, CO, NMVOCs, NH_3, and primary particles from ~700 anthropogenic sources (Li et al., 2017; Zheng et al., 2018). In its implementation in GEOS-Chem, MEIC emissions are lumped as five sectors: industry, power plants, transportation, agriculture and residential. Primary particles are emitted as hydrophobic and hydrophilic BC and OC, and speciated

NMVOCs are mapped to those in GEOS-Chem using the NMVOCs species mapping tables in Li et al. (2014).

The model includes detailed coupled gas- and aerosol-phase chemistry to represent formation and loss of $PM_{2.5}$. Individual aerosol components include sulfate, nitrate, ammonium (Park et al., 2004; Wang et al., 2013), OC (Heald et al., 2006), BC (Li et al., 2016), dust (Fairlie et al., 2007), and sea salt (Jaeglé et al., 2011). Formation of secondary sulfate-nitrate-ammonium aerosols is computed with the ISORROPIA-II thermodynamic equilibrium model (Fountoukis and Nenes, 2007). Physical loss processes include dry and wet deposition (Amos et al., 2012; Liu et al., 2001; Wang et al., 1998). We implement a revised treatment of wet scavenging described and first implemented in GEOS-Chem by Luo et al. (2019). This replaces fixed values of in-cloud condensation water used to calculate rainout of water-soluble aerosols and gases with dynamic values from MERRA-2. This increases wet deposition rates and reduces a positive bias in modelled nitrate and ammonium, in particular in winter, when compared to surface observations in China, Europe, and the US (Luo et al., 2020). We sample the model in AW2016 and AW2017 following two months spin-up before each period of interest for chemical initialization. We conduct multiple model simulations to address biases in the MEIC in the non-control period, estimate emissions for the control period, assess the importance of $PM_{2.5}$ precursor emissions of NH_3 and NMVOCs that lack observational constraints, and determine the relative contribution of emissions reductions and meteorology to changes in $PM_{2.5}$ and trace gases.

2.4 Results and discussion

2.4.1 Air pollutant concentration changes detected with monitoring networks

Figure 2.1 shows hourly CNEMN and BJMEMN $PM_{2.5}$ against those from the APHH and US Embassy sites. $PM_{2.5}$ from both networks are temporally consistent with APHH and US Embassy $PM_{2.5}$ ($r \geq 0.96$) and exhibit similar variance (slopes of 1.0-1.1). Network sites measure more $PM_{2.5}$ than APHH by 10% for CNEMN and 17% for BJMEMN. Differences to US Embassy $PM_{2.5}$ range from negligible (0.2% less) to 6.4% more. The larger discrepancies between BJMEMN and the independent measurements may be due to differences in local emissions influencing these sites, as these are further apart (~3 km) than the CNEMN and independent measurement sites (~1 km) (Table S2.1). Decline in $PM_{2.5}$ in the control period relative to the previous year is 43% according to US Embassy $PM_{2.5}$, decreasing from 97 to 55 μg m^{-3}, and is similar at the nearby BJMEMN (43% decline) and CNEMN (42% decline) sites used in Figure 2.1.

Figure 2.2 shows hourly trace gas measurements from CNEMN and BJMEMN to those from APHH. Though CO is not a $PM_{2.5}$ precursor, its abundance affects and responds to the oxidative potential of the atmosphere. It also offers an indirect assessment of $PM_{2.5}$ precursor emissions of NMVOCs that oxidize to form CO. Most network measurements exceed the instrument detection limit (indicated in Figure 2.2), except for SO_2 (31% for CNEMN, 16% for BJMEMN). The surface networks are temporally consistent with APHH ($r > 0.7$) for all trace gases. CNEMN NO_2 is ~5% more and BJMEMN NO_2 ~17% more than APHH, as the chemiluminescence instruments used at network sites are susceptible to interference from thermal decomposition of thermally unstable NO_x reservoir compounds (Dunlea et al., 2007; Reed et al., 2016). The APHH instrument is not susceptible to this interference, as it is a direct measurement (Kebabian et al., 2005). Shah et al. (2020) estimated a chemiluminescence bias of ~6% over eastern China in winter using GEOS-Chem. In other polluted locations, such as Mexico City, the bias from comparing chemiluminescence to collocated spectroscopic measurements is larger (22%) (Dunlea et al., 2007). Network measurements of SO_2 are less than APHH for CNEMN (by 19%) and more than APHH for BJMEMN (also 19%). For CO, the networks are 16% more than APHH for CNEMN and 28% more for BJMEMN.

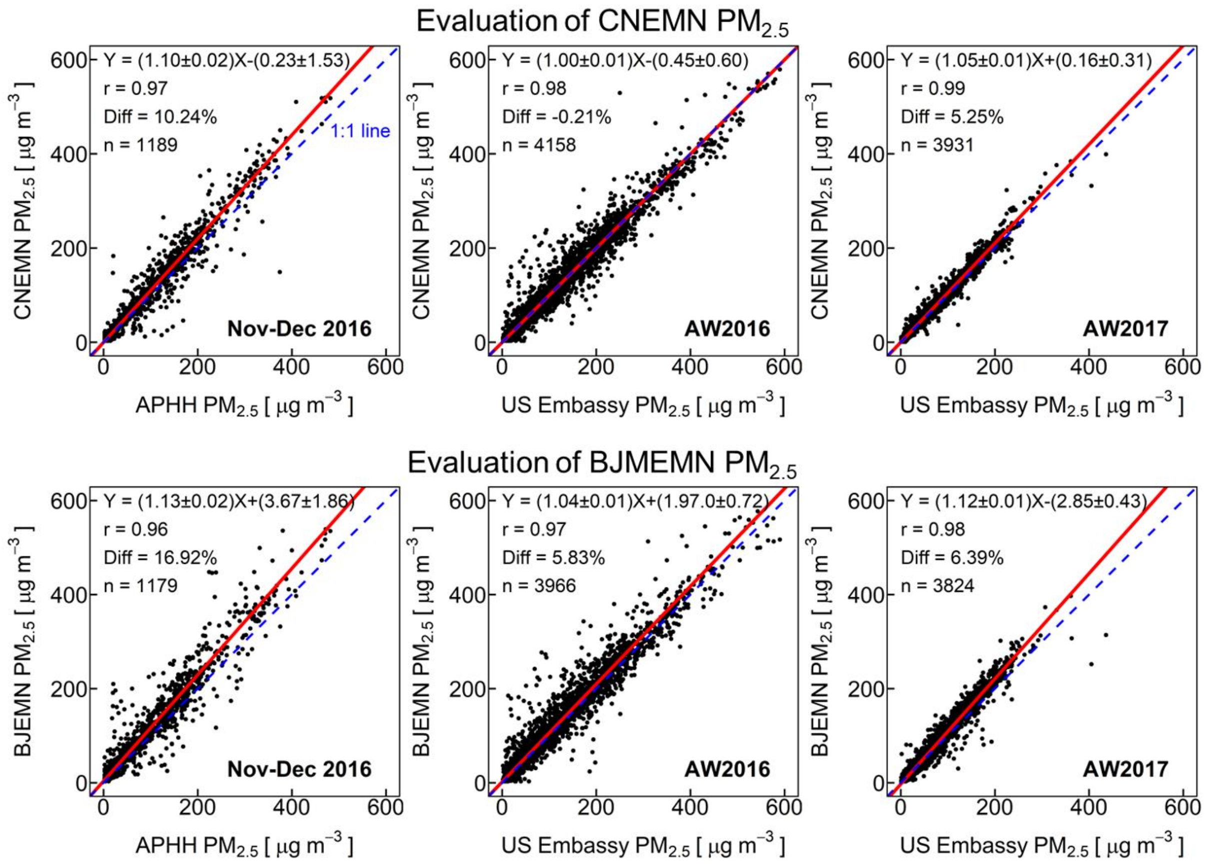

Figure 2.1: Evaluation of local and national network $PM_{2.5}$ measurements in Beijing. Points are hourly $PM_{2.5}$ measurements. The top row compares CNEMN to the APHH urban site (left), and CNEMN to the US Embassy in autumn-winter 2016/2017 (AW2016) (centre) and 2017/2018 (AW2017) (right). The bottom row compares BJMEMN to the APHH urban site (left), and BJMEMN to the US Embassy in AW2016 (centre) and AW2017 (right). Reduced major axis (RMA) regression statistics, Pearson's correlation coefficients (r), the percent difference (Diff = monitoring network minus independent measurement), and the number of points (n) are given. Lines are the RMA regression (red) and 1:1 line (blue dashed).

To aid interpretation of the differences between the network sites and independent measurements, we also assess consistency between CNEMN and BMJEMN in coincidence with APHH for the sites in Figure 2.2. These two sites are ~5 km apart and the BJMEMN site is between two busy ring roads, while the CNEMN site is located in a park. The sites are strongly correlated for $PM_{2.5}$ ($r = 0.97$) and all trace gases ($r = 0.89$-0.92), but CNEMN is less than BJMEMN by 11% for NO_2, 33% for SO_2, 9% for CO, and 6% for $PM_{2.5}$ due to greater influence of road traffic at the BJMEMN site for NO_2, CO and $PM_{2.5}$. This is consistent with the generally larger positive differences between BJMEMN and the independent APHH measurements in Figures 2.1 and 2.2. The larger difference in SO_2 result from the large scatter of the data around the 1:1 line (Figure 2.2).

Both networks also measure ozone, but ozone pollution is most severe in China in spring and summer (Yang et al., 2020). We estimate mean ozone of 15-19 µg m^{-3} at the two monitoring network sites in Figure 2.2. This is below the WHO seasonal mean ozone guideline of 60 µg m^{-3} (WHO, 2021) and almost an order of magnitude less than the summer mean ozone air quality metric, mean maximum daily 8h average ozone, of 120-160 µg m^{-3} in northern China (Li et al., 2019a). We do not consider ozone pollution further.

We show in Figure 2.3 the spatial distribution of the network observed changes in $PM_{2.5}$ and trace gas concentrations in and around BTH between the control period (autumn-winter 2017/2018) and the preceding year (autumn-winter 2016/2017). Hereafter, we refer to these time periods as AW2017 for autumn-winter 2017/2018 and AW2016 for autumn-winter 2016/2017. Decline in air pollutant concentrations in BTH is 16% for NO_2, 44% for SO_2, 31% for CO, and 29% for $PM_{2.5}$, surpassing the 15% $PM_{2.5}$ reduction target for BTH. Smaller reductions of 0.5% for NO_2, 31% for SO_2, 13% for CO, and 10% for $PM_{2.5}$ occurred in the surrounding area. Southeast of BTH, NO_2 and $PM_{2.5}$ increased by 5-9% that may be due to an increase in emissions from industries in the non-control area (Fang et al., 2019). In what follows, we use the network observations of trace gases in AW2016 to correct biases in the MEIC and the relative changes in $PM_{2.5}$ and trace gases to quantify emissions changes from AW2016 to AW2017.

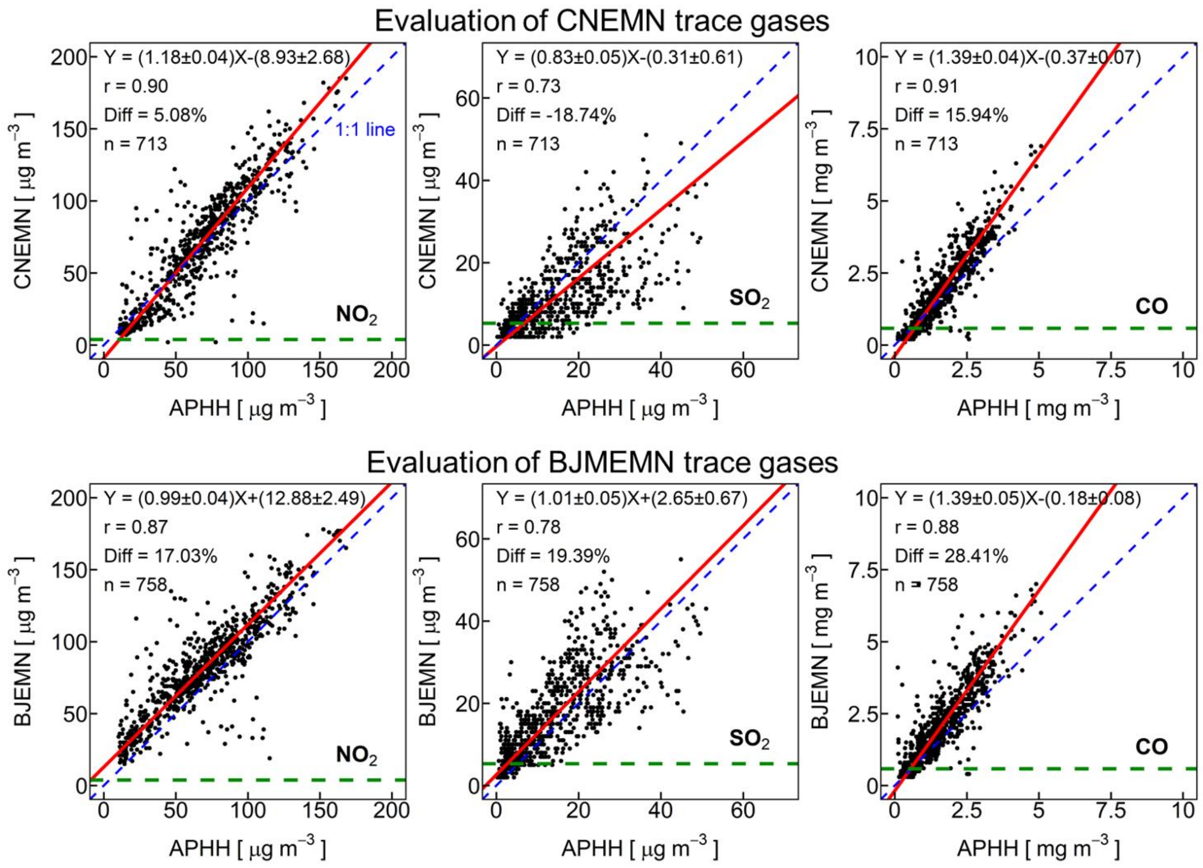

Figure 2.2: Evaluation of local and national network trace gas concentration measurements in Beijing. Points are hourly measurements. Panels compare CNEMN (top) and BJMEMN (bottom) NO_2 (left), SO_2 (centre) and CO (right) to the APHH urban site in November-December 2016. RMA regression statistics, Pearson's correlation coefficients (*r*), the percent difference (Diff = monitoring network minus independent measurement), and the number of points (n) are given. Lines are the RMA regression (red) and 1:1 line (blue dashed). The green dashed line is the reported monitoring network instrument detection limit (MEE, 2012).

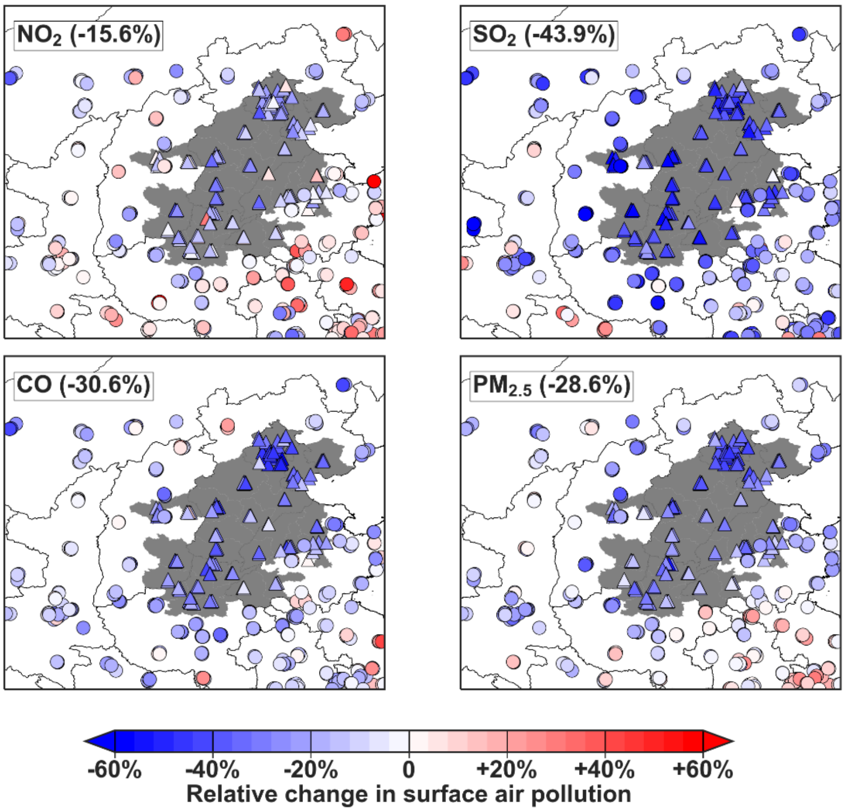

Figure 2.3: Change in observed surface air pollution in BTH and the surrounding area in AW2017 relative to AW2016. Individual points are monitoring network site changes for the control region (triangles in area shaded grey) and the surrounding area (circles in the non-shaded area). Values inset give the percent change (AW2017 minus AW2016) for sites in the control region only.

2.4.2 Addressing biases in the MEIC

Modelled surface concentrations in AW2016 driven with the MEIC are on average less than observed NO_2 (by 48%), SO_2 (by 42%), and CO (by 57%) from comparison of the model and the observations averaged onto the model grid covering the domain in Figure 2.3 (Figure S2.1). The underestimate for SO_2 is up to a factor of 6.8 for gridded observed SO_2 > 80 µg m^{-3}. We attribute this to an underestimate in precursor emissions of these in the MEIC that may result from underestimates in energy statistics (Hong et al., 2017; Zhi et al., 2017) and emission factors (Cheng et al., 2017). Previous studies reported that MEIC trends in NO_x, SO_2, and CO are consistent with those derived from satellite observations and from weather-normalised surface measurements (Vu et al., 2019; Zheng et al., 2018). Low biases in emissions of NO_x (of -28% to -11%) and CO (of -76% to -52%) have been inferred from comparison of multiple models to the network measurements in the Northern China Plain (Feng et al., 2020; Kong et al., 2020). At a very local scale, Squires et al. (2020) determined that the MEIC over- rather than under-estimates NO_x and CO emissions at the urban APHH site from comparison of MEIC to fluxes calculated using eddy-covariance, though the comparison used measurements for 2016 and the MEIC for 2013 over a time period of policy-driven decline in NO_x and CO emissions (Zheng et al., 2018).

We improve reliability of GEOS-Chem simulation of surface concentrations for AW2016 by minimizing biases in the MEIC. We do this by deriving correction factors from ratios of gridded network trace gas observations of NO_2 (for NO_x emissions), CO, and SO_2 to those from GEOS-Chem driven with the original MEIC. These are relatively spatially uniform for NO_x (mean ± standard deviation of 2.3 ± 1.4) and CO (2.6 ± 1.3). Given this and that there are potential measurement biases (Figure 2.2), errors in model chemistry, and non-linearities between concentrations and emissions, we simply apply a single scale factor over the whole domain in Figure 2.3 to MEIC NO_x (of 1.5) and MEIC CO (of 2.4). These scaling factors are decided based on our initial comparison of the model and the observations (Figure S2.1), and on the model experiments we conducted where we incrementally increased scaling factors to 1.5 for NO_x and 2.4 for CO. The 50% underestimate in modelled NO_2 is more than can be explained by positive bias in the measurements (at most 22%) or a network sampling bias. NO_2 measurements at roadside are generally higher than those at urban background sites due to emissions from nearby traffic and are affected by its surrounding micro-environment which governs accumulation and dispersion of pollution. Due to its coarse spatial resolution, the model may not well reproduce measurements at roadside sites. But this has limited effects on underestimate in modelled NO_2, as we find that average BJMEMN NO_2 only decreases by 5-8% for all non-roadside sites compared to all sites. There is no site classification data for CNEMN.

Kong et al. (2020) have also reported model underestimates in annual mean CO concentrations in the Northern China Plain by 52% to 76% when driven with the MEIC. Some of the low bias in simulated CO may be due to positive bias in the monitoring network (16-28%; Figure 2.2), though this assessment is limited to two nearby sites that may not be representative of the whole domain. CO includes contributions from primary emissions and secondary CO from oxidation of NMVOCs. MEIC NMVOCs are subject to uncertainties, due to poorly quantified industrial emissions (Li et al., 2017) and lack of reliable data for scattered sources such as residential coal burning (Li et al., 2019b; Peng et al., 2019; Shi et al., 2020). We find that modelled CO is relatively unaffected by NMVOCs emissions. A 50% increase in MEIC NMVOCs within the study area only increases GEOS-Chem surface CO concentrations by 0.2%. This suggests CO is mostly primary, though our sensitivity simulation results could be affected by model errors in NMVOCs oxidation pathways that form CO (Miller et al., 2016). Much of the low model bias for SO_2 is due to seven model grids in Shanxi province west of BTH (Figure S2.1); a region with more than twenty coal-fired power plants with a collective generating capacity ≥ 1 GW (https://globalenergymonitor.org/; last accessed 30 January 2022). We apply grid-specific scale factors ranging from 2.1 to 6.8 to MEIC SO_2 over these seven grids only (indicated in Figure S2.1), which are the ratios of measured SO_2 over modelled SO_2 with default MEIC emissions in these grids. We do not adjust AW2016 MEIC primary BC and OC, due to limited observational constraints.

Figure 2.4 compares surface concentrations of trace gases and $PM_{2.5}$ from GEOS-Chem with bias-corrected MEIC NO_x, CO and SO_2 to those from the monitoring networks averaged onto the GEOS-Chem grid. Emissions scaling of NO_x improves modelled variance in NO_2 (slope increases from 0.87 (Figure S2.1) to 0.93 (Figure 2.4)), but there is still an underestimate in modelled background NO_2 (intercept = -12.8 μg m^{-3}). If we add the modelled reservoir compounds nitric acid (HNO_3), peroxyacetyl nitrates (PANs) and alky nitrates to modelled NO_2 to capture interference from these in the chemiluminescence measurements, as suggested by Shah et al. (2020) and Dunlea et al. (2007), the model bias decreases from -33% to -13%. The remaining model bias is due to the non-linear relationship between NO_2 concentrations and NO_x emissions. This is shown in Figure S2.2, quantified by dividing the ratio of GEOS-Chem scaled-to-original surface concentrations by the MEIC correction factors (Equation (S1)). The change in NO_2 concentrations in BTH (33%) is weaker than the 50% increase in NO_x emissions. This is because NO_x loss leading to formation of HNO_3 increases with increase in NO_x emissions where sources are large. The relative increase in GEOS-Chem surface concentrations of HNO_3 (136%) exceeds the 50% increase in emissions.

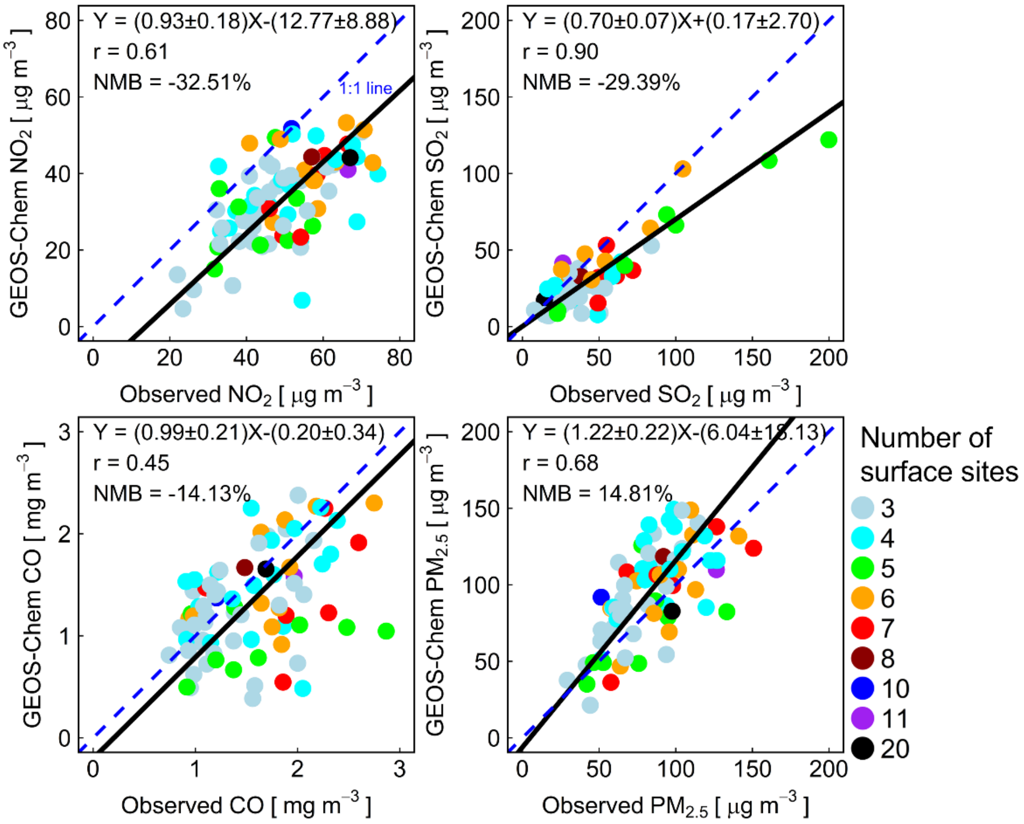

Figure 2.4: Evaluation of GEOS-Chem simulation of air pollutant concentrations in AW2016. Observations are averaged onto the GEOS-Chem grid. Points are simulated and observed NO_2 (top left), SO_2 (top right), CO (bottom left) and $PM_{2.5}$ (bottom right) in the entire domain in Figure 2.3 for grid squares with at least three coincident surface sites. Points are coloured by the number of surface sites. The model uses scaled MEIC emissions (see text for details). RMA regression statistics, Pearson's correlation coefficients (r), and model normalized mean biases (NMB) are given. Lines are the RMA regression (black) and 1:1 line (blue dashed).

The model underestimate in CO decreases from -57% to -14% and there is a small improvement in spatial correlation ($r = 0.35$ (Figure S2.1); $r = 0.45$ (Figure 2.4)). The remaining model bias is partially due to the non-linear response of CO concentrations to perturbations in emissions (Figure S2.2). Local primary emissions of CO are increased, but CO is also transported east and south of the domain shown in Figure S2.2. Also, CO emissions outside the model sampling domain are not scaled, so there is likely an underestimate in background CO concentrations. Given the relatively long lifetimes of CO of several months, CO can be transported from the background region to the study domain, a biased low CO background is expected to contribute to underestimate in the model sampling domain, which weakens the response of CO concentrations to perturbations in emissions. Emissions scaling of SO_2 improves spatial consistency of SO_2 from $r = 0.54$ (Figure S2.1) to $r = 0.90$ (Figure 2.4). There is still a model bias of -29%, as the increase in concentrations is less than the increase in emissions over the grids that are scaled (Figure S2.2), as SO_2 is advected from the scaled grids with large point sources to adjacent grids.

Scaling MEIC SO_2 and NO_x increases the $PM_{2.5}$ bias from 8% (Figure S2.1) with the original MEIC to 15% (Figure 2.4) with scaled MEIC. This bias in $PM_{2.5}$ may be due to overestimates in MEIC primary $PM_{2.5}$ emissions (BC + OC). BC fluxes estimated with eddy covariance during the winter APHH campaign suggest a large overestimate (59 times) in MEIC BC (Joshi et al., 2021), but this may be because local influence of traffic (~100 m) in the measurements is diluted at the spatial resolution of the MEIC (3 km) used in that study. To further assess modelled $PM_{2.5}$ in BTH, we compare modelled $PM_{2.5}$ components to those measured at the APHH urban and rural sites. This is shown in Figure 2.5. OC is compared instead of organic aerosol (OA), due to uncertainties in conversion of OC to OA (Xing et al., 2013). The model overestimates total $PM_{2.5}$ by 10% at the urban site and 34% at the rural site. According to the observations, OC dominates, with a carbon mass contribution to total $PM_{2.5}$ of 23% (urban) and 33% (rural). The contribution of the sum of secondary inorganic aerosols is similar (31%) at both sites and includes similar contributions from sulfate (8-9%), nitrate (13%), and ammonium (9-10%). BC is 4% of total $PM_{2.5}$ at both sites.

The model simulates similar contributions from each component at the two sites, but, compared to the observations, it underestimates OC (9-10% contribution to $PM_{2.5}$) and sulfate (4%), overestimates nitrate (28-30%), and slightly overpredicts BC (4-5%). The relative contribution of ammonium is similar to the measurements (10%). Previous studies have reported similar biases in OC, sulfate and nitrate in China from GEOS-Chem (Miao et al., 2020) and other CTMs (Chen et al., 2019; Gao et al., 2018). Miao et al. (2020) reported a year-round underestimate in OA that they attributed to biases in precursor emissions and lack of seasonality in fixed secondary OA (SOA) yields used to estimate SOA formation from NMVOCs. They also identified a year-round underestimate in sulfate that peaks at 54% in winter, similar to our 50% underestimate at the urban site. The model underestimate in sulfate may be due to remaining underestimate in MEIC SO_2 (Figure 2.4), missing sulfate formation processes during haze events (Bloss et al., 2021; Wang et al., 2016; Wang et al., 2020), and measurement interference from hydroxymethane sulfonate (HMS) (Moch et al., 2018; Song et al., 2019). Model overestimate in nitrate is a known issue (Wang et al., 2013), but the cause remains elusive. Miao et al. (2020) suggest it could be caused by uncertainties in the formation and processing of nitrate. Despite biases in $PM_{2.5}$ composition, the model reproduces temporal (day-to-day) variability in mean total $PM_{2.5}$ (r = 0.66-0.71) and its components (r = 0.50-0.78) at both sites.

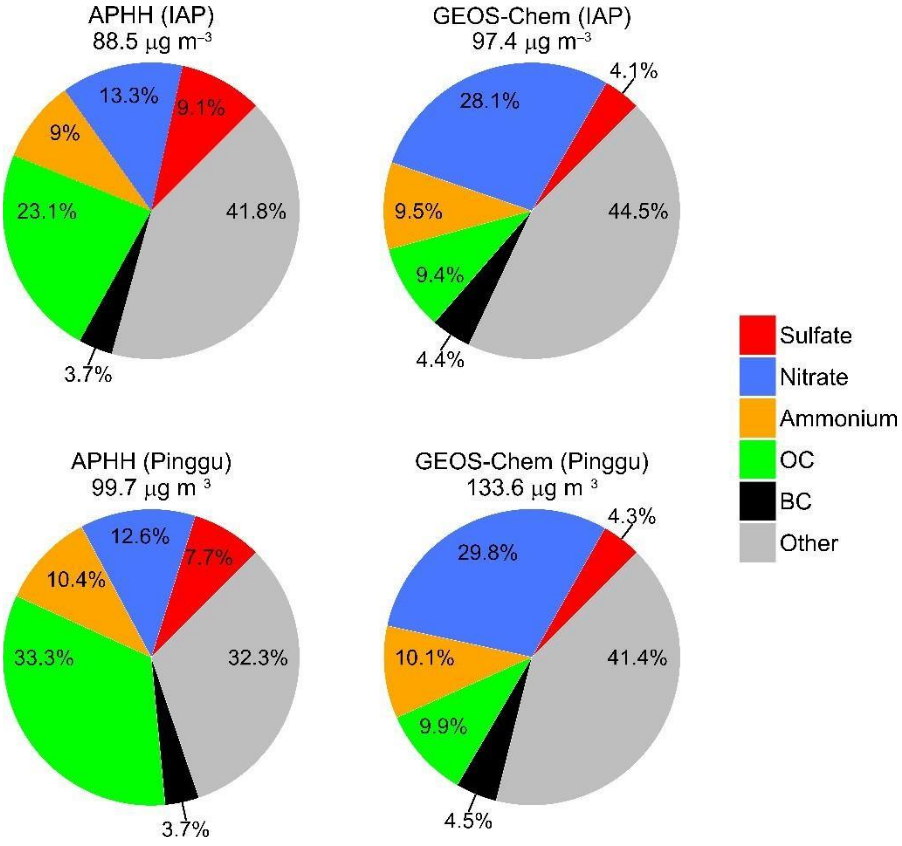

Figure 2.5: Contribution of $PM_{2.5}$ components to total $PM_{2.5}$ during the APHH campaign. Panels are measured (left) and modelled (right) percent contribution for the urban IAP (top) and rural Pinggu (bottom) sites. Components are sulfate, nitrate, ammonium, OC, BC and Other. Other is the sum of trace metals, mineral dust and other ions, the non-carbon portion of OC, and aerosol water at 33% relative humidity (RH) for the measurements and 35% RH for the model. Values above the pies give total $PM_{2.5}$.

Here we use surface measurements from monitoring networks and APHH campaign to constrain and evaluate the model performance, but there are some caveats in comparing model to observations from surface sites. The model grids are at the coarse spatial resolution of 0.5° × 0.625°, the modelled concentrations of air pollutants represent the averaged values in the entire area covered by model grids. But surface measurements are collected from sparse points and are affected by local environments. For example, wind vortices in a street canyon can control measurements at the urban traffic site, as higher levels of pollution are measured when wind blows fresh emissions from the traffic to the monitoring site which is located on one side of the street (Harrison et al., 2019). Surface measurements do not fully represent the air pollution over the area. In addition, measurement sites are normally located on the ground or on the roof of buildings with a few metres high, while the surface layer in GEOS-Chem is the lowest layer where atmospheric pressure decreases from 1013.250 to 998.051 hPa, which roughly corresponds to a height of 129-134 metres above sea level in the study domain. The difference in the elevation of measurement sites and the vertical range of surface layer in the model also contribute to discrepancies between model and observations if the lowest model layer is not well mixed.

2.4.3 Influence of emissions and meteorology on air quality in AW2017

The MEIC provides emissions estimates until the end of 2017, covering half the control period (AW2017) and limiting its direct use for the AW2017 simulation. This we address by deriving emissions for AW2017 using spatially varying scaling factors to apply to MEIC AW2016 emissions derived with observed relative concentration changes from AW2016 to AW2017. To do this for NO_x, SO_2 and CO emissions, we regrid the relative changes in trace gases in Figure 2.3 to a fixed 1° × 1.25° grid that is the best compromise between coverage and spatial resolution. We fill in missing grids (17% in the control region, 51% outside it), by interpolating across nearest neighbouring grids. The resultant scaling factors are in the supplementary (Figure S2.3). For OC and BC emissions, we use relative changes in total $PM_{2.5}$ (Figure S2.3) as an initial guess, but this underestimates decline in total observed $PM_{2.5}$ in BTH AW2017 by 9.7 %. This suggests that decline in primary $PM_{2.5}$ exceeds decline in other sources that contribute to $PM_{2.5}$ and is corroborated by greater decline in primary $PM_{2.5}$ in the bottom-up inventories used by Zhang et al. (2021) than the decline in measured total $PM_{2.5}$ for around half the 28 cities. This may be because regulations targeted sources with large primary $PM_{2.5}$ emissions, such as coal combustion, industry, vehicles, construction and biomass burning (Zhang et al., 2017b; Zheng et al., 2017). We conduct multiple model simulations with incremental 10% increases in the scaling factors derived with observed relative changes in $PM_{2.5}$ (Figure S2.3). We identify that emissions scaling factors of OC and BC that are 40% more than the values in Figure S2.3 best resolves this discrepancy.

Figure 2.6 shows the spatial distribution of modelled and observed $PM_{2.5}$ concentrations and relative changes in $PM_{2.5}$ in and around BTH. The mean decline in observed $PM_{2.5}$ is 27% in BTH, from 103 µg m^{-3} in AW2016 to 75 µg m^{-3} in AW2017. A similar decline occurs for model grids coincident with the observations (25% decrease from 112 to 85 µg m^{-3}), despite a positive model bias in total and components of $PM_{2.5}$ (Figures 2.4, 2.5). The decline in modelled $PM_{2.5}$ is 20% for all BTH grids (104 to 83 µg m^{-3}) and 15% for the whole domain (71 to 60 µg m^{-3}). In Beijing, observed $PM_{2.5}$ decreases from

96 to 57 µg m^{-3}, a 41% reduction. The decline in the model is more modest for coincident grids (33% decline of 78 to 52 µg m^{-3}) and for all Beijing grids (33% decline of 75 to 50 µg m^{-3}). All surpass the 25% target for Beijing (MEE, 2017). Our emissions estimate for AW2017 only constrains sources in and near BTH, though this only affects model consistency with observations of NO_2 and CO in the surrounding area (Figure S2.4). Regardless, the relative regional changes in $PM_{2.5}$ surrounding BTH is similar for the observations (-10%) and coincident model grids (-11%). The change is -13% for all model grids.

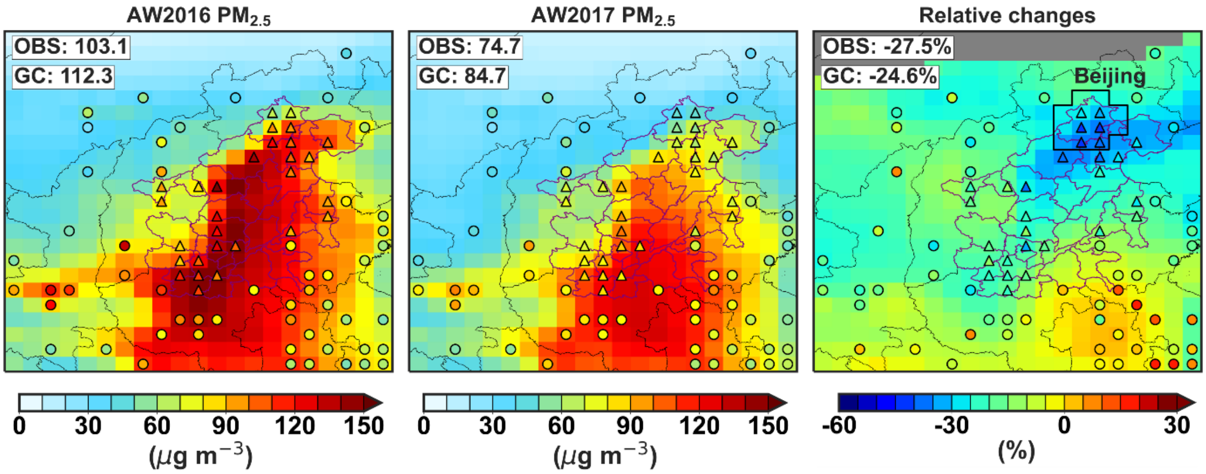

Figure 2.6: Spatial distribution of absolute and relative changes in observed and modelled $PM_{2.5}$ before and during the strict emission control period. The observed (shapes) and modelled (background) $PM_{2.5}$ are shown for AW2016 (left) and AW2017 (centre). The right panel is the relative change in observed and modelled $PM_{2.5}$ for GEOS-Chem $PM_{2.5} \geq 20$ µg m^{-3} (grey otherwise). The black boundary shows the thirteen Beijing grids. Observations are distinguished as within (triangles) and outside (circles) the emission control region (grey area in Figure 2.3). Inset values are the observed (OBS) and modelled (GC) means for sites and coincident grids in the emission control domain. Note the uneven colour scale in the right panel.

Figure 2.7 shows the total anthropogenic emissions of gaseous $PM_{2.5}$ precursors, primary $PM_{2.5}$ (OC and BC), and CO we derive for BTH in AW2016 and AW2017. These are 2.4 Tg NO_x as NO, 1.6 Tg SO_2, 150 Gg BC, 240 Gg OC, and 41 Tg CO in AW2016. The non-linear relationship between surface concentrations and emissions (Figure S2.2) suggests the AW2016 emissions are 9% too low for NO_x, 13% too low for CO, and 8% too high for SO_2. Still, this discrepancy is much less than the correction factors applied to the MEIC (50% for NO_x, >100% for CO, and >100% for SO_2 point sources). Emissions in BTH decline in AW2017 by 0.27 Tg NO_x (11% reduction), 0.66 Tg SO_2 (42%), 70 Gg OC (29%), 50 Gg BC (33%), and 9.7 Tg CO (24%). The relative decline is similar to what we infer from Zhang et al. (2021) for NO_x (~10%) and primary $PM_{2.5}$ (~30%), but more than their SO_2 (~30%). Our study focuses on the BTH region rather than individual cities, so is more influenced by point sources of SO_2 located in nearby cities in Shanxi province. The major sector contributions to anthropogenic emissions in BTH is the same in both years and includes industry for NO_x (44%), SO_2 (56%), and CO (39%), transport for NO_x (34%), and residential fuel use for SO_2 (28%), CO (42%), BC (47%) and OC (79%).

Emissions of NH_3 and NMVOCs are unchanged, due to limited constraints on these. There is an Ammonia Monitoring Network in China (AMoN-China), but there are only 8 sites in BTH, the data are not publicly available (Pan et al., 2018), and the relationship between NH_3 emissions and concentrations is complicated by reversible partitioning of NH_3 between the gas and aerosol phase to form ammonium (Fu et al., 2017; Marais et al., 2021) that depends on meteorology and abundance of acidic sulfate from SO_2 and nitrate from NO_x (Ge et al., 2019; Xia et al., 2016). According to GEOS-Chem, surface NH_3 concentrations in BTH increased by 14%, due in part to decline in SO_2 and NO_x emissions. No control measures targeted dominant NH_3 sources such as fertilizer use and livestock excreta (Huang et al., 2012). These are also at a minimum in autumn-winter (Kong et al., 2019). Controls in AW2017 targeted industries that emit NMVOCs, but we find using GEOS-Chem that a 50% increase in NMVOCs emissions only increases total $PM_{2.5}$ by 1%. In a recent study, Wang et al. (2021) propose that rapid aqueous-phase oxidation of primary OA rather than NMVOCs dominates SOA formation in Beijing and would resolve the decline in wintertime SOA while NMVOCs emissions have remained constant or increased.

We quantify the contribution of meteorology to decline in $PM_{2.5}$ in AW2017 to assess whether emissions reductions alone (Figure 2.7) are sufficient to achieve regional $PM_{2.5}$ targets. We do this by comparing GEOS-Chem AW2017 $PM_{2.5}$ (Figure 2.6) to GEOS-Chem $PM_{2.5}$ obtained with the same emissions (AW2017), but driven with meteorology for AW2016. The results of the difference between these simulations are in Figure 2.8. The mean decline in $PM_{2.5}$ in BTH due to meteorology is 12 μg m^{-3} or 57% of the total. This suggests that emission controls caused at most a 9 μg m^{-3} decline in $PM_{2.5}$ (43% of the total). This is a regional decline of ~9%; less than the 15% target. An air quality trends study focusing on polluted regions in China used WRF-CMAQ to estimate that contrasting meteorology in BTH favourable for $PM_{2.5}$ pollution in December 2016 and for $PM_{2.5}$ dispersion in December 2017 was responsible for 70% of the total decline in $PM_{2.5}$ in December 2017 relative to December 2016 (Zhang et al., 2019). The contribution of differences in December meteorology is similar (75%) according to GEOS-Chem. The meteorological factors responsible for decline in BTH $PM_{2.5}$ in AW2017 in GEOS-Chem are dilution and dispersion of pollution due to stronger south-easterly winds and a 7% higher planetary boundary layer in AW2017 than AW2016, and less efficient secondary inorganic aerosol formation due to 5% lower RH in AW2017 than AW2016. Interannual variability in RH was also the cause for sustained air pollution over BTH despite decline in precursor emissions from lockdown measures imposed to control the spread of the SARS-CoV-2 virus (Le et al., 2020) during January and February 2020.

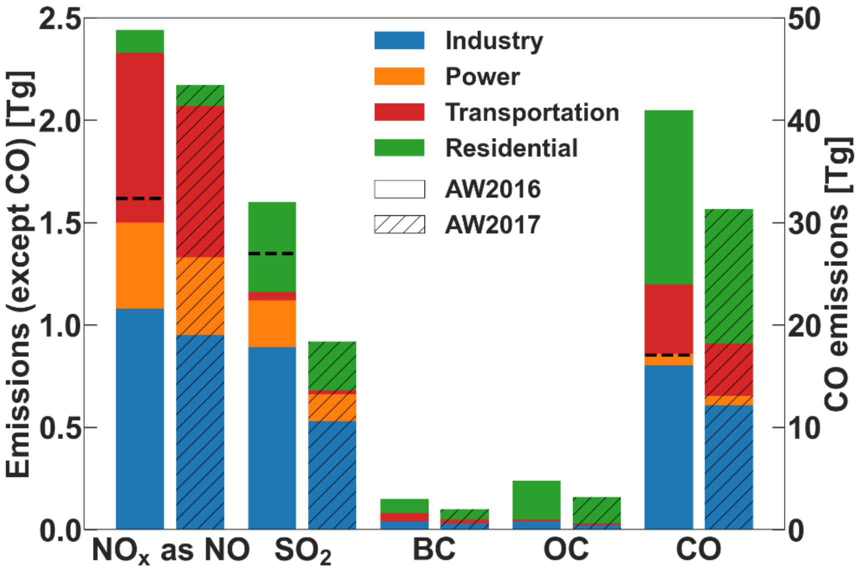

Figure 2.7: Total anthropogenic emissions in BTH in AW2016 and AW2017. Emissions are for grids covering the grey shaded area in Figure 2.3. Emissions are from the MEIC with scaling factors to address discrepancies between the model and observations for AW2016 and to reproduce the change in air pollutant concentrations in the AW2017 emission control period (see text for details). Vertical axes are emissions of NO_x, BC, OC, and SO_2 on the left axis and CO on the right. Horizontal black dashed lines show the original MEIC AW2016 emissions totals for NO_x, SO_2, and CO.

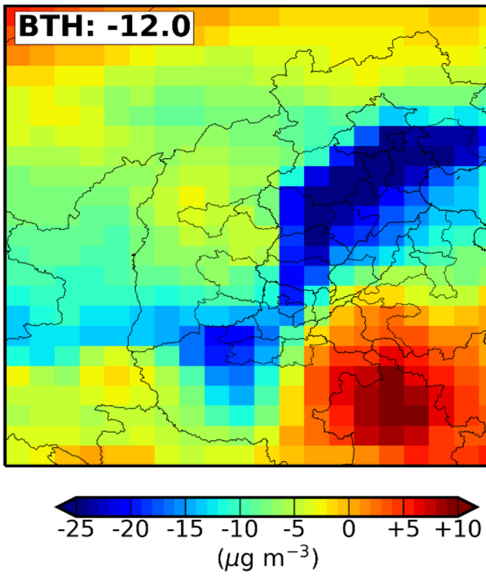

Figure 2.8: Response of $PM_{2.5}$ to interannual variability in meteorology. The map shows the difference in GEOS-Chem $PM_{2.5}$ obtained using AW2017 emissions and meteorology (Figure 2.6) and AW2017 emissions and AW2016 meteorology. Inset value is the mean decrease in BTH $PM_{2.5}$. Note the colour scale is uneven.

2.5 Conclusions

Strict emission controls were implemented across 28 cities in and around the Beijing-Tianjin-Hebei region (BTH) in autumn-winter 2017/2018 to alleviate fine particulate matter ($PM_{2.5}$) pollution. $PM_{2.5}$ reduction targets were met, leading to implementation of these seasonal control measures in other polluted regions in China. We used widespread network observations, evaluated against independent measurements, to address biases in the Multi-resolution Emission Inventory for China (MEIC) for implementation in the GEOS-Chem model to assess the efficacy of these emission controls by quantifying $PM_{2.5}$ precursor emissions reductions and determining the relative contribution of these and meteorology to decline in $PM_{2.5}$.

$PM_{2.5}$ and trace gases (NO_2, SO_2 and CO) from the surface networks are temporally consistent with independent measurements ($r > 0.9$ for $PM_{2.5}$ and $r > 0.7$ for gases) and exhibit discrepancies that are due to variability in pollution sources in the urban environment and known instrument interferences. Across all network sites in BTH, $PM_{2.5}$ decreased by 29% from 103 to 74 μg m^{-3} in the control period relative to the previous year, exceeding the regional target of 15%. The model with MEIC emissions scaled to address underestimates in NO_x (by 50%), CO (>100%), and point sources of SO_2 (>100%)

reproduce the observed spatial distribution in $PM_{2.5}$ ($r = 0.68$). Despite a 15% positive bias in total $PM_{2.5}$ and biases in the $PM_{2.5}$ components organic aerosol, nitrate, and sulfate, the model simulates the observed relative decline in $PM_{2.5}$ in BTH. According to the model, constrained with the network measurements, emissions in BTH declined by 0.27 Tg NO_x as NO, 0.66 Tg SO_2, 70 Gg OC, 50 Gg BC, and 9.7 Tg CO. These account for less than half (at most 43%) the decline in total $PM_{2.5}$ and alone would not achieve the $PM_{2.5}$ reduction targets. Most (57%) of the decline in $PM_{2.5}$ was due to interannual variability in meteorology. Specifically, a deeper planetary boundary layer, stronger winds, and lower relative humidity during the control period between October 2017 and March 2018. The ability to achieve air pollution reduction targets is an insufficient measure of the success of emission controls. Also required is diagnosis of the relative role of the emissions reductions and other influential factors like meteorology to enhance the efficacy of these measures when applied to other regions.

2.6 References

Amos, H. M., Jacob, D. J., Holmes, C. D., Fisher, J. A., Wang, Q., Yantosca, R. M., Corbitt, E. S., Galarneau, E., Rutter, A. P., Gustin, M. S., Steffen, A., Schauer, J. J., Graydon, J. A., St Louis, V. L., Talbot, R. W., Edgerton, E. S., Zhang, Y., and Sunderland, E. M.: Gas-particle partitioning of atmospheric Hg(II) and its effect on global mercury deposition, Atmos. Chem. Phys., 12, 591-603, https://doi.org/10.5194/acp-12-591-2012, 2012.

An, Z., Huang, R. J., Zhang, R., Tie, X., Li, G., Cao, J., Zhou, W., Shi, Z., Han, Y., Gu, Z., and Ji, Y.: Severe haze in northern China: A synergy of anthropogenic emissions and atmospheric processes, Proc. Natl. Acad. Sci. USA, 116, 8657-8666, https://doi.org/10.1073/pnas.1900125116, 2019.

Bei, N., Li, X., Tie, X., Zhao, L., Wu, J., Li, X., Liu, L., Shen, Z., and Li, G.: Impact of synoptic patterns and meteorological elements on the wintertime haze in the Beijing-Tianjin-Hebei region, China from 2013 to 2017, Sci. Total. Environ., 704, 135210, https://doi.org/10.1016/j.scitotenv.2019.135210, 2020.

Bloss, W. J., Kramer, L., Crilley, L. R., Vu, T., Harrison, R. M., Shi, Z. B., Lee, J. D., Squires, F. A., Whalley, L. K., Slater, E., Woodward-Massey, R., Ye, C. X., Heard, D. E., Tong, S. R., Hou, S. Q., Sun, Y. L., Xu, J. S., Wei, L. F., and Fu, P. Q.: Insights into air pollution chemistry and sulphate formation from nitrous acid (HONO) measurements during haze events in Beijing, Faraday Discussions, 226, 223-238, 10.1039/d0fd00100g, 2021.

Cheng, M. M., Zhi, G. R., Tang, W., Liu, S. J., Dang, H. Y., Guo, Z., Du, J. H., Du, X. H., Zhang, W. Q., Zhang, Y. J., and Meng, F.: Air pollutant emission from the underestimated households' coal consumption source in China, Science of the Total Environment, 580, 641-650, 10.1016/j.scitotenv.2016.12.143, 2017.

Dong, Z., Wang, S., Xing, J., Chang, X., Ding, D., and Zheng, H.: Regional transport in Beijing-Tianjin-Hebei region and its changes during 2014-2017: The impacts of meteorology and emission reduction, Sci. Total. Environ., 737, 139792, https://doi.org/10.1016/j.scitotenv.2020.139792, 2020.

Dunlea, E. J., Herndon, S. C., Nelson, D. D., Volkamer, R. M., San Martini, F., Sheehy, P. M., Zahniser, M. S., Shorter, J. H., Wormhoudt, J. C., Lamb, B. K., Allwine, E. J., Gaffney, J. S., Marley, N. A., Grutter, M., Marquez, C., Blanco, S., Cardenas, B., Retama, A., Villegas, C. R. R., Kolb, C. E., Molina, L. T., and Molina, M. J.: Evaluation of nitrogen dioxide chemiluminescence monitors in a polluted urban environment, Atmos. Chem. Phys., 7, 2691-2704, https://doi.org/10.5194/acp-7-2691-2007, 2007.

Fairlie, T. D., Jacob, D. J., and Park, R. J.: The impact of transpacific transport of mineral dust in the United States, Atmos. Environ., 41, 1251-1266, https://doi.org/10.1016/j.atmosenv.2006.09.048, 2007.

Fang, D., Chen, B., Hubacek, K., Ni, R., Chen, L., Feng, K., and Lin, J.: Clean air for some: Unintended spillover effects of regional air pollution policies, Sci. Adv., 5, eaav4707, https://doi.org/10.1126/sciadv.aav4707, 2019.

Feng, S. Z., Jiang, F., Wu, Z., Wang, H. M., Ju, W. M., and Wang, H. K.: CO Emissions Inferred From Surface CO Observations Over China in December 2013 and 2017, Journal of Geophysical Research-Atmospheres, 125, https://doi.org/10.1029/2019JD031808, 2020.

Fountoukis, C. and Nenes, A.: ISORROPIA II: a computationally efficient thermodynamic equilibrium model for K^+-Ca^{2+}-Mg^{2+}-NH_4^+-Na^+-SO_4^{2-}-NO_3^--Cl^--H_2O aerosols, Atmos. Chem. Phys., 7, 4639-4659, https://doi.org/10.5194/acp-7-4639-2007, 2007.

Fu, X., Wang, S. X., Xing, J., Zhang, X. Y., Wang, T., and Hao, J. M.: Increasing Ammonia Concentrations Reduce the Effectiveness of Particle Pollution Control Achieved via SO_2 and NO_X Emissions Reduction in East China, Environ. Sci. Tech. Lett., 4, 221-227, https://doi.org/10.1021/acs.estlett.7b00143, 2017.

Ge, B. Z., Xu, X. B., Ma, Z. Q., Pan, X. L., Wang, Z., Lin, W. L., Ouyang, B., Xu, D. H., Lee, J., Zheng, M., Ji, D. S., Sun, Y. L., Dong, H. B., Squires, F. A., Fu, P. Q., and Wang, Z. F.: Role of Ammonia on the Feedback Between AWC and Inorganic Aerosol Formation During Heavy Pollution in the North China Plain, Earth and Space Science, 6, 1675-1693, 10.1029/2019ea000799, 2019.

Harrison, R. M., Beddows, D. C. S., Alam, M. S., Singh, A., Brean, J., Xu, R. X., Kotthaus, S., and Grimmond, S.: Interpretation of particle number size distributions measured across an urban area during the FASTER campaign, Atmospheric Chemistry and Physics, 19, 39-55, 10.5194/acp-19-39-2019, 2019.

Heald, C. L., Jacob, D. J., Turquety, S., Hudman, R. C., Weber, R. J., Sullivan, A. P., Peltier, R. E., Atlas, E. L., de Gouw, J. A., Warneke, C., Holloway, J. S., Neuman, J. A., Flocke, F. M., and Seinfeld, J. H.: Concentrations and sources of organic carbon aerosols in the free troposphere over North America, J. Geophys. Res. Atmos., 111, D23S47, https://doi.org/10.1029/2006jd007705, 2006.

Hong, C. P., Zhang, Q., He, K. B., Guan, D. B., Li, M., Liu, F., and Zheng, B.: Variations of China's emission estimates: response to uncertainties in energy statistics, Atmospheric Chemistry and Physics, 17, 1227-1239, 10.5194/acp-17-1227-2017, 2017.

Huang, R. J., Zhang, Y., Bozzetti, C., Ho, K. F., Cao, J. J., Han, Y., Daellenbach, K. R., Slowik, J. G., Platt, S. M., Canonaco, F., Zotter, P., Wolf, R., Pieber, S. M., Bruns, E. A., Crippa, M., Ciarelli, G., Piazzalunga, A., Schwikowski, M., Abbaszade, G., Schnelle-Kreis, J., Zimmermann, R., An, Z., Szidat, S., Baltensperger, U., El Haddad, I., and Prevot, A. S.: High secondary aerosol contribution to particulate pollution during haze events in China, Nature, 514, 218-222, https://doi.org/10.1038/nature13774, 2014.

Huang, X., Song, Y., Li, M. M., Li, J. F., Huo, Q., Cai, X. H., Zhu, T., Hu, M., and Zhang, H. S.: A high-resolution ammonia emission inventory in China, Global Biogeochem. Cy., 26, GB1030, https://doi.org/10.1029/2011gb004161, 2012.

Jaeglé, L., Quinn, P. K., Bates, T. S., Alexander, B., and Lin, J. T.: Global distribution of sea salt aerosols: new constraints from in situ and remote sensing observations, Atmospheric Chemistry and Physics, 11, 3137-3157, 10.5194/acp-11-3137-2011, 2011.

Joshi, R., Liu, D. T., Nemitz, E., Langford, B., Mullinger, N., Squires, F., Lee, J., Wu, Y. F., Pan, X. L., Fu, P. Q., Kotthaus, S., Grimmond, S., Zhang, Q., Wu, R. L., Wild, O., Flynn, M., Coe, H., and Allan, J.: Direct measurements of black carbon fluxes in central Beijing using the eddy covariance method, Atmos. Chem. Phys., 21, 147-162, https://doi.org/10.5194/acp-21-147-2021, 2021.

Kebabian, P. L., Herndon, S. C., and Freedman, A.: Detection of nitrogen dioxide by cavity attenuated phase shift spectroscopy, Analytical Chemistry, 77, 724-728, 10.1021/ac048715y, 2005.

Kong, L., Tang, X., Zhu, J., Wang, Z., Pan, Y., Wu, H., Wu, L., Wu, Q., He, Y., Tian, S., Xie, Y., Liu, Z., Sui, W., Han, L., and Carmichael, G.: Improved Inversion of Monthly Ammonia Emissions in China Based on the Chinese Ammonia Monitoring Network and Ensemble Kalman Filter, Environ. Sci. Technol., 53, 12529-12538, https://doi.org/10.1021/acs.est.9b02701, 2019.

Kong, L., Tang, X., Zhu, J., Wang, Z. F., Fu, J. S., Wang, X. M., Itahashi, S., Yamaji, K., Nagashima, T., Lee, H. J., Kim, C. H., Lin, C. Y., Chen, L., Zhang, M. G., Tao, Z. N., Li, J., Kajino, M., Liao, H., Wang, Z., Sudo, K., Wang, Y. S., Pan, Y. P., Tang, G. Q., Li, M., Wu, Q. Z., Ge, B. Z., and Carmichael, G. R.: Evaluation and uncertainty investigation of the NO2, CO and NH3 modeling over China under the framework of MICS-Asia III, Atmospheric Chemistry and Physics, 20, 181-202, 10.5194/acp-20-181-2020, 2020.

Koukouli, M. E., Theys, N., Ding, J. Y., Zyrichidou, I., Mijling, B., Balis, D., and Johannes, V. R.: Updated SO_2 emission estimates over China using OMI/Aura observations, Atmospheric Measurement Techniques, 11, 1817-1832, 10.5194/amt-11-1817-2018, 2018.

Le, T., Wang, Y., Liu, L., Yang, J., Yung, Y. L., Li, G., and Seinfeld, J. H.: Unexpected air pollution with marked emission reductions during the COVID-19 outbreak in China, Science, 369, 702-706, https://doi.org/10.1126/science.abb7431, 2020.

Li, K., Jacob, D. J., Liao, H., Shen, L., Zhang, Q., and Bates, K. H.: Anthropogenic drivers of 2013-2017 trends in summer surface ozone in China, Proc. Natl. Acad. Sci. USA, 116, 422-427, https://doi.org/10.1073/pnas.1812168116, 2019a.

Li, K., Liao, H., Mao, Y. H., and Ridley, D. A.: Source sector and region contributions to concentration and direct radiative forcing of black carbon in China, Atmos. Environ., 124, 351-366, https://doi.org/10.1016/j.atmosenv.2015.06.014, 2016.

Li, M., Liu, H., Geng, G. N., Hong, C. P., Liu, F., Song, Y., Tong, D., Zheng, B., Cui, H. Y., Man, H. Y., Zhang, Q., and He, K. B.: Anthropogenic emission inventories in China: a review, Natl. Sci. Rev., 4, 834-866, https://doi.org/10.1093/nsr/nwx150, 2017.

Li, M., Zhang, Q., Streets, D. G., He, K. B., Cheng, Y. F., Emmons, L. K., Huo, H., Kang, S. C., Lu, Z., Shao, M., Su, H., Yu, X., and Zhang, Y.: Mapping Asian anthropogenic emissions of non-methane volatile organic compounds to multiple chemical mechanisms, Atmos. Chem. Phys., 14, 5617-5638, https://doi.org/10.5194/acp-14-5617-2014, 2014.

Li, M., Zhang, Q., Zheng, B., Tong, D., Lei, Y., Liu, F., Hong, C. P., Kang, S. C., Yan, L., Zhang, Y. X., Bo, Y., Su, H., Cheng, Y. F., and He, K. B.: Persistent growth of anthropogenic non-methane volatile organic compound (NMVOC) emissions in China during 1990-2017: drivers, speciation and ozone formation potential, Atmos. Chem. Phys., 19, 8897-8913, https://doi.org/10.5194/acp-19-8897-2019, 2019b.

Li, X. R., Zhang, C. L., Liu, P. F., Liu, J. F., Zhang, Y. Y., Liu, C. T., and Mu, Y. J.: Significant influence of the intensive agricultural activities on atmospheric $PM_{2.5}$ during autumn harvest seasons in a rural area of the North China Plain, Atmos. Environ., 241, 117844, https://doi.org/10.1016/j.atmosenv.2020.117844, 2020.

Liu, H., Jacob, D. J., Bey, I., and Yantosca, R. M.: Constraints from ^{210}Pb and ^{7}Be on wet deposition and transport in a global three-dimensional chemical tracer model driven by assimilated meteorological fields, J. Geophys. Res. Atmos., 106, 12109-12128, https://doi.org/10.1029/2000jd900839, 2001.

Liu, M. X., Huang, X., Song, Y., Xu, T. T., Wang, S. X., Wu, Z. J., Hu, M., Zhang, L., Zhang, Q., Pan, Y. P., Liu, X. J., and Zhu, T.: Rapid SO_2 emission reductions significantly increase tropospheric ammonia concentrations over the North China Plain, Atmos. Chem. Phys., 18, 17933-17943, https://doi.org/10.5194/acp-18-17933-2018, 2018.

Luo, G., Yu, F. Q., and Moch, J. M.: Further improvement of wet process treatments in GEOS-Chem v12.6.0: impact on global distributions of aerosols and aerosol precursors, Geosci. Model Dev., 13, 2879-2903, https://doi.org/10.5194/gmd-13-2879-2020, 2020.

Luo, G., Yu, F. Q., and Schwab, J.: Revised treatment of wet scavenging processes dramatically improves GEOS-Chem 12.0.0 simulations of surface nitric acid, nitrate, and ammonium over the United States, Geosci. Model Dev., 12, 3439-3447, https://doi.org/10.5194/gmd-12-3439-2019, 2019.

Ma, Q. A., Cai, S. Y., Wang, S. X., Zhao, B., Martin, R. V., Brauer, M., Cohen, A., Jiang, J. K., Zhou, W., Hao, J. M., Frostad, J., Forouzanfar, M. H., and Burnett, R. T.: Impacts of coal burning on ambient $PM_{2.5}$ pollution in China, Atmos. Chem. Phys., 17, 4477-4491, https://doi.org/10.5194/acp-17-4477-2017, 2017.

Marais, E. A., Pandey, A. K., Van Damme, M., Clarisse, L., Coheur, P. F., Shephard, M. W., Cady-Pereira, K. E., Misselbrook, T., Zhu, L., Luo, G., and Yu, F. Q.: UK Ammonia Emissions Estimated With Satellite Observations and GEOS-Chem, Journal of Geophysical Research-Atmospheres, 126, 10.1029/2021jd035237, 2021.

Martini, F. M. S., Hasenkopf, C. A., and Roberts, D. C.: Statistical analysis of $PM_{2.5}$ observations from diplomatic facilities in China, Atmos. Environ., 110, 174-185, https://doi.org/10.1016/j.atmosenv.2015.03.060, 2015.

Ministry of Ecology and Environment, the People's Republic of China (MEE).Ambient air quality standards GB3095-2012 (in Chinese), available at: https://www.mee.gov.cn/ywgz/fgbz/bz/bzwb/dqhjbh/dqhjzlbz/201203/t20120302_224165.shtml (last access: 04 March 2021), 2012.

Ministry of Ecology and Environment, the People's Republic of China (MEE).Air Pollution Comprehensive Management Action Plan in the Autumn and Winter of 2017-2018 for the Beijing-Tianjin-Hebei Region and its Surrounding Areas (in Chinese), available at: https://www.mee.gov.cn/gkml/sthjbgw/sthjbwj/201809/t20180927_630570.htm (last access: 04 March 2021), 2017.

Ministry of Ecology and Environment, the People's Republic of China (MEE).Letter on notifying the completion of air quality targets in the Beijing-Tianjin-Hebei air pollution transmission channel cities in autumn and winter (in Chinese), available at: http://www.mee.gov.cn/gkml/sthjbgw/stbgth/201805/t20180503_435855.htm (last access: 04 March 2021), 2018.

Ministry of Ecology and Environment (MEE), the People's Republic of China.Air Pollution Comprehensive Management Action Plan in the Autumn and Winter of 2020-2021 for the Beijing-Tianjin-Hebei Region and its Surrounding Areas and the Fenwei Plain (in Chinese), available at: https://www.mee.gov.cn/xxgk2018/xxgk/xxgk03/202011/t20201103_806152.html (last access: 04 March 2021), 2020a.

Ministry of Ecology and Environment (MEE), the People's Republic of China.Air Pollution Comprehensive Management Action Plan in the Autumn and Winter of 2020-2021 for the Yangtze River Delta Region (in Chinese), available at: https://www.mee.gov.cn/xxgk2018/xxgk/xxgk03/202011/t20201103_806151.html (last access: 04 March 2021), 2020b.

Miao, R. Q., Chen, Q., Zheng, Y., Cheng, X., Sun, Y. L., Palmer, P. I., Shrivastava, M., Guo, J. P., Zhang, Q., Liu, Y. H., Tan, Z. F., Ma, X. F., Chen, S. Y., Zeng, L. M., Lu, K. D., and Zhang, Y. H.: Model bias in simulating major chemical components of $PM_{2.5}$ in China, Atmos. Chem. Phys., 20, 12265-12284, https://doi.org/10.5194/acp-20-12265-2020, 2020.

Miller, C. C., Jacob, D. J., Abad, G. G., and Chance, K.: Hotspot of glyoxal over the Pearl River delta seen from the OMI satellite instrument: implications for emissions of aromatic hydrocarbons, Atmospheric Chemistry and Physics, 16, 4631-4639, 10.5194/acp-16-4631-2016, 2016.

Moch, J. M., Dovrou, E., Mickley, L. J., Keutsch, F. N., Cheng, Y., Jacob, D. J., Jiang, J. K., Li, M., Munger, J. W., Qiao, X. H., and Zhang, Q.: Contribution of Hydroxymethane Sulfonate to Ambient Particulate Matter: A Potential Explanation for High Particulate Sulfur During Severe Winter Haze in Beijing, Geophys. Res. Lett., 45, 11969-11979, https://doi.org/10.1029/2018gl079309, 2018.

Pan, Y., Tian, S., Zhao, Y., Zhang, L., Zhu, X., Gao, J., Huang, W., Zhou, Y., Song, Y., Zhang, Q., and Wang, Y.: Identifying Ammonia Hotspots in China Using a National Observation Network, Environ. Sci. Technol., 52, 3926-3934, https://doi.org/10.1021/acs.est.7b05235, 2018.

Park, R. J., Jacob, D. J., Field, B. D., Yantosca, R. M., and Chin, M.: Natural and transboundary pollution influences on sulfate-nitrate-ammonium aerosols in the United States: Implications for policy, J. Geophys. Res. Atmos., 109, D15204, https://doi.org/10.1029/2003jd004473, 2004.

Peng, L. Q., Zhang, Q., Yao, Z. L., Mauzerall, D. L., Kang, S. C., Du, Z. Y., Zheng, Y. X., Xue, T., and He, K. B.: Underreported coal in statistics: A survey-based solid fuel consumption and emission inventory for the rural residential sector in China, Appl. Energ., 235, 1169-1182, https://doi.org/10.1016/j.apenergy.2018.11.043, 2019.

Reed, C., Evans, M. J., Di Carlo, P., Lee, J. D., and Carpenter, L. J.: Interferences in photolytic NO_2 measurements: explanation for an apparent missing oxidant?, Atmos. Chem. Phys., 16, 4707-4724, https://doi.org/10.5194/acp-16-4707-2016, 2016.

Shah, V., Jacob, D. J., Li, K., Silvern, R. F., Zhai, S. X., Liu, M. Y., Lin, J. T., and Zhang, Q.: Effect of changing NO_x lifetime on the seasonality and long-term trends of satellite-observed tropospheric NO_2 columns over China, Atmos. Chem. Phys., 20, 1483-1495, https://doi.org/10.5194/acp-20-1483-2020, 2020.

Shi, Y. Q., Xi, Z. Y., Simayi, M., Li, J., and Xie, S. D.: Scattered coal is the largest source of ambient volatile organic compounds during the heating season in Beijing, Atmos. Chem. Phys., 20, 9351-9369, https://doi.org/10.5194/acp-20-9351-2020, 2020.

Shi, Z. B., Vu, T., Kotthaus, S., Harrison, R. M., Grimmond, S., Yue, S., Zhu, T., Lee, J., Han, Y., Demuzere, M., Dunmore, R. E., Ren, L. J., Liu, D., Wang, Y. L., Wild, O., Allan, J., Acton, W. J., Barlow, J., Barratt, B., Beddows, D., Bloss, W. J., Calzolai, G., Carruthers, D., Carslaw, D. C., Chan, Q., Chatzidiakou, L., Chen, Y., Crilley, L., Coe, H., Dai, T., Doherty, R., Duan, F., Fu, P., Ge, B., Ge, M., Guan, D., Hamilton, J. F., He, K., Heal, M., Heard, D., Hewitt, C. N., Hollaway, M., Hu, M., Ji, D., Jiang, X. J., Jones, R., Kalberer, M., Kelly, F. J., Kramer, L., Langford, B., Lin, C., Lewis, A. C., Li, J., Li, W., Liu, H., Liu, J. F., Loh, M., Lu, K. D., Lucarelli, F., Mann, G., McFiggans, G., Miller, M. R., Mills, G., Monk, P., Nemitz, E., O'Connor, F., Ouyang, B., Palmer, P. I., Percival, C., Popoola, O., Reeves, C., Rickard, A. R., Shao, L. Y., Shi, G. Y., Spracklen, D., Stevenson, D., Sun, Y., Sun, Z. W., Tao, S., Tong, S. R., Wang, Q. Q., Wang, W. H., Wang, X. M., Wang, X. J., Wang, Z. F., Wei, L. F., Whalley, L., Wu, X. F., Wu, Z. J., Xie, P. H., Yang, F. M., Zhang, Q., Zhang, Y. L., Zhang, Y. H., and Zheng, M.: Introduction to the special issue "In-depth study of air pollution sources and processes within Beijing and its surrounding region (APHH-Beijing)", Atmos. Chem. Phys., 19, 7519-7546, https://doi.org/10.5194/acp-19-7519-2019, 2019.

Silver, B., Reddington, C. L., Arnold, S. R., and Spracklen, D. V.: Substantial changes in air pollution across China during 2015-2017, Environ. Res. Lett., 13, 114012, https://doi.org/10.1088/1748-9326/aae718, 2018.

Song, S. J., Gao, M., Xu, W. Q., Sun, Y. L., Worsnop, D. R., Jayne, J. T., Zhang, Y. Z., Zhu, L., Li, M., Zhou, Z., Cheng, C. L., Lv, Y. B., Wang, Y., Peng, W., Xu, X. B., Lin, N., Wang, Y. X., Wang, S. X., Munger, J. W., Jacob, D. J., and McElroy, M. B.: Possible heterogeneous chemistry of hydroxymethanesulfonate (HMS) in northern China winter haze, Atmos. Chem. Phys., 19, 1357-1371, https://doi.org/10.5194/acp-19-1357-2019, 2019.

Squires, F. A., Nemitz, E., Langford, B., Wild, O., Drysdale, W. S., Acton, W. J. F., Fu, P. Q., Grimmond, C. S. B., Hamilton, J. F., Hewitt, C. N., Hollaway, M., Kotthaus, S., Lee, J., Metzger, S., Pingintha-Durden, N., Shaw, M., Vaughan, A. R., Wang, X. M., Wu, R. L., Zhang, Q., and Zhang, Y. L.: Measurements of traffic-dominated pollutant emissions in a Chinese megacity, Atmos. Chem. Phys., 20, 8737-8761, https://doi.org/10.5194/acp-20-8737-2020, 2020.

Srivastava, D., Xu, J., Vu, T. V., Liu, D., Li, L., Fu, P., Hou, S., Moreno Palmerola, N., Shi, Z., and Harrison, R. M.: Insight into $PM_{2.5}$ sources by applying positive matrix factorization (PMF) at urban and rural sites of Beijing, Atmos. Chem. Phys., 21, 14703-14724, 10.5194/acp-21-14703-2021, 2021.

Tong, R. P., Liu, J. F., Wang, W., and Fang, Y. Q.: Health effects of $PM_{2.5}$ emissions from on-road vehicles during weekdays and weekends in Beijing, China, Atmos. Environ., 223, 117258, https://doi.org/10.1016/j.atmosenv.2019.117258, 2020.

Vu, T. V., Shi, Z. B., Cheng, J., Zhang, Q., He, K. B., Wang, S. X., and Harrison, R. M.: Assessing the impact of clean air action on air quality trends in Beijing using a machine learning technique, Atmos. Chem. Phys., 19, 11303-11314, https://doi.org/10.5194/acp-19-11303-2019, 2019.

Wan, Y. T., Xu, M. Y., Huang, H., and Chen, S. X.: A spatio-temporal model for the analysis and prediction of fine particulate matter concentration in Beijing, Environmetrics, 32, e2648, https://doi.org/10.1002/env.2648, 2021.

Wang, G., Zhang, R., Gomez, M. E., Yang, L., Levy Zamora, M., Hu, M., Lin, Y., Peng, J., Guo, S., Meng, J., Li, J., Cheng, C., Hu, T., Ren, Y., Wang, Y., Gao, J., Cao, J., An, Z., Zhou, W., Li, G., Wang, J., Tian, P., Marrero-Ortiz, W., Secrest, J., Du, Z., Zheng, J., Shang, D., Zeng, L., Shao, M., Wang, W., Huang, Y., Wang, Y., Zhu, Y., Li, Y., Hu, J., Pan, B., Cai, L., Cheng, Y., Ji, Y., Zhang, F., Rosenfeld, D., Liss, P. S., Duce, R. A., Kolb, C. E., and Molina, M. J.: Persistent sulfate formation from London Fog to Chinese haze, Proc. Natl. Acad. Sci. USA, 113, 13630-13635, https://doi.org/10.1073/pnas.1616540113, 2016.

Wang, J., Li, J., Ye, J., Zhao, J., Wu, Y., Hu, J., Liu, D., Nie, D., Shen, F., Huang, X., Huang, D. D., Ji, D., Sun, X., Xu, W., Guo, J., Song, S., Qin, Y., Liu, P., Turner, J. R., Lee, H. C., Hwang, S., Liao, H., Martin, S. T., Zhang, Q., Chen, M., Sun, Y., Ge, X., and Jacob, D. J.: Fast sulfate formation from oxidation of SO_2 by NO_2 and HONO observed in Beijing haze, Nat. Commun., 11, 2844, https://doi.org/10.1038/s41467-020-16683-x, 2020.

Wang, J., Ye, J., Zhang, Q., Zhao, J., Wu, Y., Li, J., Liu, D., Li, W., Zhang, Y., Wu, C., Xie, C., Qin, Y., Lei, Y., Huang, X., Guo, J., Liu, P., Fu, P., Li, Y., Lee, H. C., Choi, H., Zhang, J., Liao, H., Chen, M., Sun, Y., Ge, X., Martin, S. T., and Jacob, D. J.: Aqueous production of secondary organic aerosol from fossil-fuel emissions in winter Beijing haze, Proc. Natl. Acad. Sci. USA, 118, e2022179118, https://doi.org/10.1073/pnas.2022179118, 2021.

Wang, Y., Jacob, D. J., and Logan, J. A.: Global simulation of tropospheric O_3-NO_x-hydrocarbon chemistry: 1. Model formulation, J. Geophys. Res. Atmos., 103, 10713-10725, https://doi.org/10.1029/98jd00158, 1998.

Wang, Y., Ying, Q., Hu, J., and Zhang, H.: Spatial and temporal variations of six criteria air pollutants in 31 provincial capital cities in China during 2013-2014, Environ. Int., 73, 413-422, https://doi.org/10.1016/j.envint.2014.08.016, 2014.

Wang, Y., Zhang, Q. Q., He, K., Zhang, Q., and Chai, L.: Sulfate-nitrate-ammonium aerosols over China: response to 2000-2015 emission changes of sulfur dioxide, nitrogen oxides, and ammonia, Atmos. Chem. Phys., 13, 2635-2652, https://doi.org/10.5194/acp-13-2635-2013, 2013.

Wang, Y. S., Li, W. J., Gao, W. K., Liu, Z. R., Tian, S. L., Shen, R. R., Ji, D. S., Wang, S., Wang, L. L., Tang, G. Q., Song, T., Cheng, M. T., Wang, G. H., Gong, Z. Y., Hao, J. M., and Zhang, Y. H.: Trends in particulate matter and its chemical compositions in China from 2013-2017, Sci. China Earth Sci., 62, 1857-1871, https://doi.org/10.1007/s11430-018-9373-1, 2019.

WHO (World Health Organization). (2021). WHO global air quality guidelines: particulate matter (PM2.5 and PM10), ozone, nitrogen dioxide, sulfur dioxide and carbon monoxide. World Health Organization. https://apps.who.int/iris/handle/10665/345329. License: CC BY-NC-SA 3.0 IGO

Wu, H. J., Tang, X., Wang, Z. F., Wu, L., Lu, M. M., Wei, L. F., and Zhu, J.: Probabilistic Automatic Outlier Detection for Surface Air Quality Measurements from the China National Environmental Monitoring Network, Adv. Atmos. Sci., 35, 1522-1532, https://doi.org/10.1007/s00376-018-8067-9, 2018.

Wu, J., Bei, N., Hu, B., Liu, S., Zhou, M., Wang, Q., Li, X., Liu, L., Feng, T., Liu, Z., Wang, Y., Cao, J., Tie, X., Wang, J., Molina, L. T., and Li, G.: Is water vapor a key player of the wintertime haze in North China Plain?, Atmos. Chem. Phys., 19, 8721-8739, https://doi.org/10.5194/acp-19-8721-2019, 2019.

Xia, Y. M., Zhao, Y., and Nielsen, C. P.: Benefits of of China's efforts in gaseous pollutant control indicated by the bottom-up emissions and satellite observations 2000-2014, Atmospheric Environment, 136, 43-53, 10.1016/j.atmosenv.2016.04.013, 2016.

Xing, L., Fu, T. M., Cao, J. J., Lee, S. C., Wang, G. H., Ho, K. F., Cheng, M. C., You, C. F., and Wang, T. J.: Seasonal and spatial variability of the OM/OC mass ratios and high regional correlation between oxalic acid and zinc in Chinese urban organic aerosols, Atmos. Chem. Phys., 13, 4307-4318, https://doi.org/10.5194/acp-13-4307-2013, 2013.

Xu, J., Liu, D., Wu, X., Vu, T. V., Zhang, Y., Fu, P., Sun, Y., Xu, W., Zheng, B., Harrison, R. M., and Shi, Z.: Source apportionment of fine organic carbon at an urban site of Beijing using a chemical mass balance model, Atmos. Chem. Phys., 21, 7321-7341, https://doi.org/10.5194/acp-21-7321-2021, 2021.

Yang, G., Liu, Y., and Li, X.: Spatiotemporal distribution of ground-level ozone in China at a city level, Sci. Rep., 10, 7229, https://doi.org/10.1038/s41598-020-64111-3, 2020.

Yun, X., Shen, G., Shen, H., Meng, W., Chen, Y., Xu, H., Ren, Y., Zhong, Q., Du, W., Ma, J., Cheng, H., Wang, X., Liu, J., Wang, X., Li, B., Hu, J., Wan, Y., and Tao, S.: Residential solid fuel emissions contribute significantly to air pollution and associated health impacts in China, Sci. Adv., 6, eaba7621, https://doi.org/10.1126/sciadv.aba7621, 2020.

Zhai, S. X., Jacob, D. J., Wang, X., Shen, L., Li, K., Zhang, Y. Z., Gui, K., Zhao, T. L., and Liao, H.: Fine particulate matter ($PM_{2.5}$) trends in China, 2013-2018: separating contributions from anthropogenic emissions and meteorology, Atmos. Chem. Phys., 19, 11031-11041, https://doi.org/10.5194/acp-19-11031-2019, 2019.

Zhang, F., Shi, Y., Fang, D., Ma, G., Nie, C., Krafft, T., He, L., and Wang, Y.: Monitoring history and change trends of ambient air quality in China during the past four decades, J. Environ. Manage, 260, 110031, https://doi.org/10.1016/j.jenvman.2019.110031, 2020.

Zhang, Q., Zheng, Y., Tong, D., Shao, M., Wang, S., Zhang, Y., Xu, X., Wang, J., He, H., Liu, W., Ding, Y., Lei, Y., Li, J., Wang, Z., Zhang, X., Wang, Y., Cheng, J., Liu, Y., Shi, Q., Yan, L., Geng, G., Hong, C., Li, M., Liu, F., Zheng, B., Cao, J., Ding, A., Gao, J., Fu, Q., Huo, J., Liu, B., Liu, Z., Yang, F., He, K., and Hao, J.: Drivers of improved $PM_{2.5}$ air quality in China from 2013 to 2017, Proc. Natl. Acad. Sci. USA, 116, 24463-24469, https://doi.org/10.1073/pnas.1907956116, 2019.

Zhang, X., Wu, Y., Liu, X., Reis, S., Jin, J., Dragosits, U., Van Damme, M., Clarisse, L., Whitburn, S., Coheur, P. F., and Gu, B.: Ammonia Emissions May Be Substantially Underestimated in China, Environ. Sci. Technol., 51, 12089-12096, https://doi.org/10.1021/acs.est.7b02171, 2017a.

Zhang, Y., Cai, J., Wang, S., He, K., and Zheng, M.: Review of receptor-based source apportionment research of fine particulate matter and its challenges in China, Sci. Total. Environ., 586, 917-929, https://doi.org/10.1016/j.scitotenv.2017.02.071, 2017b.

Zhang, Y., Chen, X., Yu, S., Wang, L., Li, Z., Li, M., Liu, W., Li, P., Rosenfeld, D., and Seinfeld, J. H.: City-level air quality improvement in the Beijing-Tianjin-Hebei region from 2016/17 to 2017/18 heating seasons: Attributions and process analysis, Environ. Pollut., 274, 116523, https://doi.org/10.1016/j.envpol.2021.116523, 2021.

Zhang, Y. P., Li, X., Nie, T., Qi, J., Chen, J., and Wu, Q.: Source apportionment of $PM_{2.5}$ pollution in the central six districts of Beijing, China, J. Clean Prod., 174, 661-669, https://doi.org/10.1016/j.jclepro.2017.10.332, 2018.

Zheng, B., Tong, D., Li, M., Liu, F., Hong, C. P., Geng, G. N., Li, H. Y., Li, X., Peng, L. Q., Qi, J., Yan, L., Zhang, Y. X., Zhao, H. Y., Zheng, Y. X., He, K. B., and Zhang, Q.: Trends in China's anthropogenic emissions since 2010 as the consequence of clean air actions, Atmos. Chem. Phys., 18, 14095-14111, https://doi.org/10.5194/acp-18-14095-2018, 2018.

Zheng, M., Yan, C. Q., Wang, S. X., He, K. B., and Zhang, Y. H.: Understanding $PM_{2.5}$ sources in China: challenges and perspectives, Natl. Sci. Rev., 4, 801-803, https://doi.org/10.1093/nsr/nwx129, 2017.

Zhi, G. R., Zhang, Y. Y., Sun, J. Z., Cheng, M. M., Dang, H. Y., Liu, S. J., Yang, J. C., Zhang, Y. Z., Xue, Z. G., Li, S. Y., and Meng, F.: Village energy survey reveals missing rural raw coal in northern China: Significance in science and policy, Environmental Pollution, 223, 705-712, 10.1016/j.envpol.2017.02.009, 2017.

2.7 Supplementary Information

Supplementary Text

Non-linear relationship between concentrations and emissions

The non-linear relationship between changes in modelled concentrations and perturbations in emissions of NO_x, SO_2 and CO are quantified by dividing the ratio of GEOS-Chem scaled-to-original surface concentrations by the MEIC correction factors:

$$\text{Non-linear response} = \frac{X_{\text{scaled}}}{X_{\text{original}} \times \left(\frac{E_{\text{scaled}}}{E_{\text{original}}}\right)} \tag{S1}$$

where X is the surface concentration of either NO_2, SO_2, or CO, ($E_{\text{scaled}}/E_{\text{original}}$) is the correction factor applied to the MEIC in AW2016 (see Section 3.2 of the main text for more details).

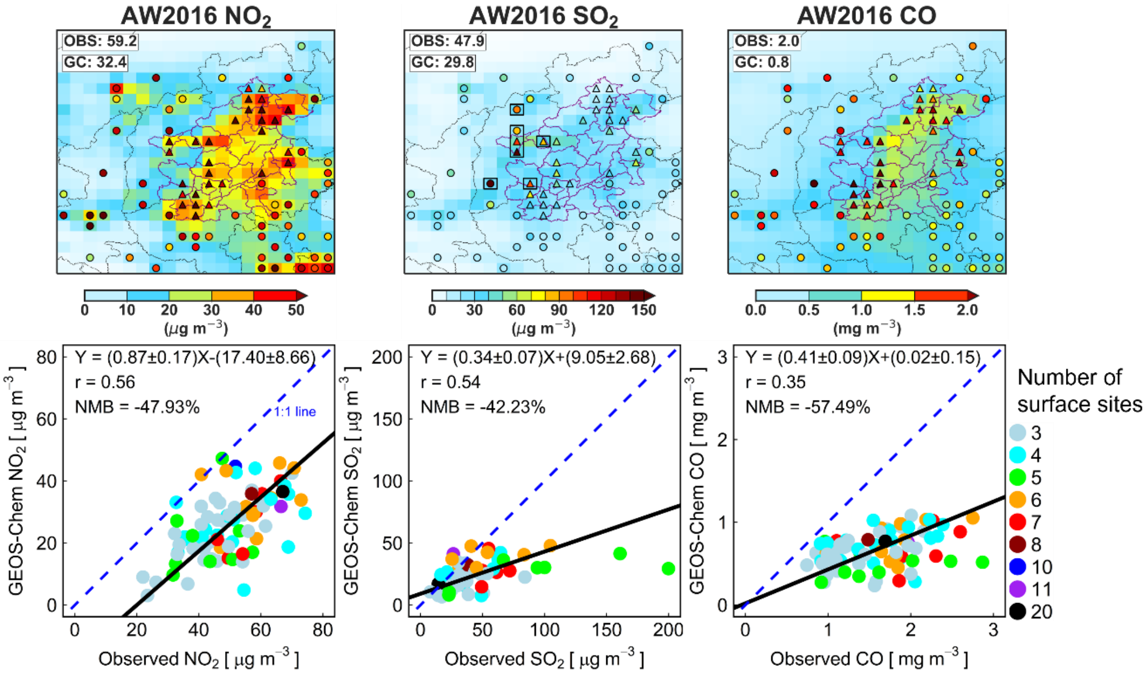

Figure S2.1: Initial comparison of observed and modelled NO$_2$, SO$_2$ and CO in AW2016. The model uses default MEIC emissions. The top row shows maps of observed (shapes) and modelled (background) NO$_2$ (left), SO$_2$ (centre) and CO (right). Shapes are means for grid squares with at least three coincident sites. Observations are distinguished as within (triangles) and outside (circles) the emission control region (grey shaded area in Figure 2.3). Inset values are the observed (OBS) and modelled (GC) means for sites and coincident grids in the emission control domain. The black boxes for SO$_2$ highlight the seven grids with model underestimates ranging from a factor of 2.1 to 6.8. The bottom row shows regresses observed vs modelled NO$_2$ (left), SO$_2$ (middle) and CO (right). Points are coloured by the number of surface sites in each model grid. RMA regression statistics, Pearson's correlation coefficients (r), and model normalized mean biases (NMB) are given. Lines are the RMA regression (black) and 1:1 line (blue dashed).

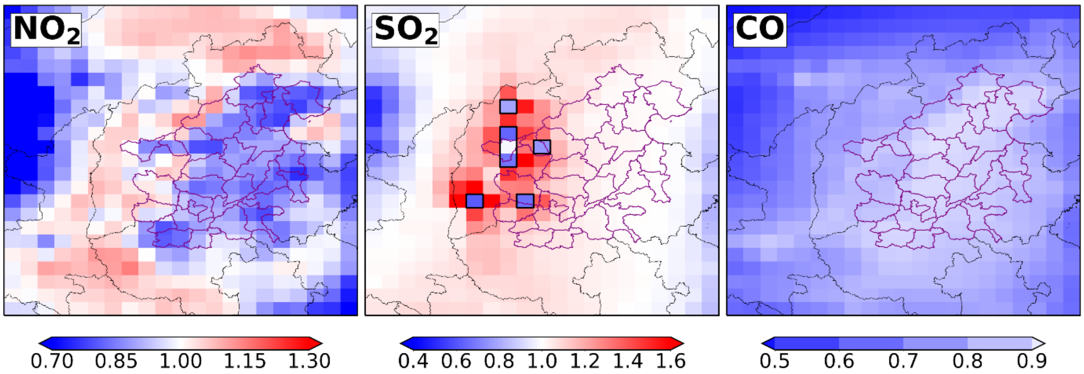

Figure S2.2: Non-linear relationship between air pollutant surface concentrations and emissions perturbations. Individual model grids are calculated using Equation (S1) in AW2016 for NO_2 concentrations and NO_x emissions, SO_2, and CO. Values of unity indicate non-linear effects are negligible.

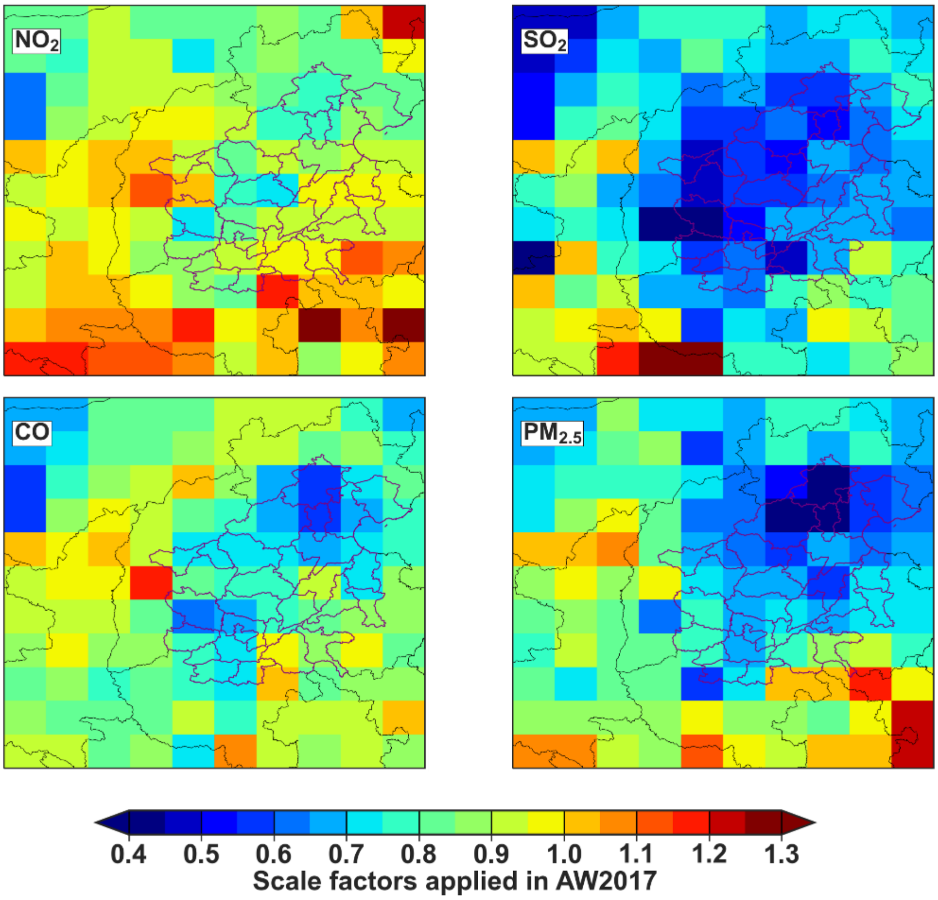

Figure S2.3: Scale factors applied to MEIC emissions in AW2016 to estimate emissions in the control period (AW2017). See Section 3.3 of the main text for more details.

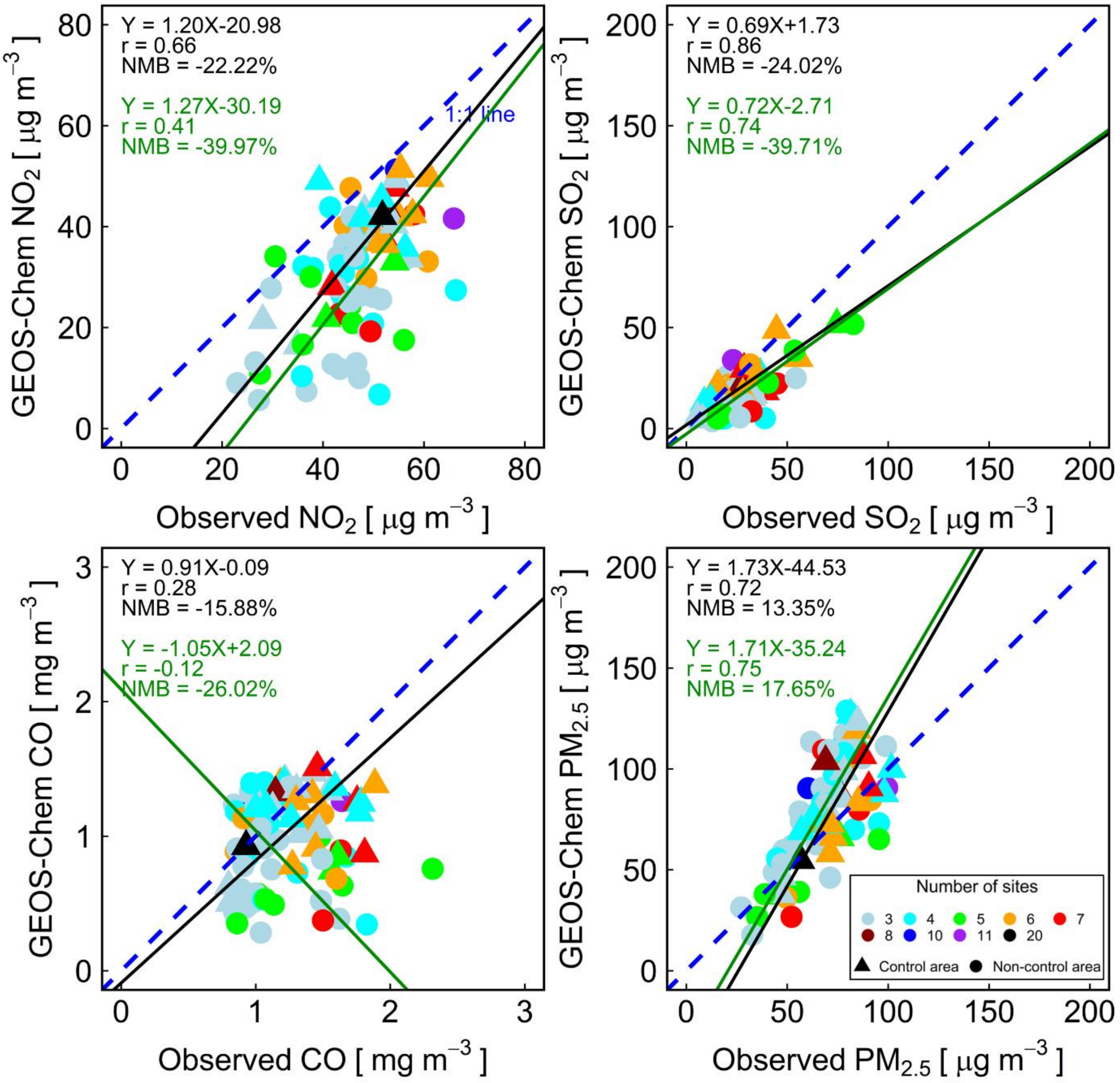

Figure S2.4: Evaluation of GEOS-Chem simulation of air pollutant concentrations in AW2017. Observations are averaged onto the GEOS-Chem grid. Panels show results for simulated and observed NO_2 (top left), SO_2 (top right), CO (bottom left) and $PM_{2.5}$ (bottom right) in the entire domain in Figure 2.3 for grid squares with at least three coincident surface sites. Triangles indicate data in BTH (grey area in Figure 2.3) and circles indicate data outside BTH coloured by the number of sites in each grid. The model uses scaled MEIC emissions (see text for details). RMA regression statistics, Pearson's correlation coefficients (r), and model normalized mean biases (NMB) are given for BTH grids (black text) and non-BTH grids (green text). Lines are the RMA regression lines (black for BTH grids and green for non-BTH grids) and 1:1 line (blue dashed).

Table S2.1: Sites used to assess national and regional air quality monitoring networks in the Beijing-Tianjin-Hebei region (BTH).

Network Site		**Independent Site**		**Distances**	**Comparison Period**	**Air Pollutants**
Name	Location	Name	Location			
CNEMN Aotizhongxin[a]	(39.98°N, 116.40°E)	APHH IAP[b]	(39.97°N, 116.37°E)	~3 km	Oct-Nov 2016	$PM_{2\ 5}$ SO_2, NO_2, CO
CNEMN Nongzhanguan[a]	(39.94°N, 116.46°E)	US Embassy[c]	(39.95°N, 116.47°E)	~1 km	Oct 2016-Mar 2017 Oct 2017-Mar 2018	$PM_{2\ 5}$
BJMEMN Xizhimenbei[d]	(39.95°N, 116.35°E)	APHH IAP		~3 km	Oct-Nov 2016	$PM_{2\ 5}$ SO_2, NO_2, CO
BJMEMN Dongsihuan[d]	(39.94°N, 116.48°E)	US Embassy		~1 km	Oct 2016-Mar 2017 Oct 2017-Mar 2018	$PM_{2\ 5}$

[a] CNEMN site, data source: http://beijingair.sinaapp.com/ (last accessed 17 October 2020), now hosted at https://quotsoft.net/air; [b] APHH campaign at IAP, data source: National Environmental Research Council Centre for Environmental Data Archive (Fleming et al., 2017); [c] US Embassy $PM_{2.5}$ measurements, data sources: http://www.stateair.net/ for October 2016-March 2017, http://www.openaq.org/ for October 2017-March 2018; [d] BJMEMN site, data source: http://beijingair.sinaapp.com/ (last accessed: 17 October 2020), now hosted at https://quotsoft.net/air

Fleming, Z. L., Lee, J. D., Liu, D., Acton, J., Huang, Z., Wang, X., Hewitt, N., Crilley, L., Kramer, L., Slater, E., Whalley, L., Ye, C., and Ingham, T.: APHH: Atmospheric measurements and model results for the Atmospheric Pollution & Human Health in a Chinese Megacity, available at: http://catalogue.ceda.ac.uk/uuid/648246d2bdc7460b8159a8f9daee7844 (last access: 04 March 2021), 2017.

CHAPTER 3:TOP-DOWN ESTIMATE OF NO_X EMISSIONS IN CITIES IN SOUTH AND SOUTHEAST ASIA

3.1 Abstract

Cities in South and Southeast Asia are developing rapidly, but routine, up-to-date and publicly available inventories of emissions are lacking for this region. Nitrogen oxides (NO_x) emissions in cities are important precursors to health-hazardous fine particulate matter ($PM_{2.5}$) and ozone (O_3). Here we estimate NO_x lifetimes and emissions over 10 large cities in South and Southeast Asia in 2019 by applying an exponentially modified Gaussian (EMG) approach with a wind rotation technique to the nitrogen dioxide (NO_2) tropospheric vertical column densities (VCDs) from the high spatial resolution TROPOspheric Monitoring Instrument (TROPOMI). Annual averaged NO_x emissions range from < 50 mol s^{-1} for Karachi, Ahmedabad, Mumbai, Lahore and Chennai, 50-100 mol s^{-1} for Manila and Jakarta, and > 100 mol s^{-1} for Delhi, Dhaka and Singapore. This is comparable to the range of emissions estimates for polluted cities in China. Bottom-up NO_x emissions from a widely used publicly available global inventory exceed the top-down estimates for most cities. The discrepancy is >100% for Chennai, Singapore and Jakarta. It was only possible to estimate top-down monthly NO_x estimates for 3 cities, due to issues with the line density fitting parameters at these fine temporal scales. These ranged from 63 to 148 mol s^{-1} for Singapore (annual mean 114 mol s^{-1}), 44 to 109 mol s^{-1} for Jakarta (68 mol s^{-1}), and 26 to 67 mol s^{-1} for Manila (53 mol s^{-1}). Month-to-month variability is absent in the bottom-up emission estimates. The discrepancies identified in this work need to be resolved to ensure the development of effective policies.

3.2 Introduction

Nitrogen oxides ($NO_x \equiv NO_2 + NO$) contribute to formation of particulate nitrate and ground-level ozone (Luo et al., 2019; Sillman, 1999), thus degrading air quality, causing adverse impacts on human health and the environment, and altering climate (Grulke and Heath, 2020; Lelieveld et al., 2015; Yue et al., 2017). Control measures have been extensively implemented to reduce NO_2 concentrations in cities in Europe, the US and China (Curier et al., 2014; de Foy et al., 2016; Silvern et al., 2019). In cities in other parts of the world, NO_2 is increasing due to fast economic development and absence of effective air quality policies. A recent study using satellite observations of NO_2 from the Ozone Monitoring Instrument (OMI) for 2005-2018 estimated that NO_2 in rapidly developing cities in South and Southeast Asia are increasing by 0.8 to 7.7 % a^{-1}, except for Jakarta, where NO_2 decreased due to emission controls (Vohra et al., 2022). Urban populations across large cities in South and Southeast Asia are projected to increase in this century to over 5 million by 2100 (Hoornweg and Pope, 2017). Controls on NO_x emissions are important to curtail adverse effects of air pollution on public health.

Bottom-up emission inventories can provide estimates of NO_x emissions based on activity data and emission factors. The Regional Emission inventory in Asia (REAS) and the MIX inventory are developed for estimating anthropogenic emissions in Asia by incorporating a collection of inventories over Asia, but these are limited to anthropogenic emissions of NO_x and are subject to uncertainties greater than ±30% in South and Southeast Asia (Kurokawa and Ohara, 2020; Li et al., 2017). Global bottom-up emission inventories such as Community Emissions Data System (CEDS) (McDuffie et al., 2020) for anthropogenic sources and the version 4 of Global Fire Emissions Database (GFED4s) for biomass burning (Randerson et al., 2017) are also used in models to understand NO_x emissions and air pollution in South and Southeast Asia. In addition to large uncertainties in these bottom-up emission estimates, it is challenging to keep bottom-up emission inventories up to date.

Top-down estimates of NO_x emissions using satellite observations of tropospheric NO_2 vertical column densities (VCDs) have been extensively developed. Beirle et al. (2011) first proposed an exponentially modified Gaussian (EMG) approach to estimate NO_x emissions from isolated high polluting cities using tropospheric NO_2 vertical column densities observed by OMI and wind data from meteorology reanalysis. In this approach, cities are treated as large point sources so that this method accounts for advection of the city plume. Beirle et al. (2011) derived NO_x emissions from 9 NO_2 hotspots around the world and found that derived NO_x emissions are generally in good agreement with bottom-up emission inventories, but are higher by a factor of 3 for Riyadh, the capital of Saudi Arabia. Many studies have since adopted similar methods to estimate city NO_x emissions (Ialongo et al., 2014; Laughner and Cohen, 2019; Verstraeten et al., 2018; Xue et al., 2022). For example, Laughner and Cohen (2019) applied this method to OM NO_2 in 30 cities in the US and found that changes in NO_x lifetime are of the same order as changes in NO_x emissions over the study periods. Their results suggest that change in NO_x lifetime must be accounted for when relating NO_x emissions and concentrations. These studies normally average long-term satellite NO_2 observations in different wind direction sections and then estimate NO_x emissions from the city under each wind direction. Valin et al. (2013) proposed a wind rotation technique which allows satellite data under different wind directions and from different days to be used together to estimate NO_x emissions from the same source. These top-down estimates of NO_x emissions from isolated cities provide an opportunity to evaluate the bottom-up emission inventories which have large uncertainties. This is especially valuable for a region like South and Southeast Asia, where NO_x emissions are poorly understood and constraints from surface measurements are lacking due to missing routine monitoring.

Here we use the wind rotation approach and tropospheric NO_2 VCDs from the high resolution TROPOspheric Monitoring Instrument (TROPOMI) to estimate annual NO_x emissions from cities in South and Southeast Asia for 2019 and compare these to bottom-up emissions calculated with the Harmonized Emissions Component (HEMCO) software.

3.3 Data and Method

TROPOMI is onboard the Copernicus Sentinel - 5P satellite launched into sun synchronous orbit on 13 October 2017. It provides daily global observations of NO_2 at 7 × 3.5 km^2 at nadir before 6 August 2019 and 5.5 × 3.5 km^2 afterwards. Its overpass time is around 13:30 pm local time. Here we use Level-2 data from the recently reprocessed TROPOMI NO_2 provided by the Sentinel-5P Products Algorithm Laboratory (S5P-PAL) system (https://data-portal.s5p-pal.com/; last acquired: 30 January 2022), as this uses the same retrieval algorithm and so provides a consistent data record. We only use high-quality data by removing data with quality flag < 0.75. This removes cloud-covered scenes, part of the scenes covered by snow/ice, errors and problematic retrievals.

As a validation for our estimates in NO_x lifetimes and emissions, we apply all the steps to Riyadh first, as it is the city for which this EMG approach is most reported (Beirle et al., 2011; Lange et al., 2022; Valin et al., 2013). We apply a physics-based oversampling algorithm (Sun et al., 2018) to the original TROPOMI NO_2 pixel data to obtain gridded annual mean tropospheric NO_2 VCDs at 0.05° × 0.05° (~5 km). This oversampling method represents each satellite observation as a sensitivity distribution on the ground, instead of a point or a polygon. This sensitivity distribution can be determined by the spatial response function of each satellite sensor. A generalized 2-D super Gaussian function is proposed to characterize the spatial response functions of TROPOMI in the along- and across-track directions. Then these sensitivity distributions are mapped over uniform latitude-longitude grids and applied to weight the TROPOMI pixel by the area of overlap.

We select 10 cities from 6 countries with isolated NO_2 hotspots in a 4° × 4° domain (Figure 3.1), as is required by the EMG approach (Beirle et al., 2011). We estimate NO_x emissions and lifetimes for each city using the EMG approach with the wind rotation technique following previous studies (Jin et al., 2021; Lange et al., 2022; Laughner and Cohen, 2019). Figure 3.2 shows an example of the three steps to derive NO_x emissions from Delhi. We first sample TROPOMI NO_2 data around each selected city within a 4° × 4° domain (Figure 3.2.a). Then we take wind data (u and v components) from the ERA-5 reanalysis product (https://cds.climate.copernicus.eu/cdsapp#!/home; last acquired: 18 March 2022) at 13:00 local time each day to coincide with the TROPOMI overpass around 13:30 pm. The ERA-5 data are at 0.25° × 0.25° horizontal resolution. At each TROPOMI NO_2 pixel, we compute the averaged wind speed and wind direction using data across layers below 900 hpa pressure levels to represent the wind conditions for the dispersion of NO_2 plumes. Then we rotate each TROPOMI NO_2 data along the city centre by the angle of the computed wind direction so that all the TROPOMI NO_2 observations are aligned to have the same "upwind-down" wind direction, which effectively show up as "North-South" direction on the map. The distance of each TROPOMI NO_2 observation to the city centre is kept the same after rotation. After rotating each satellite pixel, we regrid them to obtain the average concentrations at a consistent resolution of 0.05° × 0.05° resolution (Figure 3.2.b). Based on the regridded data, we integrate the TROPOMI NO_2 within 1° in the across-wind direction. This converts the 2D map of TROPOMI NO_2 to a 1D observed NO_2 line density (Figure 3.2.c). The observed NO_2 line density is then fitted using the EMG model following Laughner and Cohen (2019), which is based on the convolution of a Gaussian-shaped emission and an exponential decay function, following Eq. (1):

$$F(x|a, x_0, \mu_x, \sigma_x, B) = \frac{a}{2x_0} \exp\left(\frac{\mu_x}{x_0} + \frac{\sigma_x^2}{2x_0^2} - \frac{x}{x_0}\right) \operatorname{erfc}\left(-\frac{1}{\sqrt{2}}\left[\frac{x-\mu_x}{\sigma_x} - \frac{\sigma_x}{x_0}\right]\right) + B \tag{1}$$

where a, x_0, μ_x, σ_x and B are fitting parameters. a represents the total amount of observed NO_2 molecules in the domain, x_0 represents the e-folding distance which describes the length scale of the NO_2 decay, μ_x is the distance of the apparent source to the city centre, σ_x represents the Gaussian smoothing length scale and B represents the background NO_2 concentrations. We follow Laughner and Cohen (2019) to provide the best guesses of these five parameters at the beginning of the fitting. Instead of conducting a fixed number of fittings used in Laughner and Cohen (2019), we keep the fit results as our best fit if the averaged relative changes in fitted NO_2 are smaller than 0.1% of the previous iteration. The effective NO_2 lifetime (τEMG) and the NO_x emissions can be calculated using the fitted parameters a and x_0 with input of averaged wind speeds in the domain, following Eqs. (2) and (3):

$$\tau_{EMG} = \frac{x_0}{\omega} \tag{2}$$

$$E_{EMG} = \gamma \times \frac{a}{\tau_{EMG}} \tag{3}$$

where w is the averaged wind speed over the domain used for integrating NO_2, γ is the ratio of NO_x to NO_2 and is assumed to be a fixed value of 1.32 following Beirle et al. (2011). Beirle et al. (2011) reported that uncertainties exist in satellite NO_2 (about 30%), the assumed NO_x to NO_2 ratio of 1.32 (10%), the distance for integration across the wind direction (10%), the selection of wind data (30%)

and the representation of background NO_2 (10%). Here we calculate the uncertainties of NO_x emission estimates based on error propagation of the above factors. Previous studies using the EMG approach usually sample data over long-terms of multiple months or years. Here we first estimate annual NO_x emissions from each city, then we test the ability of this approach in estimating monthly NO_x emissions from each city.

We use the standalone emissions-only version of HEMCO 3.0 (https://doi.org/10.5281/zenodo.4984639; last accessed: 20 March 2022) (Lin et al., 2021) to calculate bottom-up NO_x emissions from natural and anthropogenic sources over South and Southeast Asia at 0.25° × 0.3125° (latitude × longitude) covering 47 layers throughout the atmosphere. HEMCO is used here due to its capacity to compute emissions from a user-selected ensemble of emission inventories and algorithms. Here, we use global emission inventories due to lack of up-to-date nested emission inventories in this region for the year 2019. Emission sources include anthropogenic emissions from energy production, industry, transportation, residential, solvents, agriculture, waste and shipping from the CEDS at 0.5° × 0.5° (McDuffie et al., 2020), open biomass burning emissions from the GFED4s at 0.25° × 0.25° (Randerson et al., 2017), natural lightning and soil NO_x emissions from resolution-independent offline emissions generated by HEMCO at 0.25° × 0.3125°. All these emission inventories are for 2019 in this study and emissions for all cities are taken from the same selection of emission inventories mentioned above. We use HEMCO to process the input emission inventories at varying spatial resolutions and calculate the sum of NO_x emissions at 0.25° × 0.3125° over the grids coincident with the extent of the urban area for each target city. City coordinate limits are identified using coordinate limits from Google maps. These are then compared to top-down emissions.

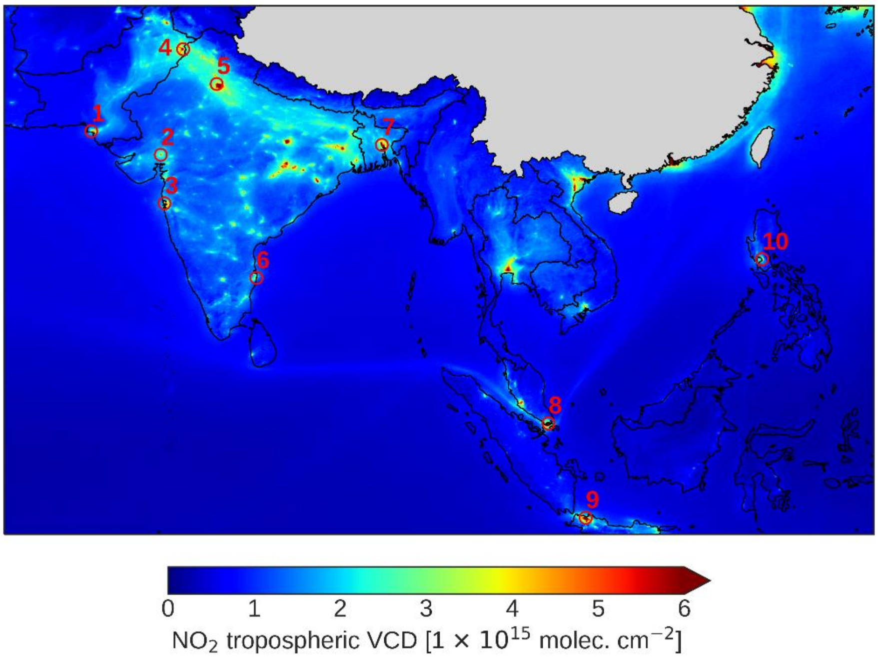

Figure 3.1: Annual mean TROPOMI tropospheric NO_2 VCDs over South and Southeast Asia in 2019. The ten selected cities are: (1) Karachi (Pakistan); (2) Ahmedabad (India); (3) Mumbai (India); (4) Lahore (Pakistan); (5) Delhi (India); (6) Chennai (India); (7) Dhaka (Bangladesh); (8) Singapore; (9) Jakarta (Indonesia) and (10) Manila (Philippines).

3.4 TROPOMI NO_2 in South and Southeast Asia

Figure 3.1 shows the annual mean TROPOMI tropospheric NO_2 VCDs in South and Southeast Asia in 2019 oversampled at 0.05° × 0.05°. Background NO_2 concentrations over the ocean are $< 2\times10^{15}$ molecules cm^{-2}. Pollution hotspots associated with cities are discernible at a number of cities. Those with very low surrounding NO_2 concentrations compared to that in the city that are ideal for deriving NO_x emissions using the wind rotation and EMG approach (Beirle et al., 2011; Valin et al., 2013) include Karachi and Lahore in Pakistan, Ahmedabad, Mumbai, Chennai in India, Dhaka from Bangladesh, Jakarta in Indonesia and Manila in the Philippines and the sovereign city Singapore. Annual mean NO_2 VCDs in these cities range from $2.3\text{-}3.8 \times 10^{15}$ molecules cm^{-2} in Manila, Chennai, Karachi, Ahmedabad and Mumbai to $4.3\text{-}5.7 \times 10^{15}$ molecules cm^{-2} in Lahore, Delhi, Dhaka, Singapore and Jakarta. TROPOMI NO_2 exhibits seasonality in these cities (Figure S3.1), which may suggest seasonality in emissions or in the lifetime and wind speeds that influence NO_2 abundance. Monthly NO_2 in Dhaka is lowest ($3.0\text{-}3.2 \times 10^{15}$ molecules cm^{-2}) in July and August and highest ($6.6\text{-}9.2 \times 10^{15}$ molecules cm^{-2}) in November, December and January. In Singapore, the highest monthly NO_2 columns are observed in March and April (7.4-9.2 × 10^{15} molecules cm^{-2}). Monthly NO_2 in Chennai and Manila show little variation throughout the year. The relative standard deviation of monthly NO_2 are 16-18% in Manila and Chennai, and 23-44% in others.

3.5 NO_x emissions estimates from TROPOMI

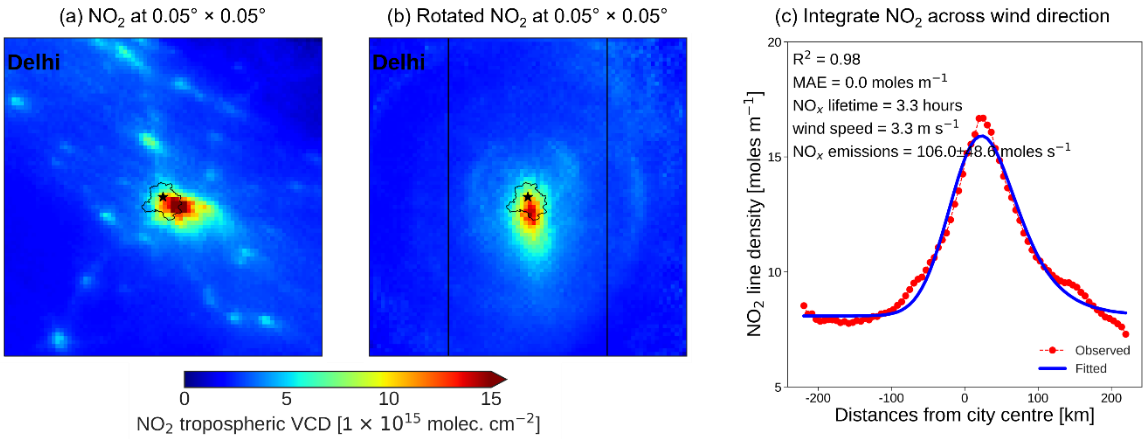

Figure 3.2: Derivation of NO_x emissions for Delhi using wind rotation and the EMG fit method. The main steps in each panel are (a) grid TROPOMI NO_2 to 0.05° × 0.05° using oversampling; (b) wind rotated and regridded TROPOMI NO_2 regridded to 0.05° × 0.05° (two black lines which are 1° away from the city centre define the area for integration across the upwind-downwind direction); and (c) TROPOMI NO_2 (red) and fit (blue) line densities within 1° of the city centre (black vertical lines in panel (b)). Values in panel (c) give the goodness of fit (R^2), Mean Absolute Error (MAE), NO_x lifetime (obtained with Eq. (2)), ERA-5 wind speed within the black vertical lines in panel (b), and NOx emissions (Eq. (3)).

Our estimates of NO_x emissions over Riyadh in 2019 are 163.3 mol s^{-1}, which is 12.5% less than the 186.1 mol s^{-1} reported by Lange et al. (2022). The difference in the estimates is mostly because we use a NO_x to NO_2 ratio of 1.32, which is 6% lower than the 1.41 used by Lang et al. (2022). Another potential cause for the discrepancy is that they used data from 360 days between March 2018 and November 2020, while here we use data from all days in 2019. The TROPOMI PAL product is reported to observe higher tropospheric NO_2 VCDs, mainly in wintertime and over polluted northern midlatitude regions (Eskes. et al., 2021). Here we used both products and yield consistent NO_x emission estimates for Riyadh.

Table 3.1 summarizes the NO_x lifetimes, emissions and averaged wind speeds in the selected cities in South and Southeast Asia obtained with the wind rotation and EMG approach for the selected cities identified in Figure 3.1. We evaluate the skill of the EMG fit (Eq. (1)) using goodness-of-fit (R^2) and

Mean Absolute Error (MAE). For all cities, the fit explains at least 92% of the variability in the data ($R^2 \geq 0.92$). The MAEs are of ~0 for all cities. Annual averaged NO_x lifetimes, obtained from the EMG fit, are 3.1-8.2 hours across the selected cities, with the shortest estimated at Dhaka, Singapore and Delhi (3.1-3.3 hours) and highest at Chennai (8.2 hours). Annual averaged wind speeds are 2.5-5.5 m s^{-1} across the selected cities, with the lowest at Lahore (2.5 m s^{-1}) and the highest at Manila (5.5 m s^{-1}). No clear relationships between NO_x lifetimes and wind speeds are found, as NO_x lifetimes during daytime are related to the rate of loss of NO_x, which is mainly via the reaction of the hydroxyl radical (OH) with NO_2 to form nitric acid (HNO_3). The relationships are nonlinear and depending on NO_x concentration (Valin et al., 2013). The estimated annual NO_x emissions range from 21.0±9.6 mol s^{-1} in Chennai to 123.6±56.6 mol s^{-1} in Dhaka. Annual averaged NO_x emissions are below 50 mol s^{-1} from Karachi, Ahmedabad, Mumbai, Lahore and Chennai, between 50-100 mol s^{-1} from Manila and Jakarta, and over 100 mol s^{-1} from Delhi, Dhaka and Singapore. This is comparable to the range of emissions estimates for polluted cities in China (Wu et al., 2021).

Table 3.1: Annual mean top-down NO_x emissions and NO_x lifetimes and ERA-5 reanalysis surface wind speeds of target cities in South and Southeast Asia.

City Number [b]	Name (Country)	NO_x emissions[a] [mol s^{-1}]	NO_x lifetime [h]	Wind speed [m s^{-1}]	R^2	MAE [mol m^{-1}]
1	Karachi (Pakistan)	48.9 ± 22.4	4.1	4.8	0.99	0.0
2	Ahmedabad (India)	26.1 ± 12.0	6.8	3.7	0.93	0.0
3	Mumbai (India)	46.1 ± 21.1	4.3	3.7	0.96	0.0
4	Lahore (Pakistan)	37.5 ± 17.2	5.3	2.5	0.93	0.0
5	Delhi (India)	106.0 ± 48.6	3.3	3.3	0.98	0.0
6	Chennai (India)	21.0 ± 9.6	8.2	5.0	0.96	0.0
7	Dhaka (Bangladesh)	123.6 ± 56.6	3.1	3.1	1.00	0.0
8	Singapore	113.8 ± 52.1	3.1	4.8	0.99	0.0
9	Jakarta (Indonesia)	68.2 ± 31.3	7.2	3.9	0.92	0.0
10	Manila (Philippines)	52.8 ± 24.2	4.6	5.5	0.93	0.0

[a] Errors in annual mean NO_x emissions are calculated by propagating errors in satellite NO_2, the NO_x to NO_2 ratio, the distance for integration across the wind direction, the selection of wind data and the representation of background NO_2 (see text for details).

[b] As given in Figure 3.1.

Figure 3.3 compares our top-down annual NO_x emissions to bottom-up emissions calculated with HEMCO. The major anthropogenic sources of NO_x are fossil fuel combustion in sectors such as energy production, transportation and residential heating. Natural sources of NO_x include lightning, biomass burning and soils. We analysed HEMCO emissions at each city, anthropogenic sources contribute to over 90% of NO_x at all cities except Lahore, where 84% of NO_x emissions are anthropogenic and 12% from soils. Bottom-up emissions for most cities exceed top-down values. Bottom-up NO_x emissions are 17-32% lower than the top-down estimates for Lahore and Dhaka, and but are 15-65% more than the top-down estimates for Karachi, Ahmedabad, Mumbai, Delhi, and Manila, and much more (>140%) for Chennai, Singapore and Jakarta. The largest discrepancies occur for Singapore and Jakarta, where the TROPOMI-based NO_x emissions and HEMCO-based NO_x emissions are 113.8 and 274.6 mol s^{-1} for Singapore, and 68.2 and 327.9 mol s^{-1} for Jakarta. Beirle et al. (2011) used OMI NO_2 from 2005-2009 and reported ~100 mol s^{-1} for Singapore and found stable estimated NO_x emissions throughout the year. Due to TROPOMI's high data density and the stable NO_x emissions throughout the year at Singapore, Lange et al. (2022) reported 94.5±11.5 mol s^{-1} of NO_x emissions for Singapore using TROPOMI data from 24 days in 2018-2020. The difference between our estimates and those reported are partially due to the differences in sampling period and selection of wind data. The differences are within the uncertainties associated with the EMG approach. Both Beirle et al. (2011) and Lange et al. (2022) found overestimates in bottom-up emissions by ~50% when comparing their estimates to EDGAR emissions at 0.1° × 0.1° (Crippa et al., 2018). The large discrepancy between our estimates for Singapore and HEMCO is likely due to the overestimates in bottom-up emission inventories caused by errors in activity data and emission factors. This may be the case for Jakarta and other cities as well, but the large discrepancies in HEMCO estimates of NO_x emissions for Jakarta is also likely because CEDS does not capture policy-driven decline in emissions in Jakarta of -2.0 % a^{-1} from 2005 to 2018 as determined with OMI tropospheric NO_2 VCDs. According to CEDS NO_x emissions have increased by 4.7% a^{-1} (Vohra et al., 2022).

But vertical sensitivities of TROPOMI NO_2 can also affect top-down NO_x emission estimates for the selected cities. In the standard TROPOMI NO_2 products, tropospheric NO_2 columns are separated from the total NO_2 columns based on a-priori vertical profiles of NO_2 that are obtained from daily global model simulations (TM5-MP) at the coarse spatial resolution of 1° × 1° (Eskes et al., 2022). Since we sample TROPOMI NO_2 over cities which normally cover areas that are much smaller than a 1° × 1° domain, using vertical profiles of NO_2 at high spatial resolution and recompute TROPOMI NO_2 tropospheric VCDs may reduce the discrepancies between top-down and bottom-up emission estimates shown in Figure 3.3. As detailed in Eskes et al. (2022), this can be done using the averaging kernel, which equals to the altitude-dependent air-mass factor (AMF) divided by the total AMF (Eskes and Boersma, 2003). For example, Jin et al. (2021) replaced vertical profiles of NO_2 from the standard TROPOMI NO_2 product with those computed by NASA GEOS-CF simulations at 0.25° resolution to estimate NO_x emissions from wildfires.

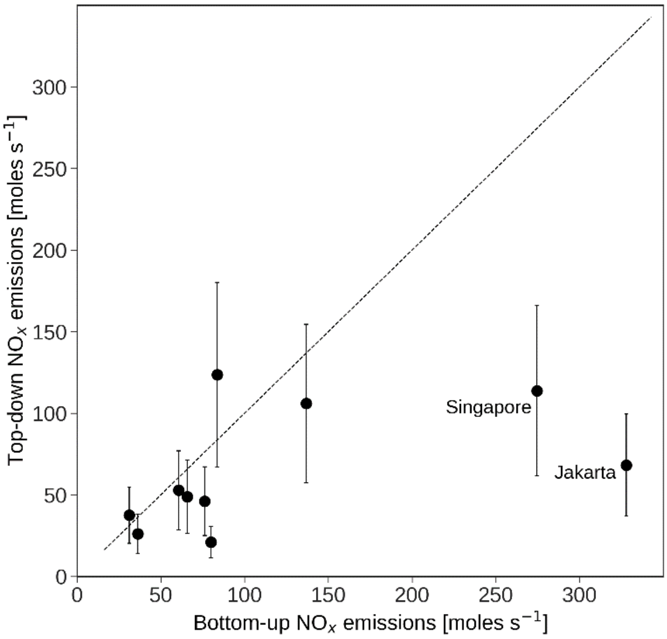

Figure 3.3: Annual average NO_x emissions derived from TROPOMI NO_2 observations compared to bottom-up emission inventories. Data points for Singapore and Jakarta are marked, TROPOMI NO_x emission estimates and emission inventories show the largest discrepancies at these two cities. The dashed line is 1:1 line.

We further exploit the large data density of TROPOMI to estimate monthly NO_x emissions for most (>10 months) of the year, limited to Singapore, Jakarta and Manila. Monthly estimated NO_x emissions, lifetimes and ERA-5 reanalysis wind speeds for these three cities are presented in Table S3.1. Data gaps, unrecognized NO_2 peak near the city centre, and a second but smaller NO_2 peak in the downwind side in the other cities results in too few successful retrievals of monthly emissions for fewer than 8 months. Previous studies have demonstrated that the EMG method works best for an ideal point source, as it is proposed to model the average outflow pattern of the NO_2 tropospheric VCDs with a decay of the signal with distance from a single point source. The EMG method reflects transport and nonlinear effects of atmospheric chemistry (Beirle et al., 2011; Lange et al., 2022; Lu et al., 2015). With the applications of high resolution TROPOMI NO_2 products, plumes from different point sources are more distinctive compared to those detected by OMI NO_2. So, with TROPOMI NO_2, this EMG method is expected to be more sensitive to the interference of nearby sources. One possible solution to reduce the interference of nearby sources is to discard TROPOMI NO_2 observations from certain wind directions during the plume rotation process (Lu et al., 2015). Another possible solution to this is to regrid TROPOMI NO_2 to coarser spatial resolutions so that multiple neighbouring sources may be captured as one single source. Degrading the spatial resolution of TROPOMI NO_2 can also fill some of the data gaps that result from cloud coverage and problematic retrievals. For those data gaps with observations in adjacent grids, they could be filled by interpolation.

Figure 3.4 compares monthly NO_x emissions at Singapore, Jakarta and Manila for 2019 from the top-down approach and from HEMCO. Consistent with the discrepancies in annual NO_x emissions, large discrepancies (> 100%) exist between monthly TROPOMI-based estimates and HEMCO for Singapore and Jakarta. In addition to differences in magnitudes of NO_x emissions estimates using these two approaches, HEMCO shows small month-to-month variability (< 1.5% at Singapore and Jakarta, 7.6% at Manila) in NO_x emission throughout the year at each city, while TROPOMI NO_x emission estimates range from 63.2 to 148.2 mol s^{-1} for Singapore, 43.6 to 108.5 mol s^{-1} for Jakarta, and 25.7 to 67.4 mol s^{-1} for Manila. Previous studies and our findings have shown that annual NO_x emissions based on TROPOMI are comparable to bottom-up emission inventories while our results also point out that monthly TROPOMI-based NO_x estimates have the potential advantage of representing seasonal variability of NO_x emissions from a city. But future research is needed to resolve challenges of deriving monthly NO_x emissions using TROPOMI discussed in this study. Figure S3.2 compares all the derived monthly NO_x emissions from all the cities in this study to bottom-up emission estimates. Similar to Figure 3.3, the derived monthly NO_x emissions are generally lower than bottom-up emissions. The largest discrepancies are observed for Singapore and Jakarta.

NO_x is an important precursor of $PM_{2.5}$ and O_3 pollution, large overestimates of NO_x emissions will lead to misinterpretation of $PM_{2.5}$ and O_3 pollution formation pathways in this region. This hinders developing effective air quality policies to protect human health and climate as tropospheric O_3 is also a greenhouse gas.

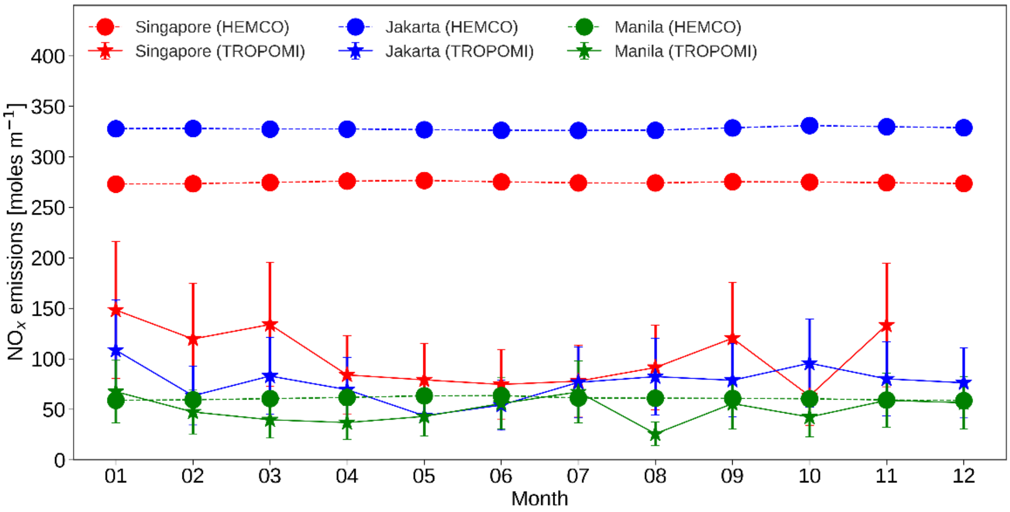

Figure 3.4: Monthly top-down and bottom-up NO_x emissions for Singapore, Jakarta and Manila. Points show bottom- up (filled circles) and top-down (filled triangles) emissions estimates for Singapore (red), Jakarta (blue), and Manila (green).

3.6 Conclusions

Here we provide top-down NO_x emission estimates over 10 large cities in South and Southeast Asia in 2019, as the region is developing rapidly, surface observations are sparse, and NO_x is an important precursor of ozone and $PM_{2.5}$ pollution. These were obtained by applying the EMG method and wind rotation technique to NO_2 tropospheric VCDs from TROPOMI and wind fields from the ERA-5 meteorology reanalysis product. Highest NO_2 concentrations are observed at Delhi, Dhaka, Singapore and Jakarta with the annual averaged oversampled TROPOMI NO_2 greater than 4.9 × 10^{15} molecules cm^{-2} Annual averaged NO_x lifetimes, obtained from the EMG fit, are 3.1-8.2 hours across the selected cities, with the shortest estimated at Dhaka, Singapore and Delhi (3.1-3.3 hours) and highest at Chennai (8.2 hours). Annual averaged NO_x emissions are below 50 mol s^{-1} from Karachi, Ahmedabad, Mumbai, Lahore and Chennai, between 50-100 mol s^{-1} from Manila and Jakarta, and over 100 mol s^{-1} from Delhi, Dhaka and Singapore. The relative error from satellite NO_2 observations, uncertainty in across-wind integration distance, selection of wind data, the NO_x:NO_2 ratio, and the choice of input background NO_2 concentration is 10%-30%. Bottom-up NO_x emissions, mostly (>85%) anthropogenic, are 17-32% lower than the top-down estimates for Lahore and Dhaka, and but are 15-65% more than the top-down estimates for Karachi, Ahmedabad, Mumbai, Delhi, and Manila, and much more (>140%) for Chennai, Singapore and Jakarta. This suggests potential errors in the activity rates or emission factors in the commonly used bottom-up emission inventories and the use of coarse emission inventories for estimating NO_x from cities in South and Southeast Asia. The ability of the top-down method to derive monthly NO_x emissions for most (>10 months) of the year is limited to Singapore, Jakarta and Manila, due to gaps in TROPOMI coverage, an indistinct peak in NO_2 relative to the background, and nearby seasonal NO_2 hotspots for the other cities. Monthly top-down NO_x estimates range from 63 to 148 mol s^{-1} for Singapore, 44 to 109 mol s^{-1} for Jakarta, and 26 to 67 mol s^{-1} for Manila, whereas there is no month-to-month variability in these bottom-up emission inventories. Discrepancies between top-down and bottom-up NO_x emissions point to errors in understanding the sources that contribute to anthropogenic NO_x sources and hinders development of effective policies.

3.7 References

Beirle, S., Boersma, K. F., Platt, U., Lawrence, M. G., and Wagner, T.: Megacity Emissions and Lifetimes of Nitrogen Oxides Probed from Space, Science, 333, 1737-1739, 10.1126/science.1207824, 2011.

Boersma, K. F., Eskes, H. J., Richter, A., De Smedt, I., Lorente, A., Beirle, S., van Geffen, J. H. G. M., Zara, M., Peters, E., Van Roozendael, M., Wagner, T., Maasakkers, J. D., van der A, R. J., Nightingale, J., De Rudder, A., Irie, H., Pinardi, G., Lambert, J. C., and Compernolle, S. C.: Improving algorithms and uncertainty estimates for satellite NO2 retrievals: results from the quality assurance for the essential climate variables (QA4ECV) project, Atmos. Meas. Tech., 11, 6651-6678, 10.5194/amt-11-6651-2018, 2018.

Chai, T. F., Carmichael, G. R., Tang, Y. H., Sandu, A., Heckel, A., Richter, A., and Burrows, J. P.: Regional NOx emission inversion through a four-dimensional variational approach using SCIAMACHY tropospheric NO2 column observations, Atmospheric Environment, 43, 5046-5055, 10.1016/j.atmosenv.2009.06.052, 2009.

Cooper, M., Martin, R. V., Padmanabhan, A., and Henze, D. K.: Comparing mass balance and adjoint methods for inverse modeling of nitrogen dioxide columns for global nitrogen oxide emissions, Journal of Geophysical Research-Atmospheres, 122, 4718-4734, 10.1002/2016jd025985, 2017.

Crippa, M., Guizzardi, D., Muntean, M., Schaaf, E., Dentener, F., van Aardenne, J. A., Monni, S., Doering, U., Olivier, J. G. J., Pagliari, V., and Janssens-Maenhout, G.: Gridded emissions of air pollutants for the period 1970-2012 within EDGAR v4.3.2, Earth System Science Data, 10, 1987-2013, 10.5194/essd-10-1987-2018, 2018.

Curier, R. L., Kranenburg, R., Segers, A. S., Timmermans, R. M. A., and Schaap, M.: Synergistic use of OMI NO2 tropospheric columns and LOTOS-EUROS to evaluate the NOx emission trends across Europe, Remote Sensing of Environment, 149, 58-69, 10.1016/j.rse.2014.03.032, 2014.

de Foy, B., Lu, Z., and Streets, D. G.: Satellite NO2 retrievals suggest China has exceeded its NOx reduction goals from the twelfth Five-Year Plan, Sci Rep, 6, 35912, 10.1038/srep35912, 2016.

Ding, J., van der A, R. J., Mijling, B., Levelt, P. F., and Hao, N.: NO_x emission estimates during the 2014 Youth Olympic Games in Nanjing, Atmos. Chem. Phys., 15, 9399-9412, 10.5194/acp-15-9399-2015, 2015.

Eskes, H. J. and Boersma, K. F.: Averaging kernels for DOAS total-column satellite retrievals, Atmospheric Chemistry and Physics, 3, 1285-1291, 10.5194/acp-3-1285-2003, 2003.

Eskes, H. J., van Geffen, J., Boersma, K. F., Eichmann, K. U., Apituley, A., Pedergnana, M., Sneep, M., Veefkind, J. P., and Loyola, D.: Sentinel-5 precursor/TROPOMI Level 2 Product User Manual Nitrogendioxide, Royal Netherlands Meteorological Institute (KNMI), De Bilt, the Netherlands, 2022.

Eskes., H., van Geffen., J., Sneep., M., Veefkind., P., Niemeijer., S., and Zehner., C.: S5P Nitrogen Dioxide v02.03.01 intermediate reprocessing on the S5P-PAL system: Readme file, 2021.

Grulke, N. E. and Heath, R. L.: Ozone effects on plants in natural ecosystems, Plant Biology, 22, 12-37, 10.1111/plb.12971, 2020.

Hanea, R. G., Velders, G. J. M., and Heemink, A.: Data assimilation of ground-level ozone in Europe with a Kalman filter and chemistry transport model, Journal of Geophysical Research-Atmospheres, 109, 10.1029/2003jd004283, 2004.

Hoornweg, D. and Pope, K.: Population predictions for the world's largest cities in the 21st century, Environment and Urbanization, 29, 195-216, 10.1177/0956247816663557, 2017.

Ialongo, I., Hakkarainen, J., Hyttinen, N., Jalkanen, J. P., Johansson, L., Boersma, K. F., Krotkov, N., and Tamminen, J.: Characterization of OMI tropospheric NO2 over the Baltic Sea region, Atmospheric Chemistry and Physics, 14, 7795-7805, 10.5194/acp-14-7795-2014, 2014.

Jin, X., Zhu, Q., and Cohen, R. C.: Direct estimates of biomass burning NOx emissions and lifetimes using daily observations from TROPOMI, Atmos. Chem. Phys., 21, 15569-15587, 10.5194/acp-21-15569-2021, 2021.

Kurokawa, J. and Ohara, T.: Long-term historical trends in air pollutant emissions in Asia: Regional Emission inventory in ASia (REAS) version 3, Atmos. Chem. Phys., 20, 12761-12793, 10.5194/acp-20-12761-2020, 2020.

Lange, K., Richter, A., and Burrows, J. P.: Variability of nitrogen oxide emission fluxes and lifetimes estimated from Sentinel-5P TROPOMI observations, Atmos. Chem. Phys., 22, 2745-2767, 10.5194/acp-22-2745-2022, 2022.

Laughner, J. L. and Cohen, R. C.: Direct observation of changing NO_x lifetime in North American cities, Science, 366, 723-727, 10.1126/science.aax6832, 2019.

Lelieveld, J., Evans, J. S., Fnais, M., Giannadaki, D., and Pozzer, A.: The contribution of outdoor air pollution sources to premature mortality on a global scale, Nature, 525, 367-+, 10.1038/nature15371, 2015.

Li, M., Zhang, Q., Kurokawa, J., Woo, J. H., He, K. B., Lu, Z. F., Ohara, T., Song, Y., Streets, D. G., Carmichael, G. R., Cheng, Y. F., Hong, C. P., Huo, H., Jiang, X. J., Kang, S. C., Liu, F., Su, H., and Zheng, B.: MIX: a mosaic Asian anthropogenic emission inventory under the international collaboration framework of the MICS-Asia and HTAP, Atmospheric Chemistry and Physics, 17, 935-963, 10.5194/acp-17-935-2017, 2017.

Lin, H., Jacob, D. J., Lundgren, E. W., Sulprizio, M. P., Keller, C. A., Fritz, T. M., Eastham, S. D., Emmons, L. K., Campbell, P. C., Baker, B., Saylor, R. D., and Montuoro, R.: Harmonized Emissions Component (HEMCO) 3.0 as a versatile emissions component for atmospheric models: application in the GEOS-Chem, NASA GEOS, WRF-GC, CESM2, NOAA GEFS-Aerosol, and NOAA UFS models, Geosci. Model Dev., 14, 5487-5506, 10.5194/gmd-14-5487-2021, 2021.

Lu, Z., Streets, D. G., de Foy, B., Lamsal, L. N., Duncan, B. N., and Xing, J.: Emissions of nitrogen oxides from US urban areas: estimation from Ozone Monitoring Instrument retrievals for 2005-2014, Atmospheric Chemistry and Physics, 15, 10367-10383, 10.5194/acp-15-10367-2015, 2015.

Luo, L., Wu, Y., Xiao, H., Zhang, R., Lin, H., Zhang, X., and Kao, S. J.: Origins of aerosol nitrate in Beijing during late winter through spring, Sci Total Environ, 653, 776-782, 10.1016/j.scitotenv.2018.10.306, 2019.

Martin, R. V., Jacob, D. J., Chance, K., Kurosu, T. P., Palmer, P. I., and Evans, M. J.: Global inventory of nitrogen oxide emissions constrained by space-based observations of NO_2 columns, Journal of Geophysical Research-Atmospheres, 108, Artn 4537

10.1029/2003jd003453, 2003.

McDuffie, E. E., Smith, S. J., O'Rourke, P., Tibrewal, K., Venkataraman, C., Marais, E. A., Zheng, B., Crippa, M., Brauer, M., and Martin, R. V.: A global anthropogenic emission inventory of atmospheric pollutants from sector- and fuel-specific sources (1970-2017): an application of the Community Emissions Data System (CEDS), Earth System Science Data, 12, 3413-3442, 10.5194/essd-12-3413-2020, 2020.

Miyazaki, K., Eskes, H. J., and Sudo, K.: Global NOx emission estimates derived from an assimilation of OMI tropospheric NO2 columns, Atmospheric Chemistry and Physics, 12, 2263-2288, 10.5194/acp-12-2263-2012, 2012.

Platt, U. and Stutz, J.: Differential Optical Absorption Spectroscopy, Springer, https://doi.org/10.1007/978-3-540-75776-4, 2008.

Qu, Z., Henze, D. K., Worden, H. M., Jiang, Z., Gaubert, B., Theys, N., and Wang, W.: Sector-Based Top-Down Estimates of NOx, SO2, and CO Emissions in East Asia, Geophysical Research Letters, 49, 10.1029/2021gl096009, 2022.

Randerson, J. T., Van Der Werf, G. R., Giglio, L., Collatz, G. J., and Kasibhatla, P. S.: Global Fire Emissions Database, Version 4.1 (GFEDv4), 10.3334/ORNLDAAC/1293, 2017.

Sillman, S.: The relation between ozone, NO_x and hydrocarbons in urban and polluted rural environments, Atmospheric Environment, 33, 1821-1845, Doi 10.1016/S1352-2310(98)00345-8, 1999.

Silvern, R. F., Jacob, D. J., Mickley, L. J., Sulprizio, M. P., Travis, K. R., Marais, E. A., Cohen, R. C., Laughner, J. L., Choi, S., Joiner, J., and Lamsal, L. N.: Using satellite observations of tropospheric NO2 columns to infer long-term trends in US NOx emissions: the importance of accounting for the free tropospheric NO2 background, Atmospheric Chemistry and Physics, 19, 8863-8878, 10.5194/acp-19-8863-2019, 2019.

Sun, K., Zhu, L., Cady-Pereira, K., Miller, C. C., Chance, K., Clarisse, L., Coheur, P. F., Abad, G. G., Huang, G. Y., Liu, X., Van Damme, M., Yang, K., and Zondlo, M.: A physics-based approach to oversample multi-satellite, multispecies observations to a common grid, Atmospheric Measurement Techniques, 11, 6679-6701, 10.5194/amt-11-6679-2018, 2018.

Valin, L. C., Russell, A. R., and Cohen, R. C.: Variations of OH radical in an urban plume inferred from NO2 column measurements, Geophysical Research Letters, 40, 1856-1860, 10.1002/grl.50267, 2013.

van Geffen, J., Eskes, H. J., Boersma, K. F., and Veefkind, J. P.: TROPOMI ATBD of the total and tropospheric NO_2 data products (issue 2.2.0), Royal Netherlands Meteorological Institute (KNMI), De Bilt, the Netherlands, 2021.

Verstraeten, W. W., Boersma, K. F., Douros, J., Williams, J. E., Eskes, H., Liu, F., Beirle, S., and Delcloo, A.: Top-Down NOX Emissions of European Cities Based on the Downwind Plume of Modelled and Space-Borne Tropospheric NO2 Columns, Sensors, 18, 10.3390/s18092893, 2018.

Vohra, K., Marais, E. A., Bloss, W. J., Schwartz, J., Mickley, L. J., Van Damme, M., Clarisse, L., and Coheur, P. F.: Rapid rise in premature mortality due to anthropogenic air pollution in fast-growing tropical cities from 2005 to 2018, Science Advances, 8, 10.1126/sciadv.abm4435, 2022.

Wu, H. J., Tang, X., Wang, Z. F., Wu, L., Li, J. J., Wang, W., Yang, W. Y., and Zhu, J.: High-spatiotemporal-resolution inverse estimation of CO and NOx emission reductions during emission control periods with a modified ensemble Kalman filter, Atmospheric Environment, 236, 10.1016/j.atmosenv.2020.117631, 2020.

Wu, N., Geng, G. N., Yan, L., Bi, J. Z., Li, Y. S., Tong, D., Zheng, B., and Zhang, Q.: Improved spatial representation of a highly resolved emission inventory in China: evidence from TROPOMI measurements, Environmental Research Letters, 16, 10.1088/1748-9326/ac175f, 2021.

Xue, R., Wang, S., Zhang, S., He, S., Liu, J., Tanvir, A., and Zhou, B.: Estimating city NOX emissions from TROPOMI high spatial resolution observations – A case study on Yangtze River Delta, China, Urban Climate, 43, 101150, https://doi.org/10.1016/j.uclim.2022.101150, 2022.

Yue, X., Unger, N., Harper, K., Xia, X. G., Liao, H., Zhu, T., Xiao, J. F., Feng, Z. Z., and Li, J.: Ozone and haze pollution weakens net primary productivity in China, Atmospheric Chemistry and Physics, 17, 6073-6089, 10.5194/acp-17-6073-2017, 2017.

3.8 Supplementary Information

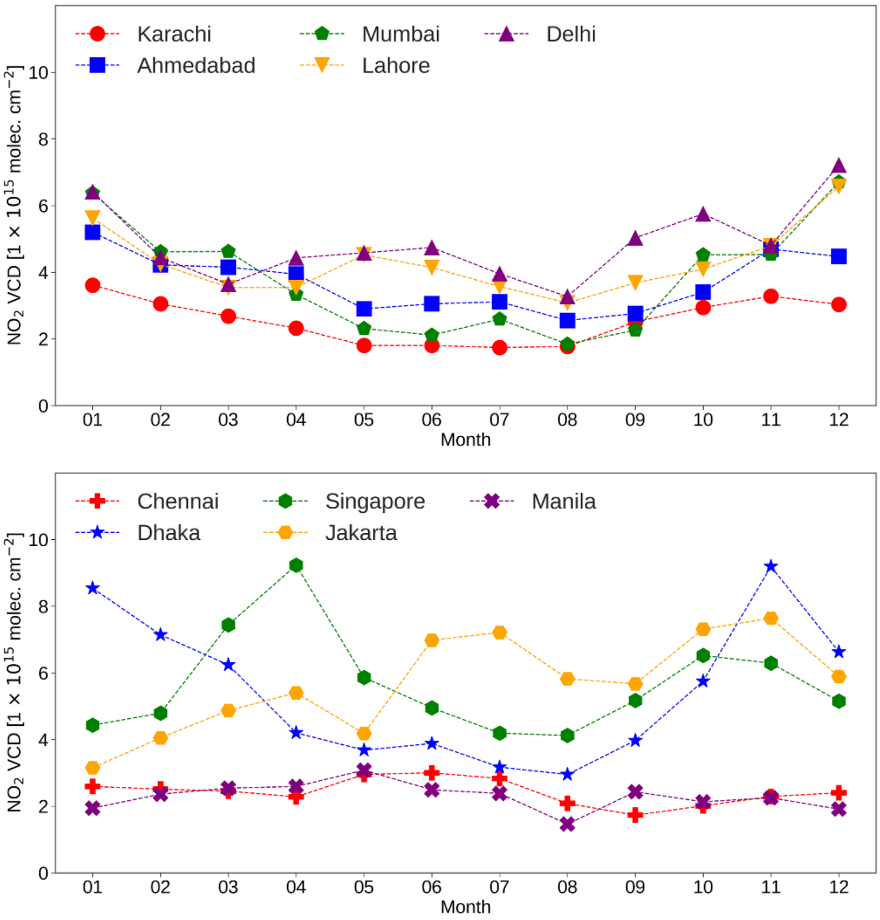

Figure S3.1: Variations of monthly averaged oversampled TROPOMI tropospheric NO_2 VCD in urban areas of selected cities in 2019.

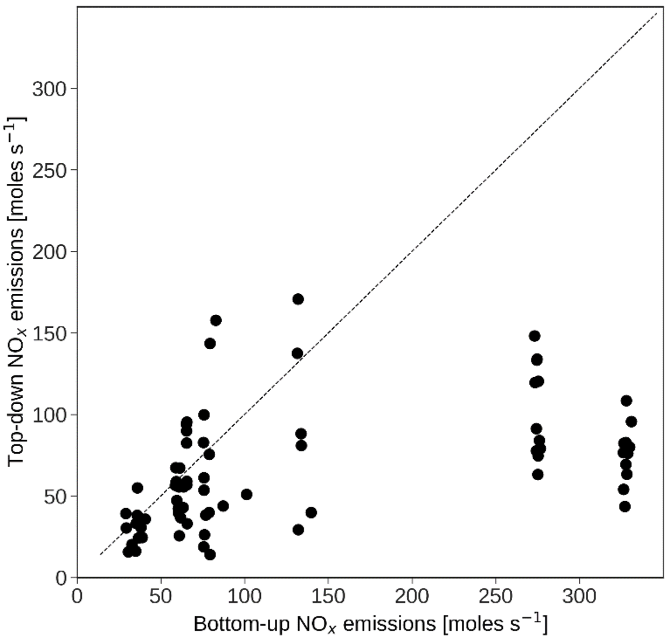

Figure S3.2: Monthly NO$_x$ emissions derived from TROPOMI NO$_2$ observations compared to bottom-up emission inventories. The dashed line is 1:1 line.

Table S3.1: Monthly mean top-down NO_x emissions and NO_x lifetimes and ERA reanalysis surface wind speeds of Singapore, Jakarta and Manila in 2019.

City	Month	NO_x emissions[a] [mol s^{-1}]	NO_x lifetime [h]	Wind speed [m s^{-1}]	R^2	MAE [mol m^{-1}]
Singapore	1	148 ± 67.9	1.8	6.7	0.95	0.0
	2	119.6 ± 54.8	2.3	5.4	0.96	0.0
	3	133.99 ± 61.4	2.7	4.0	0.97	0.0
	4	84.0 ± 38.5	5.1	2.5	0.97	0.0
	5	79.1 ± 36.2	4.1	3.8	0.99	0.0
	6	74.6 ± 34.2	5.2	5.2	0.96	0.0
	7	77.8 ± 35.7	4.3	5.8	0.97	0.0
	8	91.3 ± 41.8	3.4	6.8	0.97	0.0
	9	120.3 ± 55.1	2.5	5.1	0.97	0.0
	10	63.2 ± 29.0	6.1	2.5	0.95	0.0
	11	133.4 ± 61.1	3.0	2.8	0.97	0.0
	12	NA	NA	NA	NA	NA
Jakarta	1	108.5 ± 49.7	3.0	4.7	0.92	0.0
	2	63.4 ± 29.1	5.2	3.4	0.95	0.0
	3	82.9 ± 38.0	5.0	3.3	0.91	0.0
	4	69.4 ± 31.8	7.4	3.0	0.94	0.0
	5	43.6 ± 20.0	13.8	3.7	0.90	0.0
	6	54.1 ± 24.8	11.3	3.6	0.80	0.0
	7	76.6 ± 35.1	6.7	4.4	0.88	0.0
	8	82.3 ± 37.7	7.0	4.5	0.84	0.0
	9	78.7 ± 36.1	6.3	4.6	0.90	0.0
	10	95.6 ± 43.8	5.5	4.1	0.95	0.0
	11	80.1 ± 36.7	5.9	2.8	0.94	0.0
	12	76.2 ± 34.9	6.2	2.7	0.86	0.0
Manila	1	67.4 ± 30.9	4.5	9.2	0.98	0.0
	2	47.3 ± 21.7	5.6	6.0	0.97	0.0
	3	39.6 ± 18.1	6.7	4.5	0.96	0.0
	4	36.8 ± 16.9	9.2	4.1	0.96	0.0
	5	42.9 ± 19.7	6.3	2.7	0.93	0.0

6	55.6 ± 25.5	5.7	4.7	0.96	0.0
7	67.2 ± 30.8	2.9	4.1	0.92	0.0
8	25.7 ± 11.8	6.6	8.2	0.77	0.0
9	55.6 ± 25.5	3.2	5.0	0.96	0.0
10	42.3 ± 19.4	5.0	4.7	0.95	0.0
11	58.8 ± 26.9	4.2	6.0	0.93	0.0
12	56.5 ± 25.9	4.5	7.5	0.97	0.0

[a] Errors in annual mean NO_x emissions are calculated by propagating errors in satellite NO_2, the NO_x to NO_2 ratio, the distance for integration across the wind direction, the selection of wind data and the representation of background NO_2 (see text for details).

CHAPTER 4:CHANGES IN SURFACE AIR QUALITY DURING COVID-19 LOCKDOWNS

Statement of Author Contribution

This chapter is a component of Shi et al. (2021) which has been previously published as a research article on Science Advances (see Appendix at the end of this thesis). In Shi et al. (2021), a random forest machine learning technique is used to interpret changes in surface air quality due to COVID lockdowns in 2020 in 11 cities worldwide.

In this project, I downloaded hourly observations of surface air quality (i.e., NO, NO_2, NO_x, O_3, CO, SO_2, $PM_{2.5}$, and PM_{10}) from monitoring networks in the studied cities with contributions from co-authors on this paper. I followed the official data manual to conduct quality control of the raw datasets to remove filled values or data with bad quality flags. I determined the site types (i.e., urban background, roadside and rural) based on the official data manual and Google Maps. Then I identified and excluded sites with temporal coverage less than 75% (only if there are other available sites), or those with potential problems. For example, some sites were relocated during the sampling period, and this caused a change in site type and introduced inconsistencies. After selecting the sites, I calculated site type averaged hourly surface air quality data for each species in each city. Then I conducted analysis of the observations that I prepared. I also conducted data visualisation to support development of this research. At the time of this research project was conducted, air quality data for New York and Los Angeles were not available from the official data platform held by US EPA. So data for New York and Los Angeles were collected from a third party data platform OpenAQ. I conducted a validation of OpenAQ data against the measurements from US EPA, in response to reviewers' comments. Also, the surface air quality data for London were not yet verified by the Department for Environment, Food and Rural Affairs (DEFRA) at the time of this research project. I compared the data used in this paper against verified London data upon completion of the formal analysis.

I downloaded hourly meteorological observations of temperature, relative humidity, atmospheric pressure, wind speed, and wind direction for each selected city from the nearest meteorological observation site from the NOAA (National Oceanic and Atmospheric Administration) Integrated Surface Database (ISD) using the “worldmet” R package. Then I combined the prepared hourly air quality data with these hourly meteorological data and prepared them for use in the machine learning algorithm in the paper. In addition to air quality and meteorological data, I processed the mobility data from Google Maps for the period starting from 5 weeks before till 5 weeks after the lockdowns in 2020 for each city.

In this chapter, the selection of study cities and sites and interpretation of observed surface air quality are presented. Meteorological data were used only to train the machine learning model. So they are not analysed and not presented here. Some of the below text in this chapter is taken from Shi et al. (2021). Figures used in this chapter have not been previously published.

4.1 Abstract

The COVID-19 pandemic led to global lockdowns in early 2020, which resulted a sudden reduction in human activities and associated air pollution emissions. Here we use surface observations of air quality from monitoring networks in 11 cities worldwide to investigate the surface air quality before, during and after the COVID-19 lockdowns. Our results show that after the lockdowns, observed NO_2 levels decreased substantially in all the cities. The decrease ranges from -10.1±36.6% in London to -60.2±14.8% in Delhi at urban background sites and from -29.3±33.1% in Berlin to -53.5±18.9% in London at roadside sites. In contrast, an increase in observed O_3 is found in all cities after the lockdowns, which ranges from 16.2±16.1% in Madrid to 166.5±60.5% in Wuhan at urban background sites and from +19.5±21.0% in Madrid to +155.6±83.2% in Milan at roadside sites. As a result, smaller changes were found for total gaseous oxidant (i.e., $O_x = NO_2+O_3$), which range from a decrease of -3.6±8.1% in New York to an increase of 27.6±9.9% in Berlin. Unlike observed NO_2 and O_3, there is not a clear pattern for changes in observed $PM_{2.5}$, which range from -38.6±17.2% in Madrid to +152.9±165.0% in London at urban background sites, from -40.8±28.4% in Los Angeles to +107.6±148.5% in London at roadside sites, and from -34.2±26.8% in Delhi to +164.5±148.7% in London at rural sites. We then compare observations in 2020 to those in 2016-2019 during the equivalent periods, our results show that the observations of air quality alone cannot represent the changes in emissions due to COVID-19 lockdowns as the impact of meteorology should be considered.

4.2 Introduction

In response to the outbreak of COVID-19 in early 2020, governments around the world implemented strict lockdown measures to contain COVID-19. This led to a sudden reduction in human activities and associated emissions. Many studies have explored the impacts of COVID-19 lockdowns on air quality. Observations of air quality from surface monitoring networks and satellite platforms have been used to report abrupt changes in surface air quality due to the strict lockdown measures. Liu et al. (2020) found a 48% drop in satellite observations of tropospheric NO_2 columns over China. Lee et al. (2020) used surface measurements to report a 42% decrease in NO_2 in the UK. However, a lot of studies only focus on a limited air pollutant species or over limited spatial coverage, hindering the comprehensive interpretation of COVID-19 lockdowns on air quality (Grange et al., 2021; Hammer et al., 2021; He et al., 2021; Peralta et al., 2021). The chemical effects of COVID-19 on air quality are complex (Kroll et al., 2020). To investigate the changes in surface air quality due to the interventions caused by COVID-19 lockdowns under a range of contrasting pollution environments, we select 11 worldwide cities as our focus in this study. These are Beijing and Wuhan in China, Milan and Rome in Italy, Madrid in Spain, Paris in France, Berlin in Germany, London in the UK, New York and Los Angeles in the US, and Delhi in India. Eight of these are capitals. Wuhan was the first city to report COVID-19 and implement lockdown measures. Milan is added because it is in northern Italy, which was one of the most affected areas by COVID-19. New York was the most affected city in the US, while Los Angeles is added because a greater decline in surface air pollution levels was observed (Schiermeier, 2020). All the selected cities were significantly affected by COVID-19 and implemented strict lockdowns to contain the COVID-19 pandemic in early 2020. Lockdowns were implemented from 23 January 2020 in Wuhan, 25 January 2020 in Beijing and the entire China, 23 January 2020 in northern Italy, 13 March 2020 in the US, 14 March 2020 in Spain, 17 March 2020 in France, 22 March 2020 in Germany, 23 March 2020 in the UK, 25 March 2020 in India.

4.3 Method and data

For each city, site-level hourly surface observations of six criteria pollutants (i.e., NO_2, O_3, CO, SO_2, $PM_{2.5}$, and PM_{10}) from December 2015 to May 2020 are downloaded from local or national reference monitoring networks. Where available, NO and NO_x are also downloaded. Most data are downloaded from official sources (Table S4.1). Data for New York and Los Angeles in the US are downloaded from OpenAQ data platform (https://openaq.org/; last accessed: 14 September 2020), due to the delay in the official release of data by the US EPA. A validation of OpenAQ data against the measurements from US EPA (https://www.epa.gov/outdoor-air-quality-data; last accessed: 14 September 2020) is conducted after the analysis. The OpenAQ measurements are found to be highly consistent with official data released by US EPA (slope = ~1 and intercept = ~0) (see the example in Figure S4.1).

In this study, we group surface air quality monitoring sites by three types (i.e., urban background, roadside and rural), based on available data information from the official sources or using the site coordinates in Google Maps. Normally, data are available at multiple monitoring sites for each site for each city. In the case that rural sites are not available, we find the nearby rural site that is closest to the city. For example, we use data from Chilbolton Observatory to represent rural background air quality for London. Quality control of raw datasets are first conducted following the official data manuals to remove data with bad quality flags. In addition, sites with temporal coverage less than 75% are removed if there are other available sites of the same type for the selected city. Some sites meet the requirement of temporal coverage in the past few years, but relocation of the sites have occurred. These sites are excluded from the analysis, as the relocation may have caused a change in site type and introduced inconsistencies. Details of data source, site type, and site code for all selected sites are summarized in Table S4.1. Multiple years of air quality data are downloaded here for analysing observed air quality around the COVID-19 lockdowns in 2020, but also in equivalent periods in previous years when there were no lockdowns. Another motivation of using multiple years of data is to train the random forest machine learning model that is used in Shi et al. (2021).

Although surface sites are classified to report air quality under different environment (i.e., urban background, roadside and rural), there are still variabilities in observations from sites of the same type within the same city. Here we average the observations from sites of the same site type within each city to reduce uncertainties caused by a single site. In cases that only one site is available, the observations may be subject to nearby emission sources.

The percentage change (P) in the observed concentrations of air pollutants using the following equation:

$$P = \overline{(C_{\iota} - C)/C \times 100\%} \tag{1}$$

where C is the averaged concentration in the 2nd-3rd weeks before the lockdown date or equivalent, Ci is the average concentrations in the ith day (from 1st to 28th day) starting in the second week after the lockdown start date for each city and for each year. The week immediately before and after the lockdown date was considered a transition period so excluded in the calculations. The transition period may have started earlier than the announced lockdown date such as London. But this is highly uncertain for all the selected cities. For consistency, here we applied the same Eq. 1 for calculation for all cities.

4.4 Results and discussions

4.4.1 Changes in observed NO_2, O_3 and O_x

Figure 4.1 shows the changes in observed daily concentrations of NO_2 in early 2020 at all site types for each city. The dashed orange line in each timeseries plot represents the start of lockdown at each city. The daily urban background NO_2 correlates well ($r > 0.87$ for all cities, except $r = 0.54$ for London) and is 2-51% lower than daily roadside NO_2 for most of the cities, except for New York, where urban background NO_2 is 1% higher than roadside NO_2. The selected cities have varying observed NO_2 levels. Based on the averaged NO_2 during the period starting from 3 weeks before the lockdowns till 5 weeks after the start of the lockdowns, the highest urban background and roadside NO_2 are observed at Milan (45.1 µg m^{-3} for urban background; 53.7 µg m^{-3} for roadside), while the lowest urban background and roadside NO_2 are observed at Madrid (21.2 µg m^{-3} for roadside; 26.8 µg m^{-3} for roadside). Daily observed NO_2 are highly variable during the whole time period in early 2020. High daily NO_2 pollutions were observed even after the lockdowns in cities such as Beijing, Wuhan and Paris. In terms of averaged percentage change, observed urban background NO_2 decreased substantially, with P ranging from -10.1±36.6% in London to -60.2±14.8% in Delhi (Table S4.2). Observed roadside NO_2 also decreased significantly, with P ranging from -29.3±33.1% in Berlin to -53.5±18.9% in London. Observed rural NO_2 decreased in most cities, but increased in Paris (P = +99.2±66.7%) and London (P = +115.8±90.2%).

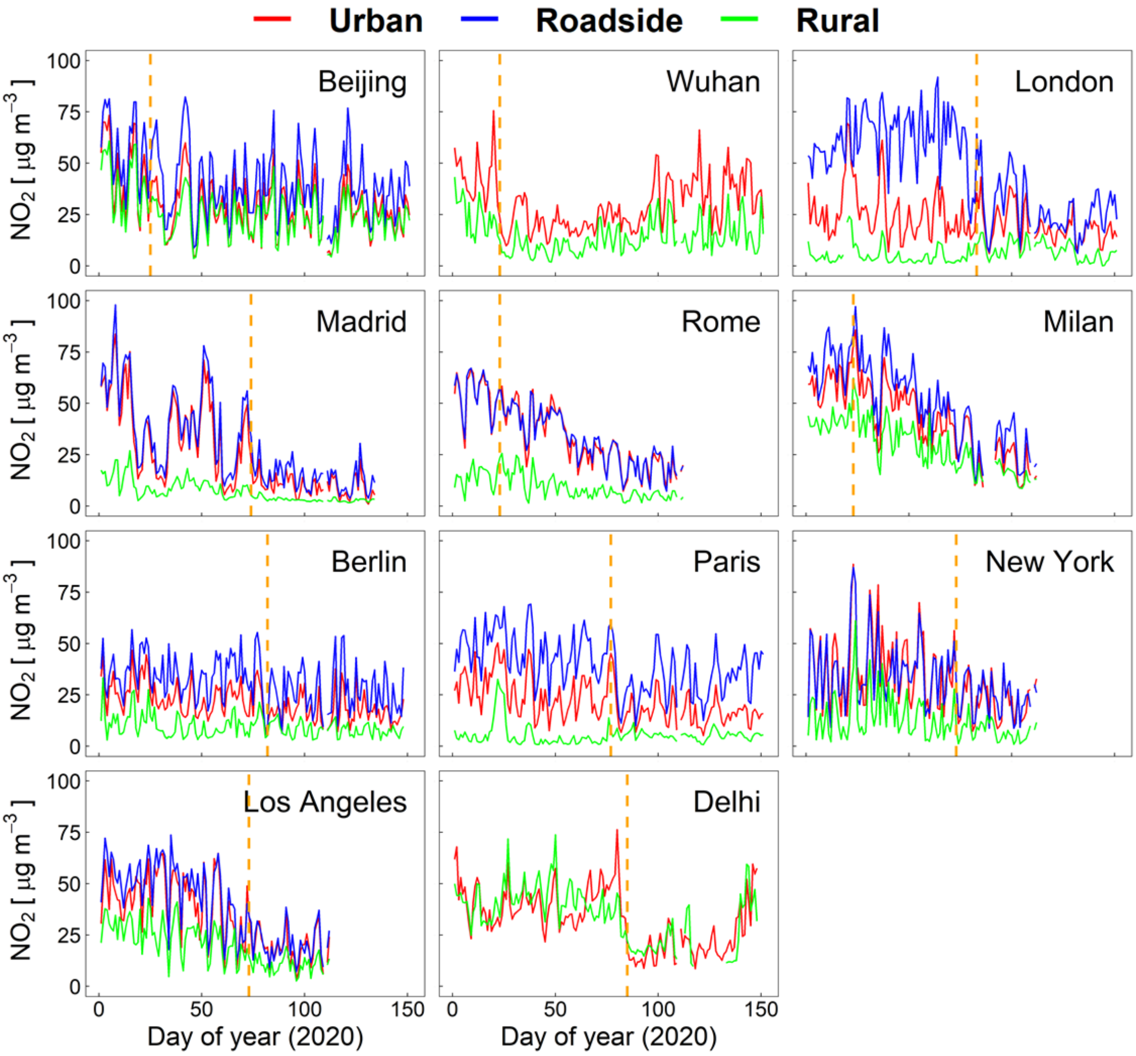

Figure 4.1: Observed daily NO_2 concentrations in each selected cities before and after the lockdown start dates or equivalent in early 2020. Data for all available site types (i.e., urban background (red), roadside (blue) and rural (green)) are provided for each city. The orange dashed line in each plot represents the start of the lockdowns for each city.

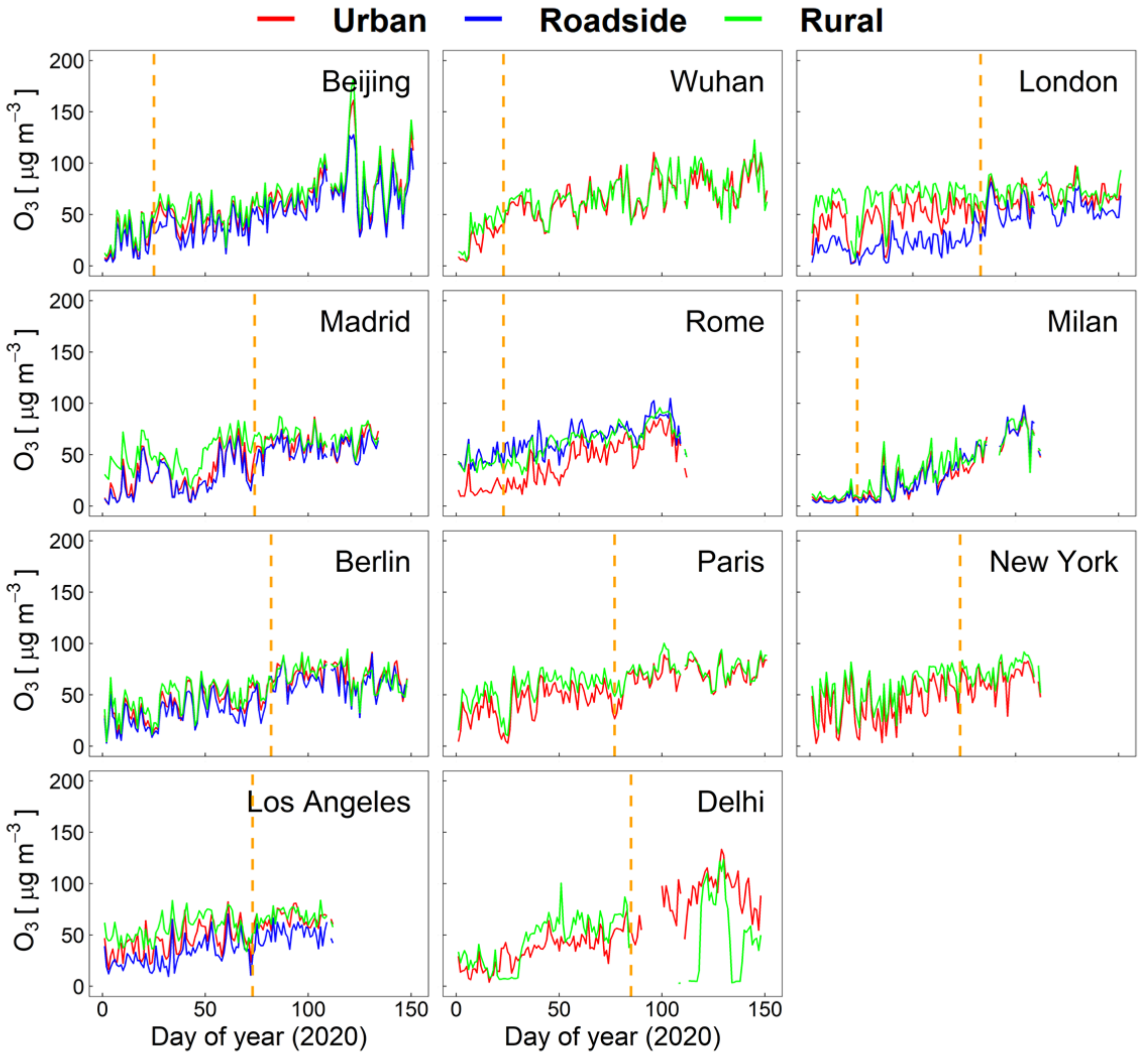

Figure 4.2: Observed daily O_3 concentrations in each selected cities before and after the lockdown start dates or equivalent in early 2020. Data for all available site types (i.e., urban background (red), roadside (blue) and rural (green)) are provided for each city. The orange dashed line in each plot represents the start of the lockdowns for each city.

Figure 4.2 shows the changes in observed daily concentrations of O_3 in early 2020 at all site types for each city. Due to a longer lifetime of O_3 of a few days, daily observed O_3 are consistent at all site types in most cities. The roadside O_3 is lower than urban background due to the titration of O_3 by NO that is emitted from vehicles (Sillman, 1999). In contrast to observed NO_2, observed O_3 increased at all sites in all cities, but with varying magnitudes. For the urban background O_3, the highest increase is observed at Wuhan (P = 166.5±60.5%), the lowest increase is observed at Madrid (P = 16.2±16.1%). For roadside

O_3, highest increase is observed at Milan (*P* = +155.6±83.2%) and the lowest increase is at Madrid (*P* = +19.5±21.0%). The increase in rural O_3 ranges from 0.2±13.3% at Madrid to 102.3±43.4% at Wuhan.

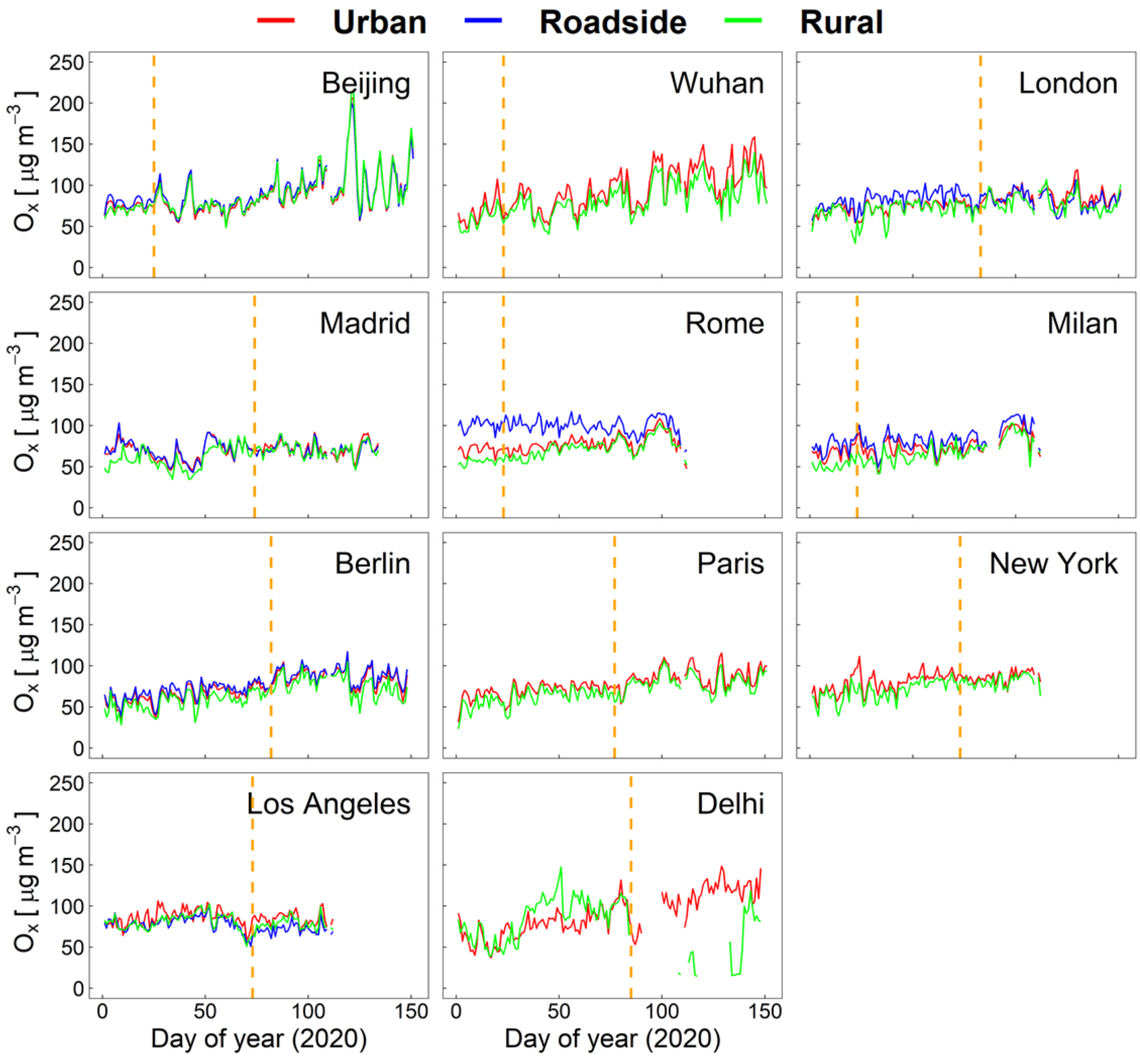

Figure 4.3: Observed daily O_x concentrations in each selected cities before and after the lockdown start dates or equivalent in early 2020. Data for all available site types (i.e., urban background (red), roadside (blue) and rural (green)) are provided for each city. The orange dashed line in each plot represents the start of lockdowns for each city.

Due to the combined effects of reduction in observed NO_2 and enhancements in observed O_3, the observed total gaseous oxidant ($O_x = NO_2 + O_3$) remained relatively stable compared to changes in observed NO_2 and O_3. Figure 4.3 shows the daily observed O_x in each city in early 2020. After the lockdowns, percentage changes in observed O_x at the urban background range from a decrease of -5.7±9.3% at Los Angeles to an increase of 27.6±9.9% at Berlin. The magnitudes of changes in observed

O_x at roadside are similar, ranging from -11.5±8.2% at Los Angeles to 23.5±10.5% at Berlin. However, most rural sites show increases of observed O_x up to 34.9±13.3% at Berlin.

As reported here, dramatic changes in observed NO_2 and O_3 are found after the lockdowns in 2020. However, these observed changes cannot be used to represent the actual changes in NO_2 and O_3 due to the lockdowns in 2020. Other factors such as meteorology and nonlinear chemistry contribute to the nonlinear relationships between emissions and concentrations of air pollutants. Here we conduct the same analysis for the observations from previous years when there were no lockdowns. Results show that dramatic decreases in NO_2 can also occur during the equivalent period in many of the selected cities. For example, during the equivalent periods in 2016-2019, observed NO_2 at the urban background sites dropped by an average of -32.3±40.6% at Beijing, -26.7±44.6% at Madrid, -20.5±24.5% at Milan. Accordingly, observed O_3 at urban sites increased by an average of 70.5±60.0% at Beijing, 28.3±35.9% at Madrid and 225.8±204.3% at Milan. Similar patterns are observed for roadside sites and rural sites. In addition, we conduct the reduced major axis regression (Ayers, 2001) to compare observed NO_2 and observed O_3 at all site types from all cities. The data are divided into three periods, before, during and after the lockdowns. Figure 4.4 shows the comparison of observed NO_2 and O_3 in each year in 2018-2020. The results show that in the equivalent periods in 2018-2020, the relationships between observed NO_2 and observed O_3 are consistent. In each year, the observed NO_2 and observed O_3 are highly correlated ($R^2 > 0.5$). The regression slopes show little differences from year to year (-0.81 in 2018, -0.78 in 2019 and -0.87 in 2020), the intercepts are also consistent (+75.82 in 2018, + 75.93 in 2019 and ++73.57 in 2020). The results show that relationships between observed NO_2 and observed O_3 are not affected by COVID-19 lockdowns. So the observed NO_2 and O_3 cannot be used directly to explain the impact of COVID-19 lockdowns on air quality in early 2020.

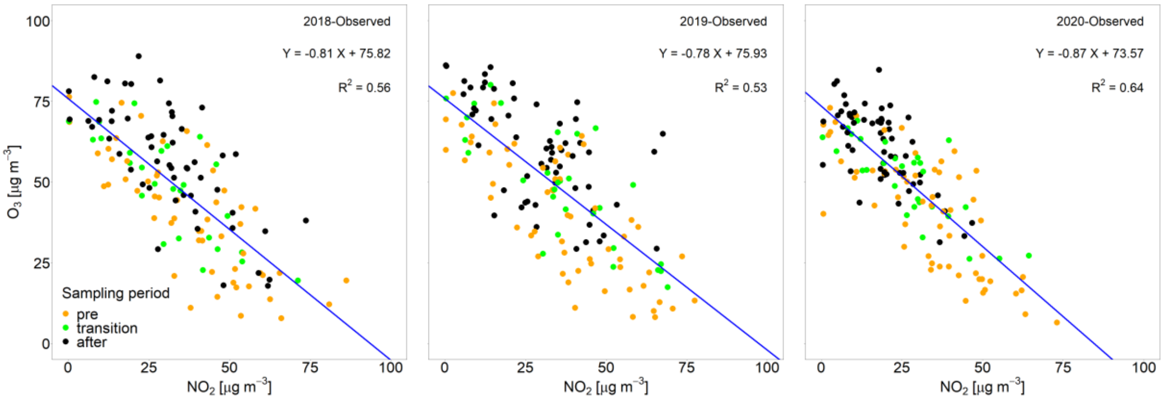

Figure 4.4: Averaged concentrations of NO_2 and O_3 before, during and after the lockdown start dates or equivalent in 2020 vs 2018 and 2019. Data are divided to three periods ("pre" for 2-5 weeks before the lockdown start, "transition" for the 2 weeks during the lockdowns and "after" for 2-5 weeks after the lockdown start.)

4.4.2 Observed changes in $PM_{2.5}$ and PM_{10}

Figure 4.5 shows the changes in daily $PM_{2.5}$ in early 2020. Berlin and Milan are not included as there were no $PM_{2.5}$ measurements available at the time of research. The selected cities have varying $PM_{2.5}$ levels. Daily $PM_{2.5}$ can exceed 200 µg m^{-3} in polluted cities such as Beijing and Delhi, while they are normally below 60 µg m^{-3} in other cities. There are no clear patterns of observed $PM_{2.5}$ after lockdowns. High $PM_{2.5}$ episodes even occurred after the lockdowns in London and Paris. The *P* values vary from -38.6±17.2% in Madrid to +152.9±165.0% in London at urban background sites, from -40.8±28.4% in Los Angeles to +107.6±148.5% in London at roadside sites, and from -34.2±26.8% in Delhi to +164.5±148.7% in London at rural sites.

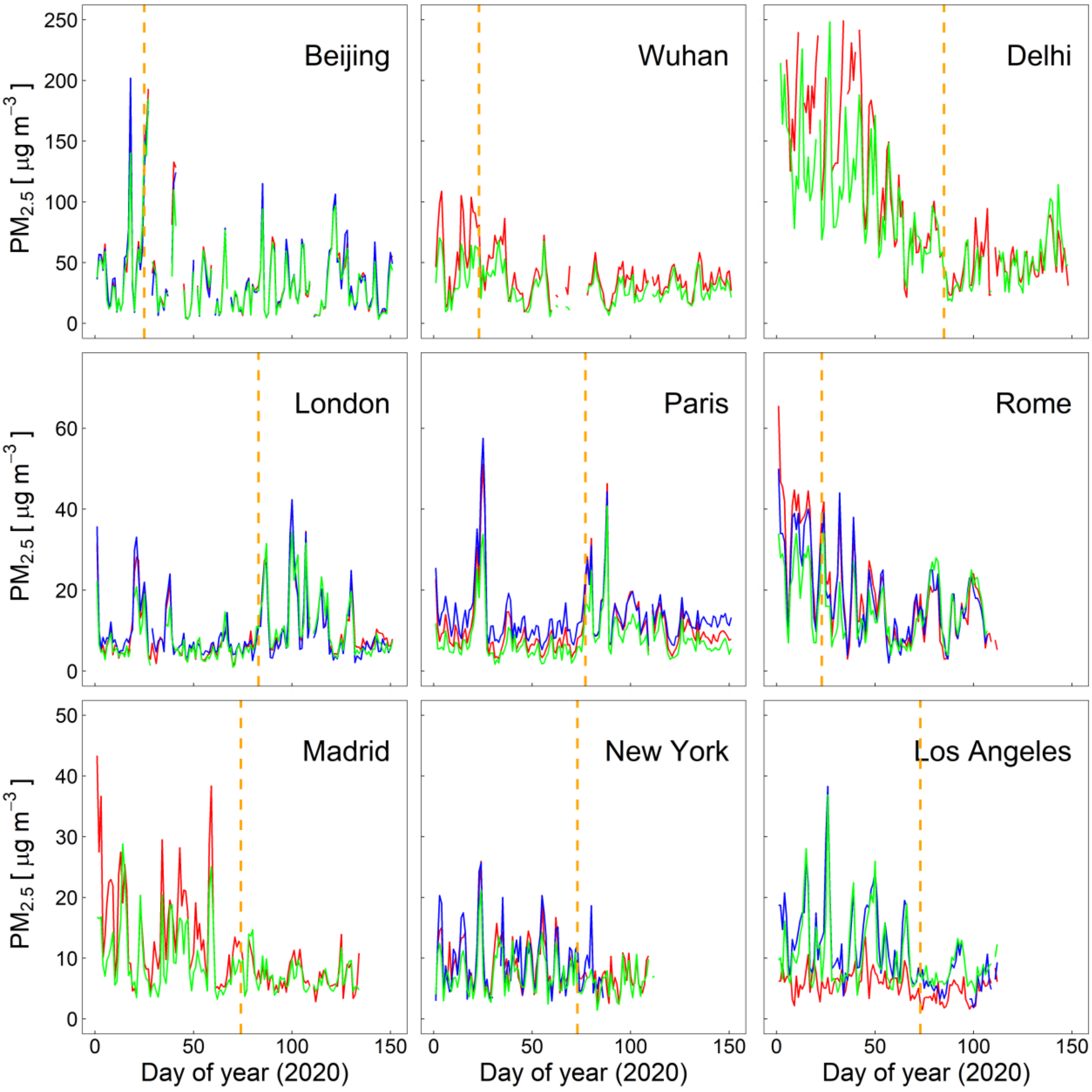

Figure 4.5: Observed daily $PM_{2.5}$ concentrations in each selected cities before and after the lockdown start dates or equivalent in early 2020. Data for all available site types (i.e., urban background (red), roadside (blue), and rural (green)) are provided for each city. The orange dashed line in each plot represents the start of the lockdowns for each city.

4.5 Conclusions

As a result of the COVID-19 pandemic outbreak, governments around the world implemented strict lockdown measures to contain COVID-19. This led to a sudden reduction in human activities and associated air pollution emissions. Here we use observations of air quality from surface monitoring networks in 11 cities worldwide to investigate the changes in surface air quality due to COVID-19 lockdown measures. We group the monitoring sites by urban background, roadside and rural sites in each city. Our results show that after the lockdowns, observed NO_2 levels decreased substantially at urban background and roadside sites in all the cities. The decrease in observed NO_2 ranges from -10.1±36.6% in London to -60.2±14.8% in Delhi at urban background sites and from -29.3±33.1% in Berlin to -53.5±18.9% in London at roadside sites. In contrast, observed O_3 increased in all cities after the lockdowns, the observed increase ranges from 16.2±16.1% in Madrid to 166.5±60.5% in Wuhan at urban background sites and from +19.5±21.0% in Madrid to +155.6±83.2% in Milan at roadside sites. As a result, little changes were observed for total gaseous oxidant (i.e., $O_x = NO_2+O_3$), which range from a decrease of -3.6±8.1% in New York to an increase of 27.6±9.9% in Berlin. Unlike observed NO_2 and O_3, there is not a clear pattern of changes in observed $PM_{2.5}$, which range from -38.6±17.2% in Madrid to +152.9±165.0% in London at urban background sites, from -40.8±28.4% in Los Angeles to +107.6±148.5% in London at roadside sites, and from -34.2±26.8% in Delhi to +164.5±148.7% in London at rural sites. But by comparing observations in 2020 to those in 2016-2019 during the equivalent periods, our results show that the observations of air quality alone cannot represent the changes in emissions due to COVID-19 lockdowns as the impact of meteorology should be considered.

4.6 References

Ayers, G. P.: Comment on regression analysis of air quality data, Atmospheric Environment, 35, 2423-2425, 10.1016/s1352-2310(00)00527-6, 2001.

Grange, S. K., Lee, J. D., Drysdale, W. S., Lewis, A. C., Hueglin, C., Emmenegger, L., and Carslaw, D. C.: COVID-19 lockdowns highlight a risk of increasing ozone pollution in European urban areas, Atmospheric Chemistry and Physics, 21, 4169-4185, 10.5194/acp-21-4169-2021, 2021.

Hammer, M. S., van Donkelaar, A., Martin, R. V., McDuffie, E. E., Lyapustin, A., Sayer, A. M., Hsu, N. C., Levy, R. C., Garay, M. J., Kalashnikova, O. V., and Kahn, R. A.: Effects of COVID-19 lockdowns on fine particulate matter concentrations, Science Advances, 7, 10.1126/sciadv.abg7670, 2021.

He, C., Yang, L., Cai, B. F., Ruan, Q. Y., Hong, S., and Wang, Z.: Impacts of the COVID-19 event on the NOx emissions of key polluting enterprises in China, Applied Energy, 281, 10.1016/j.apenergy.2020.116042, 2021.

Kroll, J. H., Heald, C. L., Cappa, C. D., Farmer, D. K., Fry, J. L., Murphy, J. G., and Steiner, A. L.: The complex chemical effects of COVID-19 shutdowns on air quality, Nat Chem, 12, 777-779, 10.1038/s41557-020-0535-z, 2020.

Lee, J. D., Drysdale, W. S., Finch, D. P., Wilde, S. E., and Palmer, P. I.: UK surface NO2 levels dropped by 42% during the COVID-19 lockdown: impact on surface O-3, Atmospheric Chemistry and Physics, 20, 15743-15759, 10.5194/acp-20-15743-2020, 2020.

Liu, F., Page, A., Strode, S. A., Yoshida, Y., Choi, S., Zheng, B., Lamsal, L. N., Li, C., Krotkov, N. A., Eskes, H., van der A, R., Veefkind, P., Levelt, P. F., Hauser, O. P., and Joiner, J.: Abrupt decline in tropospheric nitrogen dioxide over China after the outbreak of COVID-19, Science Advances, 6, 10.1126/sciadv.abc2992, 2020.

Peralta, O., Ortinez-Alvarez, A., Torres-Jardon, R., Suarez-Lastra, M., Castro, T., and Ruiz-Suarez, L. G.: Ozone over Mexico City during the COVID-19 pandemic, Science of the Total Environment, 761, 10.1016/j.scitotenv.2020.143183, 2021.

Schiermeier, Q.: Why pollution is plummeting in some cities-but not others, Nature, 508, 313, https://doi.org/10.1038/d41586-020-01049-6, 2020.

Shi, Z., Song, C., Liu, B., Lu, G., Xu, J., Van Vu, T., Elliott, R. J. R., Li, W., Bloss, W. J., and Harrison, R. M.: Abrupt but smaller than expected changes in surface air quality attributable to COVID-19 lockdowns, Sci. Adv., 7, eabd6696, https://doi.org/10.1126/sciadv.abd6696, 2021.

Sillman, S.: The relation between ozone, NO_x and hydrocarbons in urban and polluted rural environments, Atmospheric Environment, 33, 1821-1845, Doi 10.1016/S1352-2310(98)00345-8, 1999.

4.7 Supplementary Information

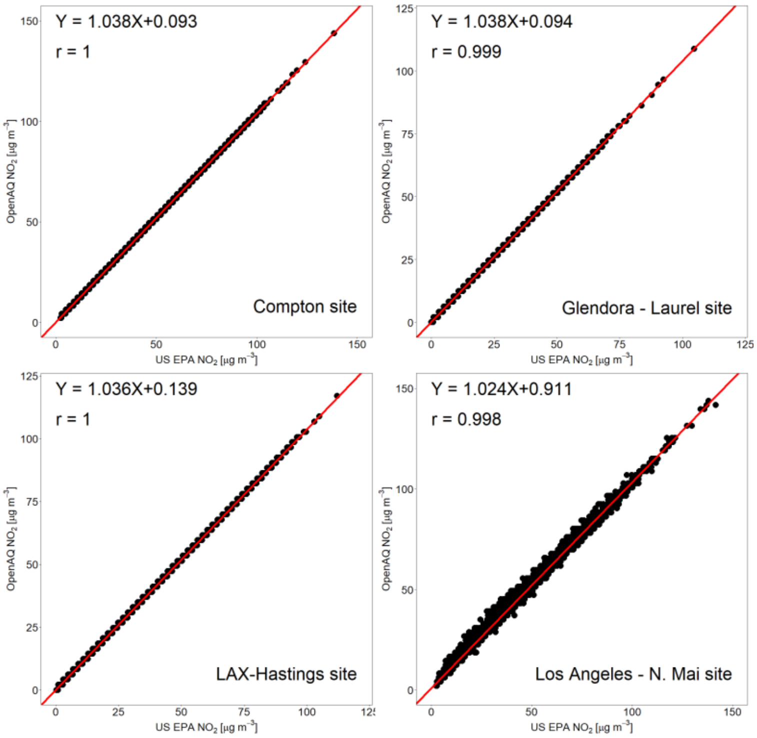

Figure S4.1: Validation of hourly NO$_2$ from OpenAQ against US EPA measurements. Sites used here are from Los Angeles.

Table S4.1: Site selection and data sources.

City	Data source	Weblink	Site type	Site name (or Site code)	Quality assurance
Beijing	Official	zx.bjmemc.com.cn/	Urban background	“Dongsi", "Tiantan", "Guanyuan", "Wanshouxigong", "Aotizhongxin", "Nongzhanguan", "Wanliu", "Beibuxincun", "Zhiwuyuan", "Fengtaihuayuan", "Yungang", "Gucheng"	Officially validated
			Roadside	"Qianmen", Yongdingmenbei", "Xizhimenbei", "Nansanhuan", Dongsihuan"	
			Rural	"Fangshan", "Daxing", "Yizhuang", "Tongzhou", "Shunyi", "Chuangping", "Menkougou", "Pinggu", "Huairou", "Miyun", "Yanqing"	
Wuhan	Official	http://106.37.208.233:20035/	Urban background	"1325A","1326A","1327A","1328A","1329A","1330A","1331A","1332A","1333A"	Officially validated
			Rural	"1334A"	
London	Official	https://uk-air.defra.gov.uk/data/data_selector_service?show=auto&submit=Reset&f_limit_was=1	Urban background	"London Bloomsbury", "London Haringey Priory Park South", "London N Kensington", "London Teddington Bushy Park"	Official validated
			Roadside	"London Marylebone Road"	
			Rural	"Chilbolton Observatory"	
Madrid	Official	http://datos.comunidad.madrid/catalogo/dataset/calidad_aire_datoshistorico	Urban background	"28007004"	Officially validated
			Roadside	"28065014", "28074007"	
			Rural	"28016001", "28067001", "28102001", "28133002", "28171001"	
Rome	Official	http://www.arpalazio net/main/aria/sci/annoincorso/chimici.php	Urban background	"2","8","15","39","48","49","56"	Officially validated
			Roadside	"3", "5", "45", "47", "55", "83", "84", "85"	
			Rural	"14","40"	
Milan	Official	https://www.dati.lombardia.it/browse?q=Dati+sensori+aria&sortBy=relevance&page=1	Urban background	"5517", "5520", "5534", "5547", "5549", "5619", "5630", "5631", "5646", "5710", "5717", "5718", "5825", "5826", "5832", "6300", "6324", "6326", "6346", "6364", "10278", "10279", "10280", "10282"	Officially validated
			Roadside	"5504", "5507", "5531", "5532", "5542", "5551", "5609", "5725", "5812", "5823", "5827", "5834", "5835", "6276", "6320", "6328", "6354", "6356", "6366", "9999", "10001", "10002"	
			Rural	"5548", "5554", "5707", "5721", "5814", "6288", "6338"	
Berlin	Official	https://luftdaten.berlin.de/lqi	Urban background	"042 Neukolln"	Officially validated
			Roadside	"174 Frankfurter Allee"	
			Rural	"032 Grunewald"	

Paris	Official	https://www.airparif.asso.fr/en/telechargement/telechargement-station	Urban background	"ARG", "AUB", "BOB", "CERGY", "CHAMP", "DEF", "EVRY", "GEN", "LOGNES", "MONTG", "NEUIL", "NOGENT", "PA07", "PA12", "PA13", "PA15L", "PA18", "STDEN", "VILLEM", "VITRY"	Officially validated
			Roadside	"A1", "AUT", "BASCH", "BONAP", "BP_EST", "CELES", "ELYS", "HAUS", "OPERA", "RD934", "RN2", "RN6","SOULT"	
			Rural	"RUR-E", "RUR-NE", "RUR-NO", "RUR-SE", "RUR-SO", "RUR_N", "RUR_S"	
New York	OpenAQ*	https://openaq.org/#/?_k=etobqa	Urban background	"Bayonne", "Newark Firehouse"	Data originated from government- and research-grade sources, and validated with official sources
			Roadside	"Fort Lee Near Road"	
			Rural	"Chester", "Flemington", "Rutgers University"	
Los Angeles	OpenAQ	https://openaq.org/#/?_k=etobqa	Urban background	"Compton", "Lancaster-Division"	
			Roadside	"Los Angeles - N. Mai"	
			Rural	"Glendora - Laurel", "LAX-Hastings"	
Delhi	Official	https://app.cpcbccr.com/ccr/#/caaqm-dashboard-all/caaqm-landing	Urban background	"Nehru Nagar"	Officially validated
			Rural	"Sonia Vihar", "Sri Aurobindo Marg"	

---

* OpenAQ data are from official sources although they are not necessarily validated before being released. We evaluated the officially released air quality data from Los Angeles (after the data analyses in this study) with OpenAQ data; they are highly correlated (both slope and correlation coefficient are either equal to or close to 1). This demonstrates that the sources of data are reliable

Table S4.2: Percentage changes in observed air pollutant concentrations (2nd-5th weeks after the lockdown began vs. 2nd-3rd weeks before the lockdown start dates).

	Beijing	Wuhan	Milan	Rome	Madrid	London	Paris	Berlin	New York	Los Angeles	Delhi
Urban background											
NO	N.A.	N.A.	N.A.	-81.1±12.5	-74.5±8.5	-53.9±38.9	N.A.	-39.2±61.8	N.A.	N.A.	-78.0±13.3
NO_2	-40.5±33.2	-47.3±17.4	-35.1±23.3	-42.2±17.3	-49.0±20.4	-10.1±36.6	-29.8±27.0	-28.1±34.2	-42.4±26.2	-49.5±21.2	-60.2±14.8
NO_x	N.A.	N.A.	-56.7±18.4	-60.1±14.4	-57.3±15.7	-23.3±33.5	N.A.	-30.0±37.0	N.A.	N.A.	-68.8±12.8
O_3	79.6±48.5	166.5±60.5	93.9±65.3	66.1±30.7	16.2±16.1	26.4±20.3	36.1±16.5	57.8±19.8	23.6±24.8	25.9±14.4	86.4±35.8
O_x	2.3±18.3	21.3±25.2	0.6±11.1	6.0±10.7	-1.6±10.3	14.6±10.4	14.0±11.5	27.6±9.9	-3.6±8.1	-5.7±9.3	11.5±12.8
CO	14.5±80.7	-16.3±17.9	-27.9±16.0	N.A.	-60.9±10.1	-19.8±16.0	N.A.	N.A.	-27.6±24.2	-55.1±20.3	-28.3±25.3
SO_2	-24.9±44.4	24.3±35.6	-1.9±7.4	-17.4±43.5	-48.2±4.7	-31.0±18.3	90.6±94.6	N.A.	N.A.	N.A.	-53.3±46.0
$PM_{2.5}$	19.2±108.6	-27.7±37.1	N.A.	-30.8±37.9	-38.6±17.2	152.9±165.0	116.0±112.7	N.A.	-30.7±33.0	-33.3±27.8	-19.1±30.3
PM_{10}	7.8±81.0	-29.9±32.2	N.A.	-23.8±29.1	-54.1±18.9	116.5±110.3	67.0±75.6	35.3±49.8	N.A.	-53.6±36.9	-18.6±30.8
Roadside											
NO	N.A.	N.A.	N.A.	-71.8±15.4	-81.5±12.7	-87.6±7.1	N.A.	-53.8±36.0	N.A.	N.A.	N.A.
NO_2	-30.8±35.5	N.A.	-38.7±21.9	-41.4±17.4	-46.0±20.1	-53.5±18.9	-34.8±23.3	-29.3±33.1	-37.3±25.9	-50.3±19.7	N.A.
NO_x	N.A.	N.A.	-52.8±20.8	-57.6±15.6	-65.0±13.4	-74.4±11.0	N.A.	-41.3±33.8	N.A.	N.A.	N.A.
O_3	81.0±67.9	N.A.	155.6±83.2	20.7±11.2	19.5±21.0	134.7±49.8	N.A.	79.4±28.1	N.A.	27.6±19.0	N.A.
O_x	-2.6±18.2	N.A.	0.6±12.3	-5.4±7.3	-4.8±11.2	-6.1±8.6	N.A.	23.5±10.5	N.A.	-11.5±8.2	N.A.
CO	9.9±76.1	N.A.	-28.6±16.0	-39.3±11.4	-14.5±28.3	N.A.	N.A.	-23.9±16.3	-22.0±23.7	N.A.	N.A.
SO_2	-25.4±39.0	N.A.	N.A.	N.A.	-4.1±4.5	-65.9±14.9	N.A.	1.7±75.9	N.A.	N.A.	N.A.
$PM_{2.5}$	3.4±94.6	N.A.	N.A.	-17.9±41.8	N.A.	107.6±148.5	45.6±69.9	N.A.	-30.0±49.9	-40.8±28.4	N.A.
PM_{10}	-5.4±70.1	N.A.	-40.0±21.2	-22.8±25.9	-61.8±9.5	48.4±74.4	25.7±47.4	21.6±48.7	N.A.	-48.5±23.8	N.A.
Rural											
NO	N.A.	N.A.	N.A.	-52.1±33.5	-34.7±3.5	161.4±66.5	N.A.	-74.5±24.0	N.A.	N.A.	-72.4±15.8
NO_2	-41.7±28.2	-64.8±18.3	-33.9±19.9	-46.1±22.0	-50.7±9.5	115.8±90.2	99.2±66.7	-25.0±33.9	-40.2±37.6	-47.8±21.7	-43.1±21.0
NO_x	N.A.	N.A.	-51.7±15.4	-54.1±19.8	-45.9±8.6	124.2±82.4	N.A.	-29.9±32.0	N.A.	N.A.	-52.2±17.5
O_3	76.3±34.8	102.3±43.4	75.5±42.6	29.6±13.8	0.2±13.3	4.2±14.6	16.8±14.2	47.6±14.5	7.0±14.4	5.8±9.9	N.A.
O_x	11.9±13.0	23.3±25.9	13.9±13.1	16.2±11.5	-4.2±12.4	11.2±14.9	20.3±13.5	34.9±13.3	0.6±9.2	-6.8±8.8	N.A.
CO	9.1±69.7	-24.6±18.1	-12.7±16.5	N.A.	-22.7±6.0	N.A.	N.A.	N.A.	N.A.	-31.2±12.9	-11.1±33.6
SO_2	-21.5±37.4	2.4±23.7	N.A.	38.6±85.5	0.8±5.3	326.1±129.7	N.A.	N.A.	N.A.	N.A.	4.4±27.0
$PM_{2.5}$	9.7±86.3	-14.3±43.4	N.A.	-0.1±61.6	-23.7±20.9	164.5±148.7	136.8±144.5	N.A.	-28.0±28.4	-13.3±27.0	-34.2±26.8
PM_{10}	6.0±70.2	-26.8±34.2	N.A.	5.6±55.0	-57.3±13.4	161.5±121.9	93.1±90.0	34.0±43.8	N.A.	-34.5±35.2	-22.5±23.9

Note: N.A.: data not available.

CHAPTER 5: SYNTHESIS

5.1 Summary and Conclusions

Observations of air quality have been extensively used to assess compliance with air quality standards, and to understand trends in air quality, effectiveness of air quality policies and impacts of air pollution on human health. But observations of air quality are not good indicators of emission changes due to limited spatial or temporal coverage, and the non-linearity between changes in observations of air quality and changes in emissions. Meteorological conditions such as wind speeds, boundary layer heights, and relative humidity are also important factors affecting the accumulation and dispersion of surface air pollution at local to regional scale. Effective air quality policy is hindered by inaccurate estimates of precursor emissions, unvalidated, sparse or absent monitoring networks, and complex causes of air pollution. The main objective of this thesis was to use a combination of surface and satellite observations and a chemical transport model to interpret changes in anthropogenic emissions underlying abrupt changes in observed air quality in time and space at local to regional scales. Findings in this thesis offer guidance on developing effective emission control measures to reduce pollution and protect human health.

This thesis focused on three key research gaps identified in Chapter 1:

- Characterising the true efficacy of strict emission controls in addressing $PM_{2.5}$ pollution in and around the Beijing-Tianjin-Hebei region in northern China in autumn-winter 2017/2018. This approach is now adopted in many regions in China, despite limited assessment of the relative contribution of emissions reductions and other factors like meteorology that is necessary for successful implementation of these control measures elsewhere.
- Estimating NO_x emissions in 10 large cities in South and Southeast Asia and assessing under-constrained bottom-up emission inventories using the now widely adopted wind rotation and EMG fit method with TROPOMI tropospheric NO_2 columns.

- Gaining insight into complex atmospheric processes affecting 11 global $PM_{2.5}$, NO_x and O_3 pollution hotspots using surface observations during abrupt changes in anthropogenic emissions during COVID-19 lockdowns in response to the outbreak of COVID-19.

Chapter 2 interpreted the contribution of autumn-winter emission controls to air quality improvements in and around the Beijing-Tianjin-Hebei region (BTH) in autumn-winter 2017/2018. Surface observations of air quality from China National Environmental Monitoring Network (CNEMN) and local Beijing Municipal Environmental Monitoring Network (BJMEMN) were evaluated against independent measurements from the intensive Atmospheric Pollution & Human Health in a Chinese Megacity (APHH) campaign in Beijing in November-December 2016. $PM_{2.5}$ and trace gases (NO_2, SO_2 and CO) from the surface networks are temporally consistent with independent measurements ($r > 0.9$ for $PM_{2.5}$ and $r > 0.7$ for gases). Any discrepancies are mostly due to spatial gradients in pollution sources in the urban environment and known instrument interferences. Results from the surface networks in BTH show that $PM_{2.5}$ decreased by 29% from 103 to 74 $\mu g\ m^{-3}$ in the control period relative to the previous year, exceeding the regional target of 15%. Large underestimates in NO_x (by 50%), CO (>100%), and point sources of SO_2 (>100%) in the monthly anthropogenic emissions from the Multi-resolution Emission Inventory for China (MEIC) were addressed with constraints from surface measurements of air quality and the GEOS-Chem model. The model with scaled MEIC emissions reproduces the observed spatial distribution in $PM_{2.5}$ ($r = 0.68$). Despite a 15% positive bias in modelled total $PM_{2.5}$ and biases in the modelled $PM_{2.5}$ components organic aerosol, nitrate, and sulfate, the model simulates the observed relative decline in $PM_{2.5}$ in BTH. According to the model, emissions in BTH declined by 0.27 Tg NO_x as NO, 0.66 Tg SO_2, 70 Gg OC, 50 Gg BC, and 9.7 Tg CO. These account for less than half (at most 43%) the decline in total $PM_{2.5}$ and alone would not achieve the $PM_{2.5}$ reduction targets. Most (57%) of the decline in $PM_{2.5}$ was due to interannual variability in meteorological factors during the emission control period. Specifically, these included a deeper planetary boundary layer and stronger winds that enhanced dilution and dispersion of pollution, and lower relative humidity that reduced formation of secondary inorganic aerosols. The ability to achieve air pollution reduction targets is an insufficient measure of the success of emission controls. The relative role of emissions reductions and other influential factors like meteorology should factor into decisions to extend similar emission control measures to other regions.

Chapter 3 provides top-down NO_x emission estimates over 10 large cities in South and Southeast Asia in 2019, as the region is developing rapidly, surface observations are sparse, and NO_x is an important precursor of ozone and $PM_{2.5}$ pollution. These were obtained by applying the EMG method and wind rotation technique to NO_2 tropospheric VCDs from TROPOMI and wind fields from the ERA5 meteorology reanalysis product. Highest NO_2 concentrations are observed at Delhi, Dhaka, Singapore and Jakarta with the annual averaged oversampled TROPOMI NO_2 greater than 4.9×10^{15} molec. Cm^{-2} Annual averaged NO_x lifetimes, obtained from the EMG fit, are 3.1-8.2 hours across the selected cities, with the shortest estimated at Dhaka, Singapore and Delhi (3.1-3.3 hours) and highest at Chennai (8.2 hours). Annual averaged NO_x emissions are below 50 mol s^{-1} from Karachi, Ahmedabad, Mumbai, Lahore and Chennai, between 50-100 mol s^{-1} from Manila and Jakarta, and over 100 mol s^{-1} from Delhi, Dhaka and Singapore. The relative error from satellite NO_2 observations, uncertainty in across-wind integration distance, selection of wind data, the NO_x:NO_2 ratio, and the choice of input background NO_2 concentration is 10%-30%. Bottom-up NO_x emissions, mostly (>85%) anthropogenic, are 17-32% lower than the top-down estimates for Lahore and Dhaka, and but are 15-65% more than the top-down estimates for Karachi, Ahmedabad, Mumbai, Delhi, and Manila, and much more (>140%) for Chennai, Singapore and Jakarta. This suggests potential errors in the activity rates or emission factors in the commonly used bottom-up emission inventories and the use of coarse emission inventories for estimating NO_x from cities in South and Southeast Asia. The ability of the top-down method to derive monthly NO_x emissions for most (>10 months) of the year is limited to Singapore, Jakarta and Manila, due to gaps in TROPOMI coverage, an indistinct peak in NO_2 relative to the background, and nearby seasonal NO_2 hotspots for the other cities. Monthly top-down NO_x estimates range from 63 to 148 mol s^{-1} for Singapore, 44 to 109 mol s^{-1} for Jakarta, and 26 to 67 mol s^{-1} for Manila, whereas there is no month-to-month variability in these bottom-up emission inventories. Discrepancies between top-down and bottom-up NO_x emissions point to errors in understanding the sources that contribute to anthropogenic NO_x sources and hinders development of effective policies.

Chapter 4 investigates surface observations of air quality in 11 cities worldwide before, during and after the COVID-19 lockdowns in 2020. Measurements of six criteria air pollutants (i.e., NO_2, O_3, CO, SO_2, $PM_{2.5}$ and PM_{10}), auxiliary pollutants (NO and NO_x), and the total gaseous oxidant (O_x) were analysed at urban background, roadside and rural sites in each city. Varying patterns were observed concentrations of these species. Observed NO_2 decreased substantially at urban background and roadside sites in all the cities, by 10.1-60.2% at urban background sites, and by 29.3-53.5% at roadside sites. In contrast, observed O_3 increased in all cities after the lockdowns, by 16.2-166.5% at urban background sites and by 19.5-155.6% at roadside sites. As a result, little changes were observed for O_x, which range from a decrease of -3.6% in New York to an increase of 27.6% in Berlin. Unlike observed NO_2 and O_3, there is not a clear pattern for $PM_{2.5}$. The percentage changes in observed $PM_{2.5}$ are -38.6-152.9% at urban background sites, -40.8-107.6% at roadside sites, and -34.2-164.5% at rural sites. But by comparing observations in 2020 to those in 2016-2019 during the equivalent periods, results in this chapter show that the observations of air quality alone cannot represent the changes in emissions due to COVID-19 lockdowns as the impact of meteorology should be considered.

This thesis integrated observations from surface monitoring networks, field campaigns and the TROPOMI satellite instrument. Observations of air quality, emission inventories, and meteorological reanalysis were used with a range of techniques including the GEOS-Chem chemical transport model, the oversampling technique, the EMG method and wind rotation technique. Findings in this thesis demonstrated that observations of air quality alone cannot be used to fully assess the compliance to air quality standards or air quality targets. The necessity of interpreting the relative role of emissions and meteorology on observed air quality is demonstrated through three research projects of different focuses and under different pollution environments. Bottom-up emission inventories can provide estimates of air pollution based on activity data and emission factors, but these are subject to large uncertainties. Surface and space-based measurements of air quality are used in this thesis to evaluate and correct biases in commonly used bottom-up emission inventories.

5.2 Limitations and Opportunities for Future Research

Limitations in the work presented in this thesis present opportunities for future research. In Chapter 2, surface measurements of air quality from monitoring networks are used to correct bottom-up emission inventories and assess changes in emissions of NO_2, SO_2, CO and primary $PM_{2.5}$. This is due to large biases in bottom-up emission inventory in China, and the missing of updated bottom-up emission inventory in the emission control period. But as discussed in Chapter 2, there is non-linearity between changes in scaled emissions and changes in modelled concentrations. Surface monitoring networks are sparse and unevenly distributed in the sampling region of the model, further hindering model's ability to reproduce changes in emissions in grids where there are few or no monitoring sites. Also, precursors to $PM_{2.5}$ such as NH_3 and VOCs are missing from the surface monitoring networks. It was not possible to use the older generation of satellite observations to assess changes in surface NO_2, SO_2, VOCs, and CO for autumn-winter in northern China. TROPOMI observations are provided with high spatial resolutions, high data density and improved data quality. But it was not available for the time period of the work in Chapter 2. In the future research, TROPOMI NO_2, SO_2 and HCHO have the potential to detect changes in emissions of NO_2, SO_2 and VOCs from high polluted areas in China in autumn-winter with improved accuracy. These can be used together with Chinese surface monitoring networks and GEOS-Chem model to evaluate the efficacy of nationwide emission controls in China as similar emission controls are now implemented every autumn-winter. Comparisons of modelled and measured $PM_{2.5}$ components are limited to comparisons using the APHH campaign measurements in Beijing, as measurements of $PM_{2.5}$ in BTH are not publicly available. More comprehensive assessment of model's ability in reproducing measured $PM_{2.5}$ components can be conducted if more measurements become available in future research.

Current studies using the EMG approach are limited to estimating NO_x emissions during a long time period of multiple months or at least a year. A recent study (Lange et al., 2022) and Chapter 3 in this thesis have identified a few causes for the EMG method fail due to data gaps, unrecognized NO_2 peak near the city centre, and a second but smaller NO_2 peak in the downwind side. Future research is needed to improve the EMG fitting approach, solve the known issues in estimating monthly NO_x emissions from isolated point sources.

Geostationary sensors such as the Geostationary Environment Monitoring Spectrometer (GEMS) over South Asia, launched in 2020 provide observations every one to two hours of air quality over East Asia during sunlight hours (Kim et al., 2020), improving on the single overpass time of TROPOMI and its predecessors. This will provide an unprecedent opportunity to monitor air quality and estimate emissions in South and Southeast Asia at different times of the day. Most crucially during morning and evening rush hours rather than at midday for TROPOMI when traffic density is at a daytime minimum. Future geostationary sensor include the Tropospheric Emissions: Monitoring of Pollution (TEMPO) to be launched in 2022 to provide observations over North America (Zoogman et al., 2017), and Sentinel-4 to be launched over Europe (Courreges-Lacoste et al., 2017).

In Chapter 4, surface observations of air quality are taken from monitoring sites that were built to represent the specific environment of each city (i.e., urban background, roadside, and rural). There may be some variabilities in the concentrations of air pollutants at different stations of the same type. This could cause potential uncertainties in our analyses if to represent the whole city. Whenever possible, we use data from multiple stations for each site type to reduce this uncertainty. But where only one or few stations are available for a site type, the data may be subject to more influence from local emission sources. Therefore, results in Chapter 4 should be treated in the context of the site availability.

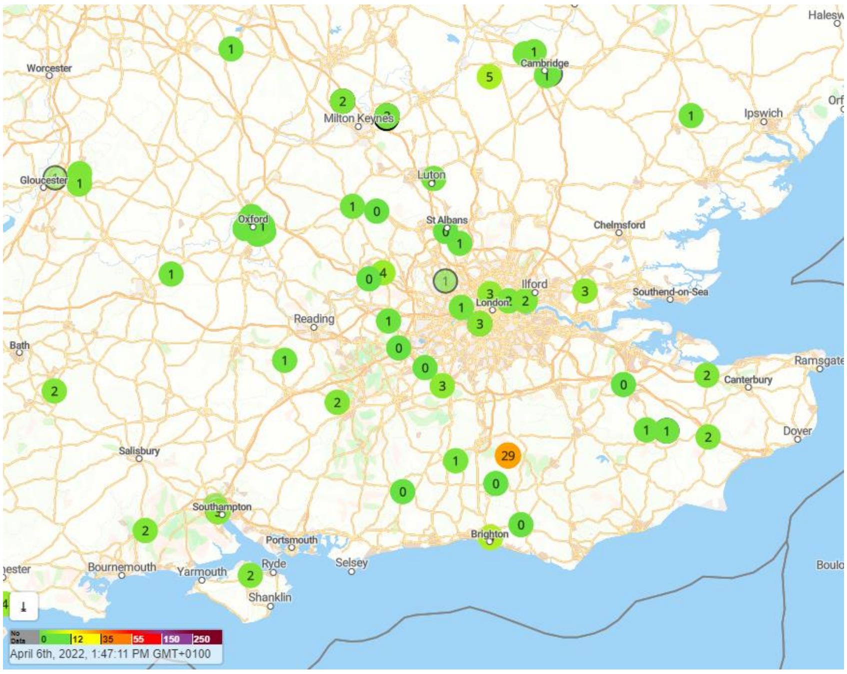

Figure 5.1: Example of real-time hourly PM$_{2.5}$ measured by low cost sensors in the Southeast UK. Source: https://www2.purpleair.com/; accessed 06 April 2022.

As shown in Figure 5.1, low-cost sensors are an emerging method to monitor surface air quality under different environments. Calibrated and reliable low cost sensors complement standard surface monitoring networks operated by governments as mentioned in Chapters 2 and 4. They are portable so that they can be deployed to monitor air quality during short term emission controls events such as the COVID-19 lockdowns mentioned in Chapter 4. Future research can combine these measurements with meteorological inputs for use in the random forest machine learning technique as described in Shi et al. (2021) to aid in interpreting changes in emissions by providing greater spatial coverage than reference monitors.

5.3 References

Courreges-Lacoste, G. B., Sallusti, M., Bulsa, G., Bagnasco, G., Veihelmann, B., Riedl, S., Smith, D. J., and Maurer, R.: The Copernicus Sentinel 4 mission - A Geostationary Imaging UVN Spectrometer for Air Quality Monitoring, Conference on Sensors, Systems, and Next-Generation Satellites XXI, Warsaw, POLAND, Sep 11-14, WOS:000418446600005, 10.1117/12.2282158, 2017.

Kim, J., Jeong, U., Ahn, M. H., Kim, J. H., Park, R. J., Lee, H., Song, C. H., Choi, Y. S., Lee, K. H., Yoo, J. M., Jeong, M. J., Park, S. K., Lee, K. M., Song, C. K., Kim, S. W., Kim, Y. J., Kim, S. W., Kim, M., Go, S., Liu, X., Chance, K., Chan Miller, C., Al-Saadi, J., Veihelmann, B., Bhartia, P. K., Torres, O., Abad, G. G., Haffner, D. P., Ko, D. H., Lee, S. H., Woo, J. H., Chong, H., Park, S. S., Nicks, D., Choi, W. J., Moon, K. J., Cho, A., Yoon, J., Kim, S. K., Hong, H., Lee, K., Lee, H., Lee, S., Choi, M., Veefkind, P., Levelt, P. F., Edwards, D. P., Kang, M., Eo, M., Bak, J., Baek, K., Kwon, H. A., Yang, J., Park, J., Han, K. M., Kim, B. R., Shin, H. W., Choi, H., Lee, E., Chong, J., Cha, Y., Koo, J. H., Irie, H., Hayashida, S., Kasai, Y., Kanaya, Y., Liu, C., Lin, J., Crawford, J. H., Carmichael, G. R., Newchurch, M. J., Lefer, B. L., Herman, J. R., Swap, R. J., Lau, A. K. H., Kurosu, T. P., Jaross, G., Ahlers, B., Dobber, M., McElroy, C. T., and Choi, Y.: New Era of Air Quality Monitoring from Space: Geostationary Environment Monitoring Spectrometer (GEMS), Bulletin of the American Meteorological Society, 101, E1-E22, 10.1175/bams-d-18-0013.1, 2020.

Lange, K., Richter, A., and Burrows, J. P.: Variability of nitrogen oxide emission fluxes and lifetimes estimated from Sentinel-5P TROPOMI observations, Atmos. Chem. Phys., 22, 2745-2767, 10.5194/acp-22-2745-2022, 2022.

Shi, Z., Song, C., Liu, B., Lu, G., Xu, J., Van Vu, T., Elliott, R. J. R., Li, W., Bloss, W. J., and Harrison, R. M.: Abrupt but smaller than expected changes in surface air quality attributable to COVID-19 lockdowns, Sci. Adv., 7, eabd6696, https://doi.org/10.1126/sciadv.abd6696, 2021.

Zoogman, P., Liu, X., Suleiman, R. M., Pennington, W. F., Flittner, D. E., Al-Saadi, J. A., Hilton, B. B., Nicks, D. K., Newchurch, M. J., Carr, J. L., Janz, S. J., Andraschko, M. R., Arola, A., Baker, B. D., Canova, B. P., Miller, C. C., Cohen, R. C., Davis, J. E., Dussault, M. E., Edwards, D. P., Fishman, J., Ghulam, A., Abad, G. G., Grutter, M., Herman, J. R., Houck, J., Jacob, D. J., Joiner, J., Kerridge, B. J., Kim, J., Krotkov, N. A., Lamsal, L., Li, C., Lindfors, A., Martin, R. V., McElroy, C. T., McLinden, C., Natraj, V., Neil, D. O., Nowlan, C. R., O'Sullivan, E. J., Palmer, P. I., Pierce, R. B., Pippin, M. R., Saiz-Lopez, A., Spurr, R. J. D., Szykman, J. J., Torres, O., Veefkind, J. P., Veihelmann, B., Wang, H., Wang, J., and Chance, K.: Tropospheric emissions: Monitoring of pollution (TEMPO), J Quant Spectrosc Ra, 186, 17-39, 10.1016/j.jqsrt.2016.05.008, 2017.

Appendix

CORONAVIRUS

Abrupt but smaller than expected changes in surface air quality attributable to COVID-19 lockdowns

Zongbo Shi[1]*†, Congbo Song[1]*†, Bowen Liu[2], Gongda Lu[1], Jingsha Xu[1], Tuan Van Vu[3], Robert J. R. Elliott[2], Weijun Li[4], William J. Bloss[1], Roy M. Harrison[1‡]

The COVID-19 lockdowns led to major reductions in air pollutant emissions. Here, we quantitatively evaluate changes in ambient NO_2, O_3, and $PM_{2.5}$ concentrations arising from these emission changes in 11 cities globally by applying a deweathering machine learning technique. Sudden decreases in deweathered NO_2 concentrations and increases in O_3 were observed in almost all cities. However, the decline in NO_2 concentrations attributable to the lockdowns was not as large as expected, at reductions of 10 to 50%. Accordingly, O_3 increased by 2 to 30% (except for London), the total gaseous oxidant ($O_x = NO_2 + O_3$) showed limited change, and $PM_{2.5}$ concentrations decreased in most cities studied but increased in London and Paris. Our results demonstrate the need for a sophisticated analysis to quantify air quality impacts of interventions and indicate that true air quality improvements were notably more limited than some earlier reports or observational data suggested.

INTRODUCTION

Air pollution (both indoor and outdoor) is the single largest environmental risk to human health globally, contributing to 8.8 million deaths in 2015 (*1*). The World Bank estimated that air pollution costs the global economy \$3 trillion in 2015 (*2*). It has been suggested that poor air quality is correlated with a higher mortality rate from COVID-19 infection (*3*). Although a causal relationship between the two is difficult to confirm, air pollution contributes to respiratory and cardiovascular diseases and thus has the potential to cause increased COVID-19 death rates (*4*).

In response to the COVID-19 crisis, governments around the world introduced severe restrictions on behavior or lockdowns, which led to the cessation of a large swathe of economic activity and thus reduced air pollutant emissions (*5*). The rapid and unprecedented reduction in the economic activity provides a unique opportunity to study the impact of a global-scale natural intervention on air pollution, which offers insights for the prioritization of future clean air actions.

Many recent studies have explored impacts of the COVID-19 lockdowns on air quality. The most common approach is to undertake a simple statistical analysis that compares air quality before and after the lockdowns began or during the lockdowns with the same periods in previous years (*6*, *7*). Some studies also compared the air quality before and after lockdown started for periods with similar meteorological conditions (*8*). Satellite observations of NO_2 have also been used to estimate the reduction in column NO_2 due to the lockdowns (*3*, *9*–*11*).

A major caveat in a number of these studies is that meteorology moderates the link between emissions and pollutant concentrations, and so, weather changes can mask the changes in emissions on air quality (*12*–*14*). Such methods cannot explain the observed severe pollution events during the lockdowns in some cities (*15*–*17*). Comparisons of pollutant levels in 2020 with previous years may assume that air pollutant emissions have not changed over the past few years, which is often not the case, particularly in those cities where clean air policy actions are in place (*14*, *18*). Furthermore, air pollutant emissions change substantially from winter to spring; thus, a direct comparison of air pollutant concentrations before and during the lockdowns could also give unreliable results. Venter *et al.* (*9*) developed statistical models (regression) to estimate the impact of lockdowns on air quality in several countries. However, the performance of the regression was often limited with correlation coefficients as low as 0.2. He *et al.* (*19*) applied a "difference-in-difference" approach, which may provide a more accurate estimate of air quality improvement; this method assumes that the control cities are not subject to any impacts.

Air quality modeling can also decouple the effect of emission changes from meteorology (*20*, *21*) and is often applied for scenario analysis. A major challenge in evaluating the impacts of short-term interventions on real-world air quality is to estimate emission changes (*16*, *20*, *21*).

Machine learning offers an alternative and reliable method in quantifying changes in air quality due to emissions and meteorological factors (*12*–*14*). Myllyvirta and Thieriot (*22*) used a random forest (RF) method (*13*), which was developed for assessing long-term air quality changes, to estimate the short-term changes in NO_2 and PM_{10} in Europe due to the COVID-19 lockdowns (see Materials and Methods).

The purpose of this study was to evaluate the impacts and implications of the natural experiment of the COVID-19 lockdowns in spring 2020 on air quality. To do this, we optimized a weather normalization technique based on Grange and Carslaw (*13*) and Vu et al. (*14*) to decouple the effects of meteorology from short-term emission changes on surface air quality monitoring data in 11 global cities that were subjected to extensive lockdown measures. The deweathered data allow us to quantitatively evaluate the real-world changes in air quality due to the lockdown measures in these cities (see Materials and Methods). These selected cities cover a range of air pollution climates, from highly to less polluted and from $PM_{2.5}$- to NO_2-dominated

---

[1]School of Geography Earth and Environment Sciences, University of Birmingham, Birmingham B15 2TT, UK. [2]Department of Economics, University of Birmingham, Birmingham B15 2TT, UK. [3]School of Public Health, Imperial College London, London W2 1PG, UK. [4]Department of Atmospheric Sciences, School of Earth Sciences, Zhejiang University, Hangzhou 310027, China.

*These authors contributed equ
†Corresponding author. Email: [redacted] (Z.S.); [redacted] (C.S.)
‡Also at: Department of Enviro and C Environmental Studies, King Abdulaziz University, P.O. Box 80203, Jeddah 21589, Saudi Arabia.

pollution. Data were divided into roadside, urban background, and rural sites to better understand the impacts of road traffic and urban emissions on air quality changes.

RESULTS

We first estimated the percentage change (P) in the observed or deweathered concentrations of air pollutants using the following equation

$$P = \overline{(C_i - C)/C \times 100\%} \tag{1}$$

where C is the average concentration in the second and third weeks before the lockdown date or equivalent (as a prelockdown baseline), and C_i is the average concentrations in the ith day (from the 1st to 28th day) starting in the second week after the lockdown start date for each city and for each year (see Fig. 1). For example

$$P_{2020} = \overline{(C_{i,2020} - C_{2020})/C_{2020} \times 100\%} \tag{2}$$

The week immediately before and after the lockdown date was considered a transition period and so was excluded in the calculations. We recognize that the transition may have started earlier in some cities such as London, but for consistency, we applied the same Eq. 1 for calculation. For clarification, we will use P_{obs} and P_{dew} to represent changes in observed and deweathered concentrations, respectively.

We then estimated the detrended percentage change (P^*) in the concentration of each air pollutant (deweathered only; Fig. 1), calculated by

$$P^* = P_{2020} - P_{2016-2019} \tag{3}$$

where P_{2020} and $P_{2016-2019}$ are percentage changes in deweathered concentrations of air pollutants in 2020 and 2016–2019, respectively. P^* was calculated by Monte Carlo simulations ($n = 10{,}000$) based on the normal distribution of P_{2020} and $P_{2016-2019}$.

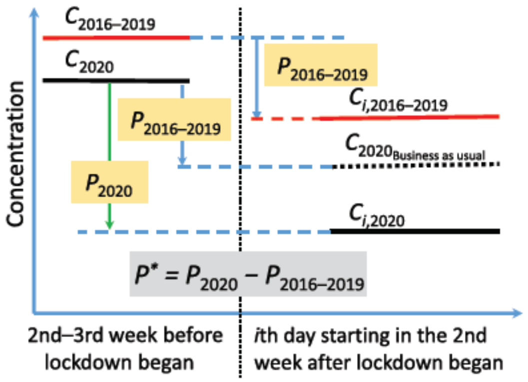

Fig. 1. Concept of detrending air pollutant levels. $C_{2016-2019}$ and C_{2020} are the average concentrations of an air pollutant in the second and third weeks before the lockdown start date or equivalent in 2016–2019 and 2020, respectively; $C_{i\,2016-2019}$ and $C_{i\,2020}$ are the daily average concentrations of an air pollutant in the ith day starting in the second week after the lockdown start date or equivalent in 2016–2019 and 2020, respectively. The vertical dashed line represents lockdown start date. $P_{2016-2019}$ and P_{2020} are the percentage changes in air pollutant levels after versus before the lockdown began or equivalent in 2016–2019 and 2020, respectively (see Eq. 2 in the main text for definition). $C_{2020\text{Business as usual}}$ is the hypothetical concentration for the ith day starting in the second week after the lockdown date under "business-as-usual" (i.e., no lockdown) conditions. This is calculated from the prelockdown concentration (C_{2020}) assuming the same percentage change as in 2016–2019 ($P_{2016-2019}$, as the "business-as-usual" change). The detrended percentage change P^* (i.e., the change in air pollutant concentration arising from lockdown effects alone) is given by $P_{2020} - P_{2016-2019}$.

P^* removes the "business-as-usual" variability in concentrations from winter to spring (i.e., 2016–2019 as a baseline, $P_{2016-2019}$) and thus represents the change attributable to lockdown measures. This business-as-usual variability can be caused by changes in anthropogenic activities (e.g., domestic heating) and natural processes [e.g., biogenic volatile organic compound (VOC) emissions]. For example, when the domestic heating demand reduces in local spring, there may be less local emissions of air pollutants; as a result, the concentrations of air pollutants are lower if emissions from other major sources do not increase and meteorological conditions are similar.

Changes in NO_2, O_3, and O_x

Observed NO_2 levels are highly variable, with daily concentrations changing notably during the study period (Fig. 2 and fig. S1). Pollution events (e.g., spikes in Fig. 2) appeared repeatedly during the lockdowns, such as in Beijing, Wuhan, and Paris. Observed NO_2 at roadside sites decreased substantially in all cities after the lockdowns began, with P_{obs} ranging from −29.3 ± 33.1% in Berlin to −53.5 ± 18.9% in London (table S1); observed NO_2 at urban background sites also decreased substantially, with the P_{obs} ranging from −10.1 ± 36.6% in London to −60.2 ± 14.8% in Delhi; and observed NO_2 at rural sites increased in London (P_{obs} = +115.8 ± 90.2%) and Paris (P_{obs} = +99.2 ± 66.7%) but decreased in other cities after lockdown started.

Deweathered NO_2 usually shows a similar pattern to the observations, but the magnitudes and sometimes even the signs of changes are different. A sudden drop, distinct from the data in 2018, is clearly observed at urban sites in 2020 after the lockdowns began in all cities except London and Los Angeles, which show a more gradual change (Fig. 2 and fig. S1). This confirms that the sudden changes in 2020 are indeed due to the lockdown measures.

Deweathered NO_2 at urban background sites in 2020 decreased in all cities after the lockdowns began, with P_{dew} ranging from −18.2 ± 6.0% in London to −52.9 ± 1.4% in Delhi (Table 1); deweathered NO_2 at roadside sites decreased more markedly in most cities (Fig. 2, fig. S1, and table S2). We also noticed that deweathered NO_2 (P_{dew}) in 2016–2019 decreased in almost all cities from winter to spring, although the magnitude of change is usually much smaller than in 2020 (Fig. 3). Thus, the absolute values of the detrended NO_2 change, P^*, is smaller than the corresponding P_{dew}. Table 1 shows that the decline in NO_2 due to the lockdown measures at urban background sites is mostly less than 30% in the studied cites.

Deweathered NO and NO_x (=NO + NO_2) in 2020 dropped more markedly (table S2) after the lockdown began than was observed for NO_2. For example, P_{dew} values for NO and NO_x at urban background sites in London were approximately −24.8 ± 6.3 and −21.0 ± 5.9%, respectively, whereas that for NO_2 was −18.2 ± 6.0%. At roadside sites in London and Rome, deweathered NO_x decreased by more than 50% during the lockdowns, a much larger change than that for NO_2 (−47.0% in London and −35.2% in Rome).

In contrast to changes in NO_2, observed O_3 at roadside sites in 2020 increased in all cases (fig. S1 and table S1) after the lockdown began, with the P_{obs} values ranging from +19.5 ± 21.0% in Madrid to +155.6 ± 83.2% in Milan. Observed O_3 at urban/rural sites also increased during the lockdowns (fig. S1). A sudden increase in

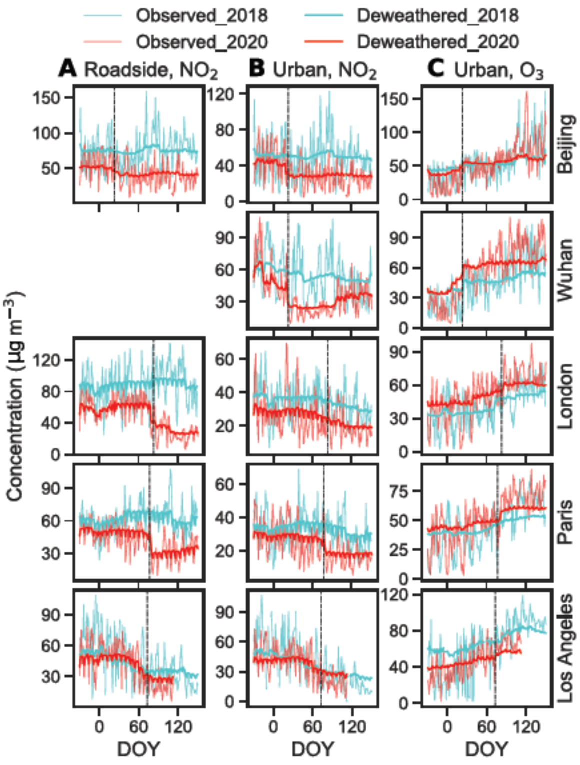

Fig. 2. Observed and deweathered daily NO_2 and O_3 concentrations in selected cities before and after the lockdown start dates or equivalent in 2020 versus 2018. Columns correspond to (**A**) NO_2 at roadside sites, (**B**) NO_2 at urban background sites, and (**C**) O_3 at urban background sites; rows show different cities as indicated. Fine and heavy lines indicate observed and deweathered concentrations, respectively. Data are shown from December to May, shown as day of year (DOY; 1 January = 1), where the vertical dashed lines represent lockdown date. The sudden drop in deweathered NO_2 and corresponding increase in deweathered O_3 are apparent in Beijing, Wuhan, and Paris, whereas London and Los Angeles show more gradual changes. The saw-like shape in the deweathered data in some cities captures the weekly cycles of NO_2 and, to a lesser extent, O_3, particularly in western cities. Results from other cities/sites are shown in fig. S1. No data are available for roadside sites in Wuhan.

deweathered O_3 after the lockdown began was observed in most of the cities (Fig. 1 and fig. S1). The P_{dew} values (Table 1 and table S2) for deweathered O_3 range from +15.0 ± 3.0% in Los Angeles to +128.5 ± 41.9% in Milan at roadside sites, from +14.8 ± 2.2% in Los Angeles to +66.8 ± 29.2% in Milan at urban background sites, and from +1.5 ± 0.9% in London to +57.9 ± 6.3% in Milan at rural sites. However, there is an increasing trend in O_3 levels at urban background sites during the same periods in 2016–2019 (Figs. 2 and 3), with P_{dew} values ranging from +12.1 ± 9.1% in New York to +51.2 ± 23.4% in Milan (auxiliary data table S1). As a result, the detrended O_3 changes (P^*) at urban background sites are much smaller than those of the corresponding P_{dew} values; there is an obvious increase in P^* in Beijing, Wuhan, Milan, and Rome, but a small change or even a decrease in other cities (Table 1).

Accordingly, the observed levels of total gaseous oxidant (i.e., $O_x = NO_2 + O_3$), a parameter unaffected by the titration reaction between NO and O_3 but representing net photochemical production of O_3, showed a different pattern to NO_2 and O_3, with little change before and during the lockdowns, whether at roadside, urban background, or rural sites (Fig. 4). Observed O_x at urban background sites in 2020 range from 35.0 ± 5.4 parts per billion (ppb) in Madrid to 44.8 ± 8.5 ppb in Delhi during the 10-week period with lockdown start date in the middle. Deweathered O_x mixing ratios at urban background sites were remarkably similar across the cities, at approximately 40 ppb (Fig. 4). Only a small change in deweathered O_x, before and after lockdown started in 2020, was observed at urban background sites in all the cities, with P_{dew} values ranging from −4.6 ± 3.5% in Delhi to +10.5 ± 0.8% in Berlin (Table 1). Small changes were also seen during the same periods in 2016–2019, with P_{dew} for deweathered O_3 ranging from −1.2 ± 7.1% in Beijing to +8.7 ± 1.7% in Berlin (Fig. 2 and auxiliary data table S1). Detrended O_x at urban background sites generally decreased during the study period in most of the cities, but the absolute change is relatively small, i.e., mostly within ±5%; changes at rural sites are more variable with almost half of the cities showing a slight increase (table S3).

Changes in $PM_{2.5}$ and PM_{10}

Figure 5 and fig. S2 show that the average observed $PM_{2.5}$ levels in 2020 reduced after lockdown started in the two more polluted cities, Wuhan and Delhi. No clear changes were observed in other cities, particularly when comparing levels to those in previous years (Fig. 5 and fig. S2). In Beijing, Paris, and London, pollution events were observed after the lockdowns began (Fig. 5). Unlike NO_2, the peak levels observed during the lockdowns were sometimes even higher than those before lockdown began (e.g., London). The P_{obs} values for observed $PM_{2.5}$ in 2020 range from −40.8 ± 28.4% in Los Angeles to +107.6 ± 148.5% in London at roadside sites, from −38.6 ± 17.2% in Madrid to +152.9 ± 165.0% in London at urban background sites, and from −34.2 ± 26.8% in Delhi to +164.5 ± 148.7% in London at rural sites (table S1).

Deweathered $PM_{2.5}$ in 2020 showed a clearer pattern than that apparent in the observations (Fig. 5). Unlike deweathered NO_2 and O_3, a sudden decrease in $PM_{2.5}$ after lockdowns started was not detected in most of the cities, with the exceptions of Wuhan and Rome (fig. S1). However, sudden decreases were observed in some cities (such as Los Angeles, New York, Beijing, and Wuhan) a few days after or before the lockdowns began. Figure 5 and fig. S2 show that the deweathered $PM_{2.5}$ before the lockdown began in 2020 was similar to that in 2018 in Beijing, lower in Wuhan, London, Paris, and Berlin, but higher in Rome and Delhi. In Beijing, there was an increase in deweathered $PM_{2.5}$ after the lockdown began initially, but there was a decrease afterward (Fig. 5). Deweathered $PM_{2.5}$ in London and Paris also increased after the lockdowns began, but in contrast, there was no obvious decrease even 3 weeks from the lockdown date.

The changes in deweathered $PM_{2.5}$ are similar at different site types (Fig. 5 and fig. S2). Deweathered $PM_{2.5}$ at roadside sites in 2020 increased slightly during the lockdowns by +1.0 ± 7.2% in London and +0.2 ± 9.1% (P_{dew}) in Paris but decreased with changes (P_{dew}) ranging from −2.8 ± 1.3% in New York to −37.8 ± 4.8% in Los Angeles (table S2). A similar trend is also observed in the deweathered $PM_{2.5}$ at urban background and rural sites (Fig. 5 and fig. S2). An obvious decrease in deweathered $PM_{2.5}$ at urban background sites during the same study periods was also observed in 2016–2019 in some cities but not in others (Fig. 3 and auxiliary data table S1). The detrended change (P^*; Table 1) in $PM_{2.5}$ at urban background sites shows a decrease in Los Angeles (−40.3 ± 26.9%), Madrid (−24.1 ± 18.4%), Wuhan (−15.7 ± 24.8%), New York (−13.9 ± 6.9%), and Delhi (−5.2 ± 4.8%), but little changes or even increases in the other cities.

Table 1. Percentage changes (%) in deweathered (P_{dew}) and detrended (P^*) NO_2, O_3, $PM_{2.5}$ mass concentrations, and O_x mixing ratios at urban background sites in the studied cities. See Eqs. 1 to 3 for definition of P_{dew} and P^*. N.A., data not available.

		Beijing	Wuhan	Milan	Rome	Madrid	London	Paris	Berlin	New York	Los Angeles	Delhi
NO_2	P_{dew}	−33.4 ± 2.2	−43.9 ± 2.2	−27.4 ± 8.3	−33.2 ± 6.1	−49.7 ± 3.1	−18.2 ± 6.0	−33.6 ± 3.3	−25.4 ± 6.0	−23.3 ± 2.0	−23.8 ± 3.4	−52.9 ± 1.4
	P^*	−18.5 ± 9.2	−33.9 ± 7.3	−16.3 ± 11.4	−27.1 ± 7.7	−35.2 ± 21.3	−7.7 ± 7.7	−25.8 ± 7.1	−11.3 ± 13.1	−17.0 ± 8.3	−9.9 ± 6.1	−51.0 ± 5.2
O_3	P_{dew}	28.9 ± 2.0	44.5 ± 3.4	66.8 ± 29.2	55.8 ± 6.7	28.0 ± 3.8	15.8 ± 1.8	22.2 ± 2.4	29.9 ± 3.0	17.4 ± 3.9	14.8 ± 2.2	26.2 ± 5.8
	P^*	14.8 ± 5.3	21.8 ± 13.6	15.4 ± 37.6	29.8 ± 10.1	11.2 ± 18.3	−1.6 ± 8.1	7.0 ± 5.1	2.6 ± 8.9	5.3 ± 9.8	2.3 ± 5.3	8.2 ± 8.4
$PM_{2.5}$	P_{dew}	−19.3 ± 9.6	−27.0 ± 18.7	N.A.	−16.4 ± 5.2	−43.1 ± 3.4	8.6 ± 8.3	16.5 ± 10.7	N.A.	−21.5 ± 2.6	−18.0 ± 5.4	−12.7 ± 2.8
	P^*	−2.4 ± 14.7	−15.7 ± 24.8	N.A.	−0.7 ± 9.6	−24.1 ± 18.4	10.9 ± 16.7	27.4 ± 15.3	N.A.	−13.9 ± 6.9	−40.3 ± 26.9	−5.2 ± 4.8
O_x	P_{dew}	−1.1 ± 2.0	1.1 ± 1.4	−1.3 ± 1.0	4.1 ± 1.2	−0.4 ± 1.3	4.2 ± 0.8	2.1 ± 0.6	10.5 ± 0.8	−1.0 ± 1.8	−2.3 ± 1.0	−4.6 ± 3.5
	P^*	0.1 ± 7.4	−0.7 ± 4.4	−7.2 ± 5.9	−2.0 ± 2.9	−3.4 ± 3.2	−2.4 ± 1.3	−0.6 ± 2.3	1.8 ± 1.9	−6.4 ± 6.8	−4.1 ± 1.7	−9.8 ± 6.3

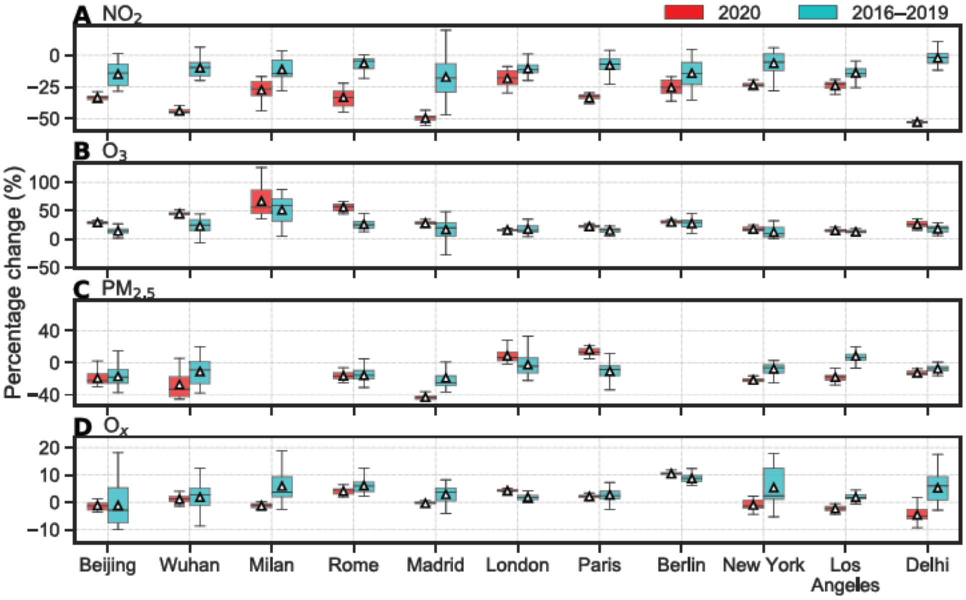

Fig. 3. Box plots of percentage change (P_{dew}) in deweathered concentrations of air pollutants in 2020 versus 2016–2019. Rows represent (**A**) NO_2, (**B**) O_3, (**C**) $PM_{2.5}$, and (**D**) O_x. Lower and upper box boundaries represent the 25th and 75th percentiles, respectively; line and triangle inside boxes represent median and mean values, respectively; lower and upper error lines represent 1.5 * IQR (interquartile range) below the third quartile and above the first quartile, respectively. Number of samples for P_{dew} in 2020 and 2016–2019 is usually 28 and 112, respectively.

The overall patterns of variations in observed and deweathered PM_{10} (fig. S4) are similar to those of the $PM_{2.5}$ (fig. S3). A slight difference in some cities is that there were more variabilities/contrasting patterns at different types of site. For example, a larger decline in P_{dew} for deweathered PM_{10} at roadside sites than that at urban background sites is observed in Beijing, Madrid, London, Paris, and Berlin (table S2), potentially reflecting a coarse particle source from road traffic (e.g., non–exhaust emissions) (*23*). Furthermore, in Los Angeles and Delhi, the decline in deweathered PM_{10} is significantly larger than that of $PM_{2.5}$ whether at urban background or rural sites (table S2), implying a reduced contribution of coarse particles to PM_{10}.

Changes in CO and SO_2

Deweathered CO levels were lower after lockdown started than before in 2020. This pattern is different from that in 2018 (fig. S4). A sudden change is observed in Rome and Wuhan only. In Beijing, deweathered CO increased slightly after the lockdown began, before falling for about 2 weeks, after which there was a substantial increase at all three types of sites. Thereafter, the deweathered CO decreased substantially, ~40% (P_{dew}) lower than that during the same period in 2018. In New York (roadside sites), a decline in deweathered CO is observed a week after the lockdown began. In Delhi, the decreasing trend in deweathered CO at urban background sites is not distinguishable from that in 2018, whereas at rural sites, CO clearly declined from a few days before the lockdown began.

The change in deweathered SO_2 after the lockdowns began is dependent on the site or city (fig. S4). No sudden change is observed in any of the cities immediately after the lockdowns. In Beijing, deweathered roadside and urban SO_2 increased initially and then decreased by ~20%. In all cases, the deweathered SO_2 concentration in 2020 is much lower than that in 2018. In London, deweathered SO_2 declined for a few days before the lockdown began at roadside sites. Deweathered SO_2 in Wuhan and Rome decreased about a month

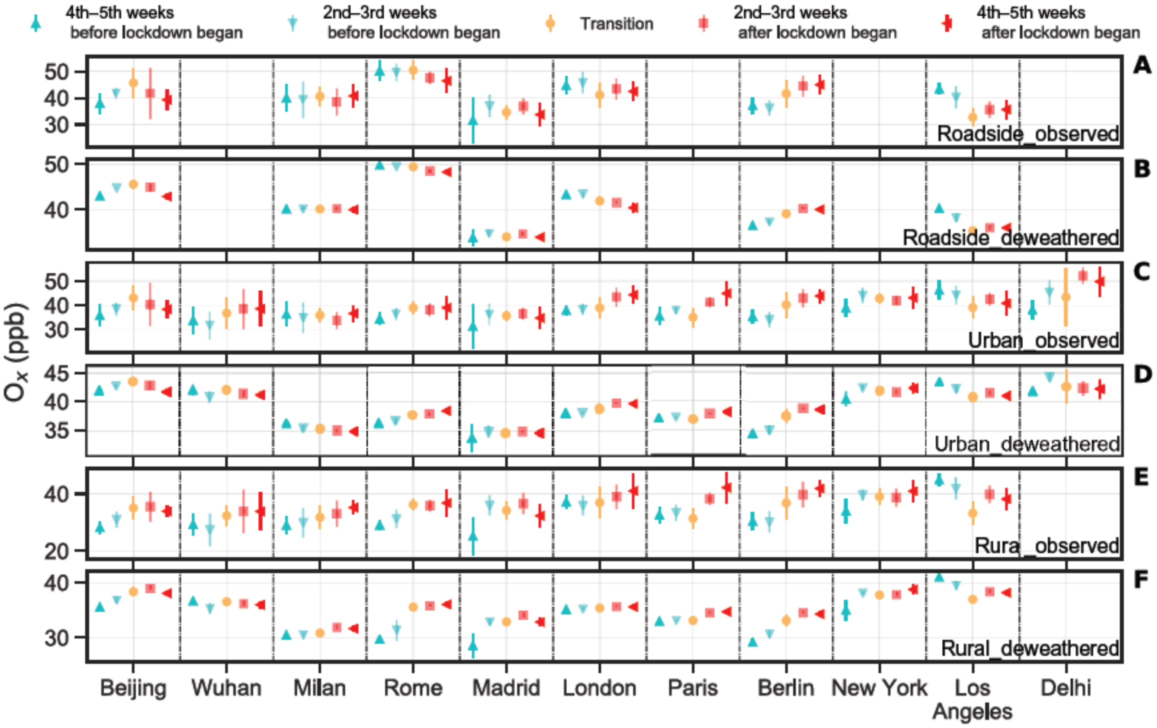

Fig. 4. Observed and deweathered O_x (i.e., $NO_2 + O_3$) mixing ratios in the 5 weeks before and after the lockdown start dates in the studied cities in 2020. The six rows (from top to bottom) show results from roadside observed (**A**) and deweathered (**B**), urban background observed (**C**) and deweathered (**D**), and rural observed (**E**) and deweathered (**F**) mixing ratios. Deweathered O_x shows little change before and after the lockdown dates in 2020 and is similar across all urban background sites (all close to 40 ppb). Error bars (included for all points) represent 1 SD ($n = 14$). Transition period refers to the 2 weeks with the lockdown start date in the middle.

before the lockdowns but did not change during the lockdowns. In New York (roadside sites), a decline in deweathered SO_2 is observed a week after the lockdown began. Delhi saw a substantial decrease in deweathered SO_2 about 2 weeks after the lockdown started, and the decrease in deweathered CO at urban background sites is not distinguishable from that in 2018, whereas at rural sites, it clearly declined from a few days before the lockdown began.

DISCUSSION

The deweathered and detrended data are used to understand how the air quality responded to the changes in activity associated with the COVID-19 lockdowns of early 2020 and the potential implications of such interventions for developing future air pollution abatement strategies and thus improving human health.

The importance of deweathering and detrending

Large differences between the deweathered and observed concentrations of air pollutants were observed in the studied cities (Fig. 2 and figs. S1 to S3). Observed daily average NO_2 concentrations are much higher than the deweathered ones during some periods. Our estimated NO_2 decline in Wuhan due to lockdown effects is much lower than that estimated by Le *et al.* (*15*), who reported up to 93% reduction in NO_2 in Wuhan during the lockdown. If we look at the observations only, we can indeed see >90% decrease from the peak concentration before the lockdown began to the lowest one afterward (Fig. 2), but this is mainly due to changes in meteorological conditions, not emissions. The observed $PM_{2.5}$ also exhibited remarkable meteorologically driven variability regardless of cities or site types and sometimes differed by more than a factor of 3 when compared with deweathered concentrations (Fig. 5 and fig. S2). In general, major differences are apparent between the observed and deweathered results when the meteorological conditions change substantially over the study period. For example, the changes in observed and deweathered $PM_{2.5}$ at urban background sites in Beijing before and after the lockdown began were +19.2 ± 108.6% (P_{obs}) and −19.3 ± 9.6% (P_{dew}), respectively. In this case, emission reductions and the unfavorable meteorological conditions drove changes of approximately −19.3 and +38.6% in the observed levels, respectively, leading to an overall +19.2% increase in $PM_{2.5}$. Our results demonstrate that meteorological variations, rather than emission changes on the scale of those occurring during the COVID-19 lockdowns, dominate short-term variability in air pollutant concentrations, which is consistent with previous studies (*12*, *14*, *20*, *24*).

Apart from deweathering, detrending the "business-as-usual" changes is also crucial in estimating real changes attributable to interventions (i.e., lockdowns). In the "business-as-usual" scenario, air pollutant emissions (both anthropogenic and natural) and, thereby, concentrations may change from winter to spring, whether there is a lockdown or not (see 2016–2019 data in Fig. 3). For example, a general increase in deweathered O_3 is observed from winter to spring in 2016–2019 in all the studied cities (Figs. 2 and 3 and fig. S1). Such an increase reflects changing photochemical steady-state partitioning from NO_2 to O_3 (Northern Hemisphere cities moving into spring with increased solar radiation intensity and day length),

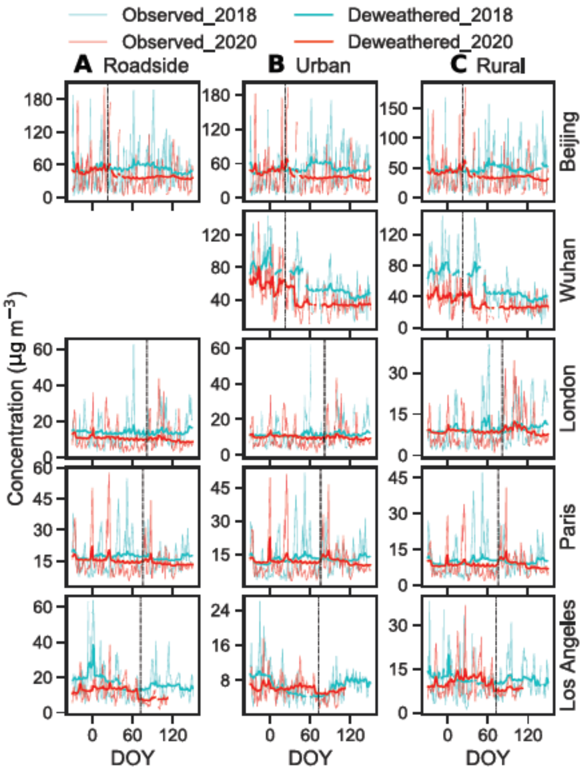

Fig. 5. Observed and deweathered daily $PM_{2.5}$ concentrations in the selected cities before and after the lockdown start dates or equivalent in 2020 versus 2018. Columns correspond to (**A**) roadside, (**B**) urban background, and (**C**) rural sites; rows show different cities as indicated. Fine and heavy lines indicate observed and deweathered concentrations, respectively. Data are shown from December to May, shown as day of year (1 January = 1), where the vertical dashed lines represent lockdown start date. Results from other cities/sites are shown in fig. S2. No data are available for roadside sites in Wuhan.

alongside wider increases in photochemical ozone formation, enhanced by increased emission and chemical reactivity of VOCs. Taking this "business-as-usual" variability into account, the detrended percentage changes (P^*) in O_3 are much smaller than the corresponding P_{dew} (Table 1 and table S3). Not accounting for this seasonality would lead to a different conclusion, as by Sicard *et al.* (*7*), that O_3 concentration increased substantially in response to the lockdowns.

In some cities, there are considerable variabilities in P_{dew} in 2016–2019 (Fig. 3). This may be partly due to specific events such as holidays around the lockdown dates, leading to a decrease in air pollutant emissions for a particular year. In this instance, the absolute value of P_{dew} in 2016–2019 could be slightly overestimated, and thus that of the P^* underestimated. However, because we included 4 years of data (2016–2019) for detrending, the impact of a specific event on the P^* values is small.

Our detrended results (Table 1 and table S3) demonstrate that the decreases in NO_2 and increases in O_3 due to the COVID-19 lockdowns are not as large as previous studies have reported (*7*, *21*) or as the raw observational data show (table S1). Note also that anthropogenic air pollutant emissions reduce year by year, such as in London and Beijing, as a result of clean air policy actions and vehicle fleet evolution (*14*, *18*). Thus, the approach widely used in the literature to estimate the lockdown effects by subtracting NO_2 during the equivalent periods in earlier years from that in 2020 (*6*, *7*, *11*, *15*) may also overestimate the effects attributed to the lockdowns (Fig. 3 and Table 1).

Considering urban background sites in Wuhan (a widely studied city) as an example, observed NO_2 and O_3 changed by −47.3 ± 17.4% and +166.5 ± 60.5% (P_{obs} values, obtained from unadjusted concentration data before/during lockdown; table S1), values similar to those reported by Shi and Brasseur [−54 ± 7% and + 220 ± 20% (*25*)]; changes of approximately −51.8 and +40.0% are obtained by subtracting NO_2 and O_3 concentrations during the second to fifth weeks after the lockdown dates in 2016–2019 from those in 2020 (i.e., without adjustment for meteorology), values which are similar to those reported by Sicard *et al.* [−57 and +36% (*7*)]. Our estimated changes in deweathered NO_2 and O_3 (P_{dew}) are −43.9 ± 2.2% and +44.5 ± 3.4%, which are similar to those reported by Zhao *et al.* [−51.7 and +58% (*21*)]. However, these estimations (*7*, *21*, *25*) are considerably higher (sometimes by a factor of 10) than our detrended results (P^*), which are −33.9 ± 7.3% for NO_2 and +21.8 ± 13.6% for O_3. This may at least partially explain why the estimated changes in NO_2 and O_3 due to the lockdown effects in the studied cities reported here are lower than those published elsewhere (*7*, *11*, *15*, *21*, *25*), and demonstrate the necessity of disentangling the changes due to meteorological variation and seasonality and from the lockdown-driven changes in emissions to understand the resulting differences in air pollutant concentrations.

Drivers of changes

The deweathered NO_2 showed a sudden decrease after the lockdown began in most of the cities (Fig. 2 and fig. S1). Detrended NO_2 at urban background sites declined the most in Delhi (−51.0 ± 5.2%), Madrid (−35.2 ± 21.3%), and Wuhan (−33.9 ± 7.3%) (Table 1). A given reduction in NO_x emission, and hence NO_x abundance, is expected to lead to a smaller reduction in ambient NO_2 levels, as the fast NO_x-O_3 photochemistry shifts the NO_2/NO_x ratio in favor of NO_2. The fact that the NO_x changes are larger than those of NO_2 supports this argument (tables S1 and S2). A substantially larger decline in NO_x and NO_2 was observed at roadside than at urban background sites, suggesting that the decline in NO_2 during the lockdowns is largely driven by changes in road traffic as the dominant source of NO_x in urban atmosphere (*16*). Mobility data from Google Maps (https://google.com/covid19/mobility/) suggest that traffic volumes reduced by 60 to 80% in the cities considered here. However, this mobility decrease does not correspond directly to the same reduction in road traffic–related NO_x emissions. For example, in London, although private car use reduced by about 80%, heavy good vehicles (HGVs) on the road only reduced by 30 to 40%. It is possible that if the change in the number of HGVs, which account for a smaller percentage of total vehicle population but a large proportion of vehicular NO_x emissions (*26*, *27*), is small, then the changes in total road traffic emissions of NO_x may be much smaller than expected. Decreases in activity levels from other combustion sources, such as power plants and industry (*22*), may have contributed to the decline in NO_2, at least in some cities, as shown by the small decline in SO_2 in some cities (fig. S4). Such changes are difficult to quantify, but the much smaller (and absence of any sudden) changes in SO_2 compared with NO_2 (Fig. 2 and fig. S2)—as indicated by the increase in SO_2/NO_2 ratio in Wuhan, London, Paris, Rome, and Delhi (auxiliary data table S1)—suggest that reductions in NO_x emissions from stationary sources were less than those from traffic emissions. This is consistent with Le Quéré *et al.* (*5*), who estimated that in Europe and the United States, electricity use reduced by 9 and 5%, respectively. Note also that domestic emissions may have increased with an increase in people working or studying from home. We recognize that our methodology is unable to attribute the actual changes in emissions on a sector-by-sector basis. This could be revisited in the future when emission inventories for the spring 2020 lockdown period are developed and evaluated against observations.

O_3 is a secondary pollutant, and its variation is driven by several factors. Dominant among these is the NO_x-O_3 photochemical steady state. The decrease in NO (tables S1 and S2) led to reduced O_3 titration, through which reductions in traffic-related NO emissions translate directly into increases in O_3, relative to the prelockdown period; the time constant for this NO_x-O_3 interaction in daylight is of the order of minutes. The fact that deweathered O_3 increased suddenly after the lockdown began and that changes in deweathered NO were more pronounced than those in NO_x and NO_2, particularly at roadside sites (fig. S1 and table S2), support this well-understood atmospheric chemistry (*28*). This effect—of a reduced urban decrement in O_3—will be partially offset by reductions in primary NO_2 emissions from traffic and, on a much longer time scale (hours to days, rather than minutes), by net O_3 production. Under an extreme condition, if all traffic-related NO_x emissions are assumed to be NO, O_x would remain unchanged in response to lockdown-driven changes in traffic (but NO_2 would decrease, and O_3 would increase). In reality, primary NO_2 emissions from road traffic decreased during the lockdowns, so O_x should fall. Detrended O_x fell slightly at roadside and urban background sites in most of the cities (Table 1 and table S3). Detrended O_x increased at rural sites in some of the cities (table S3), which indicates an increase in net photochemical production of O_3 at some of the studied sites (*28*). The different pattern of changes in detrended O_3 represents a nonlinear response of O_3 formation rates to the (relative) changes in NO_x and VOC emissions, depending on the prevailing O_3 production regime at each location, but usually with a greater impact downwind of conurbation locations (*29*, *30*).

Drivers of the response of $PM_{2.5}$ levels to the lockdown measures are more complex since both primary emissions and secondary formation contribute to $PM_{2.5}$ in ambient air. Deweathered $PM_{2.5}$ reduced after the lockdowns began at urban background sites in most of the cities, including Wuhan, Rome, New York, Los Angeles, and Delhi (fig. S2). This could be explained by (i) the expected reductions in primary emissions of $PM_{2.5}$ and its gaseous precursors (e.g., NO_2, SO_2, and VOCs) during the lockdowns and (ii) limited change in the formation rate of secondary aerosol as shown by the small variation in $PM_{2.5}$/CO ratio (fig. S5).

Deweathered $PM_{2.5}$ increased in London and Paris for an extended period (more than 3 weeks) after the lockdowns began (Fig. 5). It also increased in Beijing after the lockdown began, although for a shorter period. One possible explanation for this unexpected result is that enhanced secondary aerosol formation overwhelmed the reduced primary $PM_{2.5}$ emissions. In Chinese megacities, secondary particles typically contribute to >50% of $PM_{2.5}$ mass (*31*, *32*). In London, secondary aerosols contribute roughly half of $PM_{2.5}$ at roadside sites, increasing to ~90% of $PM_{2.5}$ at rural sites, with the contribution lying between these values at urban background sites (*33*). Such contributions are even larger during pollution events (*15*, *16*, *31*). Thus, changes in $PM_{2.5}$ are often driven by variations in secondary aerosols, particularly during pollution events. In Beijing, Sun *et al.* (*34*) noted that primary aerosol decreased by 30 to 50%, while secondary inorganic aerosol and secondary organic aerosol (SOA) increased by 60 to 110% and 52 to 175%, respectively, during the early periods of the lockdown in 2020. The fact that substantial increases in $PM_{2.5}/PM_{10}$ (Paris) or $PM_{2.5}$/CO (London; fig. S5) ratios accompanied the increase in deweathered $PM_{2.5}$ (Fig. 5 and fig. S2) also supports the greater role of secondary aerosol during the study period in Paris and London. Zhao *et al.* (*35*) suggested that SOA formation depends nonlinearly on the ratio of VOCs to NO_x; reduction in NO_x emissions may lead to increased production of SOA given imbalanced emission abatement of NO_x and VOCs. Le *et al.* (*15*) indicated that multiphase chemistry and enhanced atmospheric oxidative capacity drove haze events in China during the lockdowns. Huang *et al.* (*16*) also suggested that increase in oxidative capacity during lockdown in China/Beijing caused the observed air pollution events; however, the changes in deweathered O_x levels (P_{dew}) at urban background sites are rather small: Beijing (−1.1 ± 2.0%), London (+4.2 ± 0.8%), and Paris (+2.1 ± 0.6%) (table S2).

Another possible explanation is associated with changes in long-range transport, which brings air pollutants from nonlocal sources and thus contributes to the increase in deweathered $PM_{2.5}$. In theory, the RF models should have normalized the impacts from long-range transport by including back-trajectory clusters. However, the model may not be able to perfectly reproduce secondary formation processes arising from long-range transport if there were limited cases to learn from, especially as such events tend to be episodic in nature. In this case, the model will treat pollution events arising from long-range transport as if there are higher emissions; this attribution will be retained during deweathering. This will cause uncertainties in the model. More observational data and modeling are needed to fully understand the phenomenon of increases in $PM_{2.5}$ in London, Paris, and Beijing during the lockdowns. However, it is clear that a small reduction in primary $PM_{2.5}$ emissions (e.g., from vehicular emission changes during lockdown) could be readily overwhelmed by enhanced secondary formation and/or $PM_{2.5}$ transported from more polluted regions.

In Wuhan, the deweathered $PM_{2.5}$ decreased to a small degree during the 2 weeks after the lockdown began (Fig. 5). However, the deweathered $PM_{2.5}$/CO increased during the lockdowns (fig. S5), which suggests that enhanced secondary pollution (*36*) offsets the benefits of the reduction in primary emissions during the first 2 weeks of the lockdown. Thereafter, the deweathered $PM_{2.5}$ did decrease more significantly (P_{dew} = −27.0 ± 18.7%). Similarly, in Beijing, the deweathered $PM_{2.5}$ decreased 2 weeks after the lockdown began, so overall P_{dew} is negative (−19.3 ± 9.6%). These results suggest that if the reduction in emissions of gaseous precursors is sufficiently large, it should eventually lead to an overall decline in $PM_{2.5}$. Such a hypothesis should be tested with chemical transport models with up-to-date emission inventories when these are available.

Implications for future air pollution control

Our results demonstrate that restrictions on economic activities, particularly traffic, brought an immediate decline in detrended NO_2 in all the studied cities. If similar levels of restriction were to have remained in place, the annual average NO_2 concentration would comply with the air quality guidelines from the World Health Organization (WHO) (i.e., 40 μg m^{-3} for annual NO_2) for the cities considered under average meteorological conditions, except for a limited number of roadside sites. However, the detrended percentage decline (i.e., attributed to lockdown effects) in NO_2 is mostly below 30%. This is lower than the expected decline, partly due to the

NO_x-O_3 photochemical steady state (converting NO to NO_2), alongside seasonal effects, and partly due to the still important emissions of NO_x from stationary and mobile pollution sources. Detrended O_3 increased in most cities. This adds to the complexity of air pollution control, considering the potentially adverse impacts of O_3 on human (*37*, *38*) and environmental health, including crop yields (*39*).

$PM_{2.5}$ exhibited a more complex response to the lockdown measures. $PM_{2.5}$ did not show an immediate decline to the lockdown measures except in Wuhan, Rome, and Los Angeles, even at the roadside sites. This is not too unexpected considering the relatively small contribution of road traffic to primary $PM_{2.5}$ in most of the cities studied here and a large contribution from secondary sources (*16*, *31*). In China, much of the recent decrease in $PM_{2.5}$ came from the reductions in residential solid fuel use and industrial activity rather than traffic emissions (*18*, *40*). Nevertheless, a decrease in deweathered $PM_{2.5}$ is observed in most of the cities.

In Delhi, Wuhan, and Beijing, annual average $PM_{2.5}$ concentrations are so far in exceedance of the WHO guideline (10 μg m^{-3}) that the decline is far from sufficient to bring levels into compliance. Even in those cities where the annual average $PM_{2.5}$ is close to 10 μg m^{-3}, such as London and Paris, emission reductions on the scale of the spring 2020 COVID-19 lockdown measures may still be insufficient to bring concentrations into compliance with the current WHO guidelines. In addition, the frequent $PM_{2.5}$ pollution events during the lockdowns in some cities, such as Beijing, London, and Paris, showed that actions of a magnitude similar to the lockdown measures are far from sufficient to avoid episodic pollution events in these cities. The mechanisms driving such changes have been explored in more detail by recent studies (*15*–*17*, *20*).

Li *et al.* (*41*) suggested that aggressive reductions in NO_x and aromatic VOC emissions should be particularly effective for decreasing both $PM_{2.5}$ and O_3 in China. The huge reduction in NO_x (fig. S3) and VOCs (*16*) in response to the COVID-19 lockdowns did reduce $PM_{2.5}$ pollution in Beijing and Wuhan, but detrended O_3 increased substantially (Table 1), at least up until mid-May. A slower pace of VOC emission reduction, relative to that for NO_x, could risk a further increase in O_3 pollution.

In summary, emission changes associated with the early-2020 COVID-19 lockdown restrictions led to complex and substantial changes in air pollutant levels, but the changes are smaller than expected. The decrease in NO_2 will likely have benefits on public health, but the increase in O_3 would counteract at least some of this effect (*37*, *38*). The magnitude and even the sign of changes in $PM_{2.5}$ during the lockdowns differ significantly among the studied cities. Chemical processes of the mixed atmospheric system add complexity to efforts to abate secondary pollution (e.g., O_3 and $PM_{2.5}$) through reduction of precursor emissions (e.g., NO_x and VOCs) (*42*). Future control measures will require a systematic approach toward NO_2, O_3, and $PM_{2.5}$ tailored for specific cities, taking into account both primary emissions and secondary processes, to maximize the overall benefits to air quality and human health.

MATERIALS AND METHODS

Selected cities and data

Eleven cities were selected to ensure coverage of contrasting pollution climate: Beijing and Wuhan in China, Milan and Rome in Italy, Madrid in Spain, London in United Kingdom, Paris in France, Berlin in Germany, New York and Los Angeles in the United States, and Delhi in India. Of those, eight are capital cities. Wuhan was added because it was the first city where COVID-19 was reported and lockdown was first imposed. Milan was included because it is in northern Italy, one of the most seriously hit areas after Wuhan. In the United States, New York was the most seriously affected city, whereas Los Angeles was reported to have observed a greater decline in air pollution levels (*43*). All the study cities have been significantly affected by COVID-19 and implemented stringent lockdown measures to contain the COVID-19 pandemic in early 2020. Such measures were first implemented in Wuhan from 23 January 2020 and then 2 days later in all provinces in China (including Beijing). Tightened restrictive measures were implemented from 23 January 2020 in northern Italy, 13 March 2020 in the United States, 14 March 2020 in Spain, 17 March 2020 in France, 22 March 2020 in Germany, 23 March 2020 in the United Kingdom, and 25 March 2020 in India.

Site-specific hourly concentration of six criteria pollutants ($PM_{2.5}$, PM_{10}, O_3, NO_2, CO, and SO_2) and other auxiliary pollutants (NO and NO_x) from December 2015 to May 2020 were obtained from websites of local or national environmental agency or accredited third parties (table S4). In most cases, data from multiple stations for each site type are available. The NO_2 concentrations reported from local governments, typically performed by the widely used molybdenum conversion/chemiluminescence method, may slightly overestimate true NO_2 levels due to conversion of other labile N species to NO in the convertor stage. This problem is usually small for polluted urban sites but is larger for rural sites where overestimates of 17 to 30% have been reported (*44*). This is due to the conversion of NO_x from primary sources to secondary nitrogen compounds during its transport toward more rural locations. Hence, concentrations reported as NO_2 contain a small proportion of other NO_y species, and the "true" NO_2 levels would be lower than those officially reported, particularly at rural locations. We note that such uncertainties are effectively "built in" to monitor NO_2 with respect to regulatory standards. NO_x and NO data were obtained in cities where those data were publicly available. Data were usually downloaded from official sources, which are validated by the authorities. For those cities where data were not available from recognized official sources (i.e., Los Angeles and New York) at the time of access, we obtained the air quality data from the "OpenAQ" platform (https://openaq.org/). Data from Los Angeles were downloaded from the U.S. Environmental Protection Agency (USEPA) later (after the data analyses were done here), which were then compared with those from OpenAQ. We found that the site-specific data in Los Angeles from OpenAQ are highly correlated (slope = ~1, intercept = ~0) with those from USEPA. Air quality monitoring stations were selected to cover roadside, urban background, and rural sites when possible, and the site types were based on official classifications and maps. The downloaded data were screened and cleaned when necessary, following established methods (*24*).

The hourly temperature, relative humidity, atmospheric pressure, wind speed, and wind direction data for selected sites were obtained from the nearest meteorological observation site from the NOAA (National Oceanic and Atmospheric Administration) Integrated Surface Database (ISD) using the "worldmet" R package (https://CRAN.R-project.org/package=worldmet). In addition, hourly data for boundary layer height, total cloud cover, surface net solar radiation, and total precipitation at the selected sites were downloaded from the ERA5 reanalysis dataset (ERA5 hourly data on single levels from 1979 to present). For each site, 72-hour back trajectories at an hourly resolution were calculated using the Hybrid Single-Particle

Lagrangian Integrated Trajectory (HYSPLIT) model. The starting height was set as 100 m to ensure that the receptor was aloft but remained within the boundary layer throughout the study period. The back trajectories were then clustered into 12 clusters using the Euclidian distance by "openair" R package (https://CRAN.R-project.org/package=openair). Those clusters were used to represent the common air masses that the sites were exposed to.

Observations at the air quality stations are used for official compliance purpose. Although these stations were built to represent the specific environment of the city (i.e., roadside, urban background, and rural), there may be some variabilities in the concentrations of air pollutants at different stations of the same type. This could cause potential uncertainties in our analyses if to represent the whole city. In this study, wherever possible, we used data from multiple stations for each site type (table S4), which reduced this uncertainty. Where only one station is available for a site type, the data may be subject to more influence from local emission sources. Therefore, what we reported here should be treated in the context of the site availability (see table S4). Furthermore, we would like to emphasize that our analyses focus on the high-resolution temporal variations, and thus, the trend will be broadly representative.

RF model and weather normalization

Weather conditions change rapidly, causing variations in the concentration of air pollutants even when emissions do not change. Here, we applied a machine learning–based RF algorithm to decouple the effects of meteorological conditions. To do this, we first build an RF model for each pollutant and for each year (December to May). The RF model–based weather normalization technique was introduced in Grange *et al.* (*12*). Briefly, the RF model was built independently for each period (December 2015 to May 2016, December 2016 to May 2017, December 2017 to May 2018, December 2018 to May 2019, and December 2019 to May 2020), each pollutant, and each site type within a city. Seventy percent of the original data were randomly selected to build the model, which was then evaluated with the remainder (30%) of the dataset. Model performance for each pollutant and each time period (i.e., 2016–2020) is illustrated in fig. S6. Similar to Grange *et al.* (*12*, *13*) and Vu *et al.* (*14*), the performance of the models is usually very good, much better than that of regression models (*9*). The weather normalization was conducted using the "rmweather" R package, available at https://cran.r-project.org/web/packages/rmweather/index.html.

In the Grange *et al.* (*12*) approach, a new dataset of input predictor features including time variables (day of the year, day of the week, and hour of the day, but not the Unix time) and meteorological parameters (wind speed, wind direction, temperature, and relative humidity) is first resampled from the original observation dataset. Vu *et al.* (*14*) modified the default method to investigate the seasonal variations in trends for comparison with trends in primary emissions, by only resampling the weather variables (not the time variables). Specifically, weather variables at a specific hour of a particular day in the input datasets were generated by randomly selecting from the historical weather data (past 30 years) at the particular hour of different dates within a 4-week period (i.e., 2 weeks before and 2 weeks after that selected date). The two methods are fit for their own purposes but were not used here because (i) Grange *et al.* (*12*) normalized the diurnal and seasonal variations of the primary emissions, which is unrealistic in the real world, and (ii) although Vu *et al.* (*14*) provided diurnal and seasonal variations of the primary emissions, this is inappropriate in detecting short-term emission interventions because the normalized concentrations for a particular hour of a Julian day were not comparable with those from the different hour of a different Julian day, considering that they were resampled from different weather datasets, which would be affected by different seasonal weather conditions.

To address those limitations and better investigate the impacts of short-term lockdown on air quality, we applied a mixed method. We only normalized the weather data but not time variables, similar to Vu *et al.* (*14*), and resampled from the whole study period, similar to Grange *et al.* (*12*). The improved method is more suitable for tracking emission changes. The input features for the model included time variables (i.e., Unix time, Julian day, day of the week, and hour of the day), meteorological data from surface observations (i.e., temperature, relative humidity, wind speed, wind direction, and atmospheric pressure), meteorological data from ERA5 reanalysis dataset (i.e., boundary layer height, total cloud cover, surface net solar radiation, and total precipitation), and air mass clusters based on the HYSPLIT back trajectories. The day of week and air mass clusters were categorical variables, while all others were numeric. Following Vu *et al.* (*14*), the parameters for the RF models are as follows: a forest of 300 trees, n_tree = 300; the number of variables that may split at each node, mtry = 3; and the minimum size of terminal nodes, min_node_size = 3. For every weather normalization, the explanatory variables were resampled (excluding the time variables) without replacement and randomly allocated to a dependent variable observation. The 1000 predictions were then aggregated using the arithmetic mean to obtain the deweathered concentration.

SUPPLEMENTARY MATERIALS

Supplementary material for this article is available at http://advances.sciencemag.org/cgi/content/full/7/3/eabd6696/DC1

REFERENCES AND NOTES

1. J. Lelieveld, A. Pozzer, U. Pöschl, M. Fnais, A. Haines, T. Münzel, Loss of life expectancy from air pollution compared to other risk factors: A worldwide perspective. *Cardiovasc. Res.* **116**, 1910–1917 (2020).
2. World Bank Group, *The Cost of Air Pollution: Strengthening the Economic Case for Action (English)* (2016); http://documents.worldbank.org/curated/en/781521473177013155/The-cost-of-air-pollution-strengthening- the-economic-case-for-action.
3. Y. Ogen, Assessing nitrogen dioxide (NO_2) levels as a contributing factor to coronavirus (COVID-19) fatality. *Sci. Total Environ.* **726**, 138605 (2020).
4. D. Fattorini, F. Regoli, Role of the chronic air pollution levels in the COVID-19 outbreak risk in Italy. *Environ. Pollut.* **264**, 114732 (2020).
5. C. Le Quéré, R. B. Jackson, M. W. Jones, A. J. Smith, S. Abernethy, R. M. Andrew, A. J. De-Gol, D. R. Willis, Y. Shan, J. G. Canadell, P. Friedlingstein, F. Creutzig, G. P. Peters, Temporary reduction in daily global CO_2 emissions during the COVID-19 forced confinement. *Nat. Clim. Chang.* **10**, 647–653 (2020).
6. S. Sharma, M. Zhang, Anshika, J. Gao, H. Zhang, S. H. Kota, Effect of restricted emissions during COVID-19 on air quality in India. *Sci. Total Environ.* **728**, 138878 (2020).
7. P. Sicard, A. D. Marco, E. Agathokleous, Z. Feng, X. Xu, E. Paoletti, J. J. D. Rodriguez, V. Calatayud, Amplified ozone pollution in cities during the COVID-19 lockdown. *Sci. Total Environ.* **735**, 139542 (2020).
8. A. Tobías, C. Carnerero, C. Reche, J. Massagué, M. Via, M. C. Minguillón, A. Alastuey, X. Querol, Changes in air quality during the lockdown in Barcelona (Spain) one month into the SARS-CoV-2 epidemic. *Sci. Total Environ.* **726**, 138540 (2020).
9. Z. S. Venter, K. Aunan, S. Chowdhury, J. Lelieveld, COVID-19 lockdowns cause global air pollution declines. *Proc. Natl. Acad. Sci.* **117**, 18984–18990 (2020).
10. R. Zhang, Y. Zhang, H. Lin, X. Feng, T.-M. Fu, Y. Wang, NO_x emission reduction and recovery during COVID-19 in east China. *Atmos.* **11**, 433 (2020).
11. F. Liu, A. Page, S. A. Strode, Y. Yoshida, S. Choi, B. Zheng, L. N. Lamsal, C. Li, N. A. Krotkov, H. Eskes, R. van der A, P. Veefkind, P. F. Levelt, O. P. Hauser, J. Joiner, Abrupt decline in tropospheric nitrogen dioxide over China after the outbreak of COVID-19. *Sci. Adv.* **6**, eabc2992 (2020).

12. S. K. Grange, D. C. Carslaw, A. C. Lewis, E. Boleti, C. Hueglin, Random forest meteorological normalisation models for swiss PM$_{10}$ trend analysis. *Atmos. Chem. Phys.* **18**, 6223–6239 (2018).
13. S. K. Grange, D. C. Carslaw, Using meteorological normalisation to detect interventions in air quality time series. *Sci. Total Environ.* **653**, 578–588 (2019).
14. T. V. Vu, Z. Shi, J. Cheng, Q. Zhang, K. He, S. Wang, R. M. Harrison, Assessing the impact of clean air action on air quality trends in Beijing using a machine learning technique. *Atmos. Chem. Phys.* **19**, 11303–11314 (2019).
15. T. Le, Y. Wang, L. Liu, J. Yang, Y. L. Yung, G. Li, J. H. Seinfeld, Unexpected air pollution with marked emission reductions during the COVID-19 outbreak in China. *Science* **369**, 702–706 (2020).
16. X. Huang, A. Ding, J. Gao, B. Zheng, D. Zhou, X. Qi, R. Tang, J. Wang, C. Ren, W. Nie, V. Chi, Z. Xu, L. Chen, Y. Li, F. Che, N. Pang, H. Wang, D. Tong, W. Qin, W. Cheng, W. Liu, Q. Fu, B. Liu, F. Chai, S. J. Davis, Q. Zhang, K. He, Enhanced secondary pollution offset reduction of primary emissions during COVID-19 lockdown in China. *Natl. Sci. Rev.* 10.1093/nse/nwaa137, (2020).
17. Y. Chang, R.-J. Huang, X. Ge, X. Huang, J. Hu, Y. Duan, Z. Zou, X. Liu, M. F. Lehmann, Puzzling haze events in China during the coronavirus (COVID-19) shutdown. *Geophys. Res. Lett.* **47**, e2020GL088533 (2020).
18. Q. Zhang, Y. Zheng, D. Tong, M. Shao, S. Wang, Y. Zhang, X. Xu, J. Wang, H. He, W. Liu, Y. Ding, Y. Lei, J. Li, Z. Wang, X. Zhang, Y. Wang, J. Cheng, Y. Liu, Q. Shi, L. Yan, G. Geng, C. Hong, M. Li, F. Liu, B. Zheng, J. Cao, A. Ding, J. Gao, Q. Fu, J. Huo, B. Liu, Z. Liu, F. Yang, K. He, J. Hao, Drivers of improved PM$_{2.5}$ air quality in China from 2013 to 2017. *Proc. Natl. Acad. Sci. U.S.A.* **116**, 24463–24469 (2019).
19. G. He, Y. Pan, T. Tanaka, The short-term impacts of COVID-19 lockdown on urban air pollution in China. *Nat. Sustain.* 10.1038/s41893-020-0581-y , (2020).
20. P. Wang, K. Chen, S. Zhu, P. Wang, H. Zhang, Severe air pollution events not avoided by reduced anthropogenic activities during COVID-19 outbreak. *Res. Conserv. Recyc.* **158**, 104814 (2020).
21. Y. Zhao, K. Zhang, X. Xu, H. Shen, X. Zhu, Y. Zhang, Y. Hu, G. Shen, Substantial changes in nitrogen dioxide and ozone after excluding meteorological impacts during the COVID-19 outbreak in mainland China. *Environ. Sci. Technol. Lett.* **7**, 402–408 (2020).
22. L. Myllyvirta, H. Thieriot, *11,000 Air Pollution-Related Deaths Avoided in Europe as Coal, Oil Consumption Plummet* (CREA report, 2020).
23. A. Thorpe, R. M. Harrison, Sources and properties of non-exhaust particulate matter from road traffic: A review. *Sci. Total Environ.* **400**, 270–282 (2008).
24. J. He, S. Gong, Y. Yu, L. Yu, L. Wu, H. Mao, C. Song, S. Zhao, H. Liu, X. Li, R. Li, Air pollution characteristics and their relation to meteorological conditions during 2014–2015 in major Chinese cities. *Environ. Pollut.* **223**, 484–496 (2017).
25. X. Shi, G. P. Brasseur, The response in air quality to the reduction of Chinese economic activities during the COVID-19 outbreak. *Geophys. Res. Lett.* **47**, e2020GL088070 (2020).
26. O. Ghaffarpasand, D. C. Beddows, K. Ropkins, F. D. Pope, Real-world assessment of vehicle air pollutant emissions subset by vehicle type, fuel and EURO class: New findings from the recent UK EDAR field campaigns, and implications for emissions restricted zones. *Sci. Total Environ.* **734**, 139416 (2020).
27. C. Song, C. Ma, Y. Zhang, T. Wang, L. Wu, P. Wang, Y. Liu, Q. Li, J. Zhang, Q. Dai, C. Zou, L. Sun, H. Mao, Heavy–duty diesel vehicles dominate vehicle emissions in a tunnel study in northern China. *Sci. Total Environ.* **637**, 431–442 (2018).
28. J. H. Seinfeld, S. N. Pandis, *Atmospheric Chemistry and Physics: From Air Pollution to Climate Change* (John Wiley & Sons, 2016).
29. T. Wang, L. Xue, P. Brimblecombe, Y. F. Lam, L. Li, L. Zhang, Ozone pollution in China: A review of concentrations, meteorological influences, chemical precursors, and effects. *Sci. Total Environ.* **575**, 1582–1596 (2017).
30. K. Li, D. J. Jacob, H. Liao, L. Shen, Q. Zhang, K. H. Bates, Anthropogenic drivers of 2013–2017 trends in summer surface ozone in China. *Proc. Natl. Acad. Sci. U.S.A.* **116**, 422–427 (2019).
31. R.-J. Huang, Y. Zhang, C. Bozzetti, K.-F. Ho, J.-J. Cao, Y. Han, K. R. Daellenbach, J. G. Slowik, S. M. Platt, F. Canonaco, P. Zotter, R. Wolf, S. M. Pieber, E. A. Bruns, M. Crippa, G. Ciarelli, A. Piazzalunga, M. Schwikowski, G. Abbaszade, J. Schnelle-Kreis, R. Zimmermann, Z. An, S. Szidat, U. Baltensperger, I. E. Haddad, A. S. H. Prévôt, High secondary aerosol contribution to particulate pollution during haze events in China. *Nature* **514**, 218–222 (2014).
32. C.-S. Liang, F.-K. Duan, K.-B. He, Y.-L. Ma, Review on recent progress in observations, source identifications and countermeasures of PM$_{2.5}$. *Environ. Int.* **86**, 150–170 (2016).
33. G. McFiggans, M. R. Alfarra, J. D. Allan, H. Coe, J. F. Hamilton, R. M. Harrison, M. E. Jenkin, A. C. Lewis, S. J. Moller, D. Topping, P. I. Williams, *A Review of the State-Of-The-Science Relating to Secondary Particulate Matter of Relevance to the Composition of the UK Atmosphere: Full Technical Report to Defra, Project AQ0732* (Research Report, Defra, 2015).
34. Y. Sun, L. Lei, W. Zhou, C. Chen, Y. He, J. Sun, Z. Li, W. Xu, Q. Wang, D. Ji, P. Fu, Z. Wang, D. R. Worsnop, A chemical cocktail during the COVID-19 outbreak in Beijing, China: Insights from six-year aerosol particle composition measurements during the Chinese new year holiday. *Sci. Total Environ.* **742**, 140739 (2020).
35. Y. Zhao, R. Saleh, G. Saliba, A. A. Presto, T. D. Gordon, G. T. Drozd, A. H. Goldstein, N. M. Donahue, A. L. Robinson, Reducing secondary organic aerosol formation from gasoline vehicle exhaust. *Proc. Natl. Acad. Sci. U.S.A.* **114**, 6984–6989 (2017).
36. H. Zheng, S. Kong, N. Chen, Y. Yan, D. Liu, B. Zhu, K. Xu, W. Cao, Q. Ding, B. Lan, Z. Zhang, M. Zheng, Z. Fan, Y. Cheng, S. Zheng, L. Yao, Y. Bai, T. Zhao, S. Qi, Significant changes in the chemical compositions and sources of PM$_{2.5}$ in Wuhan since the city lockdown as COVID-19. *Sci. Total Environ.* **739**, 140000 (2020).
37. Q. Di, Y. Wang, A. Zanobetti, Y. Wang, P. Koutrakis, C. Choirat, F. Dominici, J. D. Schwartz, Air pollution and mortality in the medicare population. *N. Engl. J. Med.* **376**, 2513–2522 (2017).
38. COMEAP, *Associations of long-term average concentrations of nitrogen dioxide with mortality, Committee on the Medical Effects of Air Pollutants report, Public Health England* (2018); www.gov.uk/government/publications/nitrogen-dioxide-effects-on-mortality.
39. M. R. Ashmore, Assessing the future global impacts of ozone on vegetation. *Plant Cell Environ.* **28**, 949–964 (2005).
40. B. Zhao, H. Zheng, S. Wang, K. R. Smith, X. Lu, K. Aunan, Y. Gu, Y. Wang, D. Ding, J. Xing, V. Fu, X. Yang, K.-N. Liou, J. Hao, Change in household fuels dominates the decrease in PM$_{2.5}$ exposure and premature mortality in China in 2005–2015. *Proc. Natl. Acad. Sci. U.S.A.* **115**, 12401–12406 (2018).
41. K. Li, D. J. Jacob, H. Liao, J. Zhu, V. Shah, L. Shen, K. H. Bates, Q. Zhang, S. Zhai, A two-pollutant strategy for improving ozone and particulate air quality in China. *Nat. Geosci.* **12**, 906–910 (2019).
42. J. H. Kroll, C. L. Heald, C. D. Cappa, D. K. Farmer, J. L. Fry, J. G. Murphy, A. L. Steiner, The complex chemical effects of COVID-19 shutdowns on air quality. *Nat. Chem.* **12**, 777–779 (2020).
43. Q. Schiermeier, Why pollution is plummeting in some cities-but not others. *Nature* **580**, 313 (2020).
44. M. Steinbacher, C. Zellweger, B. Schwarzenbach, S. Bugmann, B. Buchmann, C. Ordóñez, A. S. H. Prevot, C. Hueglin, Nitrogen oxide measurements at rural sites in Switzerland: Bias of conventional measurement techniques. *J. Geophys. Res. Atmos.* **112**, D11307 (2007).

Acknowledgments: We would like to thank the University of Birmingham's BlueBEAR HPC service (www.birmingham.ac.uk/bear), which provides a high-performance computing service to run RF models and data analysis, the OpenAQ community for the open access to the air quality data, the NOAA Air Resources Laboratory (ARL) for providing the HYSPLIT model to analyze the back trajectories, and Comprehensive R Archive Network (CRAN) and authors of openair, rmweather, and worldmet R packages (particularly D. Carslaw). We thank the editor and reviewers for providing constructive comments that improved the manuscript. **Funding:** This work is funded by the Natural Environment Research Council (NE/N007190/1, NE/R005281/1, and NE/S006699/1) as part of the Atmospheric Pollution and Human Health in a Chinese Megacity program. We also acknowledge the support from the IGI Clean Air Theme in the University of Birmingham. G.L. thanks the PhD studentship funded by the China Scholarship Council. **Author contributions:** Z.S. conceived the research, designed the work, and drafted the original manuscript; G.L., J.X., B.L., and C.S. collected the air quality and meteorological data; C.S. collected the ERA5 reanalysis data, performed the back-trajectory clustering, and run the RF model, Monte Carlo simulation, and data visualization; T.V.V. and B.L. contributed to the development of the RF method for this study. W.J.B. contributed to the interpretation of the results regarding O$_3$-forming and O$_3$-depleting chemical processes. W.J.B., R.M.H., W.L., and R.J.R.E. contributed to drafting and revision of the manuscript. **Competing interests:** The authors declare that they have no competing interests. **Data and materials availability:** Codes and the auxiliary data table S1 (including observed and deweathered air quality data and deweathered and detrended percentage changes in air quality) are available at https://github.com/songnku/COVID-19-AQ. All data needed to evaluate the conclusions in the paper are present in the paper and/or the Supplementary Materials. Additional data related to this paper may be requested from the authors.

Submitted 14 July 2020
Accepted 18 November 2020
Published 13 January 2021
10.1126/sciadv.abd6696

Citation: Z. Shi, C. Song, B. Liu, G. Lu, J. Xu, T. Van Vu, R. J. R. Elliott, W. Li, W. J. Bloss, R. M. Harrison, Abrupt but smaller than expected changes in surface air quality attributable to COVID-19 lockdowns. *Sci. Adv.* **7**, eabd6696 (2021).

Science Advances

Abrupt but smaller than expected changes in surface air quality attributable to COVID-19 lockdowns

Zongbo ShiCongbo SongBowen LiuGongda LuJingsha XuTuan Van VuRobert J. R. ElliottWe jun LiWilliam J. BlossRoy M. Harrison

Sci. Adv., 7 (3), eabd6696. • DOI: 10.1126/sciadv.abd6696

Science Advances (ISSN 2375-2548) is published by the American Association for the Advancement of Science. 1200 New York Avenue NW, Washington, DC 20005. The title *Science Advances* is a registered trademark of AAAS.